



An Analytical Voltage Stability Model for Wind Power Plant Sizing and Siting in Distribution Networks

Seyed Morteza Alizadeh

B.Sc. and M.Sc. in Electrical and Electronics Engineering

College of Engineering and Science
Victoria University, Melbourne, Australia

Submitted in fulfillment
of the requirements of the degree of
Doctor of Philosophy

July, 2017

Abstract

Electrical energy is the most widely used form of energy worldwide. The world is currently experiencing severe energy shortages as the fossil-fuel deposits are decreasing at an alarming rate. The increased awareness about environmental hazards, caused by the burning of fuels, is also forcing governments towards exploiting renewable-energy resources. Wind is one the important renewable resources, abundantly available, and offers the lowest cost per MWh as compared to most other renewable-energy resources. Harvesting energy from the wind as an alternative to fossil fuels has many advantages in terms of protecting the environment and promoting sustainability. However, voltage profile of distribution networks with interconnected Wind Power Plant (WPP) can be significantly affected ascribable to the limited capability of Wind Turbine Generators (WTGs) in regulating terminal voltage through reactive power control.

The interconnection of the WPPs to distribution networks must ensure that the Point of Common Coupling (PCC) bus voltage is maintained within the allowable steady-state voltage range defined in the grid codes. Furthermore, the overall X/R ratio in distribution networks is small when compared to transmission networks. This makes the voltage regulation more challenging in distribution networks. Given all these, voltage stability at the PCC of a WPP is a key concern in the interconnection of WPPs to distribution networks. The Short Circuit Capacity (SCC), line parameters, and the corresponding system X/R ratio are the most important parameters which can be calculated at a given point looking back to the distribution substation. These parameters are very critical in dictating the voltage stability of a distribution network connected WPP.

This thesis addresses issues concerned with the interconnection of WPPs to distribution networks through detailed voltage stability analysis studies. As the main contribution of this thesis, a voltage stability analytical model has been developed for modelling the relations between the PCC bus voltage (V_{PCC}), wind power generation (P_{wind}), SCC, and the X/R ratio.

A sensitivity analysis was first carried out to gather datasets, which were used to identify a numerical relation between the voltage and X/R ratio at the PCC of various IEEE test systems with different SCR values. Analysis was carried out based on two types of WTGs commonly used in the WPPs: Induction Generator (IG) and Double Fed Induction Generator (DFIG). For each generator type, the obtained V-X/R data points were then used to develop general forms of equations capable of modelling the relations between the voltage, P_{wind} , and the PCC parameters. A Genetic Algorithm (GA) based approach was then used to identify the coefficients of the developed equations. The accuracy of the proposed equations was then evaluated using different scenarios involving a wide range of operating conditions.

The work is novel and the proposed analytical model makes significant contributions to knowledge by demonstrating the effects of key network PCC characteristics on the PCC bus voltage stability. The proposed analytical model would enable the network and grid interconnection engineers with a methodology that can be used for the initial predictive assessment of viable interconnection sites from a steady-state voltage stability view. The novel SCC and X/R based voltage-stability model has high accuracy and enables a predictive analytical assessment on siting and sizing of WPPs in distribution networks. It enables to promptly conduct three important voltage stability criteria at potential distribution network interconnection points for IG and

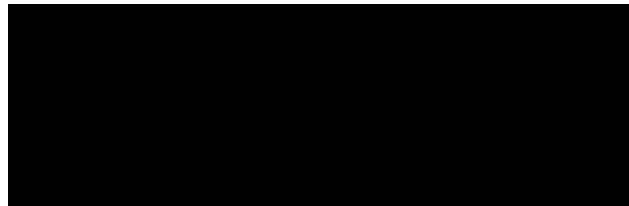
DFIG-Based WPPs. These criteria are: V_{PCC} profile, the step- V_{PCC} variation in response to the change of P_{wind} , and the maximum permissible wind power capacities that would satisfy grid code requirements in regards to steady-state voltage stability. The proposed model simplifies the challenges concerned with finding optimal allocation and sizing of WPPs in distribution networks using the existing approaches and removes the need to carry out time consuming calculations.

A follow-on benefit of this work is the fact that it would enable a predictive assessment on the quantity, structure, and cost of reactive compensation mix that would be required at a given connection point.

Student Declaration

I, Seyed Morteza Alizadeh, declare that the PhD thesis entitled “An Analytical Voltage Stability Model for Wind Power Plant Sizing and Allocating in Distribution Networks” is no more than 100,000 words in length including quotes and exclusive of tables, figures, appendices, bibliography, references and footnotes. This thesis contains no material that has been submitted previously, in whole or in part, for the award of any other academic degree or diploma. Except where otherwise indicated, this thesis is my own work.

Signature:



Date: 17 / 10 / 2017

Acknowledgements

I would like to express my sincere gratitude to the College of Engineering and Science, Victoria University, for letting me fulfil my dream of being a PhD student here. My deep gratitude goes to my supervisor, Dr. Cagil Ozansoy, for fully supporting me throughout the course of doctoral program, for patiently guiding and encouraging me on conducting high level research, and for pushing me further than I thought I could go.

To Prof. Stephen Collins, Prof. Vincent Rouillard, Dr. Valli Navaratnam, and Dr, Rudi Van Staden for giving me this opportunity to work as a tutor and lab instructor and gain an excellent experience in teaching in an international environment.

To my parents, Seyed Mohammad Alizadeh and Maryam Ghadaksaz Zadeh, for their endless support during my period of working on the thesis. Your love and constant patience have taught me so much about sacrifice, discipline, and compromise.

To my sisters, Sara and Samaneh, brothers in law, and nieces for their love and always positive vibes which felt near even from a long distance.

Finally, to my friends, especially Simon Northey, Gareth Northey, and Anne Sophie Westerdahl, who were just like a family and helped me to keep my moral on the top.

Publications

- [1] Seyed Morteza Alizadeh, Cagil Ozansoy, Tansu Alpcan, “The impact of X/R ratio on voltage stability in a distribution network penetrated by wind farms”, in 2016 Australasian Universities Power Engineering Conference (AUPEC), 2016, pp. 1-6

Under review:

- [2] Seyed Morteza Alizadeh, Cagil Ozansoy, “The Effect of Short Circuit Capacity and X/R ratio on Voltage Stability in a Distribution Network Connected Wind Power Plant”, International Review on Modelling and Simulations.
- [3] Seyed Morteza Alizadeh, Cagil Ozansoy, “An Analytical Voltage Stability Model in Site and Size Analysis for IG Wind Power Plants”, IEEE Power Engineering Letters
- [4] Seyed Morteza Alizadeh, Cagil Ozansoy, “An Analytical Voltage Stability Model in Site and Size Analysis for DFIG Wind Power Plants”, IEEE Power Engineering Letters
- [5] Seyed Morteza Alizadeh, Cagil Ozansoy, Akhtar Kalam, “Investigation into the Impact of PCC Parameters on Voltage Stability in a DFIG Wind Farm”, in 2017 Australasian Universities Power Engineering Conference (AUPEC), 2017

Table of Contents

Abstract	i
Student Declaration	iv
Acknowledgements	v
Publications	vi
Table of Contents	vii
List of Figures	xii
List of Tables	xv
Glossary and List of Acronyms	xvii
Chapter 1 Introduction	1
1.1 Background.....	1
1.2 Problem statement	2
1.3 Research objectives.....	4
1.4 Research methodologies and techniques.....	5
1.5 Research contribution and significance.....	8
1.6 Thesis structure.....	9
Chapter 2 Literature Review on Site and Voltage Stability Analysis in WPPs	11
2.1 Introduction.....	11
2.2 Wind energy systems and interconnection into distribution systems.....	14
2.2.1 Power quality standards – Voltage.....	14
2.2.2 Voltage stability challenges in WPPs.....	16
2.3 Voltage regulation in WPPs.....	18
2.3.1 Effect of generator type on voltage	19
2.3.1.1 Types 1 and 2.....	20
2.3.1.2 Types 3 and 4.....	22

2.4 Interconnection site selection.....	24
2.4.1 Analytical approaches.....	24
2.4.2 Artificial intelligence approaches.....	25
2.4.3 Mathematical formulation for selecting PCC location.....	27
2.5 Significance of the Short Circuit Ratio	29
2.5.1 Effect of SCR on voltage control	29
2.5.2 Worldwide projects.....	31
2.6 Significance of the X/R ratio in distribution systems.....	34
2.6.1 X/R value.....	35
2.6.2 Impact of X/R effect on voltage variations.....	38
2.6.3 X/R-Based voltage control schemes.....	43
2.7 Conclusion.....	45
Chapter 3 Voltage Stability Analysis at the Point of Common Coupling.....	48
3.1 Introduction.....	48
3.2 Basic theory.....	50
3.3 Test distribution systems.....	53
3.3.1 Source and distribution transformer.....	55
3.3.2 Wind power plant.....	55
3.3.3 Reactive power compensator.....	56
3.3.4 Load.....	56
3.3.5 Distribution lines.....	57
3.4 PV and QV analysis.....	58
3.4.1 PV analysis.....	59
3.4.1.1 IG-Based WPP.....	60
3.4.1.2 DFIG-Based WPP.....	65

3.4.2 QV analysis.....	69
3.4.2.1 IG-Based WPP.....	70
3.4.2.2 DFIG-Based WPP.....	74
3.5 PQ analysis.....	77
3.6 Effect of SCR and X/R ratios on voltage profile.....	80
3.7 Conclusion.....	82
Chapter 4 Genetic Algorithm-Based Analytical Model for the PCC Voltage Stability Analysis	86
4.1 Introduction.....	86
4.2 Voltage versus X/R ratio characteristic.....	87
4.2.1 IG-Based WPP.....	90
4.2.2 DFIG-Based WPP.....	91
4.3 Developing mathematical relations.....	93
4.3.1 General form of alternative functions for IG-Based WPPs.....	93
4.3.2 General form of alternative functions for DFIG-Based WPP.....	97
4.3.3 Genetic Algorithm.....	98
4.3.4 Fitness function.....	101
4.3.5 GA parameters.....	104
4.3.5.1 Selection.....	104
4.3.5.2 Crossover.....	105
4.3.5.3 Elite count.....	106
4.3.5.4 Mutation.....	106
4.3.6 GA outcomes.....	107
4.4 Evaluation of the accuracy of the proposed alternative equations.....	109
4.4.1 Statistical criteria.....	110

4.4.2 Graphical representations.....	111
4.5 Voltage stability analytical mode.....	117
4.6 Conclusion.....	121
Chapter 5 Validation of the Proposed Analytical Model.....	124
5.1 Introduction.....	124
5.2 Validation process.....	125
5.3 Validation studies for IG-Based WPP.....	126
5.3.1 Voltage profile prediction in IG-Based WPPs.....	129
5.3.2 Step-voltage variation prediction in IG-Based WPPs.....	130
5.3.3 IG-Based WPP maximum allowable sizing prediction.....	132
5.4 Validation studies for DFIG-Based WPPs.....	135
5.4.1 Voltage profile prediction in DFIG-Based WPPs.....	137
5.4.2 Step-voltage variation prediction in DFIG-Based WPPs.....	137
5.4.3 DFIG-Based WPP maximum allowable sizing prediction.....	139
5.5 Conclusion.....	141
Chapter 6 Development of the Proposed Analytical Model for Different Operational Scenarios.....	143
6.1 Introduction.....	143
6.2 Development of the analytical model for different $V_{PCC_initial}$	144
6.3 Validating proposed equations for different $V_{PCC_initial}$ values.....	153
6.3.1 Voltage profile prediction.....	153
6.3.2 Step-voltage variation prediction.....	154
6.3.3 WPP maximum allowable sizing prediction.....	156
6.4 Further validation studies.....	157
6.4.1 PV characteristics for the new test systems.....	158

6.4.2 Voltage profile prediction for the new test systems.....	161
6.4.3 Step-voltage variation prediction for the new test systems.....	162
6.4.4 WPP maximum allowable sizing prediction for the new test systems.....	165
6.5 Conclusion.....	166
Chapter 7 Conclusions and Future Work.....	168
7.1 Introduction.....	168
7.2 Key contributions of the research.....	170
7.3 Future work.....	173
References.....	177
Appendix A MATLAB/Simulink Models of Test Systems.....	191
Appendix B Test Systems Specifications.....	193
Appendix C MATLAB codes for Fitness Function 1.....	197

List of Figures

Figure 2.1	Single line diagram of a distribution system connected WPP [54].....	16
Figure 2.2	Thévenin equivalent circuit of distribution system [11].....	17
Figure 2.3	A three phase distribution line [104].....	36
Figure 2.4	Step-voltage variations versus SCR for different X/R ratios [57].....	40
Figure 2.5	Limit of ρ and X/R for $0.95 \text{ p.u.} < V_{\text{PCC}} < 1.05 \text{ p.u.}$ in a SQIG-Based WPP [56]..	41
Figure 2.6	Limit of ρ and X/R for $0.95 \text{ p.u.} < V_{\text{PCC}} < 1.05 \text{ p.u.}$ in a DFIG-Based WPP [56]..	41
Figure 3.1	Phasor diagram of the PCC voltage variation [131].....	51
Figure 3.2	Single-line diagram of the modelled 9-bus test distribution system.....	54
Figure 3.3	Single-line diagram of the modelled 37-bus test distribution system.....	55
Figure 3.4	PV curve for different X/R_{PCC} ratios in the IG-Based 9-bus test system.....	60
Figure 3.5	PV curve for different X/R_{PCC} ratios in the IG-Based 37-bus test system....	60
Figure 3.6	Voltage variation versus active power injection for different X/R ratios at the PCC of the IG-Based 9-bus test system.....	61
Figure 3.7	Voltage variation versus active power injection for different X/R ratios at the PCC of the IG-Based 37-bus test system.....	61
Figure 3.8	PV curve for different X/R ratios at the PCC of the DFIG-Based 9-bus test system.....	65
Figure 3.9	PV curve for different X/R ratios at the PCC of the DFIG-Based 37-bus test system.....	65
Figure 3.10	Voltage variation versus active power injection for different X/R ratios at the PCC of the DFIG-Based 9-bus test system.....	66
Figure 3.11	Voltage variation versus active power injection for different X/R ratios at the PCC of the DFIG-Based WPP 37-bus test system.....	66
Figure 3.12	QV curves for large X/R ratios – IG-Based WPP.....	70
Figure 3.13	QV curves for small X/R ratios – IG-Based WPP.....	73
Figure 3.14	QV curves for large X/R ratios– DFIG-Based WPP.....	75
Figure 3.15	QV curves for small X/R ratios – DFIG-Based WPP.....	77

Figure 3.16	PQ curves for different X/R ratios when $V_{PCC} = 0.95$ p.u.....	78
Figure 3.17	V_{PCC} -SCR characteristic in the IG-Based 9-bus test system.....	80
Figure 3.18	V_{PCC} -SCR characteristic in the IG-Based 37-bus test system.....	80
Figure 3.19	V_{PCC} -SCR characteristic in the DFIG-Based 9-bus test system.....	81
Figure 3.20	V_{PCC} -SCR characteristic in the DFIG-Based 37 bus test system.....	81
Figure 4.1	V_{PCC} - X/R_{PCC} characteristic for each test system – IG-Based WPP.....	90
Figure 4.2	V_{PCC} - X/R_{PCC} characteristic for each test system – DFIG-Based WPP....	91
Figure 4.3	Characteristic of the alternative Eqs. (4.1) and (4.2).....	95
Figure 4.4	Flowchart of the GA concept [146, 147].....	99
Figure 4.5	V-X/R graphs obtained by Eqs (4.20) and (4.21) for Test System 1....	112
Figure 4.6	V-X/R graphs obtained by Eqs (4.20) and (4.21) for Test System 2....	112
Figure 4.7	V-X/R graphs obtained by Eqs (4.20) and (4.21) for Test System 3....	113
Figure 4.8	V-X/R graphs obtained by Eqs (4.20) and (4.21) for Test System 4....	113
Figure 4.9	V-X/R graphs obtained by Eqs (4.22) and (4.23) for Test System 1....	114
Figure 4.10	V-X/R graphs obtained by Eqs (4.22) and (4.23) for Test System 2....	114
Figure 4.11	V-X/R graphs obtained by Eqs (4.22) and (4.23) for Test System 3....	114
Figure 4.12	V-X/R graphs obtained by Eqs (4.22) and (4.23) for Test System 4....	115
Figure 4.13	V-X/R graphs obtained by Eqs (4.24) and (4.25) for Test System 1....	116
Figure 4.14	V-X/R graphs obtained by Eqs (4.24) and (4.25) for Test System 2....	116
Figure 4.15	V-X/R graphs obtained by Eqs (4.24) and (4.25) for Test System 3....	116
Figure 4.16	V-X/R graphs obtained by Eqs (4.24) and (4.25) for Test System 4....	117
Figure 5.1	PV characteristic for Scenarios 1 and 2.....	127
Figure 5.2	PV characteristic for Scenarios 3 and 4.....	127
Figure 5.3	PV characteristic for Scenarios 5 and 6.....	127
Figure 5.4	$P\Delta V$ characteristic for Scenarios 1 and 2.....	128
Figure 5.5	$P\Delta V$ characteristic for Scenarios 3 and 4.....	128

Figure 5.6	PΔV characteristic for Scenarios 5 and 6.....	128
Figure 5.7	Predicted and simulated $P_{\max\text{-wind}}$ for Scenarios 1 to 6.....	134
Figure 5.8	PV characteristic for Scenario 7.....	135
Figure 5.9	PV characteristic for Scenario 8.....	135
Figure 5.10	PV characteristic for Scenario 9.....	136
Figure 5.11	PV characteristic for Scenario 10.....	136
Figure 5.12	PΔV characteristic for Scenario 9.....	138
Figure 5.13	Predicted and simulated $P_{\max\text{-wind}}$ for Scenarios 7 to 10.....	141
Figure 6.1	PV characteristic for Scenario A.....	145
Figure 6.2	PV characteristic for Scenario B.....	146
Figure 6.3	PV characteristic for Scenario C.....	146
Figure 6.4	PV characteristic for Scenario D.....	146
Figure 6.5	PV characteristic for Scenario E.....	147
Figure 6.6	PV characteristic for Scenario F.....	147
Figure 6.7	PV characteristic for Scenario G.....	147
Figure 6.8	PV characteristic for Scenario H.....	148
Figure 6.9	PΔV characteristic for Scenarios B and E.....	155
Figure 6.10	Predicted and simulated $P_{\max\text{-wind}}$ for Scenarios A to H.....	157
Figure 6.11	PV characteristic for Tests 5 and 6.....	159
Figure 6.12	PV characteristic for Tests 7 and 8.....	159
Figure 6.13	PV characteristic for Tests 9 and 10.....	159
Figure 6.14	PV characteristic for Tests 11 and 12.....	160
Figure 6.15	PΔV characteristic for Tests 6 and 10.....	163
Figure 6.16	Predicted and simulated $P_{\max\text{-wind}}$ for Tests 5 to 10.....	165

List of Tables

Table 2.1	Indicative planning levels for step- V_{PCC} changes as a function of the number of such changes per hour [50, 51].....	15
Table 2.2	Summary of NEM installations based on Type 1 and Type2 WTGs [60]....	21
Table 2.3	Voltage control requirement and X/R values in distribution networks [10].....	37
Table 3.1	SCC value in 9-bus and 37-bus test feeders.....	59
Table 3.2	Active power margin ensuring $0.95 \text{ p.u.} < V_{PCC} < 1.05 \text{ p.u.}$ in the IG-Based 9-bus system.....	62
Table 3.3	Active power margin ensuring $0.95 \text{ p.u.} < V_{PCC} < 1.05 \text{ p.u.}$ in the IG - Based 37-bus system.....	62
Table 3.4	Step-voltage variation in the IG-Based 9-bus test system.....	63
Table 3.5	Step-voltage variation in the IG-Based 37-bus test system.....	63
Table 3.6	Step-voltage variation in the DFIG-Based 9-bus test system.....	67
Table 3.7	Step-voltage variation in the DFIG-Based 37-bus test system.....	68
Table 3.8	Reactive power margin ensuring $0.95 \text{ p.u.} < V_{PCC} < 1.05 \text{ p.u.}$	71
Table 3.9	Maximum active and reactive power generated or absorbed by the WPP for $V_{PCC} = 0.95 \text{ p.u.}$	79
Table 4.1	Topology and SCR value for each for test distribution system.....	88
Table 4.2	Characteristics considered for developing mathematical relations for IG-Based WPPs.....	94
Table 4.3	Pseudo codes for Fitness Function 1.....	102
Table 4.4	Upper boundaries for each input variable of the GA function.....	107
Table 4.5	Values of the coefficients.	108
Table 4.6	MAE and MRE values for alternative Eqs. (4.20) to (4.25).....	110
Table 4.7	Proposed equation for each WPP type and X/R_{PCC} range.....	117
Table 4.8	Proposed analytical model assuming $V_{PCC_initial} = 0.98 \text{ p.u.}$	120
Table 5.1	Test system, generator type, and PCC parameters.....	125
Table 5.2	Error between simulated and predicted V_{PCC} profile for Scenarios 1 to 6.....	130

Table 5.3	Error between simulated and predicted ΔV_{PCC} for Scenarios 1 to 6.....	131
Table 5.4	Error between simulated and predicted V_{PCC} profile for Scenarios 7 to 10.....	137
Table 5.5	Error between simulated and predicted ΔV_{PCC} for Scenarios 7 to 10.....	139
Table 6.1	PCC parameters for Scenarios with new $V_{PCC_initial}$ values.....	145
Table 6.2	Final proposed voltage stability analytical model.....	153
Table 6.3	Error between simulated and predicted V_{PCC} profile for Scenarios A to H.....	153
Table 6.4	Error between simulated and predicted ΔV_{PCC} for Scenarios A to H.....	156
Table 6.5	New test systems topologies, PCC parameters, and $V_{PCC_initial}$ values...	158
Table 6.6	Error between simulated and predicted V_{PCC} profile for Tests 5 to 10.....	161
Table 6.7	Error between simulated and predicted ΔV_{PCC} for Tests 5 to 10.....	164
Table 7.1	Proposed voltage stability analytical model.....	169

Glossary and List of Acronyms

AEMO	Australian Energy Market Operator
DFIG	Double Fed Induction Generator
GA	Genetic Algorithm
I_{sc}	Short Circuit Current
IG	Induction Generator
MAE	Mean of Absolute Error
MRE	Mean of Relative Error
NEM	National Electricity Market
P_{margin}	Active power margin
P_{wind}	Wind Active Power
P_{max-wind}	WPP maximum permissible size ensuring the grid code requirements
PQ	Power Quality
PV	Power-Voltage
Q_{margin}	Reactive Power Margin
Q_{wind}	Wind Reactive Power
QV	Reactive Power-Voltage
R&D	Research and Development
RL	Resistor-Inductor
SCC	Short Circuit Capacity
SCR	Short Circuit Ratio
V_{PCC}	PCC Bus Voltage
V_{PCC_initial}	Initial steady-state voltage level at the point of common coupling of distribution system, before wind

	power plant connection
WPP	Wind Power Plants
WTG	Wind Turbine Generator
X/R_{PCC}	Short circuit impedance angle ratio seen at the point of common coupling
Z_{sc}	Grid Short-Circuit impedance
ΔV_{PCC}	Step-voltage variation at the point of common coupling due to the change of wind power generation
ΔQ	Reactive power variation
ρ	Integration level
σ	Standard deviation

Chapter 1 Introduction

1.1 Background

Currently, many countries are faced with increasing demands of electricity, but yet limited petroleum resources. Environmental concerns due to the release of greenhouse gas emissions in fossil fuel combustion have become a major issue all over the world [1]. These concerns have resulted in a trend towards higher penetration of renewable energy generation systems in power networks and more investment in these types of energy resources [2-5]. Wind power is one of the fastest growing and abundant renewable energy resources. In relation to the advantages of wind power, it could constitute an easily available, cost effective, sustainable, and environmentally-mild energy source [6]. The global wind capacity in 2014 was around 370 GW, 16 percent higher than the capacity in 2013. It increased by 17 percent to around 433 GW in 2015 and leaped to a new peak at around 487 GW in 2016. Considering the advancement of the wind industry and the increased size of Wind Power Plants (WPPs) all over the world, more research and investigations are needed and are being carried out into the design, control, and interconnection of WPPs to power systems [7].

A significant portion of wind power is being installed in distribution networks as small WPPs. In a distribution network, the network short circuit impedance angle ratio, called the X/R ratio, is one of the most important characteristics that can be calculated at any point looking back to the distribution substation. Short Circuit Capacity (SCC) is another important characteristic of a distribution network. SCC determines the amount of power flowing at a specific point in case of a short circuit [8]. The values of SCC and

the overall system X/R depends on the location of the PCC point. Moreover, research in the literature has demonstrated that there is a close relation between the distribution network characteristics (X/R seen at the PCC and SCC) and the voltage stability at the PCC connection point [9-12]. Considering the close relation between PCC location, PCC parameters, and PCC bus voltage stability, the WPP size and interconnection site selection must ensure the voltage stability requirements.

This thesis focuses on the issues concerned with the interconnection of WPP to distribution network and develops a novel analytical model to simplify WPP site allocation and voltage stability analysis in distribution systems.

1.2 Problem statement

As discussed in the previous section, X/R and SCC are the most important parameters seen from a given point of a distribution network. A thorough literature review about the significance of SCC and X/R seen from a given PCC point in PCC bus voltage stability has been performed in Chapter 2. The majority of the works in the literature dealt with the impact of the PCC parameters on voltage in general terms and using simple scenarios.

The X/R ratio in distribution lines is considerably smaller than that in transmission lines as the value of line resistance is high and near to line reactance [12, 13]. On the other hand, conventional approaches applied for voltage regulation through reactive power compensation are mainly based on the reactance of the distribution impedances and the resistance is ignored. Hence, these approaches are not appropriate for distribution networks where the X/R ratio is small [8]. Therefore, continuous increase in wind power penetration is likely to influence the operation of existing utility

distribution networks, especially in terms of voltage stability under the existing reactive power control schemes.

The value of SCC at a given point depends on nominal voltage and the inverse of the equivalent impedance value seen from that point [8]. In a distribution network connected WPP, the ratio between SCC of the system and rated wind active power (P_{wind}) is called Short Circuit Ratio (SCR). SCR signifies the amount of P_{wind} that can be injected to the distribution network without an adverse impact on voltage stability and Power Quality (PQ) at the PCC [14]. Larger values for the SCR parameter indicate lower PQ concerns. However, the SCR value in distribution networks connected WPP is generally small. The reason is the fact that, from planning and operation perspectives, one of the motivations for allocating WPPs is to have suitable condition for collecting efficient wind power. However, sites with a suitable wind condition are generally located far from the distribution substation. This makes Z_{eq} seen at the PCC large [15]. Furthermore, the voltage value in distribution networks is smaller than that in generation and transmission networks. Hence, at the PCC point of a distribution network connected WPP, high Z_{eq} and small voltage value make SCC small. Consequently, a small SCC results in small SCR values and imposes serious problems in terms of voltage stability and PQ requirements at the PCC point, especially in large wind power penetration [11].

In each country, the electricity markets specify particular technical rules, namely grid codes, in regards to voltage regulation according to their regional network characteristics. A comparison of several grid codes legislated in Australia, Canada, and European countries can be found in [16]. For removing the voltage stability issues mentioned earlier, the WPP size allocating process must ensure that the PCC bus

voltage (V_{PCC}) stays within the acceptable steady-state voltage range defined by the grid codes.

In Chapter 2, a detailed literature review has been performed to envisage the recent approaches proposed for finding optimal allocation and sizing of WPPs in distribution networks. The majority of these approaches are based on modelling and simulation of the whole system and/or calculating the bus impedance matrix (Z -bus), inverse of the bus admittance matrix (Y -bus⁻¹), and the Jacobean matrix [17-22]. The assumptions used for the simplifications of the calculation of these matrices are not valid in distribution systems [23]. Moreover, the simulation of distribution networks is a demanding process due to the size and complexity of these networks. Therefore, proposing a novel method which simplifies the WPP optimal size allocation process is a noticeable gap in the literature.

1.3 Research objectives

The research presented in this thesis aimed to investigate the issues related to the interconnection of WPP to distribution networks through detailed voltage stability analysis. To eliminate the various weaknesses of optimal WPP siting and sizing methods proposed in the literature, an analytical voltage stability model was proposed during the course of this research. The proposed model relies on the mathematical relation between PCC bus voltage and the PCC characteristics of a distribution network penetrated by WPP.

The specific aims of this research were to:

- Model different test distribution networks based on IEEE standard distribution models, IEEE 37-bus and IEEE 9-bus networks in Simulink, and carry out voltage stability analysis studies using these standard networks

- Investigate the effect of the PCC characteristics of a distribution system connected WPP on the PCC bus voltage stability through Power-Voltage (PV), Reactive Power-Voltage (QV), Power–Reactive Power (PQ), Voltage–SCR (V–SCR), and Voltage–X/R ratio (V–X/R) analysis studies comparing and contrasting results among the test systems.
- Propose a novel voltage stability analytical model demonstrating the mathematical relations between V_{PCC} , P_{wind} , SCC, and X/R ratio seen at the PCC using a Genetic Algorithm (GA)–Based approach.
- Validate the accuracy of the proposed analytical model in predicting three important voltage stability criteria at a given connection point of a distribution network penetrated by wind power, including: V_{PCC} profile, step variation of V_{PCC} due to the change of P_{wind} (ΔV_{PCC}), and the WPP maximum permissible size ensuring the grid code requirements ($P_{max-wind}$).

1.4 Research methodologies and techniques

In this research, a step by step approach was followed to achieve the research objectives mentioned above. These steps are summarised in the following.

- **Step 1 - Literature review on voltage stability analysis in WPPs**

A broad literature review on the voltage stability issues due to the interconnection of the WPPs to the distribution systems has been completed. Preparing this literature review resulted in achieving a holistic view of the existing knowledge as well as the problems and challenges. The effect of distribution system characteristics seen from a given PCC site on V_{PCC} stability was overviewed in details. The recent Research and Development (R&D) works concerned with the optimal PCC site selection and sizing of WPP with the aim of V_{PCC} stability improvement have been investigated in details.

Moreover, the review of the literature focused on knowledge gaps yet to be addressed and possible future work in this field of Power/Electrical Engineering.

- **Step 2 – MATLAB simulation modelling for voltage stability analysis studies**

Following the wide-scoped literature review explained above, research work has been dedicated to investigate the effects of SCC, X/R_{PCC} , and wind power injection on V_{PCC} stability. For this purpose, different distribution test systems were considered, modelled and simulated using MATLAB/Simulink. The test systems are based on IEEE standard distribution models: the IEEE 9-bus and IEEE 37-bus systems. The distribution network topologies and the PCC bus location, as well as the PCC parameters (X/R_{PCC} and SCC) values are different amongst the test models. The designed simulation models are then used to carry out voltage stability analysis studies regarding different PCC parameters. Analysis studies were carried out for two common two types of WTGs: Induction Generator (IG) and Double Fed Induction Generator (DFIG). This step was particularly important to analyse the behavior and effects of such parameters on the V_{PCC} stability since the proposed analytical model has to account for them. The development of the proposed voltage stability analytical model was heavily based on these findings.

- **Step 3 - Design of a novel voltage stability analytical model**

Once the necessary investigations concerned with the effect of PCC location and the value of the PCC parameters on the V_{PCC} stability was completed, a novel voltage stability analysing method has been designed. This new method is based on an analytical model considers a series of mathematical relations between PCC bus voltage, SCC, X/R_{PCC} , and P_{wind} . In this respect, a sensitivity analysis was carried out to find a

numerical relation between V_{PCC} and X/R_{PCC} in different test systems with different SCR values. In each test system, the X/R_{PCC} ratio was changed to monitor the V_{PCC} profile for each X/R_{PCC} value in a fixed SCR network. The obtained numerical results were used to plot the V_{PCC} - X/R_{PCC} characteristics for each test system. Taking the advantage of the V_{PCC} - X/R_{PCC} characteristics, a series of equations were developed to show the general forms of the mathematical relations between V_{PCC} , X/R_{PCC} , and SCR. This was the first step before further detailed studies on the proposed numerical models could be conducted. At this step, the values of the coefficients of the equations were not determined.

Later on, a GA based approach was used to determine the values of the coefficients of the developed equations for the lowest deviation with respect to the reference V-X/R characteristics obtained in the first step. Considering that the SCR ratio is the ratio between the grid SCC and the power injected by the WPP, the proposed equations were rewritten in terms of V_{PCC} as a function of X/R_{PCC} , SCC, and wind active power. These equations enabled to estimate the V_{PCC} value for different wind power penetrations at a given PCC site with specific SCC and X/R_{PCC} values. Furthermore, the equations were developed in terms of wind active power as a function of V_{PCC} and PCC parameters, which enabled to calculate the maximum power that could be injected by the WPP to a given connection point ensuring that the PCC voltage stays within the acceptable steady-state range defined by the grid codes.

- **Step 4 - Validation and development of the proposed analytical model**

At this step, the main idea was to evaluate the accuracy of the proposed equations in predicting the most important voltage stability criteria at a given connection point of a distribution network connected WPP, including: V_{PCC} profile for different wind power

penetration, ΔV_{PCC} , and $P_{\max\text{-wind}}$. In this regards, the proposed equations were initially verified using different scenarios based on the test systems designed and simulated in Step 3. Later on, it was shown how the proposed equations could be developed for predicting voltage stability criteria in new test distribution systems with different PCC characteristics and parameters. The presented validation results confirmed the high capability of the proposed equations in predicting the voltage stability criteria at a given connection site of a distribution network penetrated by WPP.

1.5 Research contribution and significance

As the main contribution of this research, very informative mathematical equations have been proposed to simplify the initial WPP site and size analysis challenge and enable engineers compute an initial predictive assessment on the voltage stability at a given connection point without the need to carry out complex and time consuming computational tasks or modelling of test systems.

In summary, the major contributions of this thesis are:

- **Investigation into the impact of the WPP interconnection on PCC bus voltage stability**

This research addresses issues concerned with the interconnection of WPPs to distribution networks through detailed voltage stability, PQ, QV, PQ, V-SCR, V-X/R analysis studies. The analysis provided a holistic view about the impact of PCC parameters on PCC voltage stability in grid connected WPPs.

- **Development of mathematical equations for projecting V_{PCC} and ΔV_{PCC}**

The detailed development of the mathematical relations between V_{PCC} , SCC , X/R_{PCC} , and P_{wind} has been presented for both IG and DFIG-Based WPPs. This is a very

important contribution for achieving an analytical model that enable to conduct an initial predictive assessment on voltage stability and predict the value of voltage and step–voltage variation in response to the change of wind power at a potential PCC bus in a distribution network connected to WPP.

- **Development of mathematical equations for projecting WPP maximum allowable size**

A series of mathematical equations were developed to estimate the maximum power which can be injected to the distribution system while the PCC bus voltage stays within the acceptable steady–state range. PCC parameters, which can be easily calculated at any point looking back to the distribution substation, are the only unknown of the proposed equations. PCC parameters can be easily computed using power flow analysis software. Hence, the proposed equations enable to promptly compute the size of a WPP without the need to solve complex and time consuming computational tasks.

1.6 Thesis structure

Chapter1 gives an overview of the thesis, its objectives and contribution to the knowledge. It also sheds some light on the methodologies used in the research. Chapter 2 provides a comprehensive literature review with regard to the interconnection of the WPPs to the distribution systems and introduces the concepts of X/R ratio at a given PCC point (X/R_{PCC}), SCC, and SCR. Furthermore, it envisages the recent techniques and approaches used for optimal placement and sizing of WPP in distribution systems. Correspondingly, the knowledge gaps and potential research directions for future development in this field have been identified.

Following this review and the detection of the research field, Chapter 3 investigates the significance of X/R, SCC, and SCR on voltage stability at a given PCC

point of a distribution system connected WPP. For this purpose, PV, QV, PQ, and V-SCR analysis studies have been carried out using test systems simulated in MATLAB/Simulink. The test systems are based on IEEE distribution models connected IG and DFIG-Based WPPs.

As the main contribution of this research, in Chapter 4, a novel voltage stability analytical model was developed to show the mathematical relations between V_{PCC} , X/R_{PCC} , SCC , and P_{wind} . The proposed model consists of six equations developed for predicting the most important voltage stability criteria regarding the WTG type and the range of X/R_{PCC} . Three equations were proposed to calculate the voltage profile and the step variation of voltage due to the change of wind power injection at a given connection point. Furthermore, three equations were proposed to estimate the maximum wind power could be injected to the grid while the V_{PCC} is maintained within the acceptable steady-state range.

Chapter 5 gives the details of the simulation works and numerical analysis studies undertaken to validate and confirm the intellectual contributions made in the preceding Chapters. Validation studies have been carried out using different scenarios based on test systems designed in Chapter 4 to evaluate the capability of the proposed model in estimating and calculating the considered voltage stability criteria.

Upon validating the proposed voltage stability analytical model for the test systems designed in Chapter 4, the model is further developed in Chapter 6, such that it satisfies new test distribution systems with different PCC parameters. Also, the developed model will be validated using different scenarios involving a wide range of operating conditions. Finally, Chapter 7 summarises the whole research work, highlights the contributions made and draws the conclusions.

Chapter 2 - Literature Review on Site and Voltage Stability Analysis in WPPs

2.1 Introduction

Distribution networks are one of the most important parts of the electrical networks as they are the interface between transmission system and individual consumers. Distribution systems must supply the consumer demand with an appropriate quality and continuity [24]. This signifies that a distribution network service provider must provide the requirements and limitations concerned with supply voltage range, voltage fluctuations, voltage dips, and step voltages [25].

The ability of a power system in providing proper supply of electrical energy, expressed as the reliability of that system, is an important factor in the designing and planning process [26]. Power shortage due to an unexpected mismatch between generation and demand is the most important concern in systems with low reliability. Apart from low reliability, power shortage happens as a result of voltage instability [27, 28]. The system enters into a state of voltage instability when the increase in load or changes in the system condition results in a continuous decrease in voltage. A distribution feeder has to ensure a high quality power supply to customers connected on that feeder with an appropriated voltage profile. Furthermore, a distribution network service provider has to ensure minimum loss in transferring power from source to the customers. Hence, three main criteria in the planning and design of distribution networks are increasing the reliability of the distribution system, reduction of power losses, and making improvements in the voltage profile over that network. In achieving these aims, Distributed Generation (DG) could play a key role. DG can reduce power losses, improve Power Quality (PQ) to end users, and sort out peaks in demand patterns

[29, 30]. DG technology was principally used as a backup power source to supply electricity for individual customers during grid power outages. Nowadays, the recent advances in DG technologies enabled this power solution not only to feed small personal customers but also support the entire network in parallel with the grid.

Wind power is one of the fastest growing and abundant renewable energy resources. It constitutes an easily available, cost effective, sustainable, and clean energy source [6, 31, 32]. Large installations of Wind Power Plants (WPPs) are often connected to transmission networks. However, a significant portion of wind power is being installed in distribution systems as small WPPs. The impact of WPPs on reducing power losses, voltage stability improvement, and increasing the reliability of the system are very critical in designing WPPs. However, the effect of WPPs on the voltage stability is more important than the two other criteria [33]. This effect is ignorable in low wind power penetration. However, high wind power penetration influences the voltage stability of utility distribution networks, which is a key concern from a planning and operation perspective [34, 35] .

Works in the literature have shown that there is a relation between size and location of WPPs, voltage profile and voltage variation due to the change wind power generation [10, 36-39]. Allocating WPPs in traditional distribution systems may inflict unwanted challenges in terms of voltage stability and PQ concerns. In traditional distribution networks, voltage profile at the buses is generally close to the boundaries of the allowable steady-state voltage range [14]. This adversely impacts on the system security [15]. Under these circumstances, the size and location of WPPs connected to distribution systems must ensure the voltage stability limitations [10, 36, 40, 41]. Identification of the optimal size and location of a WPP could help to reduce voltage

stability requirements and save extra costs concerned with voltage regulation. Therefore, correct WPP size allocation is of great importance in designing and planning process.

Many researchers have proposed different approaches to find optimal siting and sizing of WPPs in distribution networks. Most are based on Artificial Intelligence (IA) approaches. Few other solutions are based on analytical approaches or Optimal Power flow (OPF) [17, 42-45]. However, the main drawback of these studies is the need to compute large dimensional matrices or simulate and model test distribution systems, which is computationally demanding and takes a long time [17]. As discussed, the location of a WPP has a significant impact on voltage at the connection point. As a result, many Research and Development (R&D) needs have evolved as a necessity to allocate WPP in distribution systems. However, the problems mentioned above adversely impact the useability and simplicity of the existing WPP allocation approaches. These problems can be eliminated through developing mathematical formula that would allow a predictive assessment of a candidate Point of Common Coupling (PCC) by studying the relations between PCC voltage (V_{PCC}) and the key characteristics of distribution networks. This is highly recommended in [46]. Development of such mathematical formulations would ideally remove the need to simulate the test systems and collect data pertaining to different components of the system, and serve as a preliminary assessment tool.

A distribution system is characterised by different parameters. Short Circuit Capacity (SCC) is one of the most important parameters of a system, which measures the amount of power flowing at a specific point in case of a short circuit [8]. The ratio between SSC of the system and rated power of the WPP is called Short Circuit Ratio (SCR) and indicates the amount of power that can be accepted by the power system

without affecting PQ at the PCC [14]. Another important factor to characterise the distribution system is the system short circuit impedance angle ratio, called the X/R ratio. The X/R ratio, a means of expressing the Power Factor (PF) of the source system, is simply the ratio of the system reactance to the system resistance, and can be calculated at any point looking back to the power source [11]. It is important because it affects the operation of a power system network [41].

This chapter presents a detailed review of the literature with regard to the interconnection of the WPPs to the distribution systems by outlining the existing knowledge as well as the problems and challenges being encountered. It also provides an overview of mathematical formulations between V_{PCC} and most important parameters of distribution networks, i.e. SCR and X/R ratios. Finally, it focuses on knowledge gaps yet to be addressed and possible future work in this field of Power/Electrical Engineering.

2.2 Wind energy systems and interconnection into distribution systems

The increase in wind power penetration in power systems necessitates methods and schemes to control WPPs similar to the way that conventional power plants are controlled [47]. This signifies that the interconnection of WPPs to power grids have to satisfy grid code requirements. This section investigates challenges concerned with voltage stability in WPPs according to the acceptable voltage ranges defined by Australian grid code.

2.2.1 Power quality standards - Voltage:

Interconnection of the WPPs to distribution networks must ensure that V_{PCC} is maintained within the allowable steady-state voltage range defined in the grid codes. Referring to grid code requirements with regards to voltage control in various countries

such as UK, Australia, and Canada [48, 49], the acceptable steady-state voltage range at the PCC of a power system connected to rotating electrical machines, specifically WTGs, is between 95% and 105% of network rated voltage ($0.95 \text{ p.u.} \leq V_{\text{PCC}} \leq 1.05 \text{ p.u.}$).

Apart from V_{PCC} profile, the magnitude of V_{PCC} fluctuation is another important criterion has to be considered in the interconnection of WPPs to distribution systems. This signifies that the step voltage variation as response to the change, either increase or decrease, of wind power injection must be maintained within acceptable levels defined by the grid code. Table 2.1 includes a list of recommended limits for step voltage changes at a given PCC point regarding the grid voltage level [50, 51]. In Table 2.1, medium voltage refers to $V < 44 \text{ kV}$ and high voltage refers to $V > 44 \text{ kV}$.

Table 2.1 Indicative planning levels for step- V_{PCC} changes as a function of the number of such changes per hour [50, 51].

Number of Changes per hour (n)	Step voltage variations (%)	
	High Voltage (HV)	Medium Voltage
$n < 1$	4	3
$1 < n \leq 10$	3	2.5
$10 < n \leq 100$	2	1.5
$100 < n < 1000$	1.25	1

Distribution networks are classified as MV networks. As shown in Table 2.1, the step- V_{PCC} variation in MV networks should normally be maintained around 3%. According to the grid code requirements in regards to voltage control, it is concluded that at the point of common coupling, and under normal operating conditions, voltage profile must be maintained between 0.95 p.u. and 1.05 p.u. and a voltage fluctuation will generally not exceed 3 %, although fluctuations of up to 4% may occur.

2.2.2 Voltage stability challenges in WPPs

The continuous increase in wind power penetration is likely to influence the operation of distribution networks, especially in terms of voltage stability [52, 53]. Figure 2.1 shows a simple single line diagram of a WPP connected to a distribution network [54]. According to Figure 2.1, each Wind Turbine Generator (WTG) has a transformer to increase the WPP voltage to the level of the distribution system voltage. WTGs are connected to the distribution system through one of the network buses, called PCC bus. Reactive power compensators are often used at the PCC to regulate the voltage and maintain it within the normal operation range. From Figure 2.1, the distribution line is modelled using its reactance (X) and resistance (R) values, and the line capacitance is usually ignored.

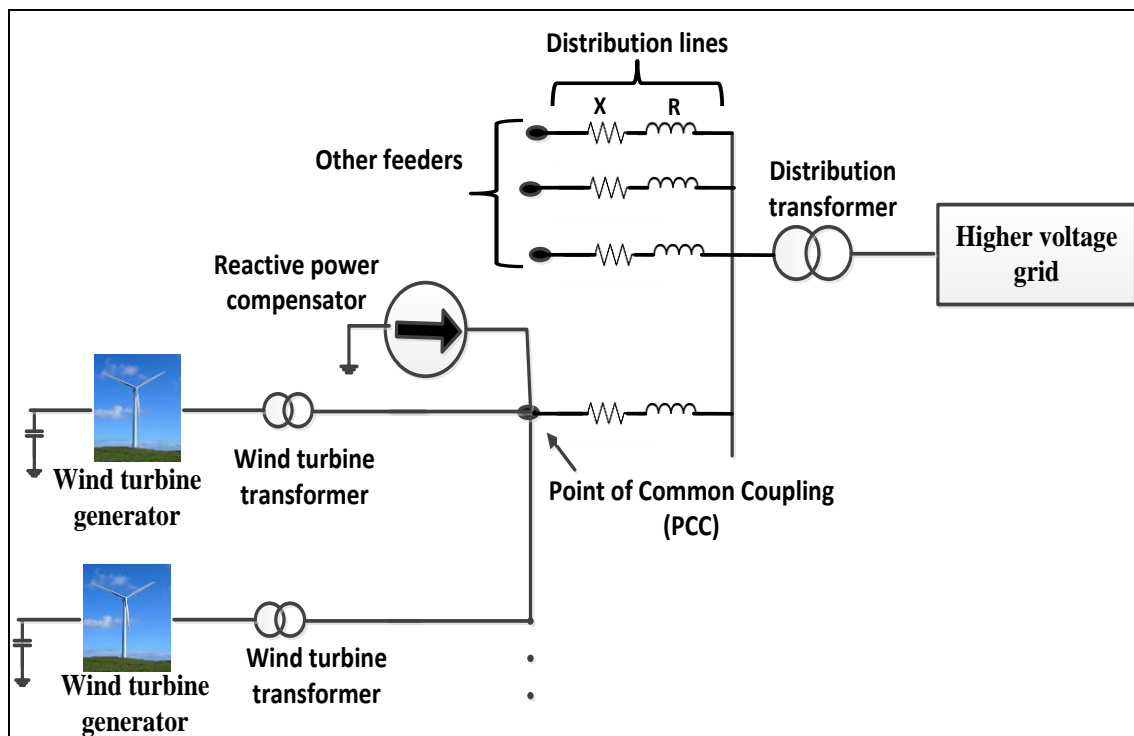


Figure 2.1 Single line diagram of a distribution system connected WPP [54].

Using the Thévenin theorem, from the perspective of a specific point on the distribution system, the whole system can be modelled as a Thévenin voltage source

connected in series with a Thévenin equivalent impedance. Figure 2.2 shows the Thévenin equivalent circuit of the distribution system as seen from PCC [11].

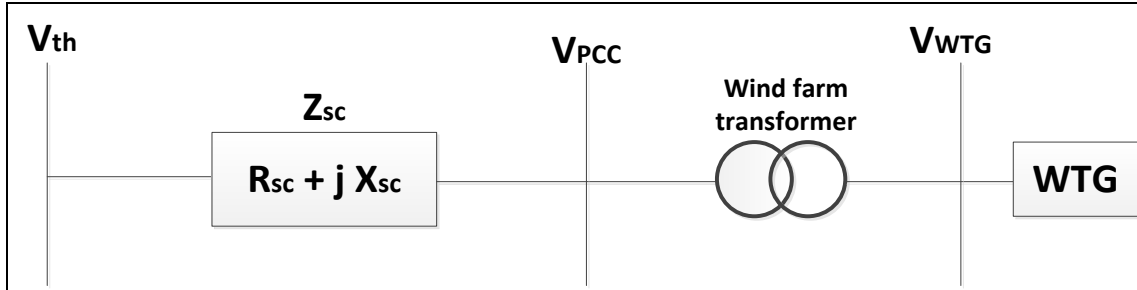


Figure 2.2 Thévenin equivalent circuit of distribution system [11].

In Figure 2.2, Thévenin voltage source (V_{th}) equals the open circuit voltage seen from the PCC. Furthermore, all the components between PCC and the distribution substation can be modelled using an equivalent Thevenin impedance, so called the grid short circuit impedance (Z_{sc}). Thévenin theorem signifies that the system short circuit impedance is the ratio between the Thévenin voltage source (V_{th}) and three phase short circuit current (I_{sc}) at the given point.

As discussed, the system short circuit impedance angle ratio, namely the X/R ratio, is one of the most important characteristics of the system [55]. Existing technologies used for voltage regulation through reactive power control are mainly based on the reactance of the distribution impedances and the resistance is ignored. Hence, these approaches are most appropriate for transmission systems where the value of the line reactance is greater than the line resistance resulting in a high system X/R value [32]. However, in distribution systems, the line reactance is low resulting in a low X/R ratio. This often hinders the feasibility of common reactive power compensation schemes and other, unconventional, ways of voltage control may need to be used [26].

Another important factor to characterise the power system is the SCC [10, 11, 55, 56]. The SCC of a distribution system can be calculated from Eq. (2.1) [57]:

$$SSC = \frac{3}{2} \times V_{rated} \times I_{sc} = \frac{3}{2} \times \frac{(V_{rated})^2}{Z_{sc}} \quad (2.1)$$

Where V_{rated} is the rated voltage of the system, which is normally 1 p.u.

The SCR is the ratio of the grid short circuit power level to the WPP MVA rating as shown in Eq. (2.2):

$$SCR = \frac{\text{Grid Short Circuit Power Level}}{\text{Rated Wind Farm MVA}} = \frac{SSC}{P_{rated}} \quad (2.2)$$

Generally, systems with an SCR greater than 20 are rated as stiff systems where grid code requirements are met [11].

Referring to Eq. (2.2), the value of SCC at a given point mainly depends on the rated voltage and the inverse of the absolute value of the equivalent impedance seen at this point [8]. Considering that sites with good wind conditions are generally located far from the substation, WPPs are usually connected to grids through long lines making Z_{sc} seen at the PCC large [54], which results in a small SCC at the PCC. Referring to Eq. (2.2), a low SCR value is therefore common in WPPs due to the high grid impedance and low SCC. This leads to PQ concerns such as poor voltage regulation, voltage dips and voltage swells depending on the network strength, connected generation capacity, type of the generator, and etc [52].

2.3 Voltage regulation in the WPPs

Existing technologies used for voltage control are based on reactive power compensation. The cost of voltage control through reactive power compensation is one of the most important challenges hindering the penetration of WPPs regardless of the generator types used in WPPs or the type of the reactive compensation approach (static

or dynamic) [58]. This problem is more critical in the small WPPs connected to the distribution system, where investors try to save costs as much as possible.

Another disadvantage of voltage regulation through reactive power compensation is that it decreases system reliability [53]. Generally, a system controller coupled with the generators controls real and reactive power generated by individual generators based on the thermal capability and/or voltage limits of the individual generators. WTGs interpret received commands and excite their generators to produce the reference reactive power. Real and reactive power commands are received by the system controller from a utility grid operator [59]. Considering that the WPP is usually at the terminal of grid, communication between the grid operator and control system for exchanging the commands is a big challenge and adversely impacts on the voltage stability margin [53].

As discussed above, voltage regulation approaches through reactive power control suffer from economic and technical problems. Therefore, investigation of the factors that impact on the voltage stability is critical in the interconnection of WPPs to distribution networks. One of the important factors that affect the V_{PCC} of the WPPs is the type of the generator connected to the wind turbine. The following sub-sections review the effect of WTG type on voltage stability.

2.3.1 Effect of generator type on voltage

There are various WTG designs, classified by machine type and control speed capabilities, which can be used in WPPs. Modern WPPs utilize machines that are designed to harvest the highest energy from wind. However, older types of WTGs have widely been installed and are expected to continue to operate for the remainder of their economic life [60]. This section investigates four common types of generators used in

the WPPs. The advantages and disadvantages of each type are discussed in terms of the capability of the generator in voltage regulation, cost, and etc.

2.3.1.1 Types 1 and 2

The use of Induction Generators (IGs) connected directly to the distribution network is one of the simplest approaches of running a WPP. In this case, WTGs are categorised into two types. Type 1 is fixed-speed wind turbine based on Squirrel Cage Induction Generator (SCIG). This type of WTGs can run within a speed range which is very close to the synchronous speed. Hence, it is required that the turbine blades rotate at a nearly constant speed.

The second type of IG-Based wind turbines are semi variable-speed wind turbine based on wound rotor IG. In this construction, a thyristor-controlled variable resistance is connected to the rotor windings. Taking the advantage of thyristor-controlled variable resistance, the generator operating point can be adjusted up to 10% greater than the synchronous speed. Type 2 wind turbine generators are generally preferred to Type 1. However, in both constructions, the generators cannot control reactive power and require reactive power support for magnetization [61].

Despite the incapability of IGs in reactive power control and voltage regulation, there are numerous installations of WPPs based on IGs throughout the world. The main advantages of IG are: simple construction, low cost, maintenance and operational simplicity, self-protection against overload and faults, etc. [62]. There are many SCIG based fixed speed WPPs operating across USA, India, and Canada with significantly high installed capacities [62]. A large number of WPPs in the National Energy Market (NEM) in Australia are based on IGs, especially Type 2. According to Australian Energy Market Operator (AEMO) report in 2013, 1160 MW or 45% of the WPP

installations in Australia are based on Types 1 or 2 [60]. Most of these installations are located in New South Wales (NSW), South Australia (SA), Tasmania (TAS), and Victoria (VIC). Few of these installations have been listed in Table 2.2 including the name of the WPP installation, region, overall size, manufacturer name, generator type and model [60].

Table 2.2 Summary of NEM installations based on Type 1 and Type2 WTGs [60].

Name	Region	Capacity (MW)	Factory	Model	Type
Blayney Wind Farm	NSW	9.9	Vestas	V47	2
Lake Bonney Stage 1 wind farm	SA	80.5	Vestas	V66	2
Woolnorth Wind Farm Stages 1 and 2	TAS	54	Vestas	V66	2
Toora Wind Farm	VIC	21	Vestas	V66	2
Starfish Hill Wind Farm	SA	34.5	NEG Micon	NM64	1
Challicum Hills	VIC	52.5	NEG Micon	NM64	1

As mentioned, IGs cannot supply reactive power. Therefore, the required reactive power is drawn from an external source such as grid. The absorption of reactive power from the grid reduces the voltage at the system buses. If the reactive power absorption reduces the voltage below the supply range, then another reactive power source would be required to compensate for the lack of reactive power and regulate the voltage. In this the use of case, fixed capacitor banks is the simplest method for reactive power control in IGs. However, the use of IGs with fixed capacitor banks increases the risk of self-excitation during off grid operation [63].

Apart from capacitor banks, Flexible Alternating Current Transmission System (FACTS) devices are also used to improve the voltage regulation process. Static Var Compensator (SVC) and Static Synchronous Compensators (STATCOMs) are the most common types of FACTS devices used in the power system. However, the main disadvantage of the former is that SVC provides reactive current proportional to the voltage. This means that reactive power supply is decreased at low voltages [64]. The

poor operation of SVCs and fixed capacitor banks is more critical when the Wind Energy Converters (WECs) do not have the Under-voltage Ride Through capability.

To overcome the problems caused by SVC, Static Synchronous Compensators (STATCOMs) have been applied in most of the WPPs. The works discussed in [65-67] proposed a reactive power control scheme based on STATCOM and Battery Energy Storage System (BESS) in a grid connected wind power system. The BESS is used as an energy storage source to control voltage. The shunt connected STATCOM with battery energy storage is connected with the interface of IG and load at the PCC in the grid system. The BESS naturally maintains DC capacitor voltage constant and sustains the real power source under fluctuating wind power. However, high costs for electrical infrastructure and additional energy storage system and the costs for STATCOM maintenance are the disadvantages of these approaches [58]. These costs could be saved using WEC with "STATCOM inside" capability [68, 69]. With this technology, the grid operator has the opportunity to constantly dispatch the reactive power of wind power plants. This type of STATCOMs also provides dynamic reactive power supply in the event of faults with transient over- and under-voltages, as well as voltage vector jumps at the WEC terminals. However, additional costs for control unit and communication link are still required [58].

2.3.1.2 Types 3 and 4

Apart from IGs, Double-Fed Induction Generator (DFIG) is another common type (Type 3) of generator used in wind power systems. The main advantage of DFIG is that this type of generators have the capability of controlling the reactive power and the reactive power demand is not sensitive to terminal voltage variations [70]. An additional advantage associated with type 3 turbines is that the grid is not significantly impacted

by variations in the prime mover, which results in a reduction in flicker levels. These turbines however require higher maintenance when compared to SQIG machines. This is due to the connection arrangements between the rotor and converter which consists of brushes and slip rings. Grid performance capability is not affected with these turbines. Due to the current trend of turbine installations across the NEM, which shows an increasing popularity for the use of Type 3 machines, it is expected that by 2020 these machines will constitute a high percentage of new installations across the NEM [60].

Generators based on Full Converter (FC) are the new generation of WTGs (Type4), in which all power extracted from the wind is managed and transferred to utility grid by a power electronics converter. Enercon and Siemens introduced the concept of FSC for Wind Turbine Systems. In this case, ABB has delivered nearly 10,000 SQIGs for FC application to leading wind turbine manufacturers since 2003. This structure is a suitable alternative to high speed Permanent Magnetic (PM) generators as SQIGs offer robust conventional technology with good efficiency and small size [71]. However, the costs for employing a full scale power electronics converter make Type 4 more expensive than Types 1 and 2 [72]. Currently, Type 4 WTGs are mainly used in large-scale WPPs and off-shore wind turbines [72].

Therefore, the cost for the voltage control through reactive power compensation is a big challenge in penetrating WPPs [10, 58, 73]. This is more problematic in the weak feeders where the high impedance seen from causes many PQ concerns [52, 54]. Therefore, a better design of the WPP plays a pivotal role in decreasing the PQ concerns and the need to voltage regulation through reactive power compensation. This increases the reliability of the systems and saves many costs.

2.4 Interconnection Site Selection

It is clear that wind resources assessment, i.e. determining the annual energy production and thus the revenue, is the preliminary step of the WPP planning process. Consequently, safe and economical grid interconnection is another issue that is being discussed upon planning the initial development of the WPP. In this respect, site selection for connecting the WPPs to the distribution network is an important phase in the design and planning process.

Effect of DG placement on the voltage variation and power losses has been widely investigated in the literature [40, 41, 43, 45, 74, 75]. DG allocation techniques proposed in the literature can be divided into two groups: analytical approaches and AI approaches. However, few other solutions such as mathematical approach have been proposed in the literature. These approaches are discussed in the following sub-sections.

2.4.1 Analytical approaches

In analytical approaches, an objective function is formulated in order to find the best site for the connection of a DG to the grid. Then, the objective function is optimised in order to ensure lowest active power losses and/or maintain V_{PCC} variation [38].

Gozel and Hocaoglu proposed an analytical methodology for the optimal allocation of DGs in distribution systems [43]. The main idea was to minimise active power losses. The authors carried out sensitivity analysis based on the equivalent current injection. Most analytical approaches are based on the exact power loss formula [17]. An exact formula-based solution for real power loss allocation was proposed in [18, 76-78]. Khan and Choudhary developed a similar method for optimal DG allocation in order to reduce the power losses and improve V_{PCC} stability [75]. However,

these approaches are based on the inverse of bus admittance matrix ($Y\text{-bus}^{-1}$), or Jacobean matrix. The calculation of the inverse of the Jacobean and $Y\text{-bus}$ matrices is not a serious concern thanks to various algorithm proposed for computing matrix inversion [79, 80]. The proposed algorithms avoid the need for large storage space in the digital computer and save computational time in off-line analysis. However, the efficiency of the proposed algorithms is adversely impacted in real-time applications and/or systems with a large number of buses [17]. More importantly, the assumptions used for the simplifications of the calculation of these matrices are often not valid in distribution systems [23]. This makes it difficult and time consuming to form the $Y\text{-bus}$ and Jacobean matrices for distribution networks. In particular, the inverse of $Y\text{-bus}$ method is not applicable to distribution systems consisting of overhead lines as the shunt admittance of these kinds of lines is ignorable resulting in singular $Y\text{-bus}$ matrix [38, 81]. The analytical approaches reviewed in this section explored technical network related optimal placement. Few papers addressed the application of DG placement approaches considering practical issues, such as the wind resource, distance to transmission and distribution lines, and etc [82, 83].

2.4.2 Artificial intelligence approaches

Artificial Intelligence (AI) approaches are heuristic techniques exhibited by computers. These techniques are used in complex optimization problems in order to optimise an objective function. The AI methods enable computers to mimic cognitive functions peculiar to human mind such as learning and problem solving [84].

DG optimal siting using IA based approaches has widely been investigated in the literature. For example, researchers from University Politehnica of Bucharest-Romania applied a GA-Based method to select the best site for the interconnection of DG to an

IEEE 69-bus distribution test system. The aim of DG siting was to improve voltage profile after the connection of DG to the distribution system. It was demonstrated that GA can provide better results compared with analytical approaches such as nonlinear optimization method when the number of DGs is high. However, for small number of DG units, the results acquired by both methods had similar accuracy. In fact, the nonlinear optimization method cannot cope with the complexity of the system as the number of DG increases, whereas in GA-Based method, there is no need for computational derivatives. However, the accuracy of GA depends on properly coding a fitness function and determining specific parameters to use [85]. The improper tuning of the parameters may increase the computational effort and adversely impact the accuracy of results [38].

Apart from GA, other IA-Based solutions such as Artificial Bee Colony (ABC) [20], Particle Swarm Optimisation (PSO) [21], evolution programming [22], GA and Tabu Search (GA-TS) [86] have been used in the literature in order to select the optimal place for the DG connection ensuring the lowest PQ concerns. However, a mathematical or simulation model of the test distribution systems is required before using these methods. Considering the size and complexity of distribution networks, modelling and simulation of these systems takes a long time [17].

Apart from time consuming computational tasks, analytical and AI-Based methods consider the DG types which can inject only active power to the system while the value of the injected or absorbed reactive power is assumed to be zero [17]. However, this assumption is not applicable to WTGs. As discussed, Types 1 and 2 draw reactive power from the grid, and only Types 3 and 4 can supply reactive power to the distribution system. Therefore, the value of the reactive power absorption or injection is

not zero. These issues indicate that the optimal placement of WPPs using suitable techniques needs further research and study.

2.4.3 Mathematical formulation for selecting the best PCC location

As an appropriate solution for allocating WPPs into the distribution networks, Golieva in [46] proposed a mathematical relation between V_{PCC} and the SCR ratio. The work was supported by the Siemens Wind Power Company. The author carried out a sensitivity analysis to find a numerical relation between V_{PCC} and SCR in an invented 4-bus test distribution system. Then, a best curve fit equation was identified for the V_{PCC} -SCR data points. It was demonstrated that the relation between V_{PCC} and SCR can be expressed through a polynomial function with an order two as in (2.3) [46]:

$$V_{PCC} = V_0 \times (0.0067 \times SCR^2 - 0.063 \times SCR + 1.1142) \quad (2.3)$$

Where V_0 is the voltage profile at the PCC before WPP connection.

The work by Golieva [46] is one of the most valuable preliminary works discussing mathematical formulation of any formula to express the relationships between V_{PCC} and SCR for the steady-state operation of the WPPs. As claimed by the author, taking advantage of this relation, the voltage profile can easily be predicted using the SCR value at each distribution feeder. This is a great achievement as it would allow WPP planning engineers select the best site for the interconnection of a WPP without the need to carry out complex and time consuming computational tasks and modelling test systems.

As mentioned earlier, In [46], the author proposed a polynomial equation with an order of two to model the relation between V_{PCC} and SCR. However, the author did not consider the results for other possible mathematical functions such as exponential or

logarithmic functions. Therefore, the work lacks the analysis of different possible functions which can be used for modelling the relation between V_{PCC} and SCR. The author also did not consider all the necessary steps for validating the proposed equation. For example, the analysis was carried out based on an invented test system with $0 \leq SCR \leq 2.5$. Referring to an AEMO documentation [87], an $SCR < 2$ adversely impacts the voltage stability in the steady-state operation and may lead to generator tripping. Therefore, an $SCR < 2$ should be avoided in WPPs [87]. This indicates that the results presented in [46] have low accuracy in real distribution systems. The most important drawback of the relation proposed in [46] is that it also did not consider the relation between V_{PCC} and the X/R ratio. As mentioned earlier, in distribution systems, the voltage regulation requirements highly depend on the X/R ratio at the PCC (X/R_{PCC}). Therefore, a lack of consideration of the relation between V_{PCC} and X/R ratio adversely impacts the accuracy and validation of (2.3).

Authors in [88] proposed an analytical approach to simplify the estimation of the maximum permissible active power that can be injected by an IG without voltage collapse. Analysis studies were carried out based on a small WPP with the total capacity of 20 MVA consists of twenty 1-MVA squirrel-cage induction generators. However, the work did not explore about the effect of SCC and X/R ratio on the voltage stability. Furthermore, the proposed formulation cannot be used for calculating other important voltage stability criteria, eg. voltage profile and voltage variation in response to changes in IG penetration. Furthermore, the work only dealt with IG systems but lacks an investigation on the permissible active power in a DFIG based systems.

Sifting the literature, it is clear that a holistic relation between V_{PCC} and the key parameters of the distribution systems, i.e. SCR and X/R ratio, is still a noticeable gap.

Obviously, investigating the effect of SCR and X/R on V_{PCC} is the mainstay of developing such a holistic relation. The next two sections review the significance of SCR and X/R ratios in distribution systems and their effects on V_{PCC} .

2.5 Significance of the Short Circuit Ratio

The grid ‘strength’ at the PCC is numerically expressed as the SCR value or parameter [54]. Generally, if the SCR is smaller than 10, then the grid is considered as weak [8, 9, 89]. As mentioned, an $SCR < 2$ should be avoided in WPPs [87]. Hence, in weak WPPs, the range of SCR is usually between 2 and 10. In this SCR range, WPP connections impose the following issues:

- Low thermal limit of cables
- High voltage variations due to the injection of wind power
- High impact of flicker and harmonic emissions

These issues are more serious as SCR gets closer to 2. As mentioned earlier, sites with good wind conditions are usually located far from the distribution substation. Therefore, long distribution lines, high grid impedance, and low SSC values are common in WPPs [9]. Consequently, large amounts of wind penetration with limited SSC results in a low SCR, weakening the system strength [54]. SCR is therefore a key parameter in choosing the best site for the WPP connection [90].

2.5.1 Effect of SCR on voltage control

Most works in the literature dealt with the effect of SCR on transient stability of weak systems under a fault condition. Few proposed solutions, such as the one in [91] where it was proposed to increase SCR values by wind active power curtailment as a means of post-fault voltage recovery, especially for the weak grids. The reason for this

solution is the fact that there is a strong connection between the feeder voltage and the active power delivered to the feeder through the WPP [92]. However, the main aim in WPPs is to harvest as much active power from the WPP as possible. Therefore, active power curtailment is against with the primary purpose of WPPs making the proposed solution far from ideal.

In most modern WPPs, voltage regulation is carried out through a Power Plant Controller (PPC). During the steady-state operation, PPC sends the reference active and reactive power values to WTGs in order to ensure a bus voltage within the $0.95 \text{ p.u.} < V_{\text{PCC}} < 1.05 \text{ p.u.}$ range [59]. Normally, a PI controller or droop controllers are used in the control loop within the PPC [54]. However, exchanging data between the WPP voltage/reactive power controller and the WTG controller causes time delays. The slow operation of the PPC imposes a coordination problem between PPC and WTG during and after fault condition. In post-fault condition, WTGs receive wrong reactive power references from PPC making voltage stability issues such as over-voltage or large voltage oscillation.

A fast voltage controller was proposed in [54] in order to control the voltage under the disturbance of sudden grid SCR change in a weak distribution test feeder. The proposed scheme was based on the PPC concept. The main idea was to provide a coordinated control by integrating slow PPC voltage/reactive power controller with fast WTG voltage controller [54]. It was presented that the proposed scheme can satisfy the grid code requirements at the PCC of the test grid connected WPP during and after the fault condition.

The proposed strategy in [54] could enable a WPP to be controlled as an integral generation unit to regulate voltage based on grid code requirements. Meanwhile, it

decreases the need for any other reactive power compensator such as STATCOM. However, the proposed method suffers from problems concerned with the reliability of a communication-based approach [53]. Furthermore, the distribution system is vulnerable to a shunt frequency resonance between the proposed controller and grid impedance when the voltage controller bandwidth is large and the grid SCR is small.

The effect of the SCR on the transient stability, Low Voltage Ride Through (LVRT), and WPP oscillations was investigated in [93]. The test system was based on DFIG (Type 3) and FC (Type 4) WTGs connected to a very weak 138 kV transmission feeder with an SCR < 2. However, this range of SCR rarely occurs in transmission feeders in the real world. Furthermore, FC is typical for all power electronic appliances and has limited SCC [46]. On the other hand, recovering voltage through increasing the reactive power requires higher current injection. This is a big issue in weak transmission networks, where dV/dQ sensitivity is particularly high as a small amount of reactive power compensation would lead to a large voltage variation [94]. The results presented in [93] did not consider distribution networks. More importantly, the study investigated generator dynamic performance, which is not expressively relevant for the WPP planning process.

2.5.2 Worldwide projects

Various research projects are being conducted to investigate the effect of wind power injection and SCR on weak grids. Majority of these studies focused on specific cases. For example, E. Muljadi and et al in [95] compared the performance of a DFIG-Based WPP with a DG unit based on conventional generator. The study was conducted on a specific portion of the Western Electricity Coordinating Council (WECC) system, the largest and most diverse of the eight Regional Entities with delegated authority from

the North American Electric Reliability Corporation (NERC) and Federal Energy Regulatory Commission (FERC). The selected area was electrically far from main generation units and was weakly connected to the bulk network. It was demonstrated that the WPP could provide a better damping performance compared with the conventional generator due to the LVRT ability in DFIG. It was shown that DFIG can improve the stability of the system. However, E. Muljadi and et al in [95] did not discuss about the problems caused by connecting WPP to the network.

A similar study was carried out in [96] where the authors carried out dynamic simulations to compare the voltage disturbance response of a DFIG-Based WPP versus a conventional synchronous generator and present relevant control design. However, the model used was developed specifically for the General Electric (GE) 1.5 and 3.6 MW WTGs and is not intended to be used as a general purpose WTG. The results were based on a constant SCR value and did not consider different values of SCR. Furthermore, only dynamic simulations were presented to analyse the transient stability problem during a fault condition. However the steady-state voltage stability which is the main issue in safe interconnection of WPP to distribution feeder was not addressed.

Researchers from ERCOT investigated the dynamic and steady-state voltage stability considering the SCR value [94]. Reference [94] is one of the few works in the literature discussing the voltage stability in the steady-state operation of a WPP in order to show SCR's role in the planning and design of a WPP. The project was supported by the Public Utility Commission of Texas. The case study was in the Panhandle area, which is a remote area from the generation center, and consists of many WPPs and SVCs making this area an extremely weak grid. PV analysis was carried out to investigate the voltage variation in response to an increase in wind power generation

under no contingency event. A significant observation was that the voltage collapse occurred at a relatively high voltage range where all bus voltages were higher than 0.96 p.u. at the nose point of the PV curve. Indeed, it was shown that a very high penetration of wind power can lead to voltage collapse even if the voltage remained in the normal operation range, i.e. $0.95 \text{ p.u.} < V_{\text{PCC}} < 1.05 \text{ p.u.}$

In the case of dynamic voltage stability, three reactive power compensation schemes were tested in [94]. The three schemes were proposed as possible solutions to enhance the SCR level in the case of a fault. These include the SVC, Synchronous Condenser (SC), and Variable Frequency Transfer (VFT) solutions. The case study considered two types of faults, including: overvoltage cascading and voltage oscillation. It was shown that SVC has not the capability of decreasing the equivalent system impedance. Hence, although SVCs are a common remedy for VRT and voltage stability issues, it cannot improve system strength and increase the SCR value. VFT is a new technology compared with SVC. VFTs can be controlled in a bidirectional way to transfer active and reactive power between asynchronous networks [97]. Reactive power flow through VFT is determined by the rotary transformer series impedance and the difference in voltage value on the primary and secondary windings [98]. However, in [94], it was demonstrated that SC installation is a better solution compared with VFT and SVC because SCs could effectively increase SCR value in weak test feeders. However, SCs has slow response times compared with SVCs.

S.H. Huang, and et al [99] presented extensive study of the voltage stability issues occurring when a large WPP is connected to a weak grid. The grid model used represented a specific case of the ERCOT region grid in Texas. Voltage quality, thermal capability and WPP stability were the three main topics discussed in [100]. The test

model was based on the Norwegian power network when the connected WPP worked at its highest capacity. Hence, the value of SCR was constant and the work failed to discuss the impacts of different values of SCR and wind power generation on the three topics considered.

Referring to Sections 2.5.1 and 2.5.2, it is clear that most works in the literature proposed dynamic voltage control solutions to improve the transient voltage stability under fault conditions. However, the works in the literature lack investigation into the impact of SCR on steady-state voltage stability at a given point of a distribution system, which is a key factor in WPP siting studies. The proposed solutions suffer from serious problems such as over-voltage, and voltage oscillations due to fast uncoordinated reactive control [101]. On the other hand, most of the transient problems can be prevented by connecting WPPs to suitable feeders to ensure lowest PQ concerns after WPP connection.

2.6 Significance of the X/R ratio in distribution systems

The grid impedance angle, called the X/R ratio, is the ratio of the Thévenin equivalent reactance and Thévenin equivalent resistance seen from a given point on the distribution system (see Figure 2.2. for further details). X/R ratio is one of the most important characteristics of a distribution system as it has a profound impact on the system voltage stability [10].

Many works in the literature have dealt with the relation between the X/R ratio and V_{PCC} in the distribution system [9-12]. The majority of these works analysed the effect of X/R variation on the V_{PCC} and V_{PCC} variation under a constant SCR value. Although the X/R ratio cannot be dynamically changed in a power system, investigating

the voltage variation in response to the change in X/R is the principal step for finding how X/R impacts the V_{PCC} .

As mentioned earlier, existing technologies used for voltage regulation through reactive power control are mainly based on large X/R ratios. However, the low X/R ratio in distribution networks often hinders the feasibility of common reactive power compensation schemes. Therefore, the effect of the X/R ratio on the system voltage stability is of great importance from a design and operation prospective. This section reviews the significance of X/R ratio on voltage control in WPPs. Consequently, the effect of X/R on V_{PCC} , and X/R-Based voltage control solutions in distribution systems are discussed below.

2.6.1 X/R value

The design of power system lines and choice of the conductor types mainly depend on two factors, the current and power carrying capacity of the line and the maximum permissible voltage drop limit. The former is more important in the design of transmission networks as the current flowing through the lines is very high [102, 103]. In transmission systems, the distance between conductors is much greater than that in distribution systems [102, 104]. Therefore, the flux linkages between the conducting phases are greater and the external component of the line inductance is noticeably high. For this reason, the inductive reactance of a transmission line is three or more times greater than its resistance, diminishing the effect of the line resistance on the modular impedance and X/R value [12]. Therefore, the value of X/R in transmission systems is high.

In the case of distribution lines, the maximum permissible voltage drop limit is the priority as the value of the current is noticeably smaller than that in transmission lines,

and the current density is small [105]. It is obvious that the reactive component of the overall system X/R ratio is affected by the reactance of distribution lines. Figure 2.3 shows a simple model of a three phase line [106].

In Figure 2.3, q and r stand for the electric charge and radius of the conductor in each phase, respectively. Parameter D is the equivalent distance between phases, called the Geometric Mean Distance (GMD), and is calculated through Eq. (2.4) [107].

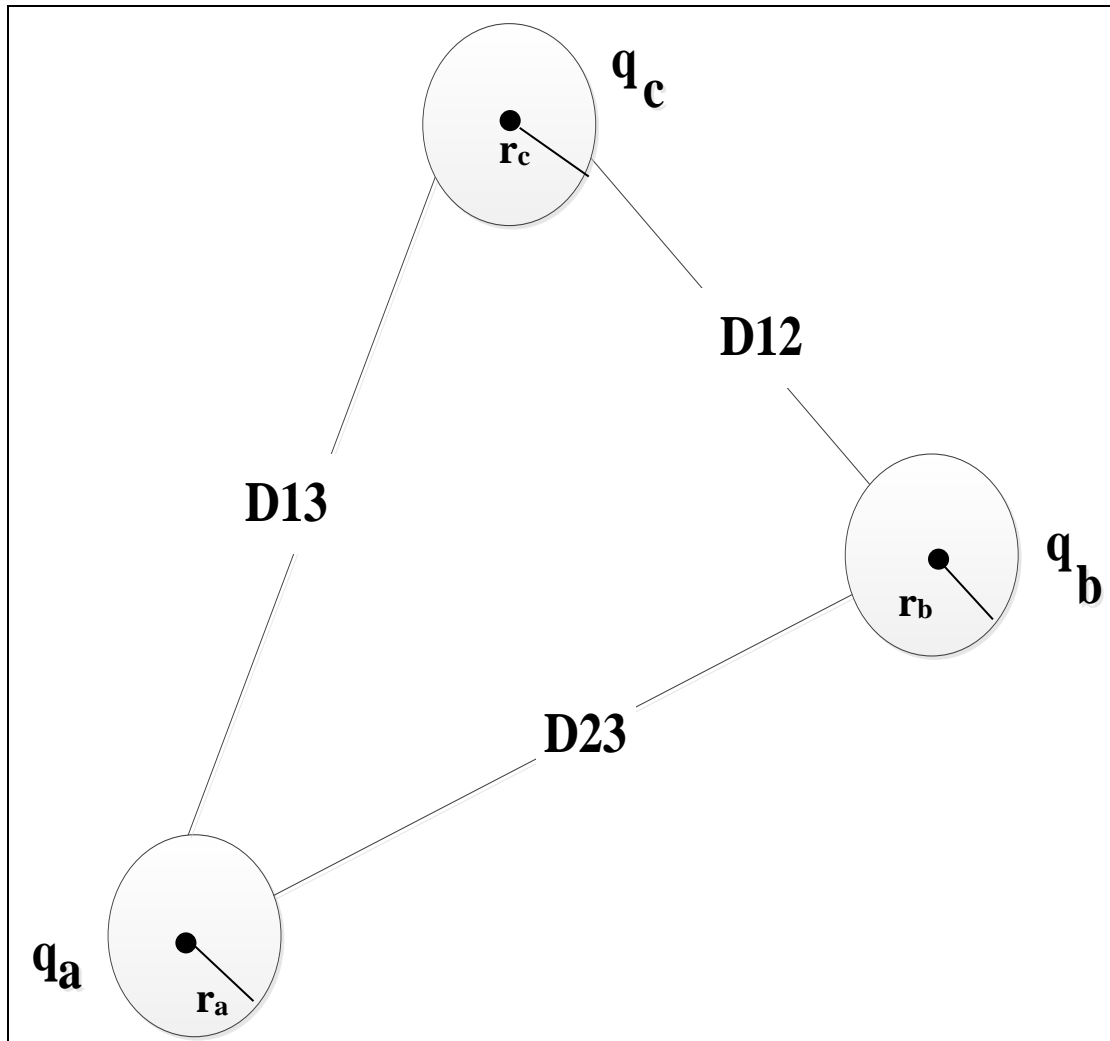


Figure 2.3 A three phase distribution line [106].

$$GMD = \sqrt[3]{D_{12} \times D_{23} \times D_{13}} \quad (2.4)$$

The reactance per meter of the line and the voltage in each phase can be formulated as follows [108]:

$$X_L = 2 \times 10^{-7} \times \ln\left(\frac{GMD}{GMR}\right) \quad (2.5)$$

$$V_p = \left(\frac{3q}{2\pi\epsilon_0}\right) \times \ln\left(\frac{GMD}{r}\right) \quad (2.6)$$

Where ϵ_0 is the permittivity of free space and equals with 8.85×10^{-12} (F/m) and V_p is the voltage in each phase of the conductor. GMR stands for Geometric Mean Radius of the conductor and is calculated from Eq. (2.7) [107, 109]:

$$GMR = r \times e^{-\frac{1}{4}} \quad (2.7)$$

From Eq. (2.5), it is clear that the line reactance depends on the GMD and GMR of the conductor. On the other hand, there is a direct relation between voltage and GMD, as shown in Eq. (2.6). Considering the fact that voltage in distribution systems is lower than in transmission networks, the value of GMD in distribution systems will be small. Referring back to Eq. (2.5), a small GMD value, in turn, leads to a small reactance value in distribution lines. Therefore, in distribution systems, the external inductance component is smaller and the reactance will be smaller. It can then be concluded that the overall X/R ratio in distribution lines is small when compared to transmission lines.

Generally, in overhead distribution lines, the value of X/R ratio is slightly greater than 1. Moreover, in cable lines, the X/R value is slightly smaller than 1 [13]. Referring to [10], the value of X/R can be divided into three ranges regarding the type of distribution line and the distance of the feeder to the distribution transformer. Table 2.3 discusses the need for voltage control through reactive power compensation in each range.

Table 2.3 Voltage control requirement and X/R values in distribution networks [10].

X/R value	distribution line	Feeder location	Voltage control
Greater than 1	Overhead line	Close to substation	rarely necessary
Nearly 1	Overhead line	The whole network	It might be necessary; however, it will be strongly limited.
	Under-ground cable	Close to substation	
Less than 1	Under-ground cable	Far from substation	It is difficult and often needed.

From Table 2.3, it can be observed that voltage control through reactive power injection is rarely needed at feeders based on overhead distribution lines located near the distribution transformer. In this case, the equivalent impedance seen from the feeder is small due to the small distance between the feeder and substation. This leads to a large SCC and strong feeder where the grid code requirements are usually met [13]. However, voltage control is required as X/R decreases.

As shown in Table 2.3, voltage control can be problematic when X/R is approximately 1. In under-ground distribution networks (based on under-ground cables), X/R will approximately equal 1 in feeders located close to the substation. For overhead distribution systems (based on overhead lines), this will be the case throughout the whole network [13].

The value of line reactance could be less than resistance ($X/R < 1$) if the feeder is located further from the substation and the network is based on under-ground cables. In this situation, the small changes in DG units' generation or load demands significantly impact on V_{PCC} . Hence, V_{PCC} cannot be maintained between the steady-state range, i.e. between 0.95p.u. and 1.05 p.u [13]. Therefore, voltage control is highly required. However, it is difficult to control V_{PCC} through reactive power compensation, as the value of line inductance is noticeably low [110] .

Next section deals with the effect of X/R ratio value on the voltage stability at distribution networks connected WPP.

2.6.2 Impact of X/R effect on voltage variations

In the steady-state operation, there is an inverse relation between V_{PCC} and X/R_{PCC} . The steady-state voltage tends to increase for small X/R_{PCC} ratios, while V_{PCC} decreases for large X/R_{PCC} ratios [9, 12]. Furthermore, the voltage drop due to an

increase in X/R_{PCC} is more serious in distribution systems with low SCR values (weak systems) compared with that in the distribution feeders with larger SCR values (stiff systems) [10, 56].

Although high X/R_{PCC} ratios lead to high V_{PCC} drops, small values of X/R_{PCC} adversely impact the step- V_{PCC} variations when V_{PCC} varies in response to an increase in wind power penetration.

The effect of variation of active load, reactive load and X/R ratio on a terminal voltage of a single line was investigated in [12]. It was concluded that high X/R ratio declines the maximum power transferred and adversely impacts voltage stability. However, the scenarios considered in this work were simple and only related to understanding the principal concepts on the effect of the X/R ratio on the terminal voltage of a single distribution line. Furthermore, the work lacks an investigation into the X/R ratio effect on voltage in a real distribution system or a system based on IEEE standard.

The effect of X/R_{PCC} on voltage variation versus wind power characteristic of a simple test distribution system was presented in [57] as shown in Figure 2.4. From Figure 2.4, it is clear that the voltage variation in response to an increase in wind active power is over 6% for the $X/R_{PCC} = 0.5$ case. However, the absolute value of ΔV_{PCC} was around 2% for high X/R_{PCC} ratios ($X/R_{PCC} = 5$). This signifies that the adverse impact of small X/R_{PCC} ratios on voltage variation is even more significant than the impact large X/R_{PCC} ratios have. Figure 2.4 shows that the lowest voltage variation happened when $X/R_{PCC} = 2$.

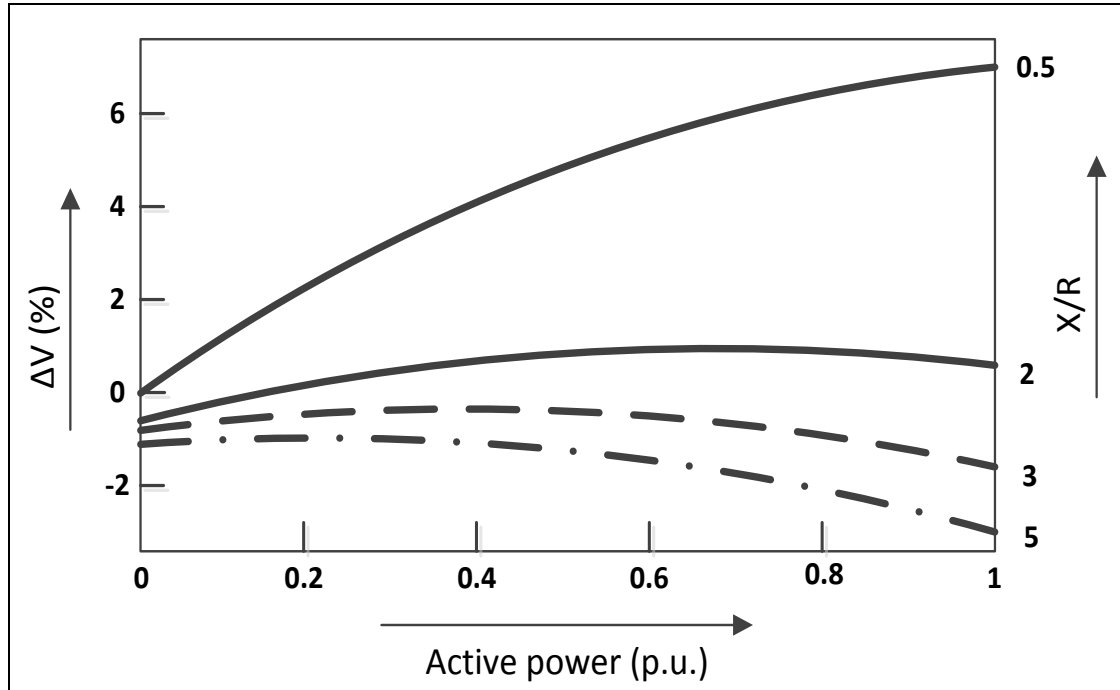


Figure 2.4 Step-voltage variations versus SCR for different X/R ratios [57].

R. Reginato, M. G. Zanchettin, and M. Tragueta carried out a similar study in [56], where the authors dealt with the effect of X/R_{PCC} and the inverse of SCR, so called the integration level (ρ), on three criteria: V_{PCC} variation, internal V_{PCC} angle, and WPP active power margin (P_{margin}). The study considered both fixed speed SQIG (Type 1) and variable speed DFIG wind turbines (Type 3). Six scenarios were considered when the system was operating under steady-state condition:

- SQ0 case: A SQIG without Power Factor (PF) compensation,
- SQN case: A SQIG without load PF compensation,
- SQF case: A SQIG with full load PF compensation,
- DFQ case: A DFIG with reactive power controller considering $Q_{ref} = 0$,
- DFP case: A DFIG with PF regulation considering $PF_{ref} = 0.95$ leading,
- DFV case: A DFIG with terminal voltage regulator considering $V_{terminal-ref} = 1pu$.

Figures 2.5 and 2.6 present the X/R- ρ characteristics for the scenarios considered when $0.95 \text{ p.u.} < V_{PCC} < 1.05 \text{ p.u.}$

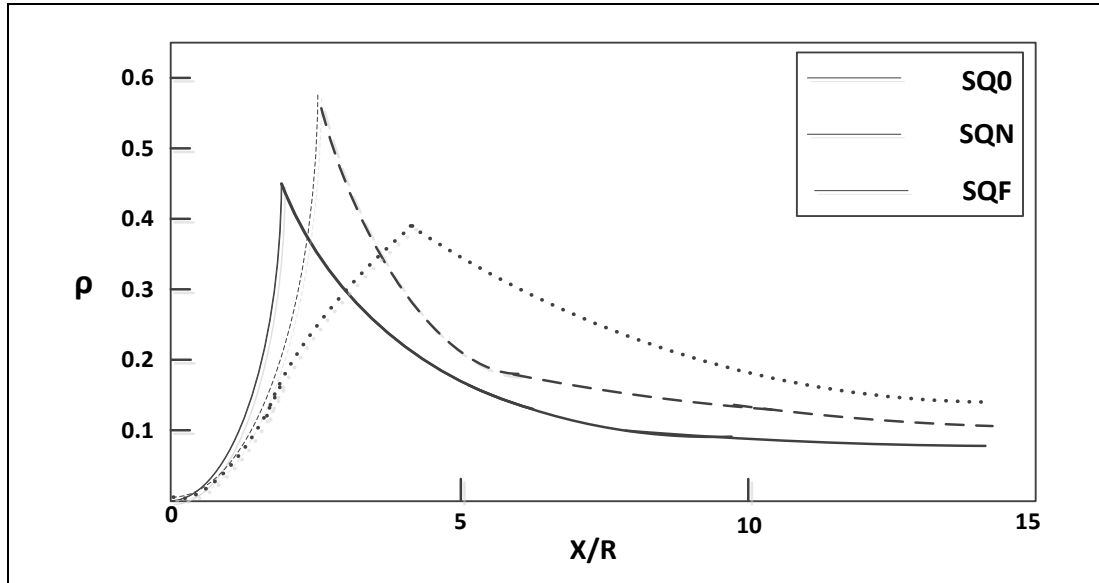


Figure 2.5 Limit of ρ and X/R for $0.95\text{p.u.} < V_{\text{PCC}} < 1.05\text{p.u.}$ in a SQIG-Based WPP [56].

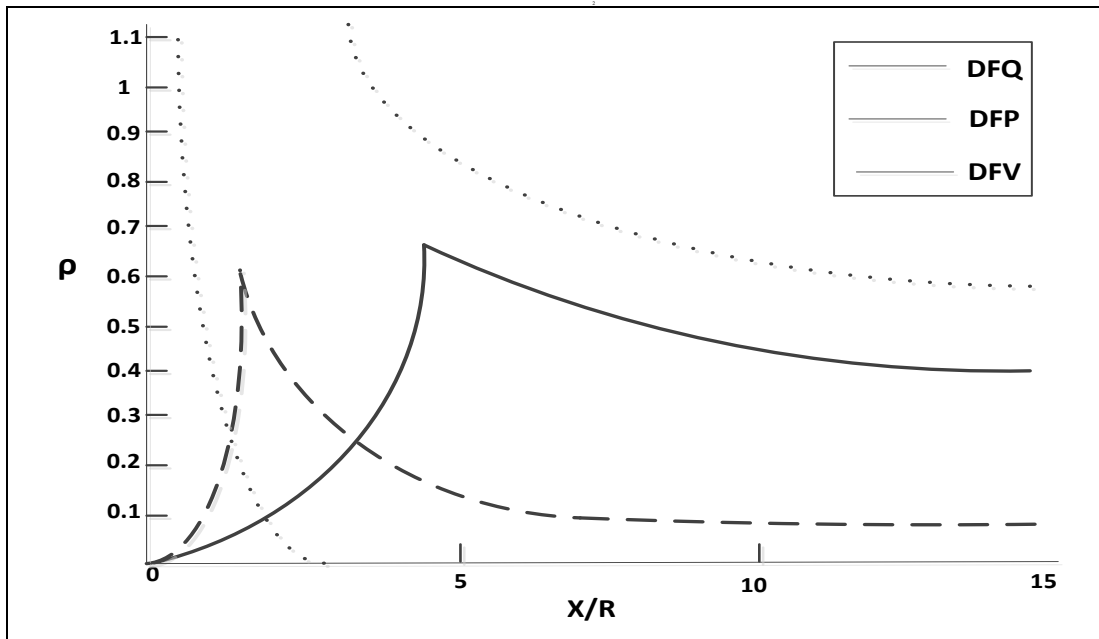


Figure 2.6 Limit of ρ and X/R for $0.95\text{p.u.} < V_{\text{PCC}} < 1.05\text{p.u.}$ in a DFIG-Based WPP [56].

From Figure 2.5, in SQIG-Based WPPs with $\text{SCR} < 10$ and without any reactive power compensation, the V_{PCC} can be maintained in the normal operation range if X/R_{PCC} is less than 5. Higher X/R_{PCC} values are attainable if $\rho < 0.1$ or $\text{SCR} > 10$. Figure 2.5 and Figure 2.6 show that ρ - X/R characteristic follows similar patterns for the two other scenarios considered for the SQIG-Based WPP and DFQ and DFP scenarios in DFIG-Based WPP.

In the case of DFIG-Based WPPs with voltage regulation set to 1 p.u., Figure 2.6 shows that the V_{PCC} increases to very high values when X/R_{PCC} is small. This necessitated the generator to absorb a large reactive power to reduce the over-voltage condition and maintain the terminal voltage within 0.95-1.05 p.u. Therefore, the generator could not comply with voltage regulation requirements when X/R_{PCC} was small. For large values of X/R_{PCC} , the generator had to inject reactive power to the feeder to increase the voltage and keep it within the normal range. In this case, the reactive power requirement demand is not beyond the generator capability and voltage requirements can be satisfied up to very large values of the wind power generation. Hence, one of the key conclusions in [56] was the fact that the DFIG has a poor efficiency in maintaining the voltage within the normal range in small X/R_{PCC} ratio, however, voltage can be maintained within the normal range for large X/R_{PCC} ratios even for a large penetration of wind power.

The authors in [56] investigated the effect of ρ and X/R_{PCC} on P_{margin} and internal V_{PCC} angle. It was demonstrated that ρ has to be high for low X/R_{PCC} ratios. Parameter ρ decreases and approaches a constant value as X/R_{PCC} increases in order to meet the P_{margin} and voltage angle requirements in all scenarios considered except the DFV. In the DFV scenario, the ρ - X/R characteristic had a different pattern where ρ decreased for small X/R_{PCC} ratios, and then increased and approached a constant value as X/R_{PCC} increased.

Reference [56] is another valuable work discussing the role of X/R_{PCC} and SCR in the safe interconnection of WPPs, but lacks proposing approaches to determine the best feeders for WPP connections where voltage variations in response to the change of wind power generation meet the grid code requirements. Relations between X/R_{PCC} , SCR,

and V_{PCC} were presented using graphs and curve characteristics; however, the work lacks formulated equations which model the mathematical relation between these three parameters. Furthermore, authors did not clarify the test system characteristics such as the grid voltage level, distribution transformer capacity, topology and construction of the system.

2.6.3 X/R-Based voltage control schemes

As previously discussed, the low X/R ratio in distribution networks often hinders the feasibility of common reactive power compensation schemes and other, unconventional, ways of voltage control may need to be used [13]. For example, Researchers from Delft University of Technology argued in [13] for the insertion of a controllable inductance in feeders as a potential solution to increase the X/R ratio in distribution systems to increase the feasibility of voltage control through reactive control schemes. The applied variable inductor circuit was based on the similar ideas used for designing the thyristor controlled reactor circuit [111] and the advanced series compensation approach proposed by [112]. The time of inserting the inductance in the circuit is adjusted through changing the firing angle of the thyristor switches. This influences the value of the line impedance and also the magnitude of the voltage drop across the device. However, the presented scheme suffers from serious shortcomings such as harmonics and frequency resonance between the proposed controller and grid impedance.

Currently, the voltage in distribution systems is mainly regulated by controllable and fixed tap changers on distribution transformers [13]. B. Neelakanteshwar et al. investigated the effect of wind power integration on tap changing of On Load Tap Changing (OLTC) transformer in a radial distribution network using voltage sensitivity

analysis [113]. The analysis was carried out for a different range of X/R ratio. It was demonstrated that the voltage sensitivity on the secondary side of the OLTC decreases with increase in tap for higher X/R ratio. For lower X/R ratios of the distribution line, voltage sensitivity was approximately same for all the taps. However, the change of tap ratios cannot ensure that the voltage will be maintained within the normal operation range [54].

In [114], the authors proposed a FC wind turbine based scheme to improve the transient voltage stability in a faulty condition. It was demonstrated that the FC WPP can contribute to a post-fault voltage support which is comparable to the support by a synchronous generator of the same capacity. However, for weak grids with small X/R values, this requires a coordinated control of active and reactive power instead of controlling voltage purely through reactive power compensation. Furthermore, it was developed that the angle current injected by the WPP during the fault must be opposite to the grid impedance angle, i.e. grid X/R ratio [114]. However, this strategy is not a specific solution for weak grids only, but rather a well-known approach to hinder LOS events in power systems [115].

The work discussed in [116] investigated the effect of X/R ratio on the voltage sag of a distribution line and its restoration using a Dynamic Voltage Restorer (DVR) after a single phase fault and double line to ground fault. DVR is a series connected custom power device which is more effective than other dynamic voltage control solutions based on FACTS devices, such as STATCOM and Unified Power Quality Conditioner (UPQC), for restoring voltage under fault conditions [111, 117-121]. The test system was based on two distribution lines supplying a total load of 50 kVA with the power factor of 0.8 lagging. It was concluded that the voltage sag and the time for restoration by

DVR does not change as X/R ratio changes. In the case of line to line fault, the voltage sag was significant but time of restoration changed slightly. However, similar to most of the works reviewed in this chapter, the authors investigated the effect of X/R ratio under a fault condition alone, but failed to investigate the significance of the grid impedance angle in safe WPPs interconnection when the system is in steady-state mode.

2.7 Conclusion

Global warming and ever increasing carbon emissions from fossil-fuel for power generation are fundamental concerns that the world is faced with today. Generating power from the wind will aid in the reduction of greenhouse gas emissions and in the conservation of natural resources for future generations. However, there are many technical challenges that hinder the large scale penetration of WPP into the power system networks. One of the biggest challenges is PQ concerns and the need to regulate voltage in WPP connected networks.

This chapter reviewed the current status of the research on the voltage regulation in process WPPs. Correspondingly, the knowledge gaps and potential research directions for future development in this field have been identified. The existing voltage regulation techniques are mainly based on reactive power compensation. Voltage control through reactive power compensation suffers from many issues such as a high cost, low reliability, shunt resonance, over-voltage, and voltage oscillation drawbacks. However, the need to regulate voltage through reactive power compensation scheme can be noticeably reduced if WPPs are appropriately integrated into network.

Optimal WPP sizing and siting is the mainstay of this process. Therefore, it is very important to develop novel technique to enable engineers and consultants,

responsible for the design and planning of distribution system connected WPPs, find the best WPP size and PCCs for the interconnection of WPPs in weak distribution systems.

The existing techniques applied for finding optimal size allocation of DG systems require computing large dimensional matrices and designing the simulation model of the test systems. Computationally, it is a very demanding and time consuming process. Sifting the literature, it was observed that there is a knowledge gaps regarding:

- **An analysing on the effect of X/R and SCR on the V_{PCC} during the steady-state operation using standard models:** Most work in the literature considered invented models or specific real cases as test systems. Therefore, the results cannot be generalised to a broad range of cases. The value of SCR in some works was less than 2. As mentioned, AEMO documentation indicates that an $SCR < 2$ adversely impacts the voltage stability in the steady-state operation and may lead to generator tripping [87]. Therefore, an $SCR < 2$ should be avoided in WPPs [87]. This indicates that the results presented in these works have low accuracy in real distribution systems.
- **A simple WPP sizing and allocation approach:** As discussed, the existing DG sizing and allocation methods suffer from time demanding calculations, modelling, and simulation issues. Therefore, a simple approach which does not require the mathematical or simulation model of distribution system is still a noticeable gap in the literature,
- **A holistic mathematical relation for WPP sizing and siting:** The problems concerned with existing DG placement and sizing methods can be removed using a holistic mathematical model between steady-state V_{PCC} and key parameters of distribution systems. However, only one reference [46], addressed

this issue by developing a mathematical relation between V_{PCC} and SCR. The work did not consider the necessary factors needed for validating the results, such as consideration of X/R as one of the parameters of the proposed equation or the realistic range of SCR ratio.

Identifying this research opportunity, author focused his research on these gaps. Consequently, the research work carried out in the subsequent chapters of this thesis is an effort to address these knowledge gaps to aid optimal WPP size allocation in distribution networks considering steady-state operation.

In a nutshell throughout this research work, a holistic mathematical relation between V_{PCC} and the key characteristics of distribution systems has been developed. Finding this relation, the relation between V_{PCC} , P_{wind} , SCC and X/R has been investigated using V-X/R characteristics sketched for different test distribution systems with different SCR values. The test systems are based on IEEE standard distribution models. Later on, mathematical relations have been developed using V-X/R curve characteristics. The coefficients of the proposed equations have been identified using one of the AI based approaches called Genetic Algorithm (GA).

Chapter 3 - Voltage Stability Analysis at the Point of Common Coupling

3.1 Introduction

Angle stability, which means the ability of interconnected synchronous machines to remain in the state of synchronism, had been the principal power systems stability concern for many years [122]. However, in the 1980s, the reduction of investments in designing new generation and transmission facilities adversely impacted on the system stability. This resulted in a new concept formerly ignored, called the voltage stability [123].

Voltage stability is the ability of the power system to maintain the voltage at all the buses within the acceptable steady-state range when the system is under normal operating conditions and after being subjected to a disturbance [122]. The system may enter into a state of voltage instability when the increase in load or changes in the system condition lead to a continuous decrease in voltage. Voltage collapse happens when a series of accidents conducting voltage instability result in a blackout or abnormally low voltages in an excessively large part of a power system.

In recent years, voltage instability has caused several network collapses and blackouts and has been drawing increasing attention. Many instances of voltage collapse have been reported around the world such as Australia, Sweden, Belgium, France, USA, Japan, etc [27, 28, 124]. The practical importance of voltage stability analysis is that it aids in designing and selecting strategies that reduce the risk of voltage collapse and increase system stability [125]. The main factors which have increased the importance of voltage stability analysis are [125]:

- Reduced ability to control voltage at the buses due to the power systems enlargement
- The incorporation of large-scale Induction Generators (IGs)
- The broad use of shunt capacitor banks for regulating voltage through reactive power compensation
- Many voltage instability cases having occurred around the world

Voltage stability has been the main concern in analysing issues related to the interconnection of WPP to power grids [126]. Numerous authors have proposed voltage stability indexes based on load flow analysis [127-132]. Indeed, voltage stability was initially considered from a load flow perspective, in which the generators were simply regarded as 'PV buses'. However, voltage stability analysis cannot be completely separated from the performance of the generators which provide power and control voltage at the load buses [122].

Voltage stability is a broad range of study analysing and observing voltage at different buses of a system especially load buses and PCC bus. As discussed in Chapter 1, the focus of this thesis is on demonstrating issues concerned with the interconnection of WPPs to distribution networks. From a voltage stability perspective, major concern at the interconnection of the WPP to the power systems is how voltage responds to the injection of wind power at a given connection point while the system is in the steady-state operation. The research aims to focus on this particular aspect of voltage-stability concerns; and specifically covers a PCC-interconnection study aimed at demonstrating the impacts of SCC and X/R ratios on the steady-state voltage profile at the PCC bus (V_{PCC}) in response to changes in wind power generation. Therefore, the voltage stability

analysis for load buses and transient stability issues are not aligned with the scope of this research.

In this chapter, the effect of the interconnection of WPPs to a distribution network is investigated through detailed voltage stability analysis studies carried out at the PCC, including: power-voltage (PV), reactive power-voltage (QV), active power-reactive power (PQ), voltage-SCR analysis. These studies have been carried out using IEEE distribution test feeders. The chapter is organized as follows: Section 3.2 introduces distribution network characteristics and parameters that would impact on voltage stability at a given connection point. The general and specific characteristics of the test systems under investigation are discussed in Section 3.3. In Section 3.4, the results of PV and QV analysis studies are presented and discussed for different SCC and X/R_{PCC} ratios. In Section 3.5, PQ analysis is used to investigate the impact of X/R_{PCC} on the maximum permissible power that could be injected by the WPP. Section 3.6 highlights the relations between the V_{PCC} , X/R_{PCC} and SCR using graphical charts and, then, Section 3.7 summarizes the major conclusions of this chapter.

3.2 Basic theory

This section introduces the network and WPP parameters that would impact on system voltage stability at the PCC. The analysis has been carried out based on the system Thévenin equivalent circuit. As discussed in Section 2.5 in Chapter 2, the supply voltage source (V_{th}) and the grid short-circuit impedance (Z_{sc}) represent the Thévenin equivalent circuit of distribution system [11] (Please refer to Figure 2.2 for further details).

The step-voltage variations in response to change of wind power generation (ΔV_{PCC}) is defined through Eq. (3.1):

$$\Delta V_{PCC} = V_{PCC_new} - V_{PCC} \quad (3.1)$$

Where V_{PCC} and V_{PCC_new} are the PCC voltage before and after the change of wind power generation, respectively.

ΔV_{PCC} has two components as expressed by Eq. (3.2) [9]:

$$\Delta V_{PCC} = \Delta V_{PCC_r} + j\Delta V_{PCC_x} \quad (3.2)$$

In (3.2), ΔV_{PCC_r} is the voltage variation caused by the effect of the resistive component of the grid short-circuit impedance and is in phase with V_{PCC} . Furthermore, ΔV_{PCC_x} is the voltage variation caused by the effect of the reactive component of the grid short-circuit impedance and is in quadrature with V_{PCC} [10].

Assigning Eq. (3.2) in Eq. (3.1), the voltage phasor after the change of wind power generation (V_{PCC_new}) can be obtained from Eq. (3.3):

$$V_{PCC_new} = (V_{PCC} + \Delta V_{PCC_r}) + j\Delta V_{PCC_x} \quad (3.3)$$

Eq. (3.3) has been used to plot a phasor diagram of the PCC voltage variation as shown in Figure (3.1) [133].

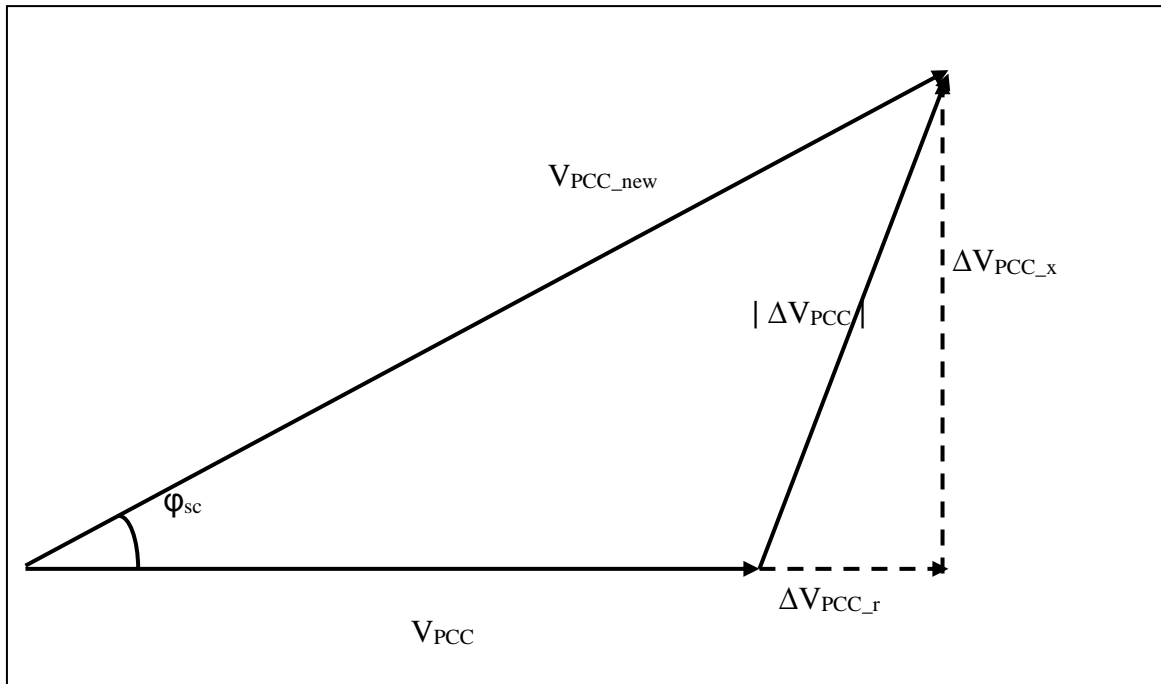


Figure 3.1 Phasor diagram of the PCC voltage variation [133].

In Figure 3.1, φ_{sc} is the system short-circuit impedance phase angle. Furthermore, $|\Delta V_{PCC}|$ is the magnitude of the ΔV_{PCC} given by Eq. (3.4):

$$|\Delta V_{PCC}| = \sqrt{\Delta V_{PCC-r}^2 + \Delta V_{PCC-x}^2} \quad (3.4)$$

From Figure 3.1, it is obvious that the ΔV_{PCC} value depends on φ_{sc} . Furthermore, referring to [10], the X/R_{PCC} ratio (X_{sc}/R_{sc}) can be calculated using Eq. (3.5):

$$\tan \varphi_{sc} = \frac{X_{sc}}{R_{sc}} \quad (3.5)$$

Therefore, it can be concluded that the ΔV_{PCC} value depends on the system overall X/R ratio. Referring to [123], the ΔV_{PCC} components can be expressed as:

$$\frac{\Delta V_{PCC-r}}{V_{PCC}} = \frac{1}{|SCC|} \times \frac{V_{th}^2}{V_{PCC}^2} [P_{wind} \times \cos \varphi_{sc} + Q_{wind} \times \sin \varphi_{sc}] \quad (3.6)$$

$$\frac{\Delta V_{PCC-x}}{V_{PCC}} = \frac{1}{|SCC|} \times \frac{V_{th}^2}{V_{PCC}^2} [P_{wind} \times \sin \varphi_{sc} - Q_{wind} \times \cos \varphi_{sc}] \quad (3.7)$$

Where P_{wind} and Q_{wind} are active and reactive power injected by the WPP to distribution network, respectively.

Generally, it is assumed that $|V_{PCC}| \cong |V_{th}|$ [10]. Therefore, Eq. (3.6) and Eq. (3.7) are simplified as:

$$\Delta V_{PCC-r} = \frac{V_{PCC}}{|SCC|} \times [P_{wind} \times \cos \varphi_{sc} + Q_{wind} \times \sin \varphi_{sc}] \quad (3.8)$$

$$\Delta V_{PCC-x} = \frac{V_{PCC}}{|SCC|} \times [P_{wind} \times \sin \varphi_{sc} - Q_{wind} \times \cos \varphi_{sc}] \quad (3.9)$$

Assigning Eq. (3.8) and Eq. (3.9) in Eq. (3.4), the magnitude of ΔV_{PCC} can be expressed as in Eq. (3.10):

$$\begin{aligned}
 |\Delta V_{PCC}| &= \frac{V_{PCC}}{|SCC|} \times \sqrt{(P_{wind} \times \cos \varphi_{sc} + Q_{wind} \times \sin \varphi_{sc})^2 + (P_{wind} \times \sin \varphi_{sc} - Q_{wind} \times \cos \varphi_{sc})^2} \\
 &= |\Delta V_{PCC}| = \frac{V_{PCC}}{SCC} \times \sqrt{P_{wind}^2 \times (\cos^2 \varphi_{sc} + \sin^2 \varphi_{sc}) + Q_{wind}^2 \times (\sin^2 \varphi_{sc} + \cos^2 \varphi_{sc})} \quad (3.10)
 \end{aligned}$$

Considering that $\sin^2 \varphi_{sc} + \cos^2 \varphi_{sc} = 1$, the following relation can be obtained [123]:

$$|\Delta V_{PCC}| = \frac{V_{PCC}}{SCC} \times \sqrt{P_{wind}^2 + Q_{wind}^2} = \frac{V_{PCC}}{SCC} \times S_{wind} \quad (3.11)$$

Where S_{wind} is the apparent power of WTG.

Eq. (3.11) is very helpful as it shows that the value of V_{PCC} variation is a function of grid SCC, active, and reactive powers (or apparent power) of the WPP. Therefore, in a distribution network penetrated WPP, the main parameters that impact the PCC voltage stability can be summarised as follows:

- The overall system X/R seen at the PCC (X/R_{PCC}) obtained by $\tan(\varphi_{sc})$,
- The ratio between rated WPP power and the grid SCC,
- The active power injected by the WPP,
- The reactive power injected or absorbed by the WPP.

As discussed earlier, in this chapter, the effects of these parameters on the V_{PCC} have been studied and plotted using PV, QV, and V-SCR studies. For this purpose, two IEEE models have individually been modelled and simulated to study the highlighted concepts. Section 3.3 describes the specifications of each model.

3.3 Test distribution systems

A distribution system consists of several feeders arranged in different ways, such as radial and meshed type. A meshed distribution system has more reliability compared to radial distribution networks. However, operating the power system is hard in a

meshed distribution system due to its complicated structure [134]. Hence, the meshed network type is not a popular structure in distribution networks and is mainly used for distribution systems feeding sensitive loads such as hospitals and factories [134]. On the other hand, radial construction is cheaper to build and has widely been used in distribution network design [135].

In this study, two IEEE radial distribution systems have been considered, modelled and simulated: the IEEE 37-bus and IEEE 9-bus systems. These two systems have been widely used in the literature as test distribution systems [136-141]. In each model, a WPP is connected to the test distribution system. The single-line diagrams of the two systems are shown in Figure 3.2 and Figure 3.3. Furthermore, the MATLAB / Simulink model of the test systems have been presented in Figures A.1 and A.2 in Appendix A. As shown in Figures 3.2 and 3.3, the main components of the test distribution systems are: source and distribution transformers, the connected WPP, loads, reactive power compensators, and distribution lines. The specification of each component is discussed in the following.

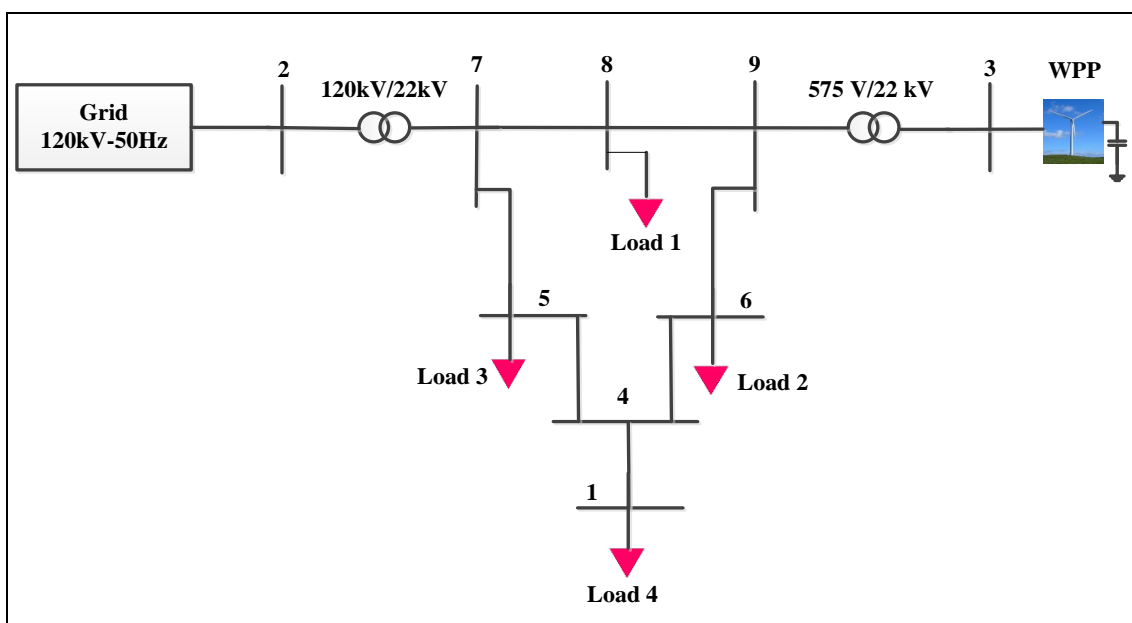


Figure 3.2 Single-line diagram of the modelled 9-bus test distribution system.

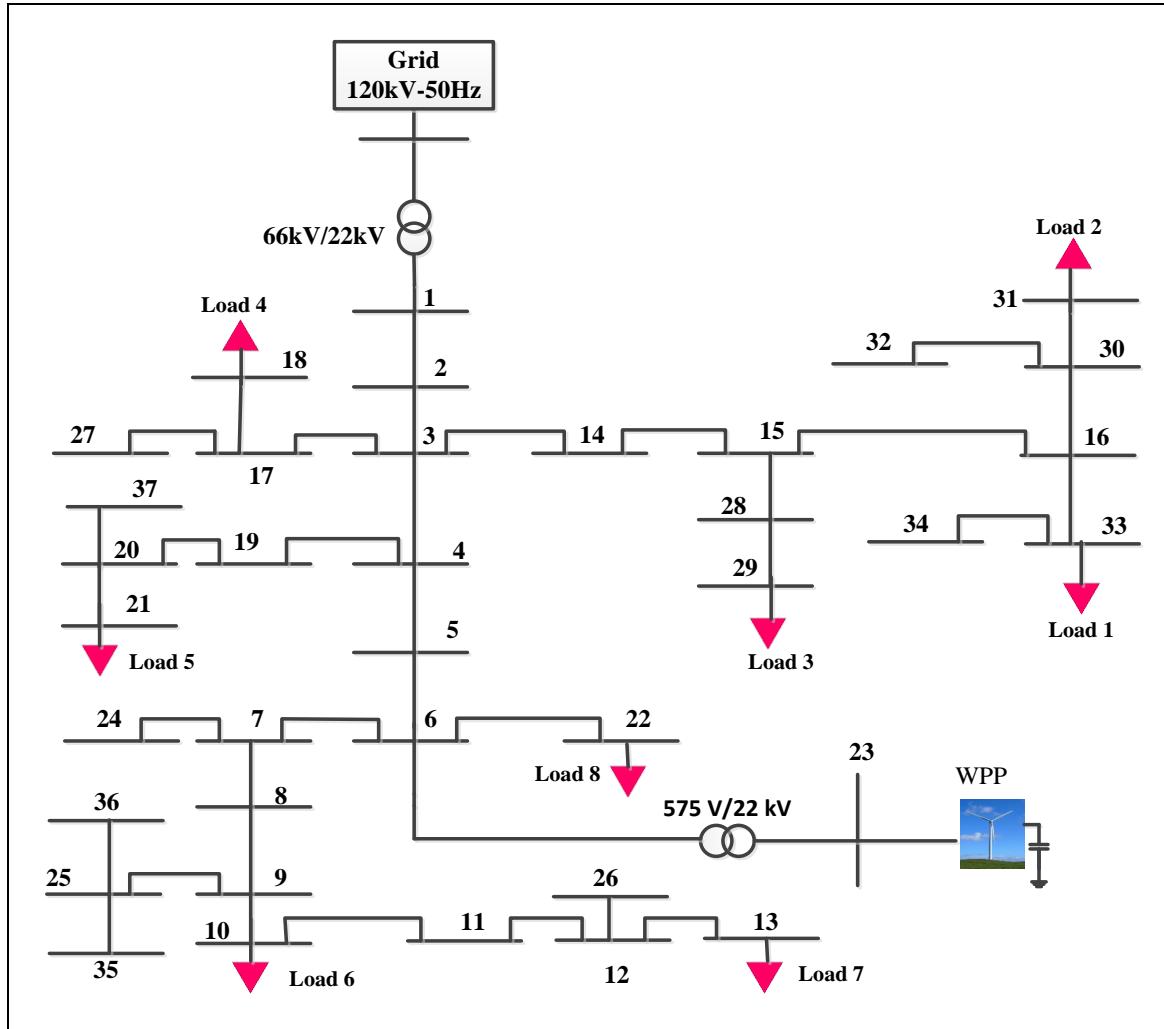


Figure 3.3 Single-line diagram of the modelled 37-bus test distribution system.

3.3.1 Source and distribution transformer

In both test systems, the distribution system is connected to a 120 kV, 50 Hz external source of infinite short circuit current through a Yg/ Δ configuration of a three-phase distribution transformer. The distribution transformer parameters are shown in Table B.1 in Appendix B.

3.3.2 Wind power plant

In each model, a small Wind Power Plant (WPP) with the total capacity of 9 MVA, provided by three 3 MVA WTGs, is connected to the distribution system at the PCC. The PCC is considered to be at Bus 9 in the 9-bus system and at Bus 6 in the 37-

bus system. Parameters used for modelling each WTG are given in Table B.2 in Appendix B. In this study, analysis studies have been carried out using two common types of WTGs: the Induction Generator (IG) and the Double Fed Induction Generator (DFIG). Referring to Table B.2, the rated voltage of WTGs is 575 V. A three-phase transformer with Yg/Yn configuration is connected to each WTG to boost voltage to the rated voltage of the distribution system, i.e. 22 kV. The values of the parameters used for simulating WPP transformers are given in Table B.3 in Appendix B.

3.3.3 Reactive power compensator

In the case of the IG-Based WPP, the reactive power absorbed by IG is partly compensated by a 0.4 MVAR capacitor bank. The rest of reactive power compensation is provided by a 3-MVAR STATCOM with a 3% droop setting to maintain the V_{PCC} in the steady-state voltage range ($0.95 \text{ p.u.} \leq V_{PCC} \leq 1.05 \text{ p.u.}$). The single-line block diagram of the STATCOM and its control system is given in Figure B.1 in Appendix B. In the case of the DFIG-Based WPP, no reactive power compensator is considered for the WPP as DFIG has the capability of controlling the reactive power and the reactive power demand is not sensitive to terminal voltage variations [70]. The block diagrams of DFIG and its converter control systems (rotor-side and grid-side converters) are presented in Figures B.2 to B.4 in Appendix B.

3.3.4 Load

Four and eight three-phase 22 kV and 50 Hz Resistor-Inductor (RL) loads are connected to the 9-bus and 37-bus test system, respectively, as shown in Figures 3.2 and 3.3. The load parameters for each test system have been listed in Table B.4. in Appendix B. Furthermore, the power factor of each load is 0.98 lagging.

3.3.5 Distribution lines

All conductors in the studied test systems are assumed to be three-wire overhead lines of AAAC type with delta configuration. AAACs have been used for transmission and distribution lines in Australia since 1984. The conductor characteristics used in the test systems are presented in Table B.5 in Appendix B [142].

It is important to mention that the X/R ratio of the lines cannot be dynamically changed in a power system, but certain design techniques can be used to reduce or minimise impedances with an effect on the X/R ratio seen at the PCC (X/R_{PCC}). Such techniques could involve retrofitting with lower impedance transformers or changing old overhead conductors with newer lower impedance conductors. While this may be expensive, it may be an option that utilities and WPP developers can resort to make an unviable feeder viable. For example, a particular feeder may be unsuitable for WPP connection, but there may be excellent wind resource in that area, and hence justifiable to retrofit the network to make it more suitable for a WPP connection. In the following sections, it is assumed that such strategies are implemented with an impact on the equivalent Thévenin impedance seen at a connection point and the respective X/R ratio.

In this thesis, for obtaining the X/R ratio at a specific connection point, the phase angle ratio of the equivalent impedance seen from that point is calculated at frequency of 50 Hz using MATLAB tool, called the impedance vs frequency measurement tool. With the knowledge of phase angle of the equivalent impedance seen at the given connection point, the equivalent impedance angle ratio seen at that point is obtained. It is obvious that the change of X/R ratios in distribution lines affects the system overall X/R_{PCC} ratio. Hence, for changing the X/R_{PCC} ratio, the X/R ratios in the distribution liners are changed while the grid SCC value seen from the PCC is constant. Changing

the X/R ratios in the distribution lines, the value of X/R_{PCC} is calculated as explained above to obtain the new value of the X/R_{PCC} .

3.4 PV and QV analysis

As discussed in Chapter 2, integration of a significant amount of wind power generation may adversely impact the voltage profile at the PCC of a WPP. Therefore, voltage exceeding specified limits is the first operating constraint in optimising P_{wind} generation. This signifies that engineers and planners have to determine the optimal amount of P_{wind} injection which ensures that the V_{PCC} stays within the steady-state voltage range as specified in the grid codes.

In a distribution system connected WPP, a PV curve describes the relationship between active power injected by WTG and steady-state voltage at the PCC. Taking advantage of a PV curve, engineers can estimate the maximum real power injection by a WPP to ensure voltage stays within acceptable steady-state limits [143]. PV analysis also makes it possible to determine ΔV_{PCC} value, which is another important parameter in voltage stability analysis. Furthermore, a QV curve shows the variation of bus voltage regarding changes in Q_{wind} at the bus. The region where dV/dQ is positive indicates stable operating region, while $dV/dQ < 0$ indicates the unstable region.

As discussed earlier, the objective is to investigate voltage stability at a given PCC bus of a grid-connected WPP. This necessitates investigations on how the steady-state voltage at a potential distribution network WPP interconnection point will change due to increases in the WPP penetration levels. Active and reactive power exchanged between WPP and the distribution network are key parameters that impact the voltage stability at the PCC point. In this respect, PV and QV analysis studies are performed to analyse the effect of WPP penetration on the V_{PCC} stability.

The analysis studies are performed assuming that the system is under steady-state mode and the load values at the PQ buses are constant. The reason for having constant load values is due to the fact that the objective is to investigate the effect of the WPP penetration, while system loads are constant. Therefore, in this Chapter, PV and QV analysis studies were carried out by changing the active and reactive power injected/absorbed by the WPP, while the load values are kept constant.

It is noted that the PV and QV characteristics in light loading condition are different with those under heavy loading conditions. The effect of heavy and light loading on PV and QV characteristics are analysed in Chapter 6.

This section presents the PV and QV analysis studies that have been carried out for both IG and DFIG-Based WPPs connected to the 37-bus and 9-bus test systems. Analysis studies have been carried out assuming that the V_{PCC} is around 0.98 p.u. in the studied test systems before WPP is connected to the PCC bus. For each test system, the SCC value was first calculated and then the PCC short circuit currents (I_{sc}) were determined. Determining short circuit currents, the grid short circuit power levels were then calculated using Eq. (2.2) presented in Chapter 2. Table 3.1 shows the SCC values for each test feeder. As shown in Table 3.1, the short circuit current and the corresponding SCC in the 37-bus test system are smaller than those in the 9-bus test system.

Table 3.1 SCC value in 9-bus and 37-bus test feeders.

Test distribution system	I_{sc} (kA)	SCC (MVA)
9-bus system	1.44	54
37-bus system	1.07	40

3.4.1 PV analysis

This section discusses how the X/R_{PCC} ratio impacts V_{PCC} in the 9-bus and 37-bus test systems as P_{wind} increases. In this respect, the PV characteristics have been plotted

for both test systems. A PV curve is formed by varying P_{wind} and monitoring the P_{wind} parameter against V_{PCC} , while the Q_{wind} value is constant.

3.4.1.1. IG-Based WPP

Figure 3.4 and Figure 3.5 show the PV curves for the two test systems for the IG-Based WPP case. Figure 3.6 and Figure 3.7 show the step- V_{PCC} variation due to an increase in wind power injection from 0 MVA to the rated power ($P_{rated} = 9$ MVA) for the 9-bus and 37-bus test systems, respectively.

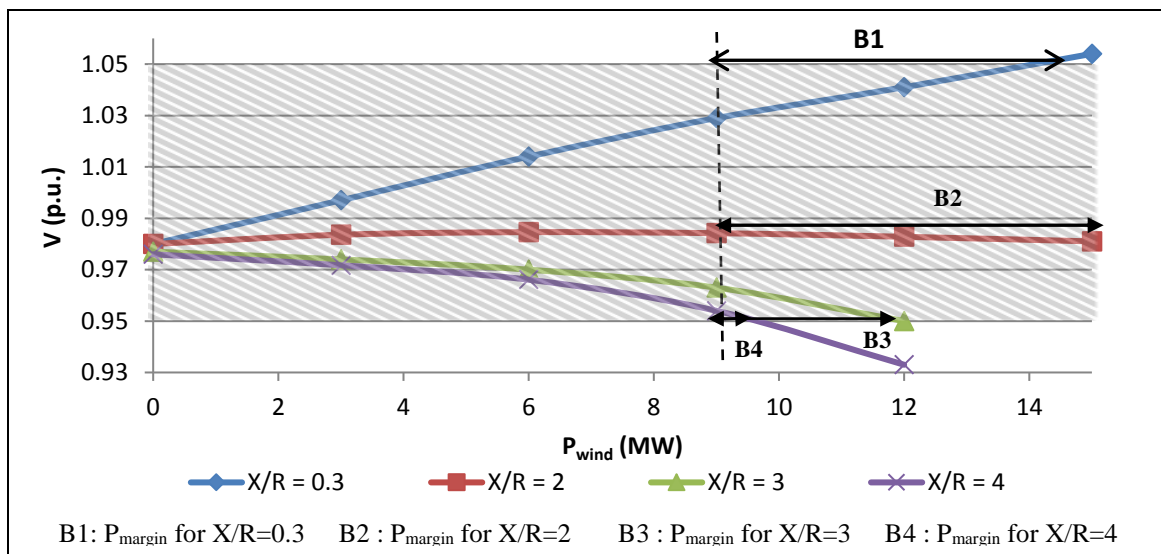


Figure 3.4 PV curve for different X/R_{PCC} ratios in the IG-Based 9-bus test system.

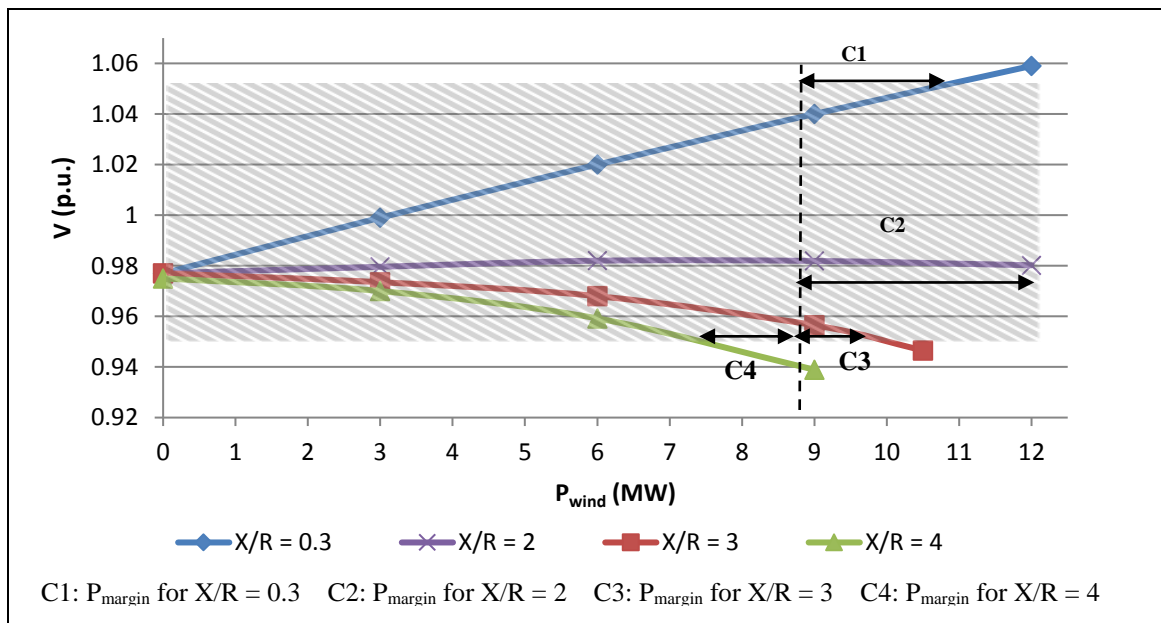


Figure 3.5 PV curve for different X/R_{PCC} ratios in the IG-Based 37-bus test system.

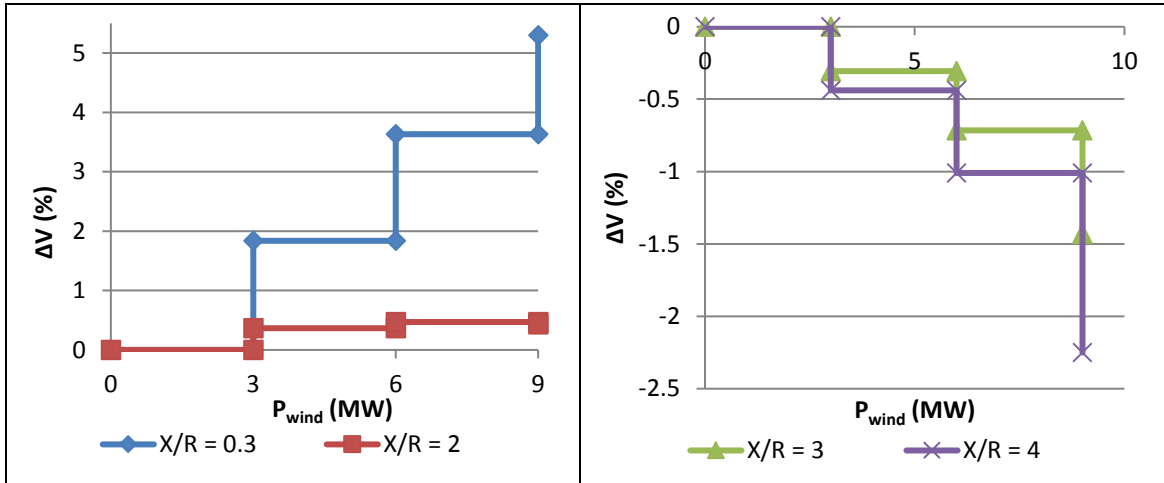


Figure 3.6 Voltage variation versus active power injection for different X/R ratios at the PCC of the IG-Based 9-bus test system.

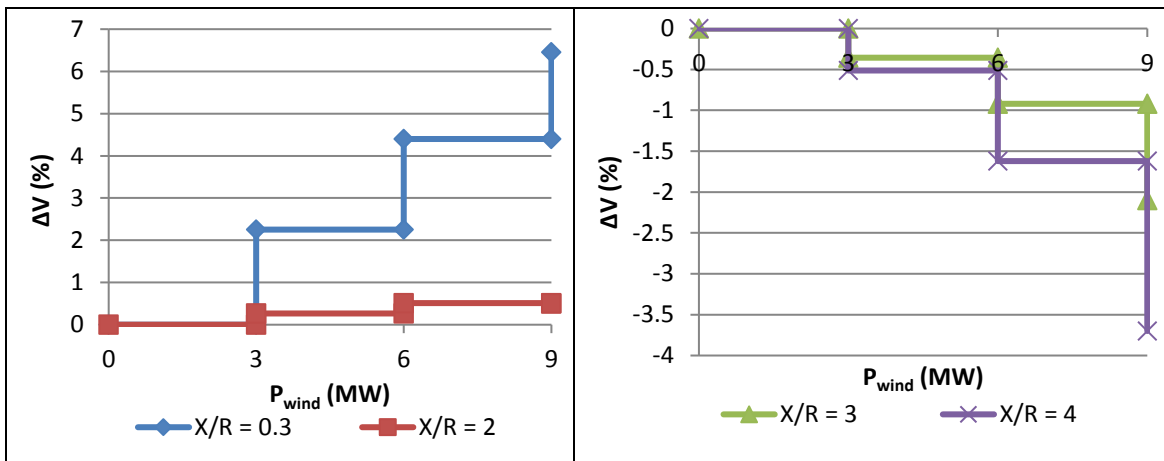


Figure 3.7 Voltage variation versus active power injection for different X/R ratios at the PCC of the IG-Based 37-bus test system.

From Figure 3.4 and Figure 3.5, it can be seen that voltage, at PCC points with small X/R ratios, increases as wind power penetration increases. In both test systems, voltage at PCC points with small X/R ratios increases beyond 1.05 p.u. for high wind power penetration. However, an increase in wind power results in voltage drops at the PCC points with large X/R ratios.

Figure 3.4 and Figure 3.5 also depict the significance of X/R_{PCC} on the active power margin (P_{margin}), which signifies the difference between the P_{rated} of a WPP and the maximum power that can be injected by the WPP ($P_{max-wind}$) for which the V_{PCC} is still in the allowable steady-state voltage range. The active power margins have been

presented by B1 to B4 for the 9-bus test system, and C1 to C4 for the 37-bus test system. P_{rated} is 9 MVA, and P_{margin} is as tabulated in Table 3.2 and Table 3.3 for the 9-bus and 37-bus test system, respectively. As shown in Table 3.2 and Table 3.3, an X/R_{PCC} of 2 provides the highest P_{margin} in both test systems, while P_{margin} decreases for $X/R_{\text{PCC}} \neq 2$ conditions.

Comparing the results between Table 3.2 and Table 3.3 also demonstrates that P_{margin} in a system with a high SCC is greater than that in a system with a small SCC. As shown in Table 3.3, P_{margin} is negative (-1.6 MVAR) for the system with a small SCC and high X/R_{PCC} ratio (SCC = 40 and $X/R_{\text{PCC}} = 4$). This indicates that in feeders with a small SCC, high X/R ratios may even not allow the WPP to transfer the rated power to the feeder; otherwise the voltage would decline out of the allowable steady-state voltage range.

Table 3.2 Active power margin ensuring $0.95 \text{ p.u.} < V_{\text{PCC}} < 1.05 \text{ p.u.}$ in the IG - Based 9-bus system.

Active power margin	Value (MW)
B1	5
B2	6
B3	3
B4	0.8

Table 3.3 Active power margin ensuring $0.95 \text{ p.u.} < V_{\text{PCC}} < 1.05 \text{ p.u.}$ in the IG - Based 37-bus system.

Active power margin	Value (MW)
C1	1.7
C2	3
C3	1
C4	-1.6

From Figure 3.6 and Figure 3.7, it is clear that the ΔV_{PCC} value for buses with small X/R ratios is more serious than ΔV_{PCC} value for buses with large X/R ratios. Tables 3.4 and 3.5 show the numerical results concerned with ΔV_{PCC} for different wind power injection levels.

Table 3.4 Step-voltage variation in the IG-Based 9-bus test system.

Wind power variation	X/R	Step – voltage variation (%)
From 0 MVA to 3 MVA	0.3	1.84
	2	0.37
	3	-0.3
	4	-0.44
From 3 MVA to 6 MVA	0.3	1.7
	2	0.1
	3	-0.41
	4	-0.57
From 6 MVA to 9 MVA	0.3	1.48
	2	-0.04
	3	-0.72
	4	-1.25
From 0 MVA to 6 MVA	0.3	3.63
	2	0.47
	3	-0.72
	4	-1
From 0 MVA to 9 MVA	0.3	5.3
	2	0.43
	3	-1.43
	4	-2.25

Table 3.5 Step-voltage variation in the IG-Based 37-bus test system.

Wind power variation	X/R	Step – voltage variation (%)
From 0 MVA to 3 MVA	0.3	2.25
	2	0.27
	3	-0.36
	4	-0.51
From 3 MVA to 6 MVA	0.3	2.3
	2	0.25
	3	-0.23
	4	-0.58
From 6 MVA to 9 MVA	0.3	2
	2	-0.01
	3	-1.1
	4	-2.05
From 0 MVA to 6 MVA	0.3	4.4
	2	0.51
	3	-0.92
	4	-1.62
From 0 MVA to 9 MVA	0.3	6.5
	2	0.5
	3	-2.1
	4	-3.7

As mentioned in Chapter 2, the grid code requirements with regards to voltage control states that the step-voltage variation in response to changes in wind power

generation should normally be maintained under 3% and not exceed 4% [50, 51]. However, results in Tables 3.4 and 3.5 show that the voltage variation in both test system does not satisfy the grid code requirements when wind power generation increases from 0 MVA to 6 MVA (when two WTGs are switched on at the same time) and 9 MVA (when three WTGs are switched on at the same time), and X/R_{PCC} ratio is small ($X/R = 0.3$).

In the case of stiffer test system (9-bus test system), the result show that the voltage variation due to an increase in wind power generation from 0 to 6 MVA is higher than 3% (3.63 %) so that the voltage variation violates the grid code requirements. The voltage variation is even higher than 4% when wind power injection increased from 0 to 9 MVA. In the case of weaker system (37-bus test system), the voltage variation is higher than 4% when wind power injection increased from 0 to 6 and 9 MVA. This signifies that voltage variation requirements can hardly be provided at PCC points with small X/R ratios. However, as shown in Tables 3.4 and 3.5, the voltage variation satisfies the grid code requirements in most cases when X/R_{PCC} is large ($X/R = 3\&4$). In this X/R_{PCC} range, the highest voltage variation which violates the grid code requirements is related to the weaker test (37-bus test system) when $X/R_{PCC} = 4$ and wind power injection increased from 0 to 9 MVA.

From a voltage stability perspective, the most optimum value of X/R_{PCC} in a distribution system would be the point where V_{PCC} has the lowest variations in response to increases in wind power generation. Analysing Figures 3.4 to 3.7, it can be concluded that this value of the X/R_{PCC} ratio is around 2 in both systems. Furthermore, reviewing the works in the literature carried out based on real systems and actual cases, it was

confirmed that the optimal X/R_{PCC} ratio in distribution system highly penetrated by IG - Based WPPs (weak distribution systems) is around 2 [56, 144].

3.4.1.2. DFIG-Based WPP

In this section, PV analysis is carried out assuming that a DFIG-Based WPP is connected to the test system. PV characteristics for the 9-bus and 37-bus test system are presented in Figures 3.8 and 3.9, respectively. Furthermore, Figures 3.10 and 3.11 show the voltage variation due to an increase in P_{wind} injection from 0 MVA to the rated power ($P_{rated} = 9$ MVA) for the 9-bus and 37-bus test systems, respectively.

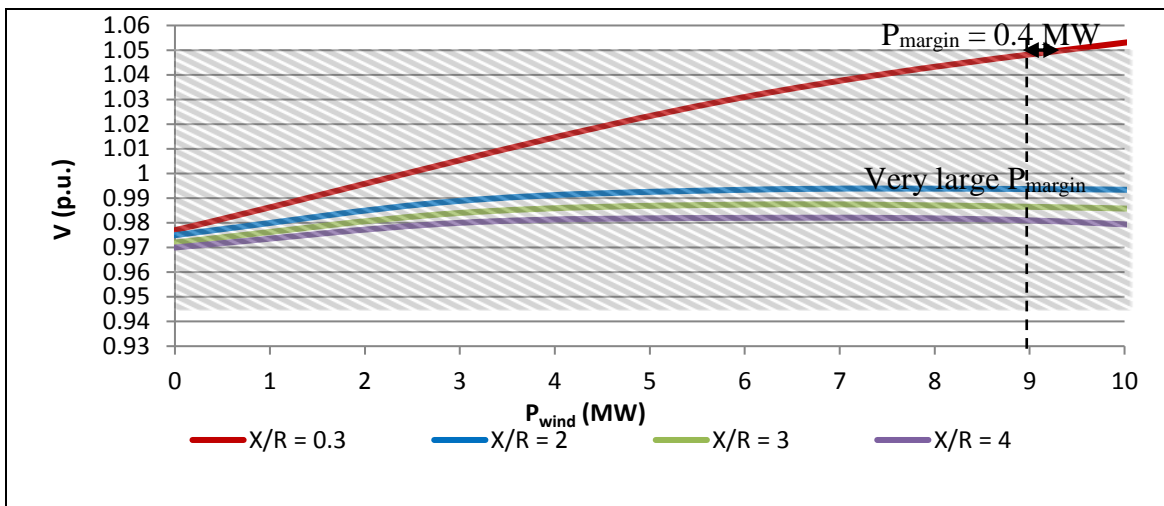


Figure 3.8 PV curve for different X/R ratios at the PCC of the DFIG-Based 9-bus test system.

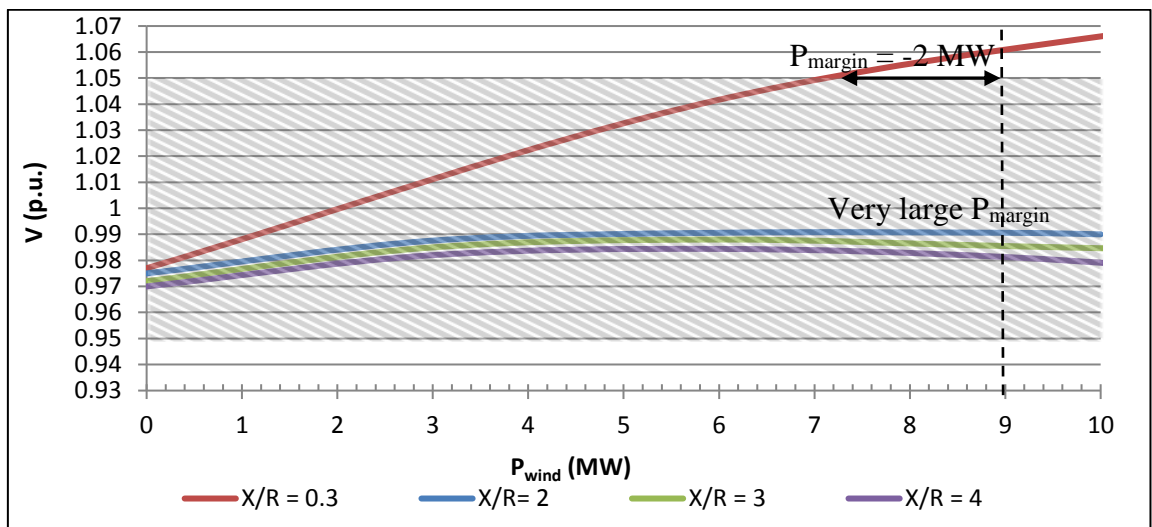


Figure 3.9 PV curve for different X/R ratios at the PCC of the DFIG-Based 37-bus test system.

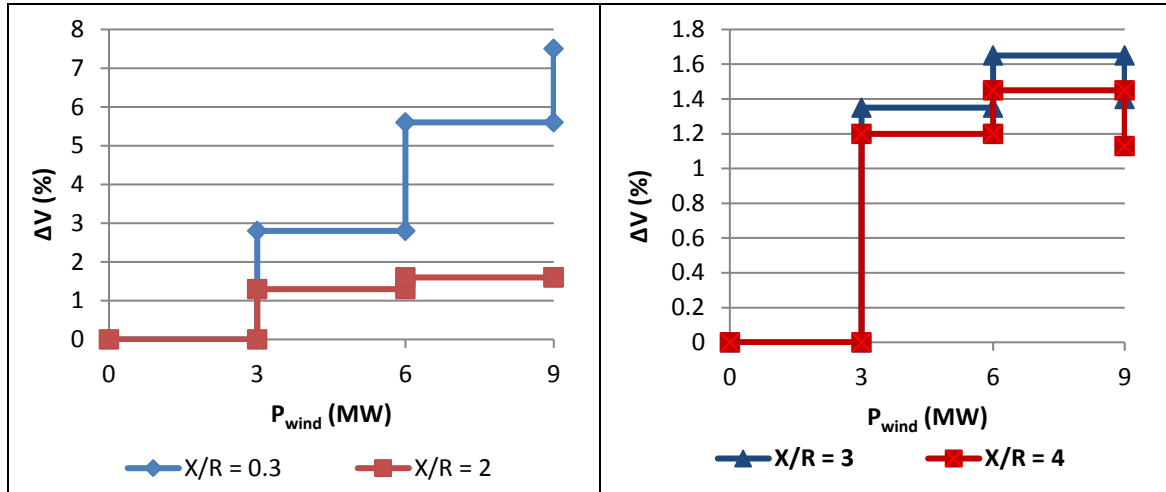


Figure 3.10 Voltage variation versus active power injection for different X/R ratios at the PCC of the DFIG-Based 9-bus test system.

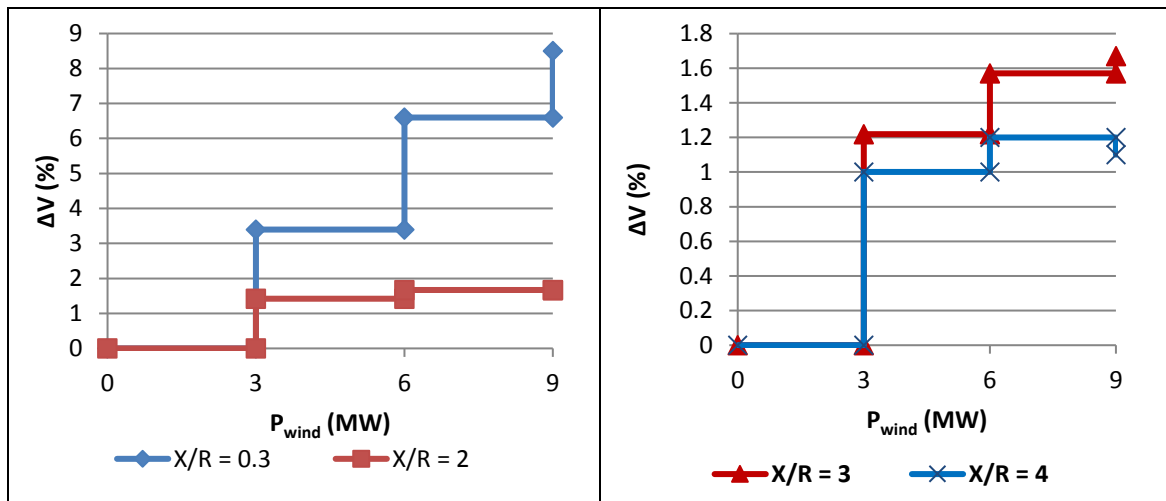


Figure 3.11 Voltage variation versus active power injection for different X/R ratios at the PCC of the DFIG-Based WPP 37-bus test system.

Figures 3.8 and 3.9 show that, for both test systems, the increase in wind power generation significantly increases the V_{PCC} , when X/R_{PCC} is small. This adversely impacts on the P_{margin} value. Figure 3.8 shows that P_{margin} for ensuring $V_{PCC} < 1.05$ p.u. in the 9-bus test system (with $SCC = 54$) is very small, around 0.4 MVA, when X/R_{PCC} ratio is small ($X/R = 0.3$). Furthermore, Figure 3.9 shows that P_{margin} is negative (-2 MVAR) for the system with small SCC and X/R_{PCC} values (37-bus system, $SCC = 40$ and $X/R_{PCC} = 0.3$). This indicates that, in a DFIG-Based WPP connected to a grid with a small SCC value, small X/R_{PCC} ratios may even not allow the WPP to transfer the rated

power to the feeder; otherwise the voltage would decline out of the steady-state range. Comparing the PV characteristics depicted for IG-Based WPP in Figures 3.4 and 3.5 with the PV characteristics depicted for DFIG-Based WPP in Figure 3.8 and 3.9, it can be observed that P_{margin} in PCC points connected to DFIG would be lower than that in PCC points connected to IG when the X/R ratio seen at the feeder is small. The reason is that, in DFIG-Based WPP, V_{PCC} increases to very high values as P_{wind} increases when X/R_{PCC} is small. This necessitated the generator to absorb a large reactive power to reduce the over-voltage condition and maintain the terminal voltage within 0.95-1.05 p.u. Therefore, one of the main drawbacks of DFIG is that the generator could not comply with voltage regulation when X/R_{PCC} was small.

For large X/R_{PCC} ratios, DFIG has to inject reactive power to the grid in order to maintain the V_{PCC} within the standard supply voltage range. DFIG can generate reactive power even two times greater than its rated power [145]. Therefore, as shown in Figures 3.8 and 3.9, for large X/R ratio, the high capability of DFIG in injecting reactive power enables DFIG to maintain the bus voltage within the normal range at PCC points with large X/R ratios even for a large penetration of wind power.

As shown in Figures 3.10 and 3.11, ΔV_{PCC} variation is high for small X/R_{PCC} ratio. However, ΔV_{PCC} is small for large X/R ratios. Tables 3.6 and 3.7 show the numerical results concerned with ΔV_{PCC} for P_{wind} injection from 0 MVA to $P_{\text{rated}} = 9$ MVA.

Table 3.6 Step-voltage variation in the DFIG-Based 9-bus test system.

Wind power variation	X/R	Step – voltage variation (%)
From 0 MVA to 3 MVA	0.3	2.8
	2	1.3
	3	1.35
	4	1.2
From 3 MVA to 6 MVA	0.3	2.8
	2	0.3
	3	0.3
	4	0.25

From 6 MVA to 9 MVA	0.3	1.9
	2	0
	3	-0.25
	4	-0.32
From 0 MVA to 6 MVA	0.3	5.6
	2	1.6
	3	1.65
	4	1.45
From 0 MVA to 9 MVA	0.3	7.5
	2	1.6
	3	1.4
	4	1.13

Table 3.7 Step-voltage variation in the DFIG-Based 37-bus test system.

Wind power variation	X/R	Step – voltage variation (%)
From 0 MVA to 3 MVA	0.3	3.4
	2	1.42
	3	1.22
	4	1
From 3 MVA to 6 MVA	0.3	3.2
	2	0.45
	3	0.35
	4	0.2
From 6 MVA to 9 MVA	0.3	1.9
	2	0
	3	-0.1
	4	-0.1
From 0 MVA to 6 MVA	0.3	6.6
	2	1.67
	3	1.57
	4	1.2
From 0 MVA to 9 MVA	0.3	8.5
	2	1.67
	3	1.47
	4	1.1

The results from Tables 3.6 and 3.7 demonstrate that ΔV_{PCC} in both test systems violates the grid code requirements when the X/R_{PCC} ratio is small ($X/R_{PCC} = 0.3$), specifically when two or all three WTGs are switched on at the same time. For small X/R_{PCC} ratios, when two 3-MVA WTGs are simultaneously connected to the 9-bus test distribution system, V_{PCC} variation becomes greater than 5%. The situation even worsens in the test system with a smaller SCC value (37-bus system) where $\Delta V_{PCC} > 6\%$. Furthermore, when all three WTGs are simultaneously connected to the test

distribution systems, V_{PCC} variation becomes far too large (7.5% in the 9-bus test system and 8.5% in the 37-bus test system).

For large X/R_{PCC} , Table 3.6 and 3.7 show that ΔV_{PCC} is within the normal range defined in the Australian standard (less than 3%) for different number of switched on generators, including: only one WTG switched on, two WTGs switched on at the same time, and three WTGs switched on at the same time. Therefore, contrary to the PCC points with small X/R ratio, the ΔV_{PCC} value for different P_{wind} penetration stays within the allowable voltage variation range at the PCC points with large X/R ratios.

To conclude, the results in PV analysis demonstrated that the voltage regulation requirements can hardly be provided at the PCC for systems with small X/R_{PCC} for both IG and DFIG-Based WPPs. In the case of systems with large X/R_{PCC} ratios connected to IG-Based WPP, the V_{PCC} may decline out of the normal range ($V_{PCC} < 0.95$ p.u.) when P_{wind} generation is large. In the case of systems with large X/R_{PCC} ratios connected to DFIG-Based WPP, the voltage regulation requirement is not an issue even for very large wind power penetration.

3.4.2 QV analysis

In this section, the impact of the X/R ratio on reactive power requirements and QV analysis at the PCC is investigated for both test feeders. In performing the QV analysis, reactive power injected & absorbed by the WPP, which is called Q_{wind} , is varied to monitor V_{PCC} while P_{wind} is at its rated value (9 MVA). For PCC buses with small X/R_{PCC} , the threshold of concern from a voltage regulation point of view is the upper boundary of the allowable voltage range (1.05 p.u.). This is because as demonstrated earlier in Sections 3.4.1 (Figures 3.4, 3.5, 3.8, and 3.9), V_{PCC} would increase as wind power generation increases for small X/R_{PCC} ratios. On the other hand,

for buses with large X/R_{PCC} ratios, the lower boundary of the allowable steady-state voltage range (0.95 p.u.) is considered as the limit for reactive power absorption. This is because as demonstrated earlier in Section 3.4.1, V_{PCC} would decrease as wind power generation increases for systems with large X/R_{PCC} ratio. Similar to the PV studies, analysis is carried out for both IG and DFIG-Based WPPs.

3.4.2.1 IG-Based WPP

The QV characteristics have been plotted for both test systems when an IG-Based WPP is connected at the PCC. Analysis has been carried out for both ranges of the X/R_{PCC} ratio: small X/R_{PCC} ($X/R_{PCC} < 2$) and large X/R_{PCC} ratio ($X/R_{PCC} > 2$).

The QV characteristics for IG-Based WPP are shown in Figure 3.12 when X/R_{PCC} ratio is large. The graphs have been plotted for the stable region where $dV/dQ > 0$. The lowest point of each QV line shows the voltage stability limit where further absorption of Q by IG results in $dV/dQ < 0$ and voltage collapse. This point also defines the maximum reactive power that can be absorbed by the WPP before voltage collapse.

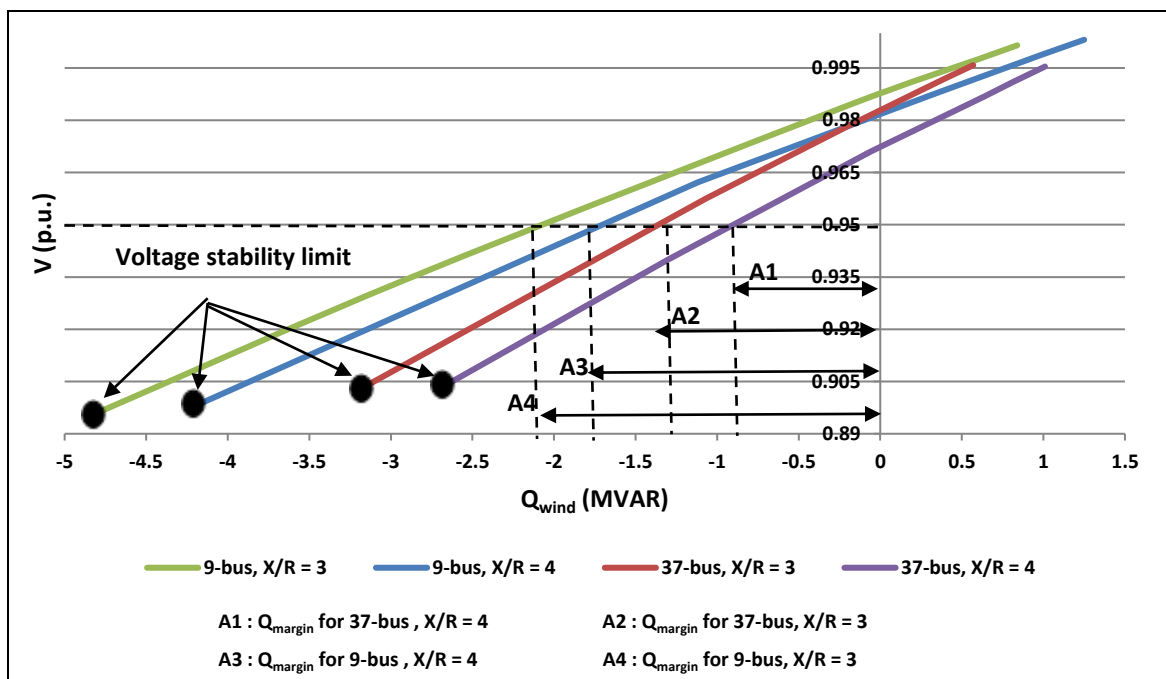


Figure 3.12 QV curves for large X/R ratios – IG-Based WPP.

From Figure 3.12, it is observed that the voltage stability limit and the amount of reactive power that can be absorbed by the IG before voltage collapse in a system with a large SCC at the PCC (9-bus system with SCC = 54) is greater than that in a system with a small SCC at the PCC (37-bus with SCC = 40). Also, large X/R_{PCC} adversely impacts on the voltage stability limits at the connection points with small SCC. Figure 3.12 shows that the lowest stability limit is observed for the case with the lowest SCC and highest X/R_{PCC} ratio (37-bus system, SCC = 40, and $X/R_{PCC} = 4$).

According to Figure 3.12, voltage at the connection points with large X/R ratio will fall below the lower boundary of the allowable steady-state voltage range, if reactive power drawn by IG is greater than a specific value. This value is called the reactive power margin (Q_{margin}). In Figure 3.12, the reactive power margins have been presented by A1 to A4. The values of these parameters are as tabulated in Table 3.8. From Table 3.8, it is clear that Q_{margin} in the test system with the smallest SCC and largest X/R_{PCC} ratios (37-bus system, SCC = 40, and $X/R_{PCC} = 4$) is lower than that in the other test distribution systems.

Table 3.8 Reactive power margin ensuring $0.95 \text{ p.u.} < V_{PCC} < 1.05 \text{ p.u.}$

Active power margin	Value (MW)
A1	- 0.9
A2	- 1.3
A3	- 1.8
A4	- 2.1

The equations representing the lines plotted in Figure 3.12 were obtained using MS Excel. These equations are as in Eq. (3.12) to Eq. (3.15):

$$\text{9-bus system, SCC} = 54, X/R_{PCC} = 3: \quad V = \frac{1}{54} \times Q + 0.9808 \quad (3.12)$$

$$\text{9-bus system, SCC} = 54, X/R_{PCC} = 4: \quad V = \frac{1}{54} \times Q + 0.9727 \quad (3.13)$$

$$37\text{-bus system, } SCC = 40, X/R_{PCC} = 3: \quad V = \frac{1}{40} \times Q + 0.9825 \quad (3.14)$$

$$37\text{-bus system, } SCC = 40, X/R_{PCC} = 4: \quad V = \frac{1}{40} \times Q + 0.9712 \quad (3.15)$$

From Eq. (3.12) to Eq. (3.15), it was observed that for each case, the slope of the line equals to the inverse of the SCC value. Considering that for a linear equation, derivative of the function equals to the slope of the line, the relation between reactive power variation (ΔQ), voltage variation (ΔV), and SCC is generally expressed as in Eq. (3.16) when X/R_{PCC} ratio is large.

$$\Delta V = \frac{1}{SCC} \Delta Q \quad (3.16)$$

Eq. (3.16) signifies that voltage variation in response to reactive power variation will be larger in PCC points with a small SCC concluding that PQ concerns will be more critical in connection points with a small SCC.

It is important to mention that Eq. (3.16) has been constantly proposed in the literature to express the relation between voltage and reactive power with regard to the grid SCC value. Following the findings explained above, Eq. (3.16) has been dedicated to investigate the PCC points where the $X_{PCC} \gg R_{PCC}$ (large X/R_{PCC}). However, there is no consensus in the literature about the relation between voltage and reactive power at the PCC points with a small X/R ratio. This shortcoming has been addressed in the following.

The QV characteristics, for IG-Based WPP when the X/R_{PCC} ratio is small (e.g. $X/R_{PCC} = 0.5$), are shown in Figure 3.13. Similar to the QV analysis for the large X/R_{PCC} ratio case, the graphs have been plotted for the stable region where $dV/dQ > 0$. The voltage stability limits have also been shown using circles for both test systems.

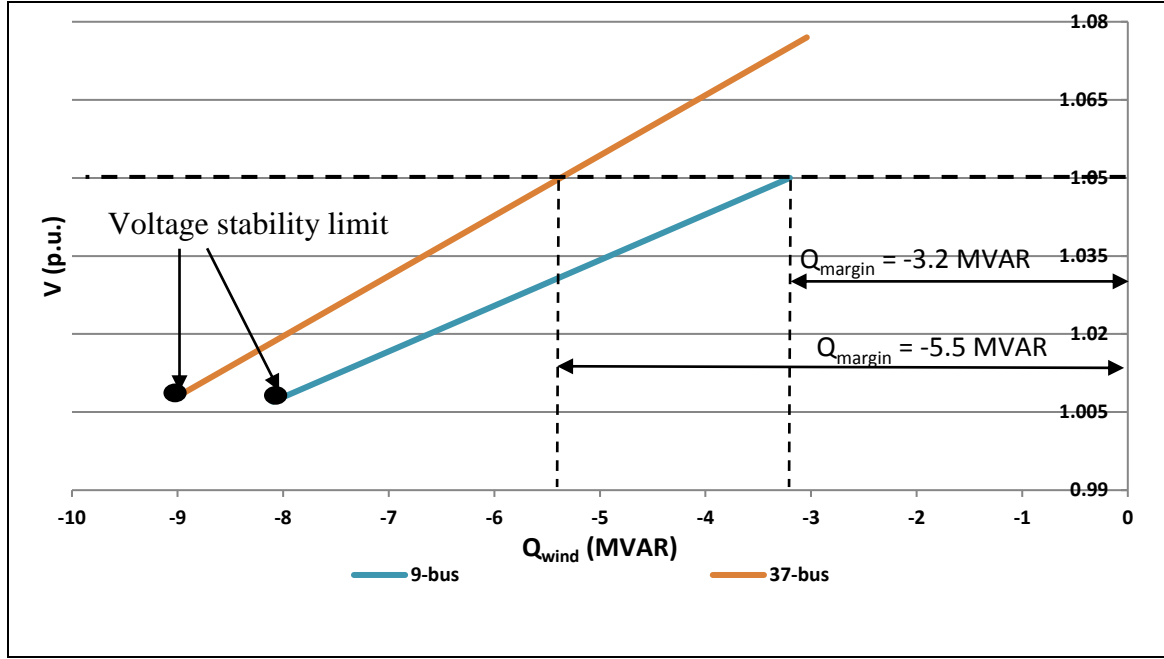


Figure 3.13 QV curves for small X/R ratios – IG-Based WPP.

The results in Figure 3.13 show that a large amount of reactive power absorption is needed to ensure that $0.95 \text{ p.u.} < V_{\text{PCC}} < 1.05 \text{ p.u.}$, when X/R_{PCC} is small. According to Figure 3.13, the reactive power absorption less than 3.2 MVAR and 5.5 MVAR causes the V_{PCC} to increase to higher than the upper boundary of the allowable steady-state voltage range (1.05 p.u.) for the 9-bus and 37-bus test systems, respectively. Figure 3.13 also shows that the voltage stability limit for both feeders is between 0.95 p.u. and 1.05 p.u. This signifies that a very large reactive power absorption at connection points with small X/R ratios can lead to voltage collapse even if the voltage remained in the normal operation range, i.e. $0.95 \text{ p.u.} < V_{\text{PCC}} < 1.05 \text{ p.u.}$

The equations representing the QV lines when $X/R_{\text{PCC}} = 0.5$ were obtained using MS Excel. The equations are as Eq. (3.17) and Eq. (3.18):

$$\text{9-bus system, SCC} = 54: \quad V = \frac{1}{115} \times Q + 1.0784 \approx \frac{1}{2 \times 54} \times Q + 1.0784 \quad (3.17)$$

$$\text{37-bus system, SCC} = 40: \quad V = \frac{1}{86} \times Q + 1.1122 \approx \frac{1}{2 \times 40} \times Q + 1.1122 \quad (3.18)$$

From Eq. (3.17) and Eq. (3.18), it was observed that for each case, the slope of the line approximately equals to the inverse of $2 \times \text{SCC}$ value. Considering that for a linear equation, derivative of the function equals to the slope of the line, the relation between ΔQ , ΔV , and SCC is generally expressed as in Eq. (3.19) when the X/R_{PCC} ratio is small.

$$\Delta V \approx \frac{1}{2 \times \text{SCC}} \Delta Q \quad (3.19)$$

From Eq. (3.19), it is demonstrated that the rate of voltage variation in response to reactive power variation at the PCC points with a small X/R ratio is approximately the inverse of $2 \times \text{SCC}$ value.

As mentioned earlier, the relation between ΔV and ΔQ for the buses with small overall X/R has not been addressed in the literature. Therefore, the first major contribution of this project is investigating the relation between ΔV , ΔQ , and SCC at the PCC points with a small X/R ratio. Comparing Eq. (3.16) and Eq. (3.19), it can be demonstrated that in two PCC points with the same SCC values and different X/R_{PCC} ratios, V_{PCC} variation due to a change of reactive power at the PCC point with the larger X/R_{PCC} ratio will be greater than that at the PCC point with the smaller X/R_{PCC} ratio. It can also be concluded that the V_{PCC} variation at PCC points with a small SCC value is more serious than that at PCC points with a high SCC value. Furthermore, large X/R_{PCC} increases the rate of voltage variation in response to the change of reactive power absorbed by the WPP. Therefore, PQ concerns will be more critical in distribution systems with small SCC and large X/R ratio at the PCC.

3.4.2.2 DFIG-Based WPP

In this section, QV analysis is carried out and presented for a DFIG-Based WPP connected to the test systems. The results consider the impacts of both small and large

X/R_{PCC} ratios. Figure 3.14 represents the QV graphs for large X/R_{PCC} ratios. The graphs have been plotted for the stable region where $dV/dQ > 0$.

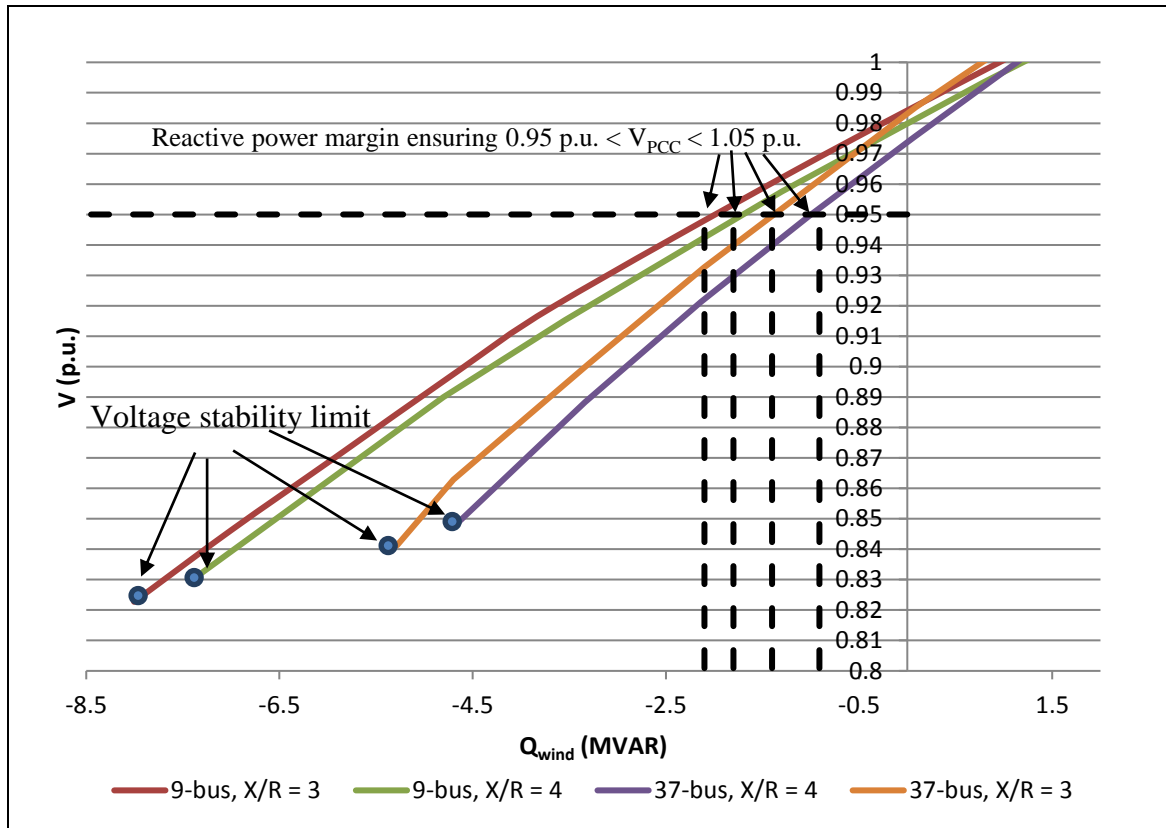


Figure 3.14 QV curves for large X/R ratios– DFIG-Based WPP.

Comparing the QV graphs obtained for DFIG in Figure 3.14 with the graphs obtained for IG in Figure 3.12, it is observed that Q_{margin} ensuring $V_{PCC} > 0.95$ p.u. in both cases is the same. However, the voltage stability limits in DFIG are far greater than those in IG. As an example, the maximum voltage drop and reactive power absorption (before voltage collapse) for the IG-Based WPP was around 0.88 p.u. and -5 MVAR as shown in Figure 3.12, while the corresponding voltage and Q values are around 0.82 p.u. and -8 MVAR for the DFIG-Based WPP as represented in Figure 3.14. Therefore, the use of DFIG increases the voltage stability limit.

The equations representing the QV lines in Figure 3.14 were obtained using MS Excel. The equations can be mathematically as in Eq. (3.20) to Eq. (3.23):

$$\text{9-bus system, SCC} = 54, \text{X/R}_{\text{PCC}} = 3: \quad V = \frac{1}{54} \times Q + 0.98 \quad (3.20)$$

$$\text{9-bus system, SCC} = 54, \text{X/R}_{\text{PCC}} = 4: \quad V = \frac{1}{54} \times Q + 0.973 \quad (3.21)$$

$$\text{37-bus system, SCC} = 40, \text{X/R}_{\text{PCC}} = 3: \quad V = \frac{1}{40} \times Q + 0.9755 \quad (3.22)$$

$$\text{37-bus system, SCC} = 40, \text{X/R}_{\text{PCC}} = 4: \quad V = \frac{1}{40} \times Q + 0.9721 \quad (3.23)$$

The QV equations obtained for DFIG, Eq. (3.20) to Eq. (3.23), are very similar with the QV equations obtained for IG, Eq. (3.12) to Eq. (3.15). Similar to the IG-Based WPP with a large X/R_{PCC} , for the PCC points with large X/R ratios connected to the DFIG-Based WPP, the ratio between ΔV and ΔQ equals to the inverse of the grid SCC (refer to Eq. (3.16)).

The QV characteristics for the DFIG-Based WPP are shown in Figure 3.15 for a small X/R_{PCC} ratio ($\text{X/R}_{\text{PCC}} = 0.5$). The graphs have been plotted for the stable region where $dV/dQ > 0$ and the voltage stability limits have been shown with circles for both test systems.

Figure 3.15 shows that the voltage stability limit for both systems is between 0.95 p.u. and 1.05 p.u. Furthermore, the QV graphs show that a minimum of 2 MVAR and 4.5 MVAR reactive power has to be drawn by the DFIG in the stiffer test system (9-bus system) and weaker test system (37-bus system), respectively, to ensure that the V_{PCC} stays below the upper boundary of allowable steady-state voltage range (1.05 p.u.). This amount of reactive power absorption could be beyond the capability of a small 9 MVA DFIG-Based WPP connected to the test systems, especially in the weaker test system, and results in shut down of the generator and voltage collapse.

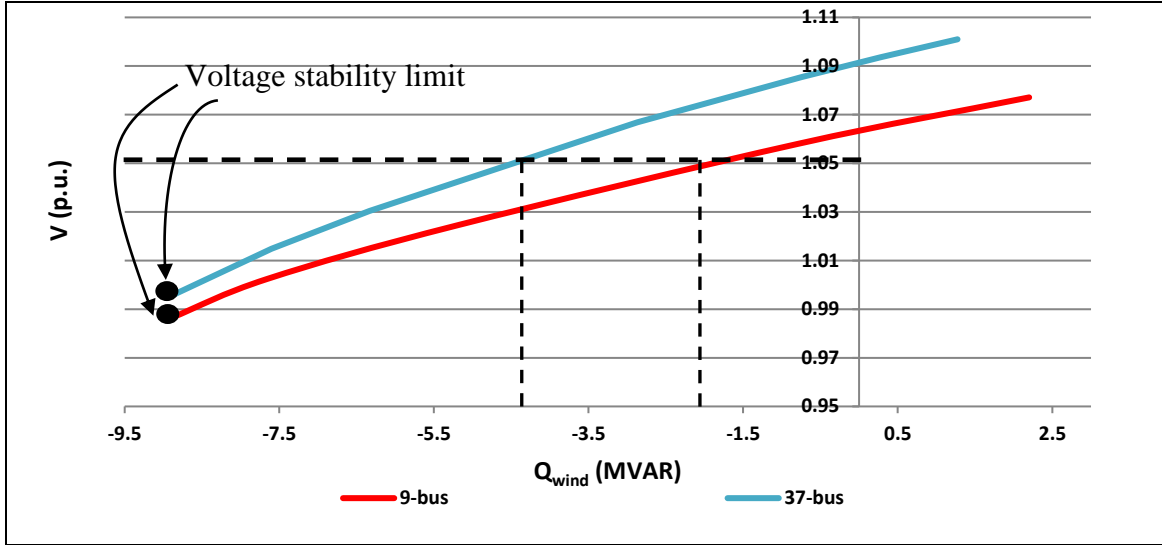


Figure 3.15 QV curves for small X/R ratios – DFIG-Based WPP.

The best fit equations for the QV lines shown in Figure 3.15 were obtained using MS Excel. The equations are as in Eq. (3.24) and Eq. (3.25):

$$\text{9-bus system, SCC} = 54: \quad V = \frac{1}{120} \times Q + 1.0624 \approx \frac{1}{2 \times 54} \times Q + 1.0624 \quad (3.24)$$

$$\text{37-bus system, SCC} = 40: \quad V = \frac{1}{90} \times Q + 1.0917 \approx \frac{1}{2 \times 40} \times Q + 1.0917 \quad (3.25)$$

According to Eq. (3.24) and Eq. (3.25), the slope of the line approximately equals with the inverse of the $2 \times \text{SCC}$ value. Therefore, similar to the equations obtained for the IG-Based WPP with a small X/R_{PCC} , the ratio between ΔV and ΔQ approximately equals to the inverse of $2 \times \text{SCC}$ values (Refer to Eq. (3.19)). This signifies that large X/R_{PCC} ratios increase the rate of voltage variation in response to changes in reactive power. It can be concluded that the V_{PCC} variation in response to changes in reactive power absorption or injection by the DFIG will be more critical in distribution systems with small SCC and large X/R ratio at the PCC.

3.5 PQ analysis

As discussed in the previous sections, PV and QV analysis can show the maximum active ($P_{\text{max-wind}}$) and reactive power ($Q_{\text{max-wind}}$) generated (or absorbed) by

the WPP while V_{PCC} stays in the allowable steady-state voltage range. PQ analysis is another method which can be used to find $P_{\max\text{-wind}}$ and $Q_{\max\text{-wind}}$ parameters. In this section, PQ analysis is used to investigate the impact of X/R_{PCC} on $P_{\max\text{-wind}}$ and $Q_{\max\text{-wind}}$. In this respect, IG-Based WPP has been selected to carry out PQ analysis for both test systems.

PQ analysis shows the amount of reactive power to be injected or absorbed by the WPP keeping V_{PCC} constant as the real power generated by the WPP increases. If the PQ curve is plotted for the boundaries of the acceptable steady-state voltage range, the $P_{\max\text{-wind}}$ and $Q_{\max\text{-wind}}$ parameters can be determined [146].

In a PQ characteristic, the $P_{\max\text{-wind}}$ occurs when the tangent to the curve becomes vertical [46]. Figure 3.16 shows the significance of the X/R ratio in the PQ characteristics for both test systems. The PQ curves have been plotted for large X/R ratios ($X/R = 3$ & 4) when the $V_{PCC} = 0.95$ p.u., as shown in Figure 3.16. The $P_{\max\text{-wind}}$ has been marked with a circle for each case. The $P_{\max\text{-wind}}$ values and the corresponding reactive power demand have also been shown in Table 3.9. In Table 3.9, positive sign signifies that power is being generated by the WPP and negative sign means power is being absorbed by the WPP.

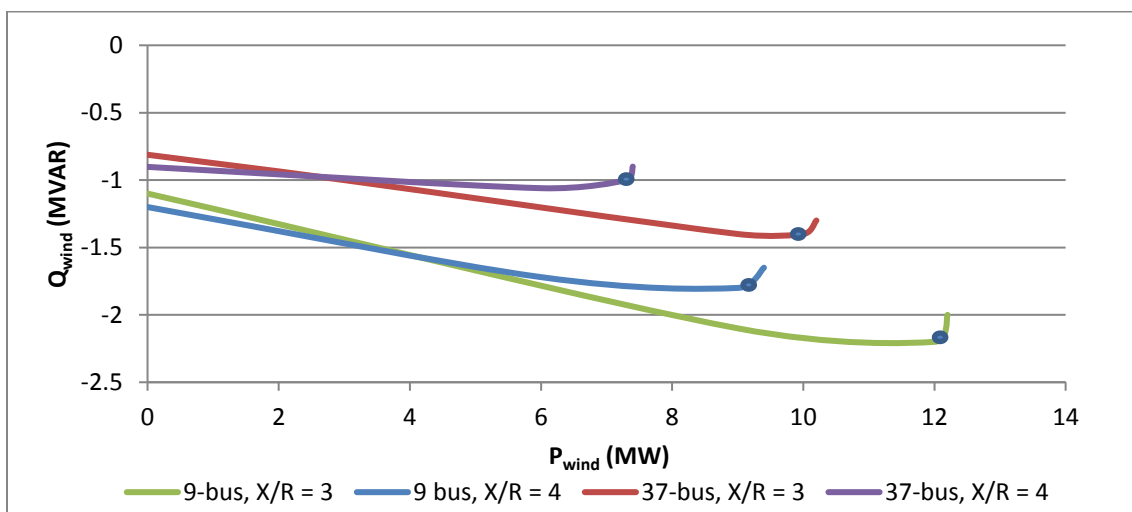


Figure 3.16 PQ curves for different X/R ratios when $V_{PCC} = 0.95$ p.u.

Table 3.9 Maximum active and reactive power generated or absorbed by the WPP for $V_{PCC} = 0.95$ p.u.

Test system	$P_{\max\text{-wind}}$ (MW)	$Q_{\max\text{-wind}}$ (MVA)
9-bus, X/R = 3	12	-2.2
9-bus, X/R = 4	9.4	-1.7
37-bus, X/R = 3	10	-1.35
37-bus, X/R = 4	7.6	-1

The results from Figure 3.16 and Table 3.9 demonstrate that the $P_{\max\text{-wind}}$ in a system with a large SCC at the PCC (9-bus system with SCC = 54) is greater than that in a system with a smaller SCC at the PCC (37-bus with SCC = 40). This means that a bus with a large SCC can accept greater levels of wind power generation. Also, higher X/R_{PCC} ratios decrease $P_{\max\text{-wind}}$ in each feeder. For example, $P_{\max\text{-wind}}$ reduced from 12 MW to 9.4 MW in X/R_{PCC} going from 3 to 4 in the 9-bus test feeder. The highest $P_{\max\text{-wind}}$ was observed for the case with the highest SCC and lowest X/R_{PCC} (9-bus system, SCC = 54, and X/R_{PCC} = 3), while the lowest $P_{\max\text{-wind}}$ was observed for the case with the lowest SCC and highest X/R_{PCC} ratio (37-bus system, SCC = 40, and X/R_{PCC} = 4). As discussed in the previous section, $P_{\max\text{-wind}}$ is the sum of P_{margin} and P_{rated} ($P_{\max\text{-wind}} = P_{\text{margin}} + P_{\text{rated}}$). Considering that P_{rated} is 9 MW and comparing the results from Table 3.2, Table 3.3, and Table 3.9, it can be demonstrated that the PV and PQ analysis studies also gave the same results for the $P_{\max\text{-wind}}$.

Results also show that small SCC and large X/R_{PCC} ratios decrease the capability of the system to provide reactive power requirements. The highest reactive power that could be delivered from the grid to the IG is for the case with the highest SCC and lowest X/R ratio (9-bus system, SCC = 54, and X/R_{PCC} = 3), while the lowest reactive power that the grid can deliver to an IG was observed for the case with the lowest SCC and highest X/R_{PCC} ratio (37-bus system, SCC = 40, and X/R_{PCC} = 4).

3.6 Effect of SCR and X/R ratios on voltage profile

As mentioned in Section 3.2, the ratio between rated wind power and grid SCC impacts on the voltage stability of a distribution system. Referring to Section 2.5 in the previous chapter, the ratio between these two parameters is expressed by the SCR value. This section investigates the effect of X/R_{PCC} and SCR ratios on the V_{PCC} profile. The V_{PCC} -SCR characteristic was plotted for different X/R_{PCC} ratios. Similar to the QV and PV studies, analysis has been carried out for both IG and DFIG-Based WPP systems connected to the 9-bus test system with an SCC of 54 MVA and 37-bus test system with an SCC of 40 MVA. For each case, the SCC was divided by different WPP ratings in order to plot the characteristics of the V_{PCC} versus SCR for different X/R_{PCC} ratios. The results are presented as shown in Figures 3.17 to 3.20.

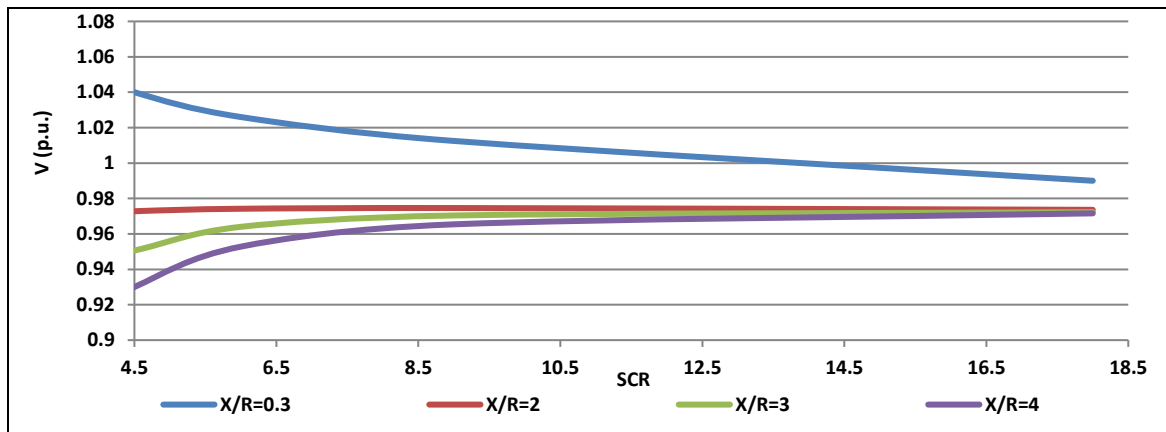


Figure 3.17 V_{PCC} -SCR characteristic in the IG-Based 9-bus test system.

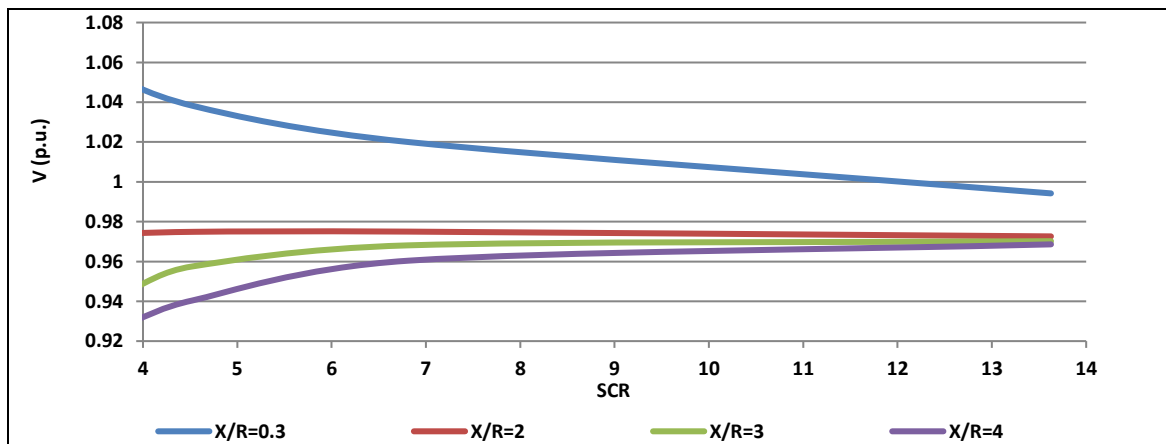


Figure 3.18 V_{PCC} -SCR characteristic in the IG-Based 37-bus test system.

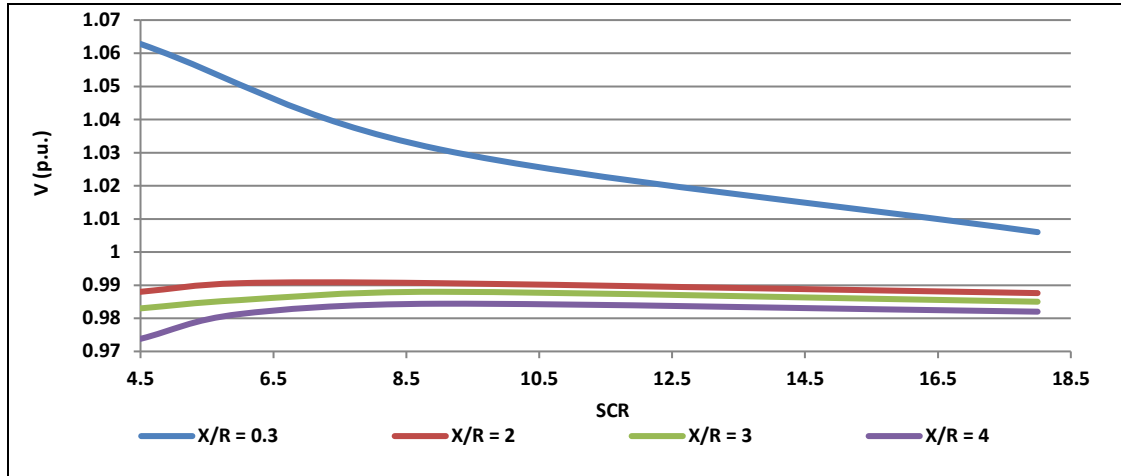


Figure 3.19 V_{PCC} -SCR characteristic in the DFIG-Based 9-bus test system.

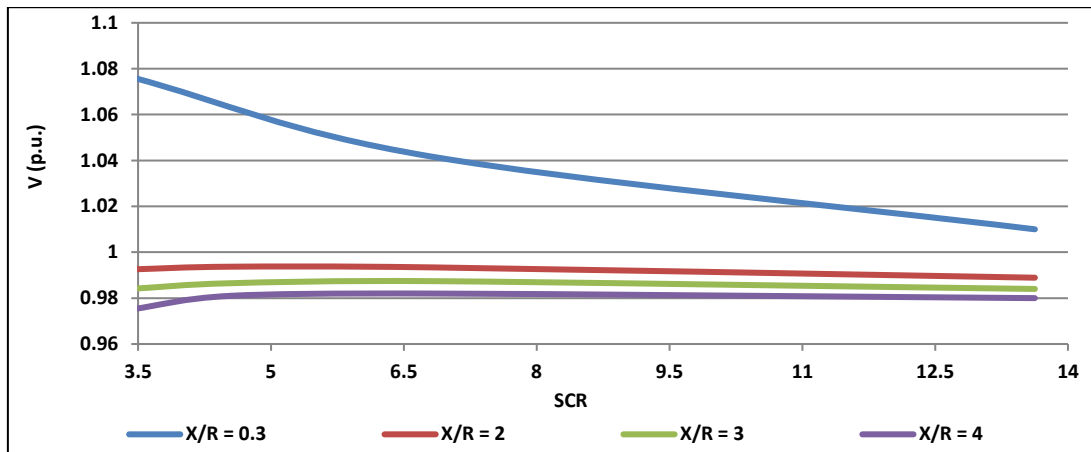


Figure 3.20 V_{PCC} -SCR characteristic in the DFIG-Based 37-bus test system.

For the IG-Based WPP, Figures 3.17 and 3.18 show that the change of SCR significantly changes V_{PCC} when the system is weak ($SCR < 10$). In this SCR range, the voltage variation at the PCC points with a small X/R_{PCC} ratio is more serious than that at the PCC points with a large X/R ratio. In the case of DFIG-Based WPP, the graphs in Figures 3.19 and 3.20 show that the V_{PCC} variation due to the changes in the SCR ratio is small for large X/R_{PCC} ratios even for $SCR < 10$. This is because as demonstrated in Section 3.4.1.2, DFIG has a high capability in injecting reactive power in order to regulate the voltage within the allowable steady-state voltage range. However, for a small X/R_{PCC} where the V_{PCC} is generally high and the reactive power has to be

absorbed by the DFIG, V_{PCC} variation in response to the changes in SCR is significant when $SCR < 10$.

The results for both IG and DFIG-Based WPP show that the voltage variation in response to a change in SCR in WPP with an $SCR > 10$ is not as significant as that in WPPs with an $SCR < 10$ for different X/R ratios. This demonstrates that the PQ concerns will not be critical in stiff PCC buses where $SCR > 10$ regardless of the X/R ratios. Furthermore, the results demonstrate that $X/R_{PCC}=2$ is the optimum X/R ratio where V_{PCC} variation in response to a change in wind power penetration and SCR value is minimum.

Generally, it was observed that there is a relation between V_{PCC} and two important characteristics of a distribution system: X/R_{PCC} and SCR. Considering that the SCR ratio represents the relation between the grid SCC and P_{rated} of the WPP, proposing a mathematical relation between V_{PCC} , SCR, and X/R_{PCC} enables to plot the PV curve for the feeders with different SCC and X/R_{PCC} values. This achievement, in turn, can provide insightful information to identify the stiffer buses, where the X/R and SCC values would ensure that the V_{PCC} profile and ΔV_{PCC} would be in accordance with the grid code requirements. These buses, then, can be chosen as potential common coupling points to connect the WPP to. In this respect, next chapter proposes a voltage stability analytical model to mathematically define the relation between V_{PCC} and the PCC parameters.

3.7 Conclusion

In the recent years, voltage stability is considered as an important concern in the assessment of power systems reliability. This chapter has addressed issues concerned with the interconnection of WPP to distribution systems through detailed voltage

stability analysis. The highlights of the research carried out in this chapter are itemized below.

- It was shown that V_{PCC} variations depend on the short-circuit impedance angle ratio (X/R), the grid SCC, the SCR ratio, the active power injected by the WPP, and the reactive power injected or absorbed by the WPP.
- PV analysis for the IG-Based WPP demonstrated that an increase in P_{wind} may push voltage out of the acceptable steady-state range at connection points with large or small X/R ratios. It was shown that ΔV at PCC buses with a small X/R ratio was larger than that at PCC buses with a large X/R ratio. Furthermore, it was observed that the ΔV value at PCC points with a small SCC was greater than that at PCC points with a large SCC.
- PV analysis for the DFIG-Based WPP demonstrated that step changes in V_{PCC} due to changes in wind power penetration is significant at PCC points with a small X/R ratio. Similar to the IG scenario, DFIG is not able to regulate V_{PCC} and maintain it within the allowable steady-state voltage range at PCC points with a small X/R ratio when wind power penetration is high. Therefore, DFIG is not suitable for low X/R ratio PCCs.
- The ΔV value at the PCC point of a DFIG-Based WPP with a small X/R is greater than that at the PCC of an IG-Based WPP with a small X/R_{PCC} . Hence, P_{margin} for a DFIG WPP would be lower than the P_{margin} of an IG-Based WPP at small X/R_{PCC} ratio connections points. This study has therefore proven that IG is a better option for PCC points with low X/R_{PCC} ratios.
- PV analysis for the DFIG-Based WPP also demonstrated that voltage regulation would not be an issue at PCC points with large X/R ratios. The high capability

of DFIG in injecting reactive power enables DFIG to maintain V_{PCC} within the acceptable steady-state range at PCC points with large X/R_{PCC} ratios even for very large penetration of wind power.

- The QV analysis showed that the voltage stability limit for a DFIG-Based WPP is greater than that of an IG-Based WPP at PCC points with a large X/R ratio. QV analysis for both IG and DFIG demonstrated that V_{PCC} variation at PCC points with a small SCC value and a large X/R_{PCC} ratio is more serious than V_{PCC} variation at PCC points with a high SCC value and a small X/R_{PCC} ratio.
- As one of the major contributions of this project, it was shown that the rate of change in voltage in response to changes in the reactive power absorbed or injected by the IG or DFIG-Based WPPs at PCC points with a small X/R ratio is smaller than that at PCC points with a large X/R ratio. Large X/R_{PCC} increases the rate of voltage variation in response to changes in reactive power absorbed by the WPP. For both IG and DFIG, the voltage collapse may occur when V_{PCC} is within the allowable steady-state voltage range for small X/R_{PCC} ratios.
- PQ analysis demonstrated that the maximum allowable wind power generation is greater in a system with a large SCC than in a system with a smaller SCC. Also, higher X/R_{PCC} ratios decrease $P_{max-wind}$ at the PCC point.
- The V-SCR characteristics showed that for weak connection points, where $SCR < 10$, PQ requirements will be problematic in an IG-Based WPP at connection points with very small or large X/R_{PCC} ratios, and in the case of a DFIG-Based WPP at connection points with very small X/R_{PCC} ratio. On the other hand, for both IG and DFIG-Based WPP, it was demonstrated that the PQ concern will

not be significant in strong PCC points where $SCR > 10$ regardless of the X/R ratio.

- It was discussed that $X/R = 2$ is the optimal X/R_{PCC} ratio where V_{PCC} has the lowest variations in response to a change in wind power penetration and SCR value.

Generally, the results in this Chapter revealed that there is a relation between V_{PCC} , X/R_{PCC} , the grids SCC, and the wind power penetration. Next chapter introduces an analytical model to mathematically define the relation between these parameters.

Chapter 4 - Genetic Algorithm-Based Analytical Model for the PCC Voltage Stability Analysis

4.1 Introduction

Chapter 3 dealt with the analysis of the interconnection effects of WPPs on the voltage stability at a specific connection point. As mentioned therein, it was demonstrated that the PCC bus voltage (V_{PCC}) variation depends on three factors: the short-circuit impedance angle ratio seen at the PCC (X/R_{PCC}), the grid's SCC, and the rated wind power capacity of the proposed WPP. As discussed in Chapter 2, the need for mathematical formula expressing the relationship between these grid parameters and the network voltage is still a noticeable gap in the literature. Such formula would allow an initial predictive analysis on the voltage stability at a given connection point to check conformance with the grid codes. In this chapter, the focus is on the derivation of mathematical relations between V_{PCC} , the WPP size, and the PCC parameters, i.e. SCC and the X/R ratio.

The major concern was to select an appropriate method and strategy for developing such an analytical model. In this respect, a sensitivity analysis was carried out to find a numerical relation between V_{PCC} and X/R_{PCC} in different test systems with different SCR values. As discussed in Chapter 2, the ratio between the grid's SCC and the rated wind power is expressed by the SCR parameter. The obtained numerical results were used to plot the V_{PCC} - X/R_{PCC} characteristics for each test system. This was the first step before further detailed studies on the proposed numerical models could be conducted. Later on, a Genetic Algorithm (GA)-Based analytical model was developed capable of predicting the V_{PCC} profile given the X/R_{PCC} and SCR ratios for a particular

PCC bus. The proposed equations were then rewritten in terms of V_{PCC} as a function of X/R_{PCC} , SCC , and wind active power (P_{wind}). In this case, a series of mathematical equations were developed using the V-X/R characteristics obtained in the first step. The GA approach was used to determine the values of the coefficients of the proposed equations for the lowest deviation with respect to the reference V-X/R characteristics obtained in the first step. The key advantages of the analytical model are:

- It allows steady-state voltages to be determined at the PCC given P_{wind} , SCC and X/R ratios
- It allows step changes on the steady-state voltage levels (ΔV_{PCC}), resulting from switching operations, to be predicted at a given bus
- It would allow maximum real-power output ensuring voltage stay within the acceptable steady-state range ($P_{max-wind}$) to be estimated at a given connection point

4.2 Voltage versus X/R ratio characteristic

This section aims to demonstrate how V_{PCC} will behave for different X/R ratios at a particular connection point. In this respect, a sensitivity analysis was carried out to gather datasets, which were used to identify a numerical relation between V_{PCC} and X/R_{PCC} . Four test systems were investigated using IEEE distribution models: two test systems based on 9-bus IEEE distribution network model and two systems based on 37-bus IEEE distribution network model. The reason for analysing four different test systems is to increase the validity of the developed ideas in considering different topologies and SCR values.

The values of frequency, nominal voltage, and base power of the test distribution systems, the specification of the WPPs, and the line parameters are as discussed in

Chapter 3, Section 3.3. For the two 9-bus test systems, the PCC bus and the buses connected to the load (PQ buses) are as presented in Figures 3.2 in Chapter 3. Furthermore, for the two 37-bus test systems, the PCC bus and the PQ buses are as shown in Figure 3.3 in Chapter 3. The load values for the 9-bus and 37-bus test systems are as presented in Table B.4 in Appendix B.

In each test distribution system, the reactive power compensation before the WPP connection is provided through capacitor banks in a way that V_{PCC} is around 0.98 p.u. while the WPP is not connected to the grid. Hereinafter, the value of the voltage at the PCC bus before the WPP connection is called $V_{PCC_initial}$. Hence, in this chapter, the mathematical relations have been developed regarding that the $V_{PCC_initial} = 0.98$ p.u. The lines length and number of connected WTGs are different amongst the test systems resulting in different SCR values. Table 4.1 shows the topologies considered, SSC value, the number of connected WTG, and the SCR value for each test. Similar to the analysis studies carried out in Chapter 3, the active power injected by each WTG is considered to be 3 MW.

Table 4.1 Topology and SCR value for each for test distribution system.

Case study	Topology	Connection point	SCC	No. of connected WTGs	P_{rated}	SCR
Test 1	IEEE 37 - bus system	Bus 6	27	3	9	3
Test 2	IEEE 37 - bus system	Bus 6	40	3	9	4.5
Test 3	IEEE 9 - bus system	Bus 9	54	3	9	6
Test 4	IEEE 9 - bus system	Bus 9	21	1	3	7

As mentioned in Chapter 2, the grid strength at the PCC is numerically expressed as the SCR value [54]. Furthermore, it was discussed that the SCR value depends on SCC and the inverse of P_{wind} . As shown in Table 4.1, the SCR ratios in all four tests are less than 10 classifying the test systems as weak distribution systems. The first test system has the lowest SCR value and is, therefore, the weakest system amongst the test systems considered. In Test 4, although the SCC value is smaller than that in the other

test systems, the wind power penetration is smaller than that in the other tests. As shown, only one 3 MVA WTG has been connected to the PCC point of Test 4. Therefore, the consequent ratio between SSC and wind power penetration in Test 4 is larger than that in the other tests (SCR=7) making the PCC point in Test 4 stiffer than that in the other test systems.

As discussed in previous Chapters, very small or large X/R_{PCC} ratios may push the voltage out of the acceptable steady-state range at a given connection point. It was also shown that X/R_{PCC} ratio has a larger adverse impact on voltage stability as the wind power penetration increases and the SCR ratio decreases. Hence, in V-X/R analysis studies, the X/R ratio limits the SCR range for which steady-state voltage stability can be achieved.

The X/R ratio range, analysed in this study, was derived from an analysis of real-world distribution networks. Reginato et. al [56] carried out a research study concerned with an analysis of potentially viable X/R range, to satisfy the grid code requirements, for a given integration level (ρ). The main idea was to investigate how V_{PCC} varies in response to changes in P_{wind} for a specific value of X/R_{PCC} . Given that SCC was fixed, the integration level changed as wind power changed. In V-X/R characteristics presented in this section, the range of X/R and the corresponding SCR value, are based on the ρ -X/R graphs presented in [56].

In each test system, the X/R_{PCC} ratio was changed to monitor the V_{PCC} profile for each X/R_{PCC} value in a fixed SCR network. However, the value of SCR is different among the four test systems as mentioned in the previous section. Therefore, comparing and contrasting the V-X/R characteristics among the four test systems will demonstrate

the effect of X/R_{PCC} ratio on V_{PCC} for different SCR values. Analyses have been carried out based on two types of WTGs widely used in the WPPs, i.e. the IG and DFIG.

4.2.1 IG-Based WPP

Figure 4.1 shows the V_{PCC} - X/R_{PCC} characteristic for each test where an IG-Based WPP is connected to the test distribution network.

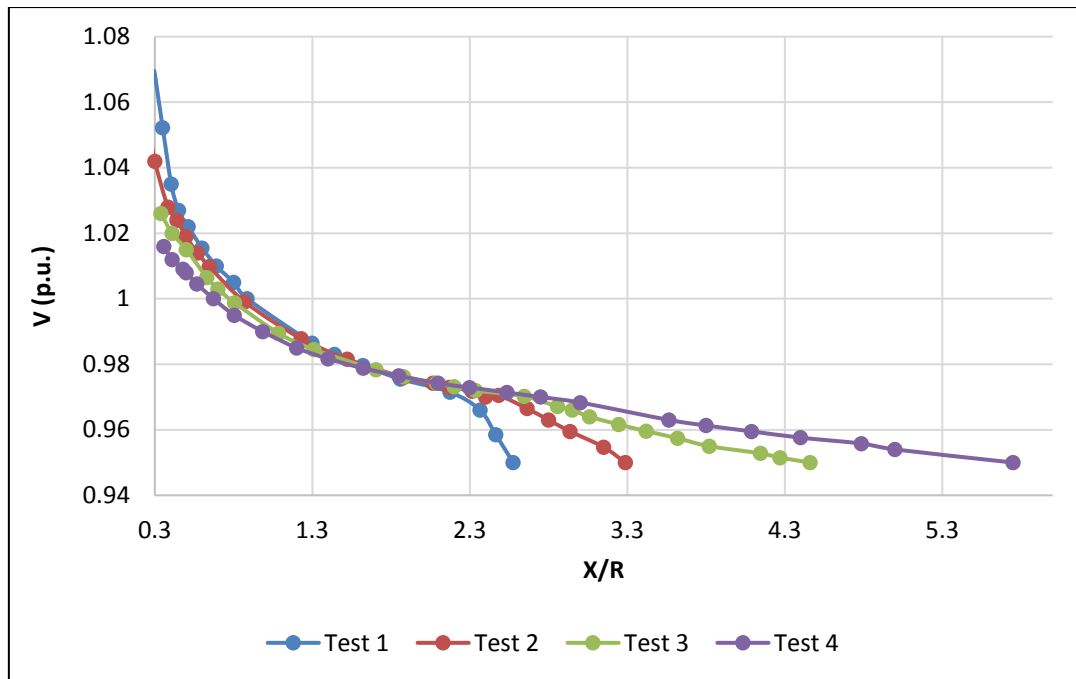


Figure 4.1 V_{PCC} - X/R_{PCC} characteristic for each test system – IG-Based WPP.

As shown in Figure 4.1, V_{PCC} is high for small X/R_{PCC} ratios, especially in test systems with a small SCR ratio. For example, voltages is higher than the upper boundary of allowable steady-state range ($V_{PCC} > 1.05$) in the weakest test system (Test 1 with SCR = 3) for a small X/R_{PCC} ratio ($X/R_{PCC} = 0.3$). However, for the stiffest test system (Test 4 with SCR = 7), small X/R_{PCC} ratios do not increase voltage significantly.

Figure 4.1 also shows that V_{PCC} is generally lower for large X/R_{PCC} ratios. The impact of an increase in the X/R_{PCC} ratio on voltage will be even more critical in the weaker systems. For example, for the weakest test system (Test 1), the X/R_{PCC} margin is around 2.6, after which the bus voltage would collapse below 0.95 p.u. On the other

hand, in the stiffest test system (Test 4), the X/R_{PCC} margin is almost 5.5 before the bus voltage collapses below the lower bound of the steady-state voltage range. This shows that in stiff systems, a greater range of connection points can potentially be used for the interconnection of wind farms, whereas the range of the connection points in a weak network is limited to buses with a relatively low X/R value. This also potentially signifies that in weak systems, heavier voltage regulation may potentially be required if the wind farm is to be connected to a PCC point with a high X/R value.

The SCR value is different among the four tests, but the V - X/R characteristics of all four systems intersect each other when X/R is around 2, as shown in Figure 4.1. This confirms the discussion presented in the Chapter 3 (Section 3.6) that $X/R = 2$ causes the lowest voltage variation regardless of the SCR value in an IG based WPP [56, 144].

4.2.2 DFIG-Based WPP

Figure 4.2 shows the V_{PCC} - X/R_{PCC} characteristic for each test distribution system when a DFIG-Based WPP is connected to the network.

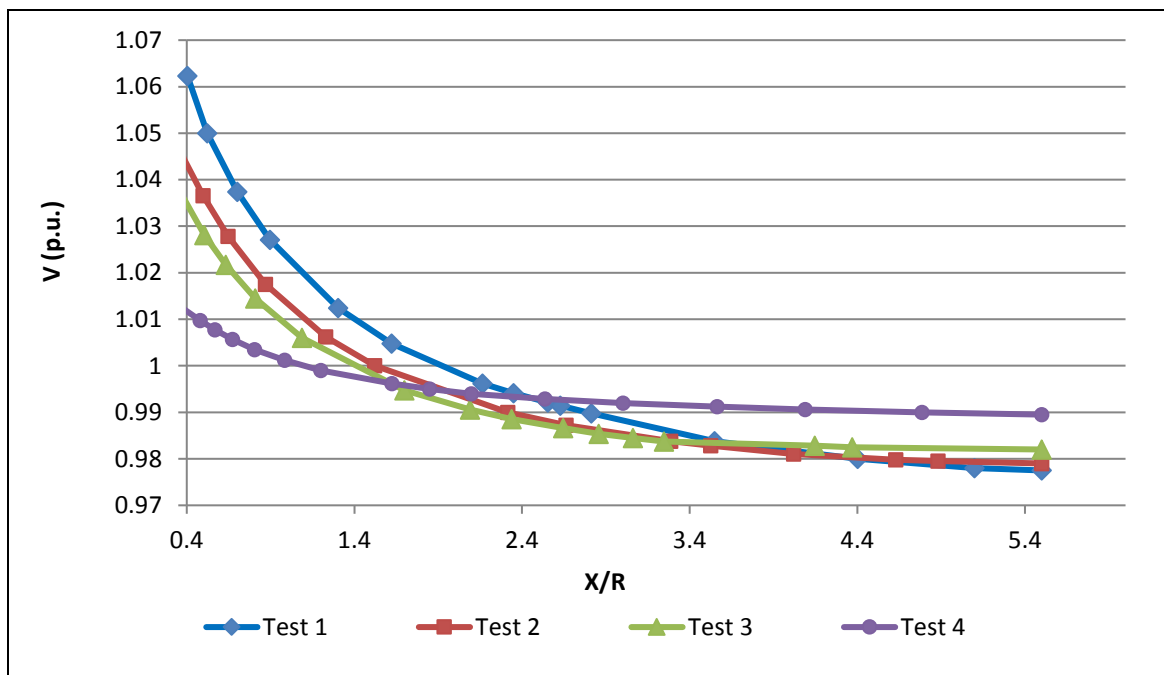


Figure 4.2 V_{PCC} - X/R_{PCC} characteristic for each test system - DFIG-Based WPP.

For the DFIG-Based WPP, similar to the IG-Based WPP, V_{PCC} is high when X/R_{PCC} is small. This may result in voltages higher than the upper boundary of allowable steady-state range (1.05 p.u.) especially when the SCR ratio seen from the connection point is very small. From Figure 4.2, it is clear that V_{PCC} is greater than 1.05 p.u. when the X/R_{PCC} ratio is very small ($X/R < 0.5$) and the test system is weak (Test 1). However, V_{PCC} is within the acceptable range for all other test systems even when $X/R < 0.5$. The results demonstrate that, in a DFIG-Based WPP, the sensitivity and variation of bus voltage with respect to changes in the X/R_{PCC} and SCR ratios is high only when X/R_{PCC} is less than 2. Comparing the V-X/R characteristics in Figures 4.1 and 4.2, it can be observed that the sensitivity of V_{PCC} to changes in the X/R_{PCC} and SCR ratios for the DFIG-Based WPP is similar to that in an IG-Based WPP when X/R_{PCC} is small ($X/R_{PCC} < 2$). However, for the DFIG-Based WPP, the variation of V_{PCC} with respect to changes in X/R_{PCC} and SCR is very small when X/R_{PCC} is large ($X/R_{PCC} > 2$), as shown in Figure 4.2. This is because as discussed earlier in Chapter 3, DFIG has a high capability in maintaining V_{PCC} within the allowable steady-state range through reactive power injection when the X/R_{PCC} ratio is high. Hence, for a DFIG-Based WPP connected to a distribution network with a large X/R_{PCC} ratio, the voltage regulation requirement is not an issue even for large wind power penetration (low SCR ratio).

Generally, the V-X/R characteristics show that both small and large X/R_{PCC} ratios adversely impact the V_{PCC} and may push the voltage out of the allowable steady-state range in IG-Based WPPs. For DFIG-Based WPPs, the voltage regulation requirement is problematic only at the connection points with a small X/R ratio, while V_{PCC} usually stays between the 0.95 p.u. and 1.05 p.u. at connection points with large X/R ratios.

The following section presents how the numerical datasets and V-X/R characteristics presented in this section have been used in this study to develop mathematical formulations between V_{PCC} , X/R_{PCC} , and SCR for both IG and DFIG-Based WPPs.

4.3 Developing mathematical relations

As the main contribution of this research, this section proposes mathematical formulations between V_{PCC} , and the key parameters of a distribution network, i.e. X/R_{PCC} and SCR. The relations have been developed for both IG and DFIG-Based WPPs. In the case of the IG-Based WPP, the mathematical relations were developed for both small and large X/R_{PCC} ratio ranges. This is because as demonstrated in Figure 4.1, both small and large X/R_{PCC} ratios impose PQ concerns and voltage regulation challenges at the PCC of IG-Based WPP. In the case of the DFIG-Based WPP, the numerical model has only been developed for small X/R_{PCC} ratios. This is due to the fact that as demonstrated in Figure 4.2, large X/R ratios do not cause a major impact on the V_{PCC} of a DFIG-Based WPP, or voltage regulation requirements at the PCC.

For both IG and DFIG-Based WPPs, general forms of alternative equations, which can be used to describe the relation between V_{PCC} , X/R_{PCC} , and SCR, were first developed, and the coefficients of the equations were later identified using a GA based approach. Finally, the accuracy of each alternative equation was investigated in order to identify the best fit equation for each X/R ratio range.

4.3.1 General form of alternative functions for IG-Based WPPs

In this section, a numerical model is developed to mathematically express the relation between voltage, X/R, and SCR at the PCC of an IG-Based WPP. The main

idea is to develop mathematical formulations which fit the V-X/R curve characteristics presented in Figure 4.1. Mathematical formulas have been developed as the best curve-fit expressions to mathematically define the V_{PCC} - X/R_{PCC} characteristic shown in Figure 4.1, for the $X/R_{PCC} < 2$ and the $X/R_{PCC} > 2$ ranges separately. The mathematical relations were developed for two important characteristics observed and illustrated in Figures 3.4 and 3.5 in Chapter 3. Table 4.2 summarises these characteristics.

Table 4.2 Characteristics considered for developing mathematical relations for IG-Based WPPs.

Characteristic	Description
Characteristic 1	The increase in wind power penetration (small SCR ratio) increases V_{PCC} at feeders with a small X/R ratio
Characteristic 2	The increase in wind power penetration decreases V_{PCC} at feeders with a large X/R ratio

Considering the shape of the V-X/R characteristic curves in Figure 4.1, two possible mathematical functions can be considered for expressing the relationships between V_{PCC} , X/R_{PCC} and SCR ratio for both small and large X/R_{PCC} ranges. The general forms of these functions are as shown in Eqs. (4.1) and (4.2).

Function 1 - V_{PCC} - X/R_{PCC} (Polynomial with an order of 2)

$$V_{PCC} = A_0 - A_1 \times \left(\alpha \times \frac{X}{R}\right) + A_2 \times \left(\alpha \times \frac{X}{R}\right)^2 \quad (4.1)$$

Function 2 - V_{PCC} - X/R_{PCC} (Exponential function)

$$V_{PCC} = B_0 + B_1 \times e^{(-\beta \times \frac{X}{R})} \quad (4.2)$$

Where A_0 , A_1 , A_2 , B_0 , and B_1 are positive coefficients. And, α and β are polynomial and exponential decay coefficients, respectively.

Eqs. (4.1) and (4.2) are two possible equations which can fit the reference graphs shown in Figure 4.1. Mathematically, it was tested and verified that the V-X/R characteristics plotted by the polynomial equation (4.1) and exponential equation (4.2)

are similar to each other. Therefore, both Eqs. (4.1) and (4.2) can be utilised to model the relation between voltage and X/R. Investigating different mathematical functions enabled the author to compare the accuracy of each function and choose the best-fit function with the highest accuracy.

Figure 4.3 shows the V-X/R characteristic given by the alternative equations for different values of decay coefficients.

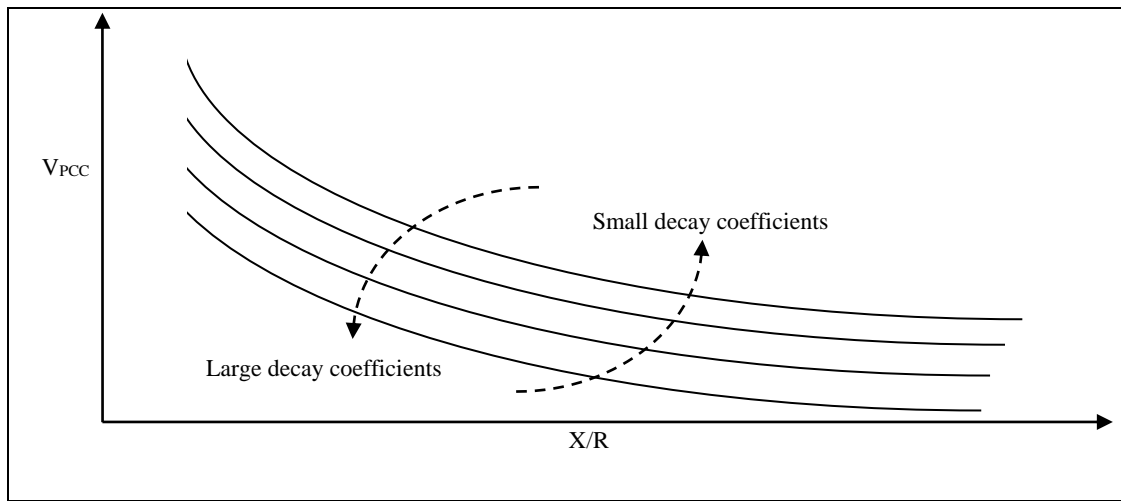


Figure 4.3 Characteristic of the alternative Eqs. (4.1) and (4.2).

From Figure 4.3, it can be mathematically verified that in exponential and polynomial functions such as Eq. (4.1) and Eq. (4.2), lower values of decay coefficients (α and β) increase the value of the function, while higher values of decay coefficient decrease the value. Referring to Characteristic 1 in Table 4.2, V_{PCC} increases in response to an increase in wind power penetration when the X/R_{PCC} ratio is small ($X/R_{PCC} < 2$). On the other hand, an increase in wind power penetration makes SCR smaller. Therefore, small SCR ratios increase V_{PCC} when $X/R_{PCC} < 2$. Hence, it can be concluded that there must be a direct relation between decay coefficients and SCR when X/R_{PCC} is small ($X/R_{PCC} < 2$), and these can be expressed as shown in Eqs. (4.3) and (4.4):

$$\alpha = a \times \text{SCR} \quad \text{when } X/R_{PCC} < 2 \quad (4.3)$$

$$\beta = b \times SCR \quad \text{when } X/R_{PCC} < 2 \quad (4.4)$$

Where a and b are positive values.

In the case of decay coefficients (α and β) for large X/R_{PCC} ratios ($X/R_{PCC} > 2$), referring to Characteristic 2 in Table 4.2, V_{PCC} decreases in response to an increase in wind power penetration. On the other hand, an increase in wind power penetration makes SCR smaller. Therefore, small SCR ratios decrease V_{PCC} when $X/R_{PCC} > 2$. It can then be concluded that there must be an inverse relation between decay coefficients and SCR for large X/R_{PCC} ($X/R_{PCC} > 2$) ratios, and these can be expressed as in Eqs. (4.5) and (4.6):

$$\alpha = \frac{c}{SCR} \quad \text{when } X/R_{PCC} > 2 \quad (4.5)$$

$$\beta = \frac{d}{SCR} \quad \text{when } X/R_{PCC} > 2 \quad (4.6)$$

Where c and d are positive values

Considering the relations between decay coefficients (α and β) and the SCR ratio given in Eqs. (4.3) to (4.6), the general forms of the alternative Eqs. (4.1) and (4.2) can be rewritten as follows:

$$V_{PCC} = A_{sr0} - A_{sr1} \times \left(SCR \times \frac{X}{R} \right) + A_{sr2} \times \left(SCR \times \frac{X}{R} \right)^2 \quad \text{when } \frac{X}{R} < 2 \quad (4.7)$$

$$V_{PCC} = B_{sr0} + B_{sr1} \times e^{(-B_{sr2} \times SCR \times \frac{X}{R})} \quad \text{when } \frac{X}{R} < 2 \quad (4.8)$$

$$V_{PCC} = A_{lr0} - A_{lr1} \times \left(\frac{1}{SCR} \times \frac{X}{R} \right) + A_{lr2} \times \left(\frac{1}{SCR} \times \frac{X}{R} \right)^2 \quad \text{when } \frac{X}{R} > 2 \quad (4.9)$$

$$V_{PCC} = B_{lr0} + B_{lr1} \times e^{(-B_{lr2} \times \frac{1}{SCR} \times \frac{X}{R})} \quad \text{when } \frac{X}{R} > 2 \quad (4.10)$$

Where A_{sr0} , A_{sr1} , A_{sr2} , B_{sr0} , B_{sr1} are the coefficients for the $X/R < 2$ range, and A_{lr0} , A_{lr1} , A_{lr2} , B_{lr0} , B_{lr1} are the coefficients for the $X/R_{PCC} > 2$ range.

Referring to Eqs. (4.1) to (4.6), the coefficients of the alternative equations can be formulated as follows:

$$A_{sr1} = a \times A_1 \quad (4.11) \quad A_{sr2} = a^2 \times A_2 \quad (4.12)$$

$$A_{lr1} = c \times A_1 \quad (4.13) \quad A_{lr2} = c^2 \times A_2 \quad (4.14)$$

$$B_{sr2} = b \quad (4.15) \quad B_{lr2} = d \quad (4.16)$$

4.3.2 General form of alternative functions for DFIG-Based WPP

Similar to the IG-Based WPP, the general forms of two possible equations can be formulated for modelling the relation between V_{PCC} , X/R_{PCC} , and SCR in a DFIG-Based WPP. These were developed using the V-X/R characteristics presented in Figure 4.2. As mentioned earlier, in a DFIG-Based WPP, V_{PCC} can be easily maintained within the allowable steady-state range at large X/R connection points because of the high capability of the DFIG in regulating the terminal voltage through reactive power injection.

However, the limited capacity of DFIG in absorbing reactive power under overvoltage conditions imposes serious voltage stability problems at weak connection points with a small X/R ratio. Therefore, the proposed alternative equations were only developed for the small X/R_{PCC} range, i.e. $X/R_{PCC} < 2$. As discussed in Section 4.2.2, in this X/R range, the V-X/R characteristic for DFIG-Based WPPs are similar to the V-X/R characteristics of the IG-Based WPPs. Hence, for the DFIG-Based WPP with a small X/R_{PCC} , the same alternative equations developed for the small X/R_{PCC} IG-Based WPP case can be used, the general forms of which are as follows:

$$V_{PCC} = C_0 - C_1 \times \left(SCR \times \frac{X}{R}\right) + C_2 \times \left(SCR \times \frac{X}{R}\right)^2 \quad \text{when } \frac{X}{R} < 2 \quad (4.17)$$

$$V_{PCC} = D_0 + D_1 \times e^{(-D_2 \times SCR \times \frac{X}{R})} \quad \text{when } \frac{X}{R} < 2 \quad (4.18)$$

Where C_0 , C_1 , C_2 , D_0 , D_1 , and D_2 are positive coefficients.

Eqs. (4.7) to (4.10), and Eqs. (4.17) and (4.18) provide insightful information enabling the mathematical formulation of relations between V_{PCC} , X/R_{PCC} , and SCR . However, determination of the coefficients was the most important step and proven quite challenging. The following section discusses how a GA-Based approach was used in this study to identify the coefficients.

4.3.3 Genetic Algorithm

In the previous section, the general forms of the mathematical relations between V_{PCC} , X/R_{PCC} , and SCR were developed. Yet, the values of the coefficients of the developed relations must be precisely determined before these can be applied for predicting the voltage behavior at a given PCC bus.

Regression analysis is one of the approaches used in the literature for estimating the coefficients of a statistical model given data. However, as an advanced technique, this work proposes a Genetic Algorithm (GA) technique for identifying the coefficients' values. The values of the coefficients must ensure that the V-X/R characteristics predicted by the proposed equations provide the best fit for the reference V-X/R graphs shown in Figures 4.1 and 4.2.

The Genetic Algorithm is a searching method for solving both constrained and unconstrained optimization problems based on probabilistic search methods developed

using the ideas of evolutionary processes [147]. GA approach is based on the Darwinian concept of the continuity of the fittest. Figure 4.4 shows a flowchart of the GA concept.

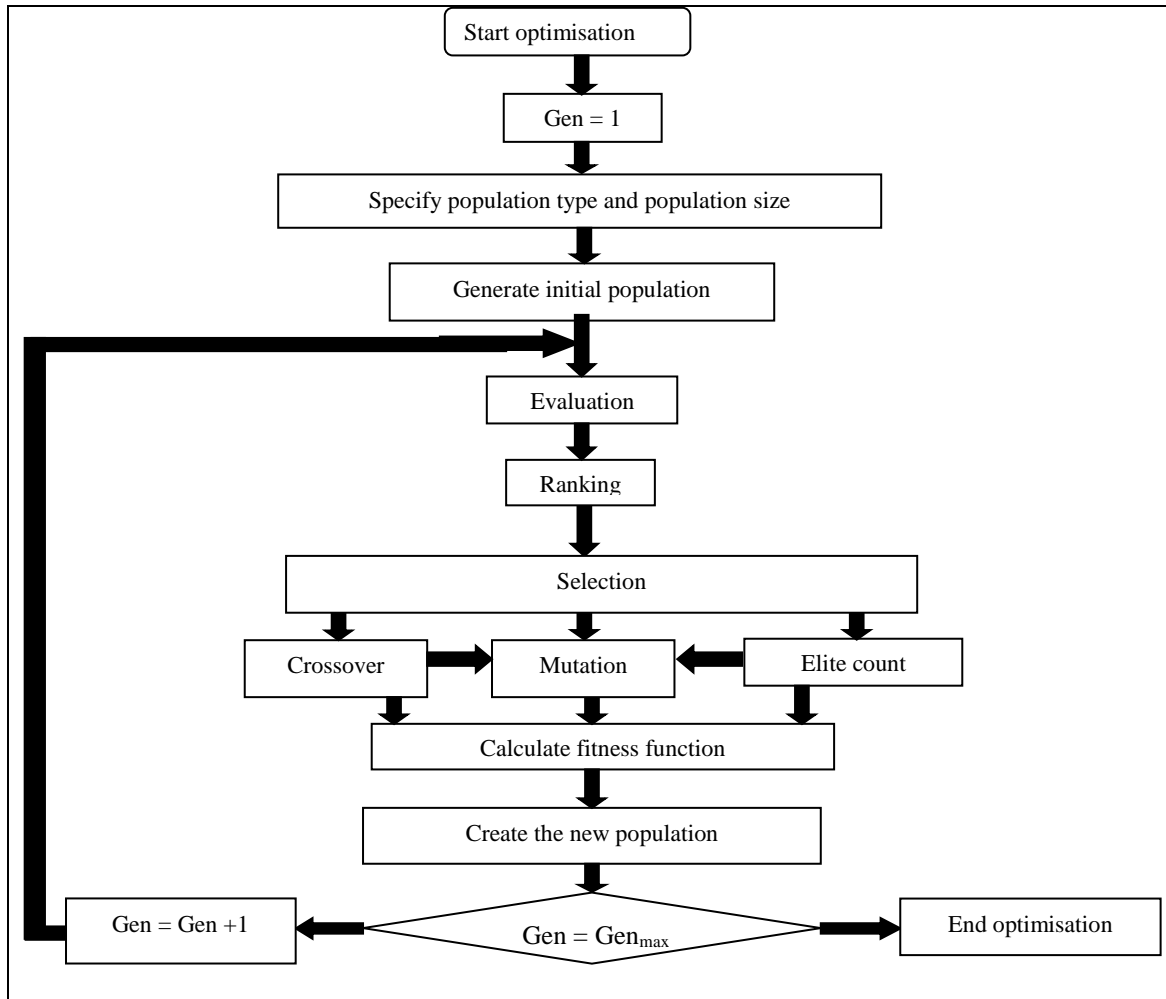


Figure 4.4 Flowchart of the GA concept [148, 149].

As shown in Figure 4.4, the GA concept involves creating a primary population involving a predefined number of individuals or solutions. In this project, individuals or solutions represent potential values of the coefficients of the alternative equations developed in Section 4.3.1 (Eqs. (4.7) to (4.10)) and Section 4.3.2 (Eqs. (4.17) and (4.18)). Each solution or population is represented by a genetic string or chromosome. Each individual has an associated fitness measure, which represents an objective value. The concept of fittest individuals in a population producing fitter offspring is then implemented to reproduce the next population. The individuals are tested and ranked.

Selected individuals are selected for elite count or crossover at each generation. Meanwhile the genes of an individual are randomly modified using a suitable mutation factor to develop the population. Later on, better individuals or solutions are created through carrying out biased random selection and mixing of the evaluated searches. Therefore, a new generation of individuals is resulted based on the indigenous subjects leading to following populations with better individual fitness. The algorithm will expel the individuals with lower fitness value from the population, and recognises the individuals with optimal fitness values [30].

Compared with other regression techniques, GA is more popular in solving engineering, scientific, and business optimisation problems due to its ease of use and higher accuracy [150]. The ability of GA in exploiting parent solutions which are closer to the optimal solution is higher than heuristic searching techniques, such as structural models and structural stiffness methods [151]. Compared with regression and heuristic approaches, which can find only one solution for optimising a given problem, GA selects the best solution among the all possible solutions which can be applied for the problem optimisation. Therefore, the final solution proposed by GA is guaranteed to be the global-optimal [151]. The global-optimal ability increases the accuracy of GA in problem optimisation as the proposed optimal solution is the best solution among all possible answers. Reviewing the literature, it was clear that many researchers have applied GA to forecast model parameters [150, 152-155], which shows the wide-spread application of GA in problem optimisation and estimating the parameters of a given model. The main advantages of GA over the regression techniques in optimising problems are [156]:

- The evolutionary nature of GA enables to search for solutions with a reasonably small number of mathematical requirements.
- Contrary to traditional optimisation methods based on local search by a convergent stepwise procedure, such as regression approaches, the evolution operators make GA effective at performing global search. Local search means to compare the values of nearby points and move to the relative optimal points. However, global optimum is the optimal solution among all possible solutions, not just those in a particular neighbourhood of values [151].
- GA is very flexible in terms of hybridising with domain dependent heuristics to make an efficient implementation for a specific problem.

Considering the advantages mentioned above, GA was preferred optimisation method in this study. GA function is one of the solvers for optimising a given problem, and a GA toolbox is available in MATLAB. In a GA function, the procedure of optimisation mainly depends on three factors: Fitness function definition, constraint definition, and determination of GA parameters. Each one of these factors is discussed in the following sub-sections.

4.3.4 Fitness function

As mentioned, GA is responsible to find the best solution for optimizing a given problem. The problem is coded as a function, usually called the fitness function, using MATLAB instructions and commands. In a GA approach, individuals or solution space is a population of binary strings. For the whole population, fitness function is applied to binary strings to determine which candidates are included in each gene.

In this study, the GA solver is applied to find the values of the coefficients of the alternative Eqs. (4.7) to (4.10) (developed for IG WPP) and Eqs. (4.17) and (4.18)

(developed for DFIG WPP). The graph plotted by each equation must have the lowest error with respect to the reference V-X/R data points. The reference V-X/R data points were shown in Figures 4.1 and 4.2 for the IG and DFIG-Based WPPs, respectively. One fitness function has been considered, defined, and coded for each alternative equation. In each fitness function, the coefficients of the relevant alternative equation are considered as the input variables. Furthermore, the output of the fitness function is standard deviation (σ) between the V_{PCC} predicted by the equation (V_{PCC}) and the reference voltage (V_{PCC_ref}) given by Eq. (4.19).

$$\sigma = \sqrt{\frac{1}{n} \sum_{i=1}^n (Y_i - \bar{Y}_i)^2} \quad (4.19)$$

Where Y_i expresses reference values and \bar{Y}_i expresses predicted values and n represents the number of \bar{Y}_i .

The objective is to find values of the input variables for which the output of the fitness function becomes minimum. For elaborating the fitness functions operation, Table 4.3 shows pseudo codes and the description of each code for one of the fitness functions. As an example, Fitness Function 1 was selected, which was used for finding the values of the coefficients in the first alternative equation, i.e. Eq. (4.7). Moreover, the MATLAB codes written for this fitness function have been included in Appendix C.

Table 4.3 Pseudo codes for Fitness Function 1.

Pseudo code	Description
Procedure function_name (input vector)	Declare Fitness Function 1 named FF1 which accepts vector K as input variable and returns output variable σ . K is a row vector with length = 3. The elements in vector k represent the value of coefficients in Eq. (4.7), i.e. A_{sr0} , A_{sr1} , and A_{sr2} . Output parameter (σ) is the sum of the standard deviation of reference vs. predicted V-X/R characteristics for the four test systems.
$A_{sr0} \leftarrow$ First element of input vector $A_{sr1} \leftarrow$ Second element of input vector $A_{sr2} \leftarrow$ Third element of input vector	Assign the first element of vector K into variable A_{sr0} , the second element of vector K into A_{sr1} , and the third element of vector K

	into A_{sr2} .
$[xr_1, v_ref_1] \leftarrow$ Reference X/R and voltage data points for Test 1	Assign the reference X/R and voltage data points obtained for Test 1 into variable xr_1 and variable v_ref_1 , respectively.
$SCR_1 \leftarrow 3$ $v_pre_1 \leftarrow A_{sr0} * \exp(A_{sr1} * (xr_1 / SCR_1)) + A_{sr2}$	For Test 1, calculate voltage value named v_pre_1 using Eq. (4.7) considering that $SCR = 3$.
Error $\leftarrow 0$ For $i=1$ to length of v_pre_1 do Error \leftarrow Error + $(v_ref_1(i) - v_pre_1(i))^2$; end for $\sigma(1) \leftarrow \sqrt{\text{Error} / \text{length of } v_pre_1}$	Calculate standard deviation between v_ref_1 and v_pre_1 and assigned it into variable $\sigma(1)$.
$[xr_2, v_ref_2] \leftarrow$ Reference X/R and voltage data points for Test 2	Assign the reference X/R and voltage data points obtained for Test 2 into variable xr_2 and variable v_ref_2 , respectively.
$SCR_2 \leftarrow 4.5$ $v_pre_2 \leftarrow A_{sr0} * \exp(A_{sr1} * (xr_2 / SCR_2)) + A_{sr2}$	For Test 2, calculate voltage value named v_pre_2 using Eq. (4.7) considering that $SCR = 4.5$
Error $\leftarrow 0$ For $i=1$ to length of v_pre_2 do Error \leftarrow Error + $(v_ref_2(i) - v_pre_2(i))^2$; end for $\sigma(2) \leftarrow \sqrt{\text{Error} / \text{length of } v_pre_2}$	Calculate standard error between v_ref_2 and v_pre_2 and assigned it into variable $\sigma(2)$.
$[xr_3, v_ref_3] \leftarrow$ Reference X/R and voltage data points for Test 3	Assign the reference X/R and voltage data points obtained for Test 3 into variable xr_3 and variable v_ref_3 , respectively.
$SCR_3 \leftarrow 6$ $v_pre_3 \leftarrow A_{sr0} * \exp(A_{sr1} * (xr_3 / SCR_3)) + A_{sr2}$	For Test 3, calculate voltage value named v_pre_3 using Eq. (4.7) considering that $SCR = 6$
Error $\leftarrow 0$ For $i=1$ to length of v_pre_3 do Error \leftarrow Error + $(v_ref_3(i) - v_pre_3(i))^2$; end for $\sigma(3) \leftarrow \sqrt{\text{Error} / \text{length of } v_pre_3}$	Calculate standard deviation between v_ref_3 and v_pre_3 and assigned it into variable $\sigma(3)$.
$[xr_4, v_ref_4] \leftarrow$ Reference X/R and voltage data points for Test 4	Assign the reference X/R and voltage data points obtained for Test 4 into variable xr_4 and variable v_ref_4 , respectively.
$SCR_4 \leftarrow 6$ $v_pre_4 \leftarrow A_{sr0} * \exp(A_{sr1} * (xr_4 / SCR_4)) + A_{sr2}$	For Test 4, calculate voltage value named v_pre_4 using Eq. (4.7) considering that $SCR = 7$.
Error $\leftarrow 0$ For $i=1$ to length of v_pre_4 do Error \leftarrow Error + $(v_ref_4(i) - v_pre_4(i))^2$; end for $\sigma(4) \leftarrow \sqrt{\text{Error} / \text{length of } v_pre_4}$	Calculate standard deviation between v_ref_4 and v_pre_4 and assigned it into variable $\sigma(4)$
$\sigma \leftarrow \sigma(1) + \sigma(2) + \sigma(3) + \sigma(4)$	Assign the sum of $\sigma(1)$, $\sigma(2)$, $\sigma(3)$, and $\sigma(4)$ into output variable named σ
End	End procedure

4.3.5 GA parameters

Referring to Figure 4.4, the operation of a GA function depends on the value or type of several parameters. In this section, the main parameters that must be identified while using a GA function are defined and explained in detail. Furthermore, the value and type of the parameters considered in the numerical model proposed in this project are presented.

Generation and population size are the basic parameters that need to be identified before running GA. The maximum number of iterations that GA performs is specified by the generation parameter. Furthermore, the number of individual in each generation is determined by the population size. The default values for the number of generation and population size in MATLAB are 100 and 20, respectively. However, in this study, the specified values for generation and population size are 300 and 200, respectively, which are very larger than the default values. This increases the accuracy of the results and ensures that GA determines appropriate values for the unknown variables (coefficients of the alternative equations). Apart from the number of generation and population size, selection, crossover, elite count, and mutation are the other important parameters of a GA function that must be identified by the operator.

4.3.5.1 Selection

The selection parameter chooses individuals which are available in current generation as the parents for the next generation based on their scaled values from the fitness function [157]. An individual can be selected more than once as a parent so that it contributes its genes to more than one child. Roulette-wheel and stochastic uniform are two common functions used for selecting the individuals in GA. The former is a fitness-based function where the chance of an individual to be chosen as a parent in the

next population is based on its relative fitness in the current population. However, the roulette wheel is not a good search strategy, as towards the end, the fitness values of the individuals slightly change in the last generations. This issue was removed in stochastic uniform search strategy. Stochastic uniform does not select the parents regarding their relative fitness, but their rank in the population. Therefore, stochastic uniform function is a better search strategy compared with roulette wheel function. In this study, stochastic uniform function has been selected for the selection parameter.

4.3.5.2 Crossover

Crossover categorises two individuals (parents) of the intermediate generation to create a new individual (child) for the next generation. Single point, two-point, and scattered crossover are three basic crossover functions [148].

Single point crossover function cuts both parents bit strings at the same point which is randomly chosen by the function. The child is created by taking the first part of the first parent and the second part of the second parent. Two-point crossover function works similar to the previous crossover function, however, this time the parents' bit strings are cut at two points. The child is created by taking the first part of the first parent, the second part of the second parent, and the third part of the first parent. In the case of scatter operator, the crossover process is carried out within two steps. Initially, the function generates a random binary vector. Later on, the function selects the strings of the first parent if the corresponding bit string in the random binary vector is 1, and selects the string of the second parents if the corresponding gen in the random binary vector is zero, and concatenates these pieces to create the child [148]. Comparing the crossover process in scattered, single point, and two-point crossover functions, it can be

concluded that scattered crossover function provides higher flexibility [148]. Therefore, in this study, the scattered function has been selected as the crossover operator.

4.3.5.3 Elite count

In a GA function, elite count is one of the options in reproduction process. It determines the number of the individuals which survive to the next generation. The value of elite count is between one and population size [149]. However, large elite number results in unrealistic results. Similar to the real world, the appropriate value for the number of elite gens is a small portion (around 1%) of the total population size. As mentioned earlier, in GA function applied for this study, the specified value for the population size is 200. Hence, the number of elite gens of the GA function is considered to be 2 which is 1% of the total population ($2 = 1\% * 200$).

4.3.5.4 Mutation

The algorithm makes small randomly changes in the genes of individual parents to create mutation children [158]. By default, for unconstrained problems, GA function adds an incidental vector from a Gaussian distribution to the parent. For bounded or linearly constrained problems, the child stays attainable. In this study, the mutation function type is constraint dependent. The constraints are concerned with the maximum and minimum boundaries of the input variables of the fitness functions. Referring to Sections 4.3.1 and 4.3.2, in all six alternative functions, the values of the coefficients are positive. Hence, for all input variables, the minimum value is zero. In the case of upper boundaries, for each variable, a large positive domain was initially set. Later on, the GA function was run for several iterations to discover an approximate answer for the input variable considered. Once an approximate solution was discovered in the positive

large domain, the GA function was repeated based on the boundaries close to the approximate solution to achieve a more accurate answer. Table 4.4 presents the upper boundaries of each input variable. The lower boundaries were set to zero in each case.

Table 4.4 Upper boundaries for each input variable of the GA function.

Variable	Value
A_{sr0}	2
A_{sr1}	0.1
A_{sr2}	0.01
B_{sr0}	2
B_{sr1}	0.1
B_{sr2}	1
A_{lr0}	2
A_{lr1}	0.1
A_{lr2}	0.01
B_{lr0}	2
B_{lr1}	0.1
B_{lr2}	1
C_0	2
C_1	0.1
C_2	0.01
D_0	2
D_1	1
D_2	1

4.3.6 GA outcomes

Upon defining the fitness functions and GA parameters, the GA function was individually run in order to determine the values of the input variables for each fitness function. For each fitness function, the number of times that the algorithm is iterated equals with the multiplication of population size and the number of generation. Considering that the population size and the number of generation are 200 and 300 (refer to Section 4.3.5) respectively, the number of iterations for each fitness function equals $200 \times 300 = 6 \times 10^4$.

For each fitness function, GA obtains the values of the input variables ensuring that the value of the fitness function in the current iteration is less than the value of the fitness function in the previous iteration. Therefore, for each input variable, the value

obtained in the last iteration is considered as the optimal value. The optimal values of the input variables are, then, considered as the values of the coefficients of the alternative equations developed in Section 4.3.1 and 4.3.2.

Table 4.5 shows the optimal value of each one of the input variables determined by GA for the fitness functions.

Table 4.5 Values of the coefficients.

Fitness function	Variable	Value
Fitness function 1	A _{sr0}	1.068
	A _{sr1}	0.015
	A _{sr2}	0.001
Fitness function 2	B _{sr0}	0.9867
	B _{sr1}	0.0912
	B _{sr2}	0.29
Fitness function 3	A _{lr0}	0.9813
	A _{lr1}	0.0427
	A _{lr2}	0.002
Fitness function 4	B _{lr0}	0.788
	B _{lr1}	0.195
	B _{lr2}	0.24
Fitness function 5	C ₀	1.102
	C ₁	0.03
	C ₂	0.002
Fitness function 6	D ₀	0.99
	D ₁	0.101
	D ₂	0.347

Assigning the values of the coefficients presented in Table 4.6 in the corresponding alternative equations developed in Section 4.3.1 and 4.3.2, Eqs. (4.7) to (4.10) and Eq (4.17) to Eq (4.18)) can be rewritten as: follows:

$$\text{IG WPP} \quad \left\{ \begin{array}{l} V_{PCC} = 1.068 - 0.015 \times \left(\frac{X}{R} \times SCR\right) + 0.001 \times \left(\frac{X}{R} \times SCR\right)^2 \end{array} \right. \quad (4.20)$$

$$\text{X/R}_{PCC} < 2 \quad \left\{ \begin{array}{l} V_{PCC} = 0.9867 + 0.0912 \times e^{(-0.29 \times \frac{X}{R} \times SCR)} \end{array} \right. \quad (4.21)$$

$$\begin{cases} \text{IG WPP} \\ \text{X/R}_{PCC} > 2 \end{cases} \left\{ \begin{aligned} V_{PCC} &= 0.9813 - 0.0427 \times \left(\frac{X}{R} \times \frac{1}{SCR} \right) + 0.002 \times \left(\frac{X}{R} \times \frac{1}{SCR} \right)^2 & (4.22) \\ V_{PCC} &= 0.788 + 0.195 \times e^{(-0.24 \times \frac{X}{R} \times \frac{1}{SCR})} & (4.23) \end{aligned} \right.$$

$$\begin{cases} \text{DFIG WPP} \\ \text{X/R}_{PCC} < 2 \end{cases} \left\{ \begin{aligned} V_{PCC} &= 1.102 - 0.03 \times \left(\frac{X}{R} \times SCR \right) + 0.002 \times \left(\frac{X}{R} \times SCR \right)^2 & (4.24) \\ V_{PCC} &= 0.99 + 0.101 \times e^{(-0.347 \times \frac{X}{R} \times SCR)} & (4.25) \end{aligned} \right.$$

Eqs. (4.20) to (4.25) are the final forms of numerical models, which can be used to express the relations between V_{PCC} , X/R_{PCC} , and SCR for different types of wind turbines and in different X/R_{PCC} ranges. In the following sections, the accuracy of each equation is evaluated using statistical criteria and graphs presented to highlight the best-fit equation for each WPP type and X/R_{PCC} range.

4.4 Evaluation of the accuracy of the proposed alternative equations

This section presents the validation testing of Eqs. (4.20) to (4.25). The proposed equations must provide the lowest error with respect to the reference V-X/R data points. The reference V-X/R data points were presented in Section 4.2 for the IG and DFIG WPP (please refer to Figures 4.1 and 4.2). As mentioned therein, the V-X/R characteristics were plotted for four test systems based on IEEE distribution system models with different topologies and SCR values seen from the connection point. Consequently, for each WPP type and X/R_{PCC} range of considered in Eqs. (4.20) to (4.25), the accuracy of the relevant alternative equations must be evaluated for each test system. Later on, the equation with the highest accuracy can be selected as the proposed equation for modelling the mathematical relation between V_{PCC} , X/R_{PCC} , and SCR .

4.4.1 Statistical criteria

As mentioned in Section 4.3.4, the output variable of each fitness function is the standard deviation (σ) between reference and predicted values. In this section, apart from σ , two other well-known evaluation criteria: Mean of Absolute Error (MAE) and Mean of Relative Error (MRE) are used to measure the accuracy of the alternative Eqs. (4.20) to (4.25). These criteria are commonly used in estimation methods.

The formulas of these criteria can be defined as follows [159-161]:

$$MAE = \frac{1}{n} \sum_{i=1}^n |\hat{M}_i - M_i| \quad (4.26)$$

$$MRE = \frac{1}{n} \sum_{i=1}^n \left| \frac{\hat{M}_i - M_i}{M_i} \right| \quad (4.27)$$

The reference values of V_{PCC} , is expressed as M_i , and its predicted values are expressed as \hat{M}_i . Also, the total number of reference values is given as n .

The lower the value for each evaluation criteria, the higher would be the relative accuracy [33]. Table 4.6 presents the value of each evaluation criterion for each alternative equation.

Table 4.6 MAE and MRE values for alternative Eqs. (4.20) to (4.25).

WPP type	X/R _{PCC} range	Test system	Alternative equation	Σ	MAE	MRE
IG-Based WPP	X/R _{PCC} < 2	1	4.20	0.0324	0.0314	0.0305
			4.21	0.0264	0.026	0.0254
IG-Based WPP	X/R _{PCC} > 2	1	4.22	0.0144	0.013	0.0137
			4.23	0.015	0.014	0.0144
DFIG-Based WPP	X/R _{PCC} < 2	1	4.24	0.0068	0.006	0.0058
			4.25	0.0038	0.0035	0.0034
IG-Based WPP	X/R _{PCC} < 2	2	4.20	0.0247	0.0223	0.0218
			4.21	0.0155	0.0145	0.0143
IG-Based WPP	X/R _{PCC} > 2	2	4.22	0.0097	0.0087	0.0091
			4.23	0.0102	0.0091	0.0095
DFIG-Based WPP	X/R _{PCC} < 2	2	4.24	0.0103	0.0093	0.009
			4.25	0.0014	0.0012	0.0012
IG-Based WPP	X/R _{PCC} < 2	3	4.20	0.0318	0.0274	0.0267

			4.21	0.0117	0.0116	0.0115
IG-Based WPP	$X/R_{PCC} > 2$	3	4.22	0.0052	0.0044	0.0046
			4.23	0.0055	0.0047	0.0049
DFIG-Based WPP	$X/R_{PCC} < 2$	3	4.24	0.0361	0.0234	0.0223
			4.25	0.0036	0.0031	0.003
IG-Based WPP	$X/R_{PCC} < 2$	4	4.20	0.2876	0.2523	0.194
			4.21	0.0122	0.0121	0.012
IG-Based WPP	$X/R_{PCC} > 2$	4	4.22	0.0046	0.0045	0.0047
			4.23	0.0051	0.005	0.0052
DFIG-Based WPP	$X/R_{PCC} < 2$	4	4.24	0.0327	0.0225	0.0215
			4.25	0.0088	0.0065	0.0064

In the case of the IG-Based WPP with a low X/R_{PCC} ($X/R_{PCC} < 2$), as per Table 4.6, σ , MAE, and MRE for the exponential function (Eq. 4.21) are less than those for the polynomial function (Eq. 4.20) for all four test connection points. Therefore, Eq (4.21) is more accurate than Eq (4.20) in representing the relationship between V_{PCC} , X/R_{PCC} , and SCR.

In the case of IG-Based WPP with a large X/R_{PCC} PCC ($X/R_{PCC} > 2$), σ , MAE, and MRE values for Eq. (4.22) are slightly less than those of Eq. (4.23). Therefore Eq. (4.22) is proposed for modelling the relation between V_{PCC} , X/R_{PCC} , and SCR for the IG-Based WPP in the $X/R_{PCC} > 2$ range. For the DFIG-Based WPP, σ , MAE, and MRE values for the exponential function (Eq. 4.25) are less than those for the polynomial (Eq. 4.24) and hence the exponential function has been chosen to model the relation between the voltage, X/R, and SCR.

4.4.2 Graphical representations

In this section, the accuracy of the alternative equations has been investigated using graphical representations. In this case, for each test system presented in Table 4.1, the V-X/R curve characteristic predicted by each alternative equation is compared with the

corresponding reference curve characteristics. The predicted and reference V-X/R curve characteristics are as shown in Figures 4.5 to 4.16.

For the IG-Based WPP with a small X/R_{PCC} , Figures 4.5 to 4.8 show that the V-X/R curve predicted by Eq. (4.21) follows the reference V-X/R curve for all four test systems. The highest error was around 2.5% in the first test system when $X/R_{PCC} = 2$. However, the error between the reference V-X/R curve and the V-X/R curve predicted by the polynomial alternative equation, Eq. (4.20), was significant, especially for stiffer test systems (Test 3 and Test 4). As shown in Figures 4.7 and 4.8, the graphs given by Eq. (4.20) could not track the reference curve characteristics. Therefore, the results demonstrate that Eq. (4.21) provides a better accuracy compared with Eq. (4.20).

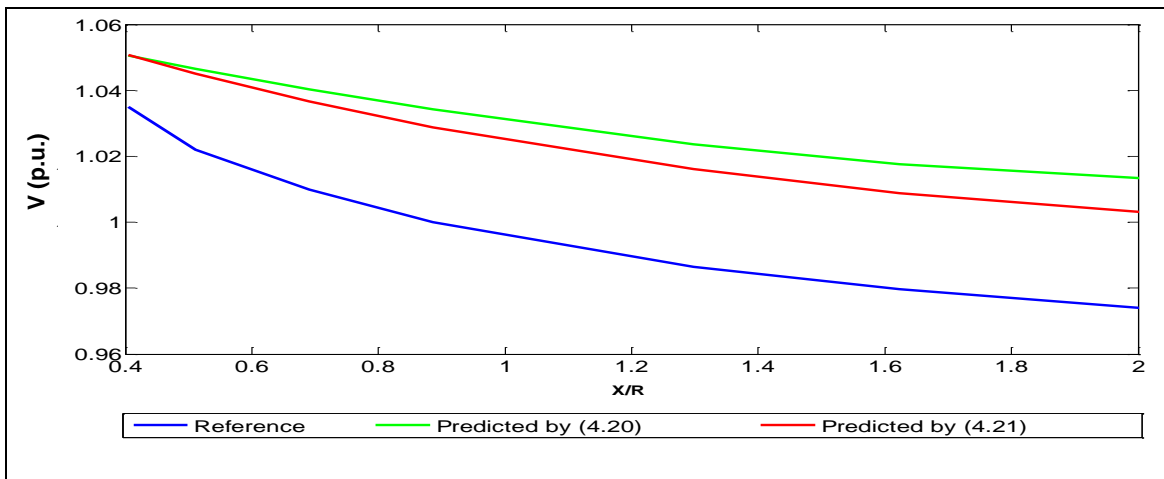


Figure 4.5 V-X/R graphs obtained by Eqs (4.20) and (4.21) for Test System 1.

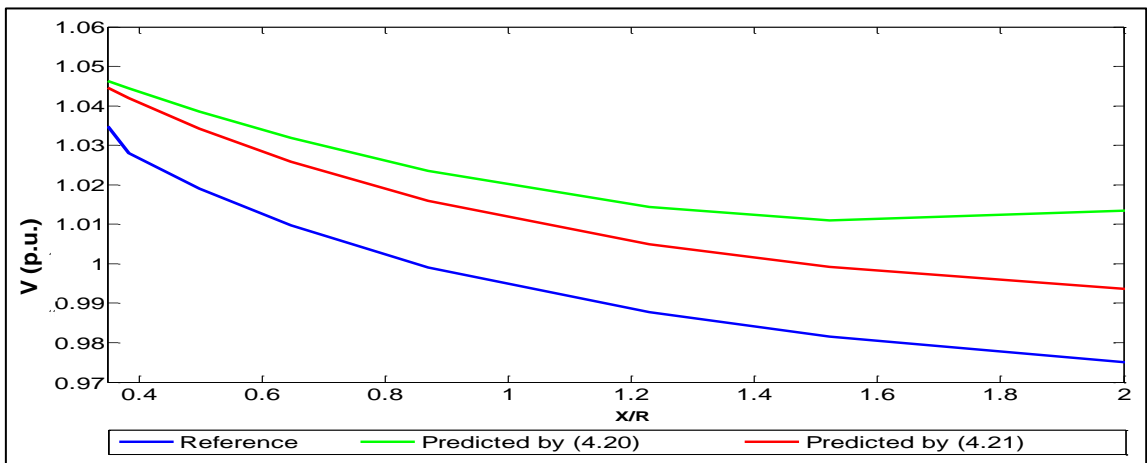


Figure 4.6 V-X/R graphs obtained by Eqs (4.20) and (4.21) for Test System 2.

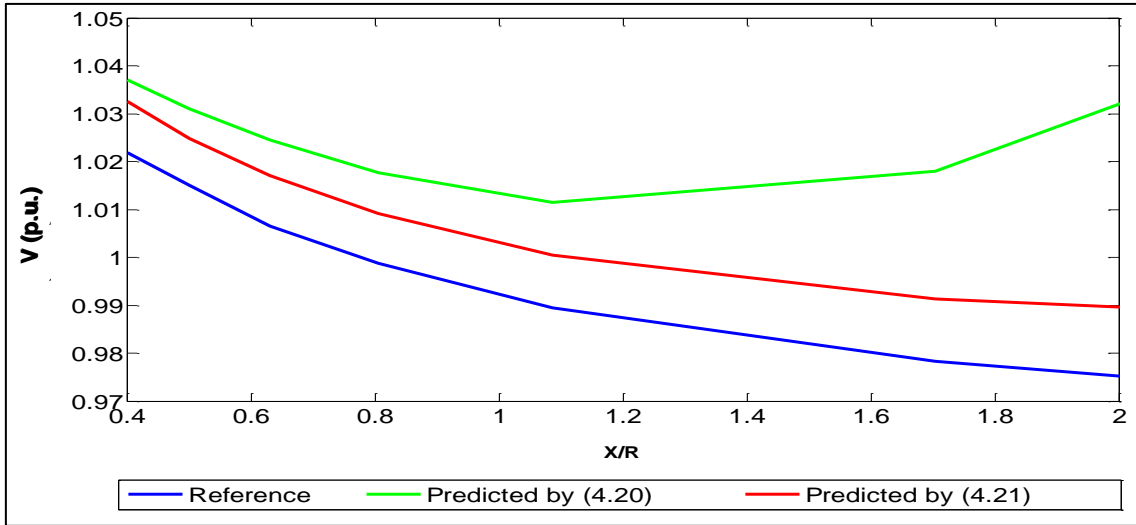


Figure 4.7 V-X/R graphs obtained by Eqs (4.20) and (4.21) for Test System 3.

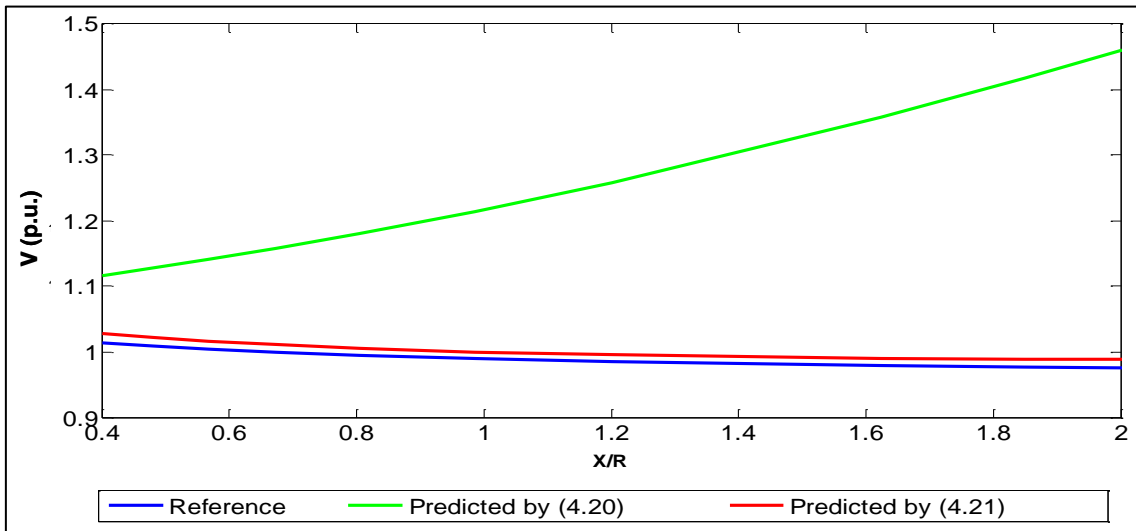


Figure 4.8 V-X/R graphs obtained by Eqs (4.20) and (4.21) for Test System 4.

For the IG-Based WPP with a large X/R_{PCC} , the accuracy of the graphs obtained by Eqs. (4.22) and (4.23) were close to each other as shown in Figures 4.9 to 4.12. However, for all test systems, the error between the curves given by Eq. (4.22) and reference graphs were lower than the error between the curves predicted by Eq. (4.23) and reference graphs. For both Eqs. (4.22) and (4.23), the highest error was concerned with the first test system when X/R_{PCC} is around 2. In this case, as can be seen from Figure 4.9, the error between the reference and predicted graphs is around 1.6%.

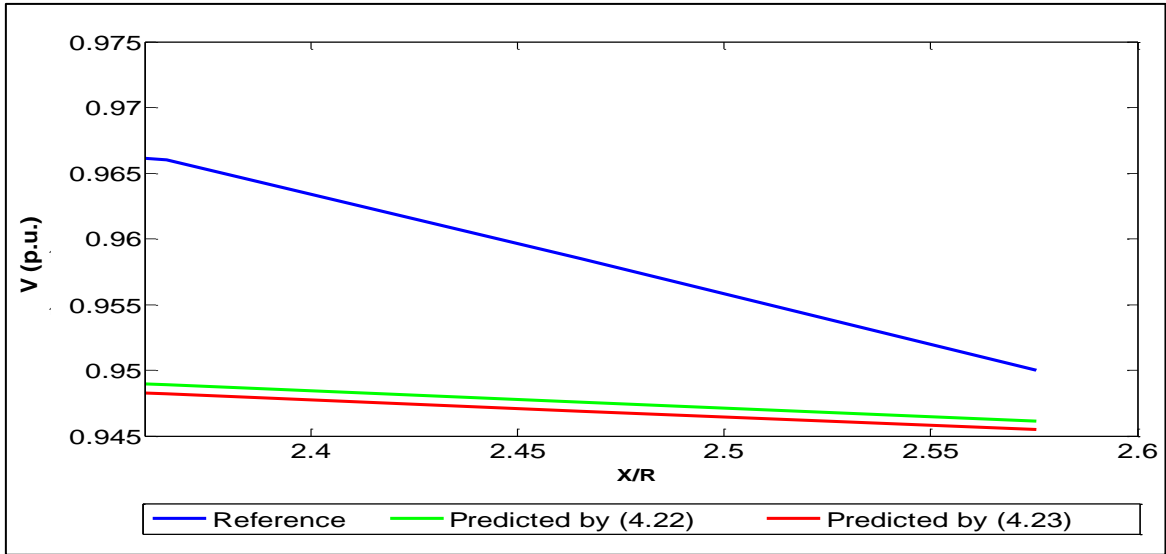


Figure 4.9 V-X/R graphs obtained by Eqs (4.22) and (4.23) for Test System 1.

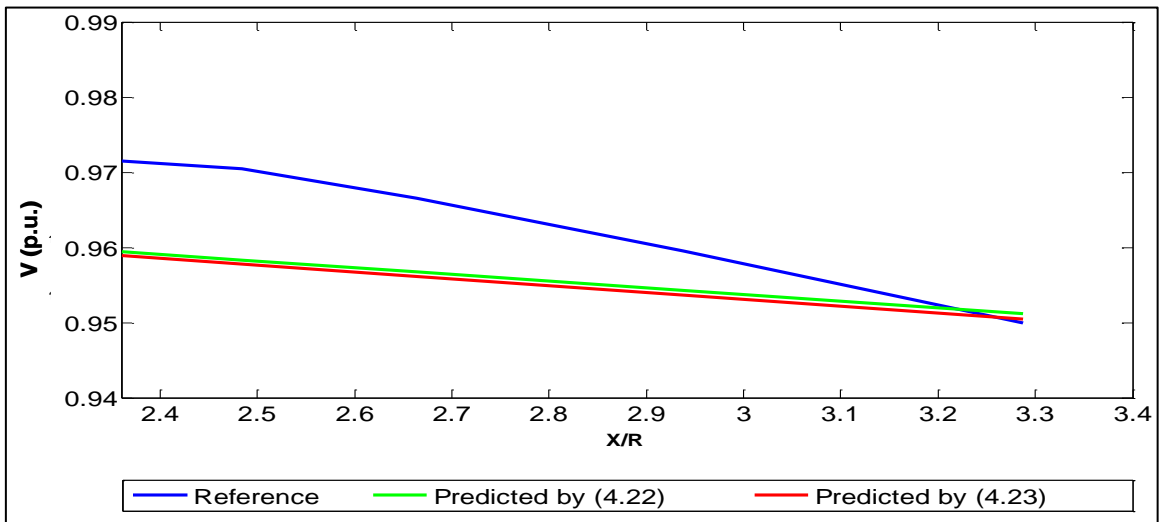


Figure 4.10 V-X/R graphs obtained by Eqs (4.22) and (4.23) for Test System 2.

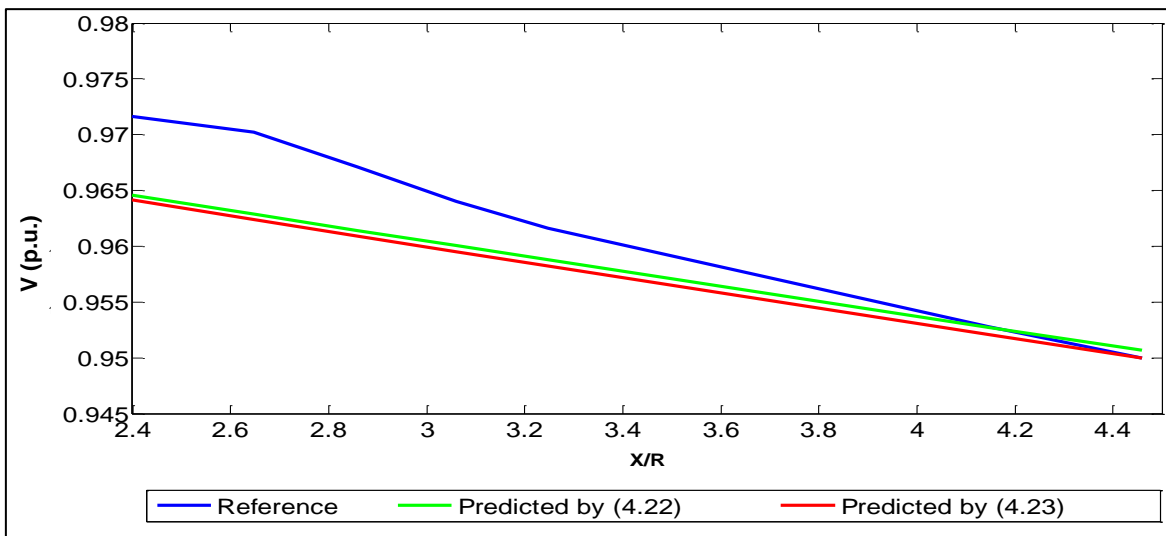


Figure 4.11 V-X/R graphs obtained by Eqs (4.22) and (4.23) for Test System 3.

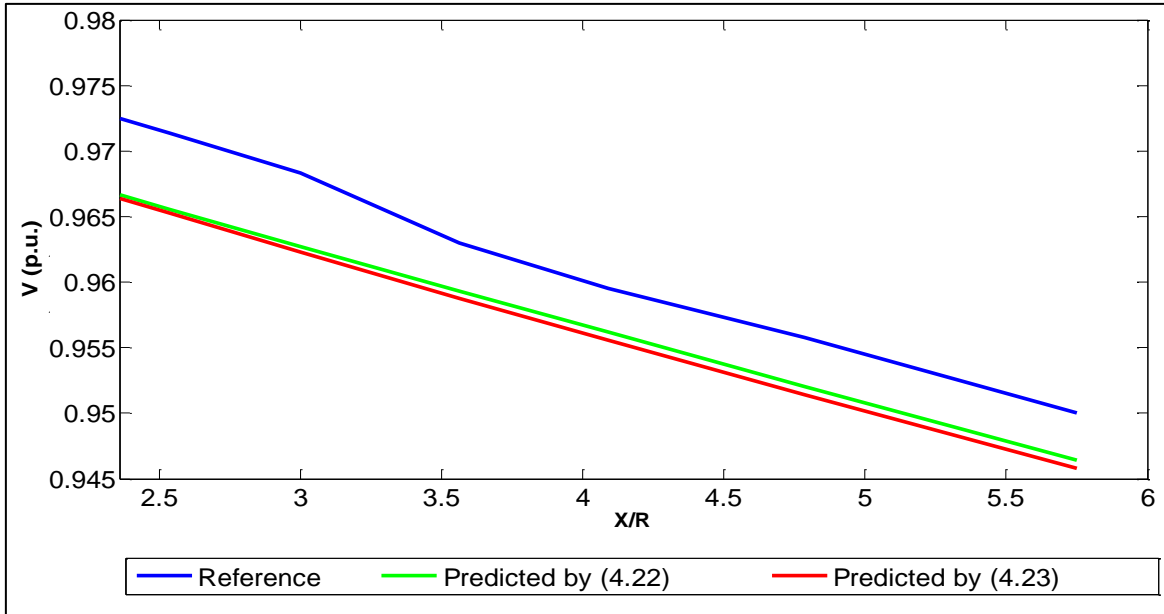


Figure 4.12 V-X/R graphs obtained by Eqs (4.22) and (4.23) for Test System 4.

Finally, for the DFIG-Based WPP, the results in Figures 4.13 to 4.16 show that the accuracy of the graphs gained by the relevant exponential alternative equation, Eq. (4.25), is better than the accuracy of the graphs given by the relevant polynomial alternative equation, Eq. (4.24).

For all test systems, the error between the reference curve and the curves given by Eq. (4.25) is less than 1%. However, the error between the graphs given by Eq. (4.24) and the reference curves is high, especially for Test 3 and Test 4. For Test 3, according to Figures 4.15, the highest error caused by Eq. (4.25) is nearly 0.5%, while the error caused by Eq. (4.24) is around 4%. Similarly, for Test 4, Figure 4.16 shows that the highest error of the graph plotted by Eq. (4.25) is around 0.5%, however, the highest error between the reference curves and the graphs given by Eq. (4.24) is over 6%. Therefore, the results demonstrate that, contrary to Eq. (4.24), the accuracy of Eq. (4.25) is very high.

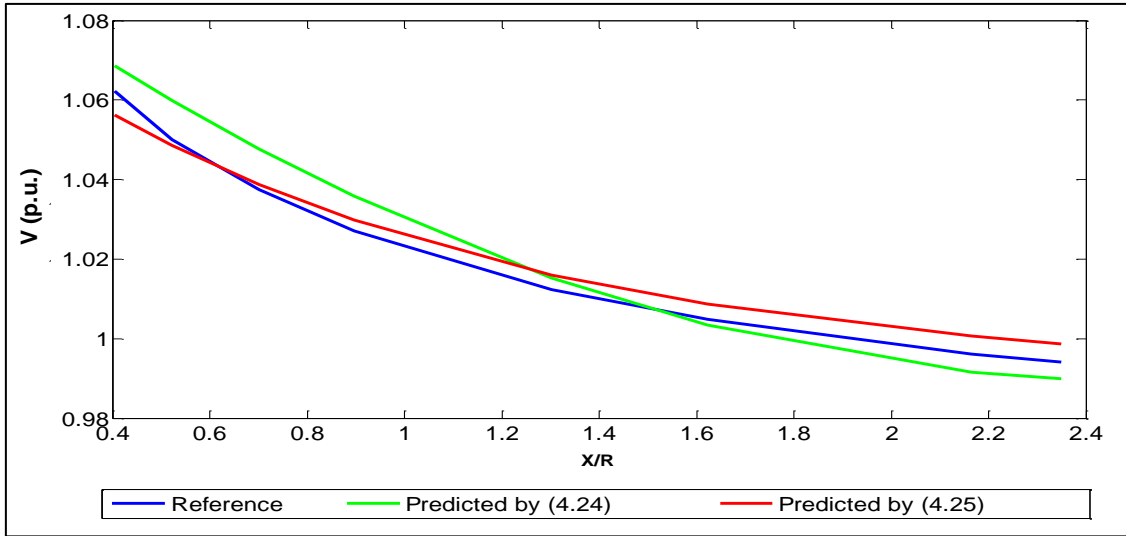


Figure 4.13 V-X/R graphs obtained by Eqs (4.24) and (4.25) for Test System 1.

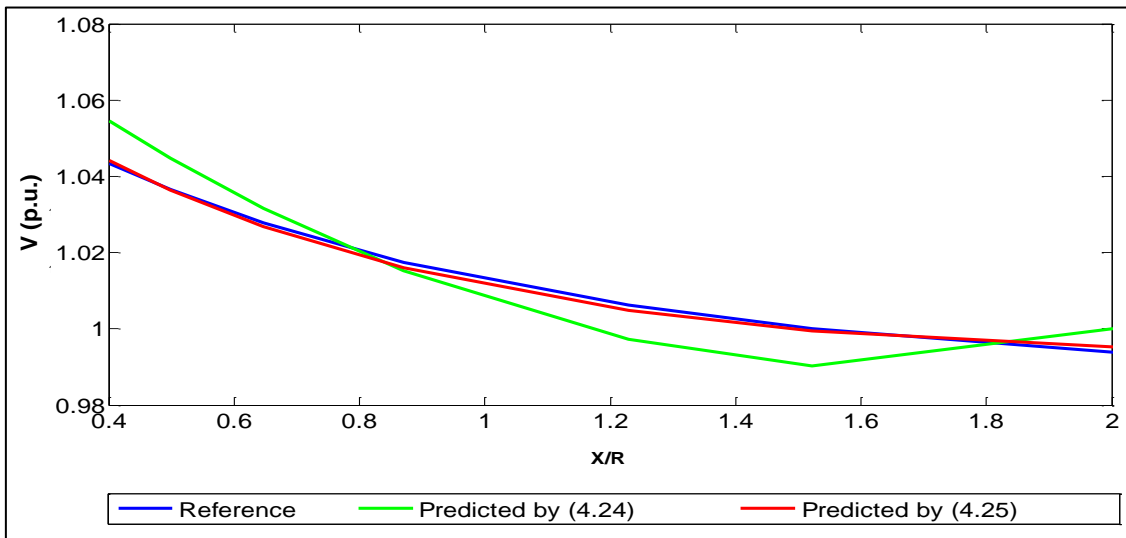


Figure 4.14 V-X/R graphs obtained by Eqs (4.24) and (4.25) for Test System 2.

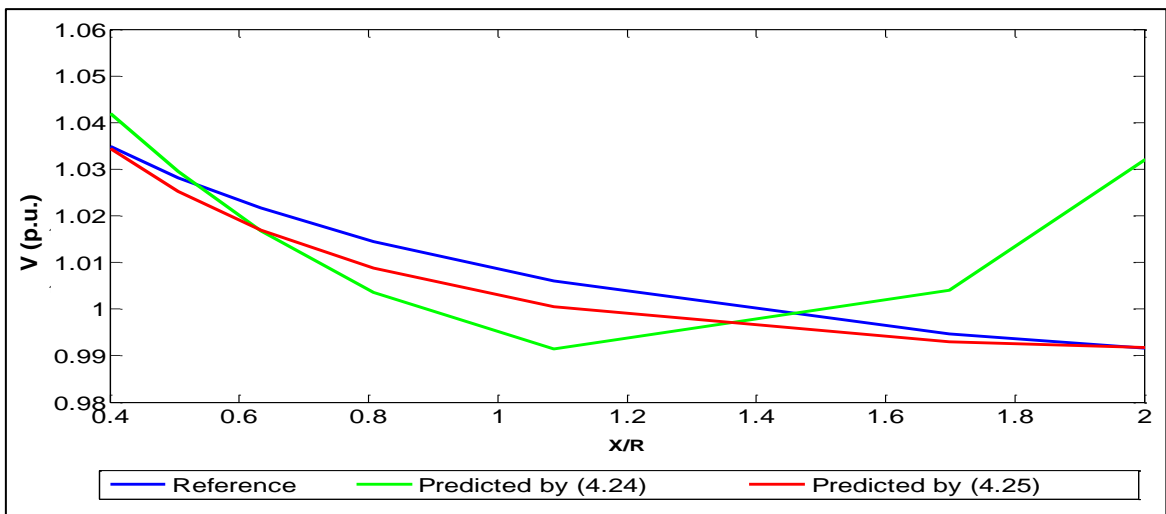


Figure 4.15 V-X/R graphs obtained by Eqs (4.24) and (4.25) for Test System 3.

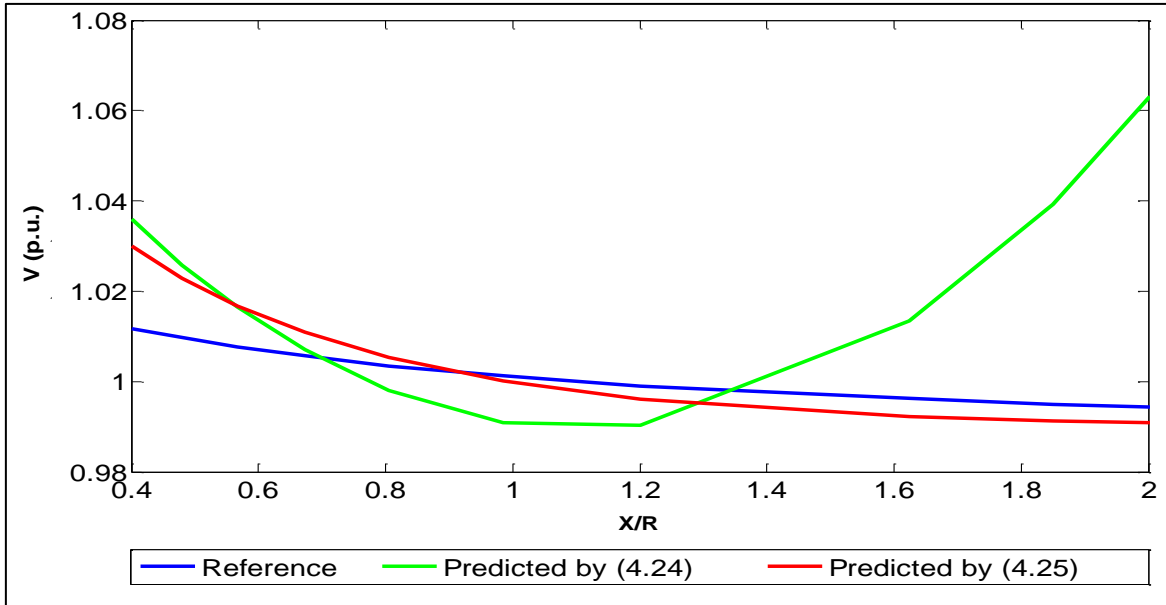


Figure 4.16 V-X/R graphs obtained by Eqs (4.24) and (4.25) for Test System 4.

Comparing the accuracy of the alternative Eqs. (4.20) to (4.25) using the statistical criteria and graphical representation, the equations proposed for modelling the relation between V_{PCC} , X/R_{PCC} , and SCR are as listed in Table 4.7.

Table 4.7 Proposed equation for each WPP type and X/R_{PCC} range.

WPP type X/R_{PCC} range	Proposed equation
IG WPP $X/R_{PCC} < 2$	4.21
IG WPP $X/R_{PCC} > 2$	4.22
DFIG WPP $X/R_{PCC} < 2$	4.25

4.5 Voltage stability analytical model

As shown in the previous section, the relation between voltage, X/R, and SCR at the PCC of the IG and DFIG-Based WPPs can be modelled using three equations developed for two key X/R_{PCC} regions of interest, the $X/R_{PCC} < 2$, and $X/R_{PCC} > 2$ regions. Considering that SCR is the ratio between the grid's SCC and P_{wind} , the proposed equations can be expressed in terms of V_{PCC} as a function of P_{wind} and SCC as shown in Eqs. (4.28), (4.33), and (4.41). These equations enable to calculate the voltage profile and voltage variations at a given connection point with a specific X/R and SCC.

Eqs. (4.28), (4.33), and (4.41) can be developed in terms of P_{wind} as a function of V_{PCC} , as shown in Eqs. (4.32), (4.39), and (4.45). In the case of the IG-Based WPP with $X/R_{PCC} > 2$, the P_{wind} parameter can be expressed by Eq. (4.39) or Eq. (4.40). In Eq. (3.40), the P_{wind} value is given by the multiplication of the ratio between SCC and X/R and the sum of two phrases: a constant value (10.675) and a square root relation. The SCC value is normally very larger than X/R value making the ratio between SCC and X/R large. Multiplication of the sum of the two phrases by a large value makes P_{wind} value larger than the grid's SCC, which is not realistic. Hence, the acceptable value of P_{wind} is given by Eq. (4.39).

Eqs. (4.32), (4.39), and (4.45) enable to estimate the WPP maximum permissible size which ensures that V_{PCC} is maintained within the acceptable steady-state range. This is another significance of the voltage stability model proposed in this study.

- **IG WPP with $X/R_{PCC} < 2$**

$$V = 0.9867 + 0.0912 e^{(-0.29 \times \frac{X}{R} \times \frac{SCC}{P_{wind}})} \quad (4.28)$$

$$\rightarrow \frac{V - 0.9867}{0.0912} = e^{(-0.29 \times \frac{X}{R} \times \frac{SCC}{P_{wind}})} \quad (4.29)$$

$$\rightarrow \ln\left(\frac{V - 0.9867}{0.0912}\right) = -0.29 \times \frac{X}{R} \times \frac{SCC}{P_{wind}} \quad (4.30)$$

$$\rightarrow P_{wind} = -0.29 \times \frac{\frac{X}{R} \times SCC}{\ln\left(\frac{V - 0.9867}{0.0912}\right)} \quad (4.31)$$

$$\rightarrow P_{wind} = 0.29 \times \frac{\frac{X}{R} \times SCC}{\ln\left(\frac{0.0912}{V - 0.9867}\right)} \quad (4.32)$$

• **IG WPP with $X/R_{PCC} > 2$**

$$V_{PCC} = 0.9813 - 0.0427 \times \left(\frac{X}{R} \times \frac{P_{wind}}{SCC} \right) + 0.002 \times \left(\frac{X}{R} \times \frac{P_{wind}}{SCC} \right)^2 \quad (4.33)$$

$$\xrightarrow{\times \frac{1}{0.002}} 500V = \left(\frac{X}{R} \times \frac{P_{wind}}{SCC} \right)^2 - 21.35 \times \left(\frac{X}{R} \times \frac{P_{wind}}{SCC} \right) + 500 \times 0.9813 \quad (4.34)$$

$$\rightarrow 500 \times (V - 0.9813) = \left(\frac{X}{R} \times \frac{P_{wind}}{SCC} \right)^2 - 21.35 \times \left(\frac{X}{R} \times \frac{P_{wind}}{SCC} \right) \quad (4.35)$$

$$\rightarrow 500 \times (V - 0.9813) = \left(\frac{X}{R} \times \frac{P_{wind}}{SCC} \right)^2 - 21.35 \times \left(\frac{X}{R} \times \frac{P_{wind}}{SCC} \right) + 114 - 114 \quad (4.36)$$

$$\rightarrow 500 \times (V - 0.9813) = \left(\frac{X}{R} \times \frac{P_{wind}}{SCC} - 10.675 \right)^2 - 114 \quad (4.37)$$

$$\rightarrow \frac{X}{R} \times \frac{P_{wind}}{SCC} - 10.675 = \pm \sqrt{500 \times (V - 0.9813) + 114} \quad (4.38)$$

$$\left\{ \begin{array}{l} P_{wind} = SCC \times \frac{R}{X} \times \left(10.675 - \sqrt{500 \times (V - 0.9813) + 114} \right) \quad \checkmark \quad (4.39) \\ \\ P_{wind} = SCC \times \frac{R}{X} \times \left(10.675 + \sqrt{500 \times (V - 0.9813) + 114} \right) \quad \times \quad (4.40) \end{array} \right.$$

• **DFIG WPP with $X/R_{PCC} < 2$**

$$V = 0.99 + 0.101 e^{(-0.347 \times \frac{X}{R} \times \frac{SCC}{P_{wind}})} \quad (4.41)$$

$$\rightarrow \frac{V - 0.99}{0.101} = e^{(-0.347 \times \frac{X}{R} \times \frac{SCC}{P_{wind}})} \quad (4.42)$$

$$\rightarrow \ln \left(\frac{V - 0.99}{0.101} \right) = -0.347 \times \frac{X}{R} \times \frac{SCC}{P_{wind}} \quad (4.43)$$

$$\rightarrow P_{wind} = -0.347 \times \frac{\frac{X}{R} \times SCC}{Ln\left(\frac{V-0.99}{0.101}\right)} \quad (4.44)$$

$P_{wind} = 0.347 \times \frac{\frac{X}{R} \times SCC}{Ln\left(\frac{0.101}{V-0.99}\right)}$	(4.45)
--	--------

Referring to Eqs. (4.28) to (4.45), the proposed analytical model is summarised as Table 4.8. Next chapter investigates and verifies the accuracy of the proposed equation in predicting V_{PCC} profile, ΔV_{PCC} , and $P_{max-wind}$ using the four test systems designed and simulated in this chapter.

Table 4.8 Proposed analytical model assuming $V_{PCC_initial} = 0.98$ p.u.

Eq.	Equation	Application
(4.28)	$V = 0.9867 + 0.0912 e^{(-0.29 \times \frac{X}{R} \times \frac{SCC}{P_{wind}})}$	Projecting V_{PCC} and ΔV_{PCC} for IG-Based WPPs for $X/R_{PCC} < 2$
(4.33)	$V_{PCC} = 0.9813 - 0.0427 \times \left(\frac{X}{R} \times \frac{P_{wind}}{SCC}\right) + 0.002 \times \left(\frac{X}{R} \times \frac{P_{wind}}{SCC}\right)^2$	Projecting V_{PCC} and ΔV_{PCC} for IG-Based WPPs for $X/R_{PCC} > 2$
(4.41)	$V = 0.99 + 0.101 e^{(-0.347 \times \frac{X}{R} \times \frac{SCC}{P_{wind}})}$	Projecting V_{PCC} and ΔV_{PCC} for DFIG-Based WPPs for $X/R_{PCC} < 2$
(4.32)	$P_{wind} = 0.29 \times \frac{\frac{X}{R} \times SCC}{Ln\left(\frac{0.0912}{V-0.9867}\right)}$	Projecting P_{wind} for IG-Based WPPs for $X/R_{PCC} < 2$
(4.39)	$P_{wind} = SCC \times \frac{R}{X} \times \left(10.675 - \sqrt{500 \times (V - 0.9813) + 114}\right)$	Projecting P_{wind} for IG-Based WPPs for $X/R_{PCC} > 2$
(4.45)	$P_{wind} = 0.347 \times \frac{\frac{X}{R} \times SCC}{Ln\left(\frac{0.101}{V-0.99}\right)}$	Projecting P_{wind} for DFIG-Based WPPs for $X/R_{PCC} < 2$

4.6 Conclusion

In a distribution system connected WPP, the short-circuit impedance angle ratio (X/R) and the grid SCC are the key characteristics that affect the voltage at the PCC. Development of mathematical relations between V_{PCC} , P_{wind} , X/R_{PCC} , and SCC will enable the understanding on how the steady-state voltage will behave in response to increases in wind power generation at a particular PCC, based on the SCC and X/R ratios observed at that point. In this chapter, the key objective was to mathematically determine the relations between V_{PCC} , P_{wind} , SCC, and X/R_{PCC} . The analysis paid emphasis on assessing the likely impacts of an increased X/R ratio on the steady-state voltage stability at the PCC of a WPP connected to a distribution network. Analysis studies were carried out based on two types of WTGs widely used in the WPPs: IG and DFIG.

Four distribution test feeders were modelled and simulated based on two different IEEE distribution system models to consider different network topologies and impacts of the network strength on the relationship between V_{PCC} and X/R . Later on, for each type of WTGs, a system X/R ratio sensitivity analysis was introduced and presented to quantify the impacts of the X/R ratio variation on the voltage-stability at the PCC and in order to determine how voltage responds to such changes. The realistic range of X/R_{PCC} and V_{PCC} has been taken into account in the V - X/R characteristics presented. It was demonstrated that both small and large X/R_{PCC} ratios adversely impact V_{PCC} and may push the voltage out of the allowable steady-state range in IG-Based WPPs. In the case of DFIG-Based WPPs, however, the voltage regulation requirement is problematic only at feeders with small X/R_{PCC} ratio.

The V-X/R characteristics were, then, used to develop the proposed voltage stability analytical model. The main idea was to find the equations which can fit the V-X/R curve characteristics presented for the four test systems. Six alternative equations were considered: two alternative equations for the IG-Based WPP with small X/R_{PCC} , two alternative equations for the IG-Based WPP with large X/R_{PCC} , and two alternative equations for the DFIG-Based WPP with small X/R_{PCC} . The coefficients of the equations were determined using a GA-Based approach. In this respect, for each alternative equation, a fitness function was coded in MATLAB. The error between the V-X/R curves given by the alternative equation and the reference V-X/R characteristic was considered as the output variable of the fitness function. Moreover, the coefficients of the alternative equation were considered as the input variables of the fitness function. GA was used to obtain the optimal values of the input variables in a way that the output of the fitness function becomes minimum.

Upon determining the values of the coefficients for each alternative equation, the accuracy of the equations was evaluated using statistical criteria and through visual observations of the graphs presented. It was demonstrated that the relation between V_{PCC} , X/R_{PCC} , and SCC, and P_{wind} can be modelled using three mathematical functions: an exponential function for IG-Based WPP with small X/R_{PCC} , a polynomial with an order of two for IG-Based WPP with large X/R_{PCC} , and an exponential function for DFIG-Based WPP with small X/R_{PCC} .

The graphical result demonstrated that the error between the reference voltage values and the values predicted by the proposed equations is very small. The graphical results showed that the V-X/R characteristics predicted by the developed model could

track the reference V-X/R graphs with an acceptable margin of error. This signifies that the proposed model is conservative.

The relation, then, were developed to calculate the active power injected by the WPP for a specific voltage value at the PCC point.

Next chapter investigates how these equations can be used for a predictive PV analysis study and for estimating three important voltage stability criteria, including: V_{PCC} profile, ΔV_{PCC} , and the WPP maximum permissible size.

Chapter 5 - Validation of the Proposed Analytical Model

5.1 Introduction

Preceding chapters have presented the novel analytical method developed during the course of this research to model the relation between the PCC voltage and PCC parameters in a distribution network penetrated by WPPs. In Chapter 3, PV, QV, and V–SCR analysis studies were carried out to investigate the impact of PCC parameters on voltage stability at a given connection point from a number of aspects using modelling and simulation studies. Chapter 4 focused on the development of analytical model of a series of mathematical relations between the bus voltage and network parameters at the interconnection of a WPP. Six mathematical equations were proposed to model the analytical correlation between PCC bus voltage (V_{PCC}), wind power generation (P_{wind}), the X/R ratio seen from the PCC (X/R_{PCC}), and the grid's SCC for two key types of WTG: IG and DFIG.

This chapter presents simulation works and numerical analysis studies undertaken to validate and confirm the intellectual contributions made in the area of development of an analytical voltage stability model for site and size analysis in wind farms. Referring to Chapter 4, the analytical model was developed using data from the simulation of four test systems with different PCC parameters. In developing the analytical formulae, the initial steady-state voltage level at the PCC of the four test systems, when $P_{wind} = 0$ kW, was assumed to be around 0.98 p.u ($V_{PCC_initial}=0.98$ p.u.). In this Chapter, the focus is on validating the capability of the proposed analytical model in estimating and projecting three important voltage stability criteria at a given PCC point of each one the

four test systems. These criteria are: the V_{PCC} profile, step-voltage variations in response to changes in P_{wind} (ΔV_{PCC}), and the maximum wind power transfer for grid codes compliance ($P_{max-wind}$). The validation studies have been performed using different scenarios for both IG and DFIG-Based WPPs.

5.2 Validation process

This section details the validation process applied for validating the analytical model proposed in Chapter 4. As discussed in the previous section, the validation studies have been carried out using four test systems designed in Chapter 4 with a known set of PCC Buses and SCC values detailed in Table 4.1.

Different voltage values at the candidate PCC buses will impact the voltage behaviour in response to the injection of wind power when the WPP is connected to the PCC bus. Referring to Chapter 4, the voltage value at the candidate PCC buses of the test systems was considered to be 0.98 p.u.

Ten different scenarios have been considered, including six scenarios for the IG-Based WPP and four scenarios for the DFIG-Based WPP. Different potential X/R ratio possibilities have been considered at the PCC points to validate the proposed model for a range of X/R_{PCC} at a fixed SCC bus. The test system, generator type, and the PCC parameters in each scenario are tabulated as shown in Table 5.1.

Table 5.1 Test system, generator type, and PCC parameters.

	Scenario	Test system	SCC	X/R_{PCC}
IG-Based WPP	1	Test 1	27	0.3
	2	Test 2	40	3
	3	Test 2	40	4
	4	Test 3	54	0.3
	5	Test 3	54	4
	6	Test 4	21	3
DFIG-Based WPP	7	Test 1	27	0.5
	8	Test 2	40	0.4
	9	Test 3	54	0.3
	10	Test 4	21	0.6

For each scenario, PV and PΔV characteristics were plotted using the analytical models developed in Chapter 4. For this purpose, Eq. (4.28), Eq. (4.33), and Eq (4.41) were used for calculating V_{PCC} and ΔV_{PCC} data points for different P_{wind} penetrations. Then, the PV and PΔV characteristics were plotted using the obtained data points. Hereinafter, the PV and PΔV characteristics given by the proposed analytical model are called the ‘predicted PV curve’ and ‘predicted PΔV characteristic’, respectively.

For each scenario, PV and PΔV characteristics were also plotted using the data points gained from the network Simulink models. Hereinafter, the PV and PΔV characteristics plotted using datasets from the Simulink model are called the ‘simulated PV curve’ and ‘simulated PΔV characteristic’, respectively. With the knowledge of the simulated and predicted PV and PΔV characteristics, each equation was evaluated in terms of accuracy in predicting the V_{PCC} , ΔV_{PCC} , and $P_{max-wind}$ characteristics at a given bus.

5.3 Validation studies for IG-Based WPPs

This section investigates the accuracy of the proposed analytical model in predicting PV and PΔV characteristics for Scenarios 1 to 6. Figures 5.1 to 5.6 show the simulated and predicted PV and PΔV characteristics for each scenario. V_{PCC} was plotted in the $0.95 \text{ p.u.} < V_{PCC} < 1.05 \text{ p.u}$ range in accordance with the Australian grid codes.

In Figures 5.1 to 5.6, Eq. (4.28) was used for predicting the PV and PΔV curves for Scenarios 1 and 4 where X/R_{PCC} is small. Also, Eq. (4.33) was applied for predicting the PV and PΔ curves for Scenarios 2, 3, 5, and 6 where X/R_{PCC} is large.

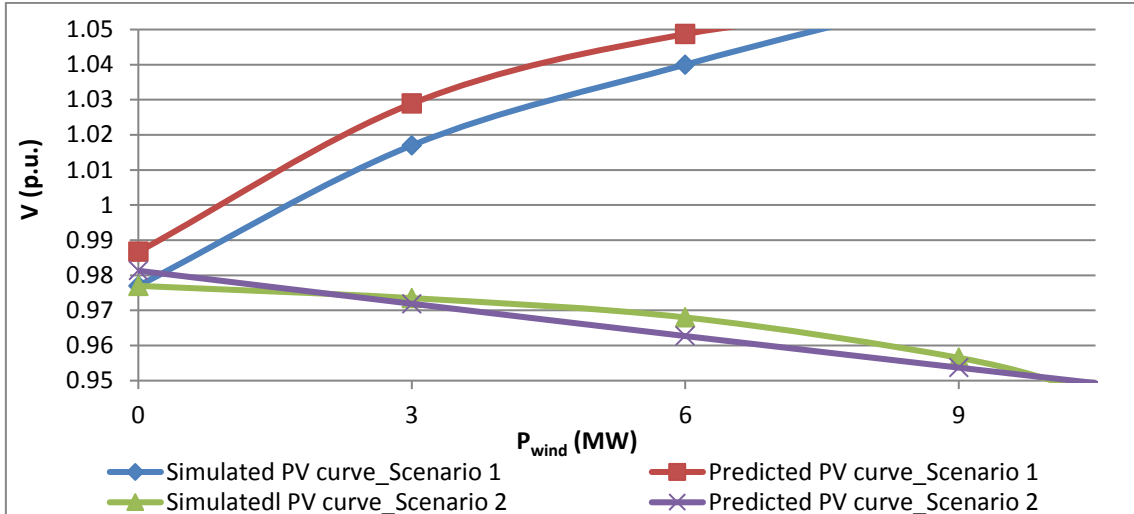


Figure 5.1 PV characteristic for Scenarios 1 and 2.

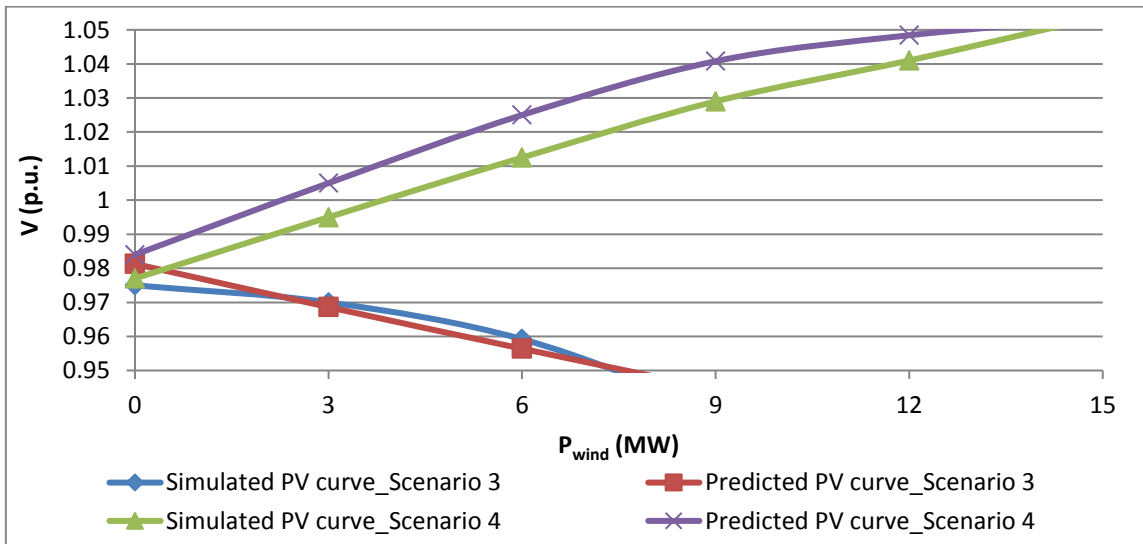


Figure 5.2 PV characteristic for Scenarios 3 and 4.

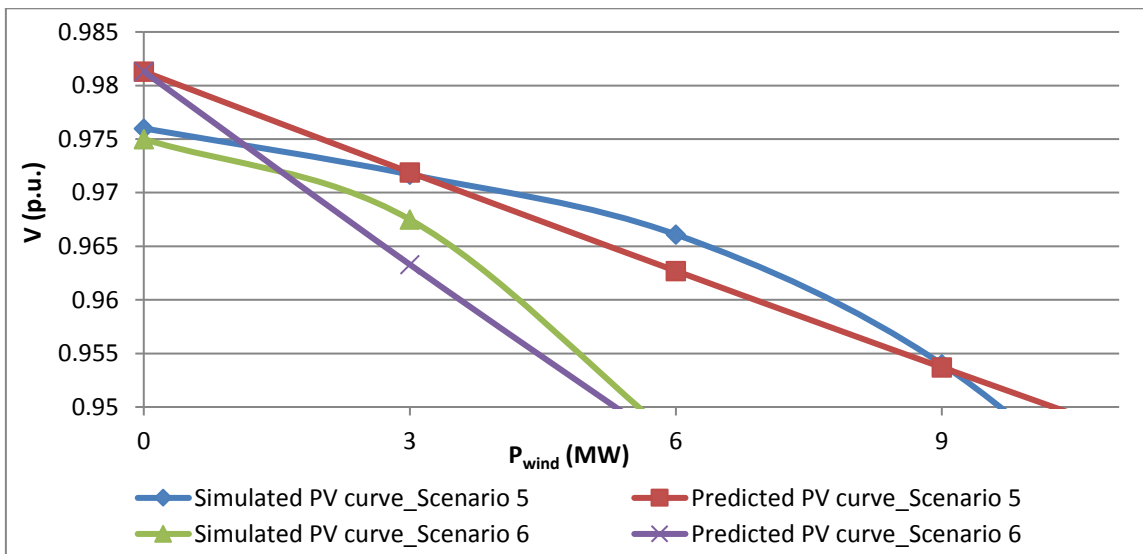


Figure 5.3 PV characteristic for Scenarios 5 and 6.

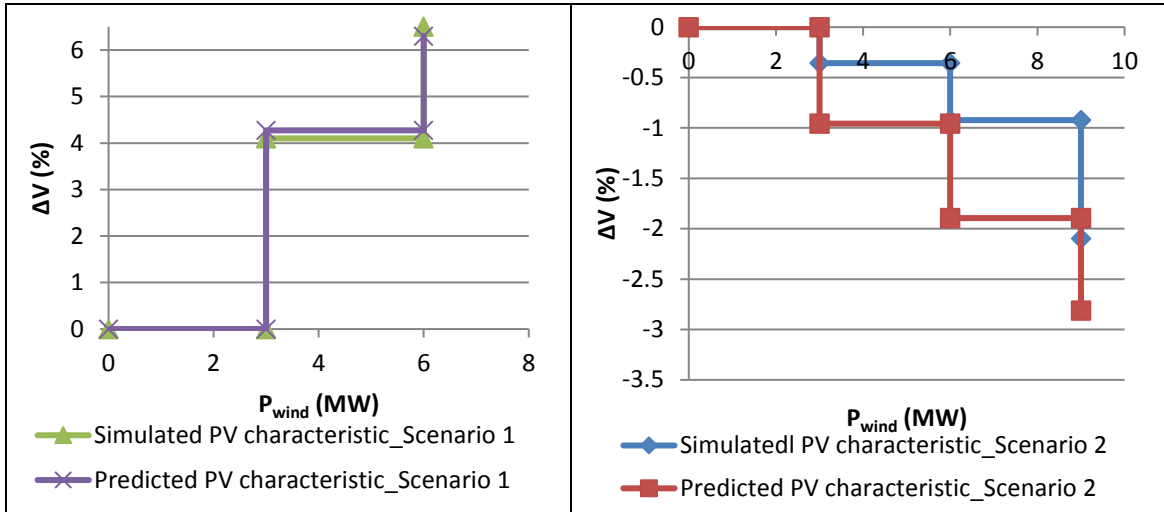


Figure 5.4 PΔV characteristic for Scenarios 1 and 2.

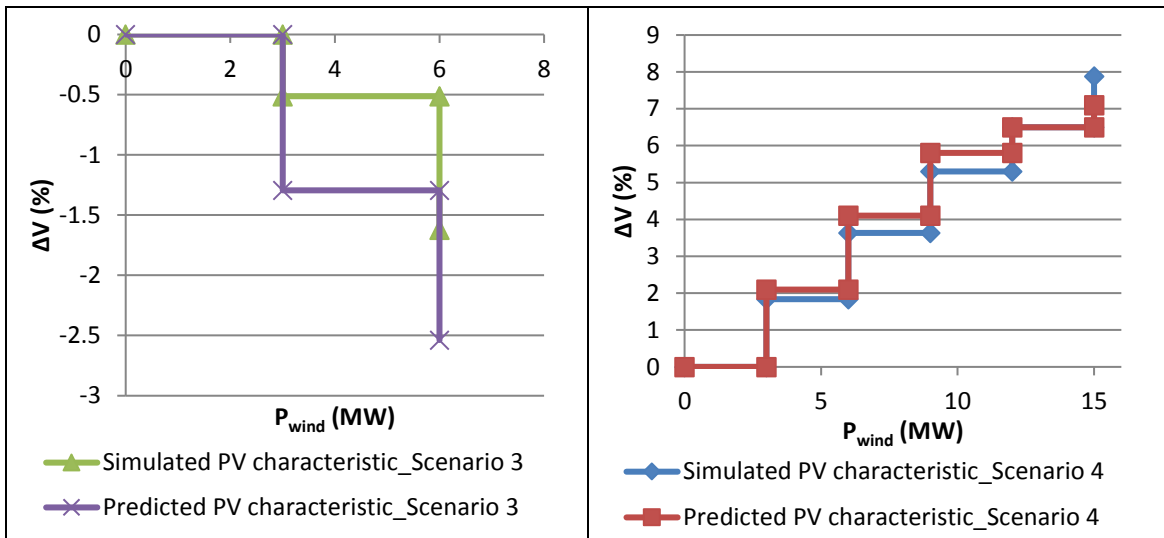


Figure 5.5 PΔV characteristic for Scenarios 3 and 4.

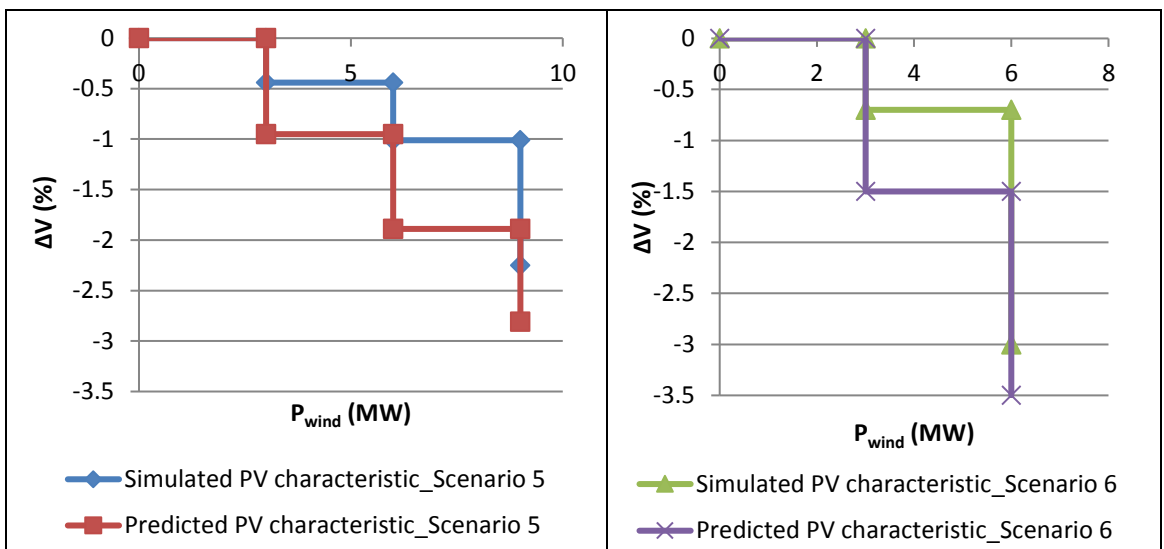


Figure 5.6 PΔV characteristic for Scenarios 5 and 6.

In Chapter 3, it was shown that V_{PCC} increases due to an increase in P_{wind} at small X/R ratio PCC points, while V_{PCC} decreases as P_{wind} increases at large X/R ratio PCC points. These findings could be observed from the PV characteristics presented in Figures 5.1 to 5.6. This confirms that the analytical model developed can accurately be used in projecting the V_{PCC} profile at the WPP connection point.

As discussed in Chapter 3, ΔV at connection points with a small SCC and X/R value would be higher than that at connection points with a large SCC and X/R value. In this case, both simulated and predicted results in Figure 5.4 show that the highest ΔV_{PCC} occurred in Scenario 1 where SCC and X/R values are both small. According to Figure 5.4, in Scenario 1, ΔV_{PCC} is around 4% when P_{wind} increases from 0 to 3 MVA, around 2.5% when P_{wind} increases from 3 to 6 MVA, and about 6.5% when P_{wind} increases from 0 to 6 MVA.

The next three sections investigate the accuracy of the proposed analytical model in predicting V_{PCC} , ΔV_{PCC} , and $P_{max-wind}$ for the IG-Based scenarios using the predicted and simulated PV and P ΔV characteristics presented in Figures 5.1 to 5.6.

5.3.1 Voltage profile prediction in IG-Based WPPs

In this section, the accuracy of the proposed equations in predicting the voltage profile is evaluated using the PV characteristics presented in the previous section (Figures 5.1 to 5.3). The percent error between the simulated and predicted voltage profiles was calculated for different P_{wind} penetration levels for each IG-Based WPP scenario listed in Table 5.1. The results are shown in Table 5.2. According to Table 5.2, twenty five cases have been investigated to evaluate the accuracy of the proposed equations. The results demonstrate that the error between the simulated and predicted values was less than 1% in most cases (21 cases).

The error in scenarios with small X/R_{PCC} ratio, i.e. Scenarios 1 and 4, was slightly higher than that in the other scenarios. This signifies that small X/R_{PCC} impacts the accuracy of the proposed relations. Generally, the results given in Table 5.2 demonstrate that the proposed equations could provide a high accuracy in predicting the voltage profile at a given connection point for the IG-Based scenarios.

Table 5.2 Error between simulated and predicted V_{PCC} profile for Scenarios 1 to 6.

Scenarios	P_{wind} (MW)	$V_{simulated}$ (p.u.)	$V_{predicted}$ (p.u.)	Percent error (%)
Scenario 1	0	0.977	0.9867	0.9928
	3	1.017	1.0289	1.17
	6	1.04	1.0487	0.84
	9	1.06	1.0572	-0.2642
Scenario 2	0	0.977	0.9813	0.4401
	3	0.9735	0.9719	-0.1644
	6	0.968	0.9627	-0.5475
	9	0.9565	0.9537	-0.2927
Scenario 3	0	0.975	0.9813	0.6462
	3	0.97	0.9686	-0.1443
	6	0.9592	0.9564	-0.2919
	9	0.9389	0.9445	0.5964
Scenario 4	0	0.977	0.984	0.7165
	3	0.995	1.005	1
	6	1.0125	1.025	1.57
	9	1.03	1.0408	1.44
	12	1.04	1.0484	0.8077
	15	1.054	1.0534	-0.0569
Scenario 5	0	0.976	0.9813	0.543
	3	0.9717	0.9719	0.02
	6	0.9661	0.9627	-0.3519
	9	0.954	0.9537	-0.0314
Scenario 6	0	0.975	0.9813	0.64
	3	0.9683	0.9633	-0.5
	6	0.948	0.9461	-0.2

5.3.2 Step-voltage variation prediction in IG-Based WPPs

The value of step-voltage variation due to the change of P_{wind} (ΔV_{PCC}) has to satisfy the grid code requirements and should normally be maintained under 3% and not

exceed 4% [50, 51]. This section investigates the accuracy of the proposed analytical models in predicting ΔV profile at potential connection points. For this purpose, the P ΔV characteristics presented in Figure 5.4 to 5.7 were used to calculate the simulated and predicted ΔV_{PCC} for different P_{wind} penetrations for each IG–Based WPP scenarios. For each change in P_{wind} , ΔV_{PCC} was checked to confirm whether it satisfies or violates the grid code requirements while V_{PCC} is between 0.95 and 1.05 p.u. The results are as shown in Table 5.3.

Table 5.3 Error between simulated and predicted ΔV_{PCC} for Scenarios 1 to 6.

Scenarios	P_{wind} (MW)		$\Delta V_{simulated}$ (%)		$\Delta V_{predicted}$ (%)	
	From	To	Value	Evaluating based on grid codes	Value	Evaluating based on grid codes
Scenario 1	0	3	4.1	Violates the grid code	4.2769	Violates the grid code
	3	6	2.2	Satisfies the grid code	1.9244	Satisfies the grid code
	0	6	6.5	Violates the grid code	6.3	Violates the grid code
Scenario 2	0	3	-0.3582	Satisfies the grid code	-0.9579	Satisfies the grid code
	3	6	-0.5650	Satisfies the grid code	-0.9466	Satisfies the grid code
	6	9	-1.188	Satisfies the grid code	-0.9349	Satisfies the grid code
	0	6	-0.9212	Satisfies the grid code	-1.8954	Satisfies the grid code
	0	9	-2.1	Satisfies the grid code	-2.8126	Satisfies the grid code
	3	9	-1.7463	Satisfies the grid code	-1.8726	Satisfies the grid code
Scenario 3	0	3	-0.5128	Satisfies the grid code	-1.2942	Satisfies the grid code
	3	6	-1.1134	Satisfies the grid code	-1.2595	Satisfies the grid code
	0	6	-1.6205	Satisfies the grid code	-2.5375	Satisfies the grid code
Scenario 4	0	3	1.84	Satisfies the grid code	2.1	Satisfies the grid code
	3	6	1.76	Satisfies the grid code	2	Satisfies the grid code
	6	9	1.6	Satisfies the grid code	1.55	Satisfies the grid code
	9	12	1.16	Satisfies the grid code	0.75	Satisfies the grid code
	12	15	1.25	Satisfies the grid code	0.5	Satisfies the grid code
	0	6	3.63	Violates the grid code	4.1	Violates the grid code
	0	9	5.3	Violates the grid code	5.8	Violates the grid code
	0	12	6.5	Violates the grid code	6.5	Violates the grid code
	0	15	7.88	Violates the grid code	7.1	Violates the grid code
	3	9	3.42	Violates the grid code	3.56	Violates the grid code
	3	12	4.6	Violates the grid code	4.32	Violates the grid code
	3	15	5.93	Violates the grid code	4.82	Violates the grid code
	6	12	2.8	Satisfies the grid code	2.3	Satisfies the grid code
	6	15	4	Violates the grid code	3	Violates the grid code
	9	15	2.4	Satisfies the grid code	1.21	Satisfies the grid code
Scenario 5	0	3	-0.44	Satisfies the grid code	-0.95	Satisfies the grid code
	3	6	-0.58	Satisfies the grid code	-0.94	Satisfies the grid code
	6	9	-1.25	Satisfies the grid code	-0.94	Satisfies the grid code
	0	6	-1.01	Satisfies the grid code	-1.89	Satisfies the grid code

	0	9	-2.25	Satisfies the grid code	-2.81	Satisfies the grid code
	3	9	-1.82	Satisfies the grid code	-1.87	Satisfies the grid code
Scenario 6	0	3	-0.7	Satisfies the grid code	-1.5	Satisfies the grid code
	3	6	-2.1	Satisfies the grid code	-2	Satisfies the grid code
	0	6	-3	Violates the grid code	-3.5	Violates the grid code

Both simulated and predicted results in Table 5.3 show that the ΔV_{PCC} is high and may violate the grid code requirements in scenarios where X/R_{PCC} is small, i.e. Scenarios 1 and 4. For example, in Scenario 4, both predicted and simulated results show that ΔV_{PCC} would be greater than 3% in some cases where the increase in P_{wind} is greater than 3 MW. This signifies that ΔV_{PCC} would violate grid code requirements when two or more 3 MVA generators are simultaneously connected to the grid. In other scenarios, such as Scenario 2, both predicted and simulated results show that ΔV_{PCC} for different P_{wind} penetration levels would satisfy grid code requirements as $\Delta V_{simulated}$ and $\Delta V_{predicted}$ are less than 3% in all six cases where $0.95 \text{ p.u.} < V_{PCC} < 1.05 \text{ p.u.}$

Comparing and contrasting the results in Table 5.3 justifies that the simulated results confirm the results estimated and calculated by the proposed equations in all cases. Therefore, these validation studies have successfully confirmed the high accuracy of the proposed equations in predicting ΔV_{PCC} for all IG-Based scenarios detailed in Table 5.1.

5.3.3 IG-Based WPP maximum allowable sizing prediction

This section validates the accuracy of the proposed analytical model in predicting the maximum power can be injected by the WPP ensuring $0.95 \text{ p.u.} < V_{PCC} < 1.05 \text{ p.u.}$ ($P_{max-wind}$) in Scenarios 1 to 6. Although, the $P_{max-wind}$ value can be estimated using the predicted graphs shown in Figures 5.1 to 5.3, the use of predicted PV characteristics is not a straight forward solution for finding the $P_{max-wind}$ value.

Referring to Chapter 4, Eqs. (4.32) and (4.39) were proposed to calculate how much P_{wind} must be provided to have a specific voltage value at a given connection point of an IG-Based WPP. Moreover, as discussed in Chapter 3, the increase in P_{wind} increases voltage at small X/R ratio PCC points and decreases voltage at PCC points with a large X/R ratio. Therefore, taking the advantage of Eqs. (4.32) and (4.39), the $P_{max-wind}$ parameter could be calculated if the V_{PCC} value is considered to be the upper boundary of the acceptable range (1.05 p.u.) when $X/R_{PCC} < 2$, and the lower boundary of the allowable range (0.95 p.u.) when $X/R_{PCC} > 2$. Eqs (4.32) and (4.39) can then be rearranged as shown below to produce Eqs (5.2), (5.4), using which the $P_{max-wind}$ parameter can be calculated.

- **IG-Based WPP with $X/R_{PCC} < 2$**

Eq. (4.32) developed in Chapter 4:
$$P_{wind} = 0.29 \times \frac{\frac{X}{R} \times SCC}{Ln\left(\frac{0.0912}{V - 0.9867}\right)}$$

$$\xrightarrow{V=1.05(p.u.)} P_{max-wind} = 0.29 \times \frac{\frac{X}{R} \times SCC}{Ln\left(\frac{0.0912}{1.05 - 0.9867}\right)} \quad (5.1)$$

$$\rightarrow P_{max-wind} = 0.7941 \times \frac{X}{R} \times SCC \quad (5.2)$$

- **IG-Based WPP with $X/R_{PCC} > 2$**

Eq. (4.39) developed in Chapter 4:
$$P_{wind} = SCC \times \frac{R}{X} \times \left(10.675 - \sqrt{500 \times (V - 0.9813) + 114}\right)$$

$$\xrightarrow{V=0.95(p.u.)} P_{max-wind} = SCC \times \frac{R}{X} \times \left(10.675 - \sqrt{500 \times (0.95 - 0.9813) + 114}\right) \quad (5.3)$$

$$\rightarrow P_{max-wind} = 0.7578 \times SCC \times \frac{R}{X} \quad (5.4)$$

Eq (5.2) was used for calculating $P_{\max\text{-wind}}$ in Scenarios 1 and 4 where $X/R_{\text{PCC}} < 2$ and Eq (5.4) was used for calculating $P_{\max\text{-wind}}$ in Scenarios 2, 3, 5, and 6 where $X/R_{\text{PCC}} > 2$. The predicted values are, then, compared with the $P_{\max\text{-wind}}$ values gained by the simulated PV characteristics shown in Figures (5.1) to (5.3).

Figure 5.7 shows the simulated and predicted $P_{\max\text{-wind}}$ values for each scenario listed in Table 5.1. As shown, the highest difference between the predicted and simulated results is around 1 MW, which is corresponding with 13% error, in Scenario 1, where both X/R_{PCC} and SCC values are small. Therefore, small SCC values slightly impact the accuracy of the proposed analytical model in predicting $P_{\max\text{-wind}}$ in IG-Based WPP with a small X/R_{PCC} ratio ($X/R_{\text{PCC}} < 2$). In this case, as shown in Figure 5.7, the proposed equation (Eq. (5.2)) has a worst case 87 % accuracy in Scenario 1. However, in the other cases where $X/R_{\text{PCC}} > 2$ or SCC value is large, the error is less than 0.5 MW.

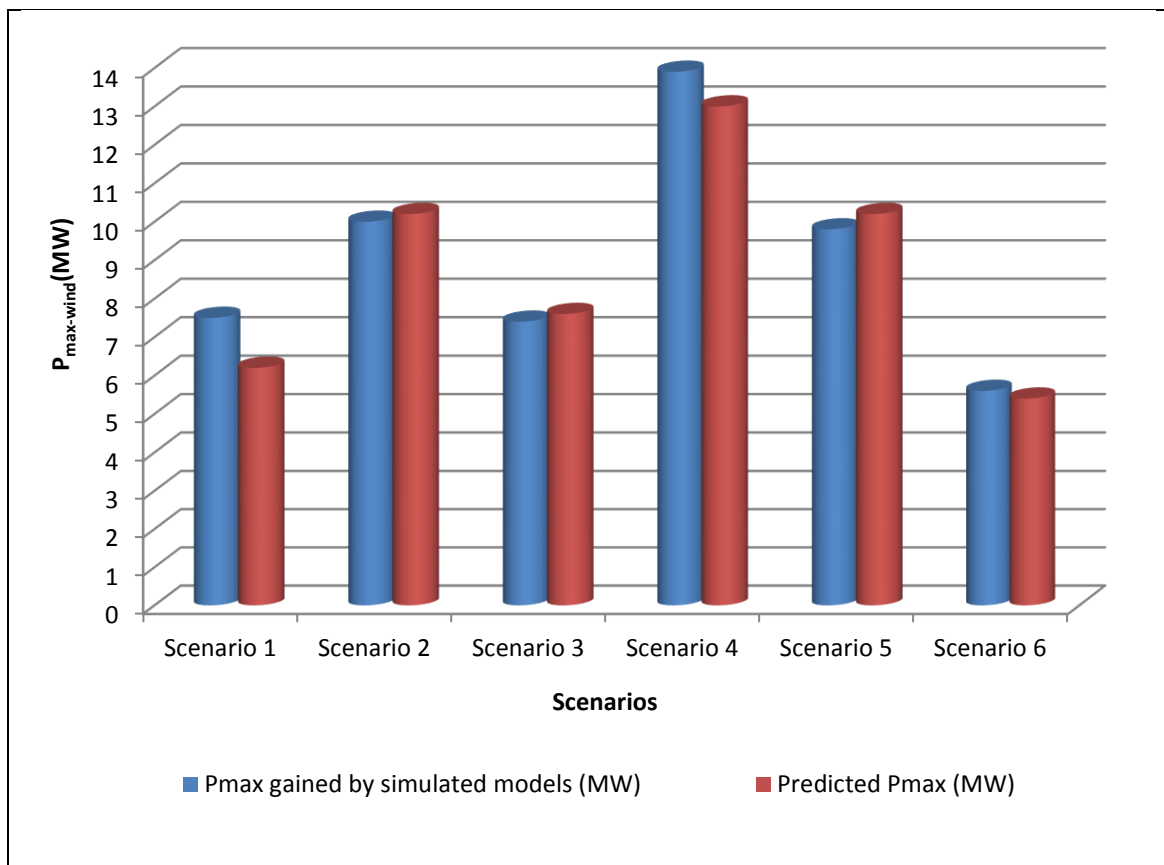


Figure 5.7 Predicted and simulated $P_{\max\text{-wind}}$ for Scenarios 1 to 6.

5.4 Validation studies for DFIG–Based WPPs

Similar to the IG–Based WPPs, validation studies were also carried out for the DFIG–Based WPP. To evaluate accuracy of the developed analytical models, simulated PV characteristics and those predicted and plotted by Eq. (4.41) were analysed and compared for the four different scenarios detailed in Table 5.2 (Scenarios 7 to 10). Figures (5.8) to (5.11) show the simulated and predicted PV characteristics for each scenario.

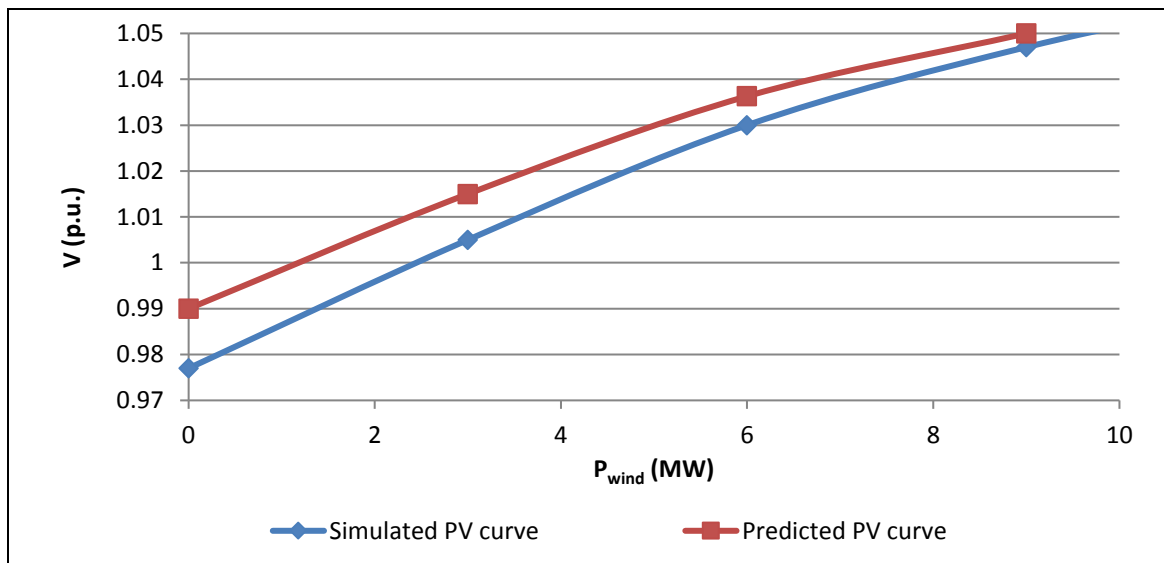


Figure 5.8 PV characteristic for Scenario 7.

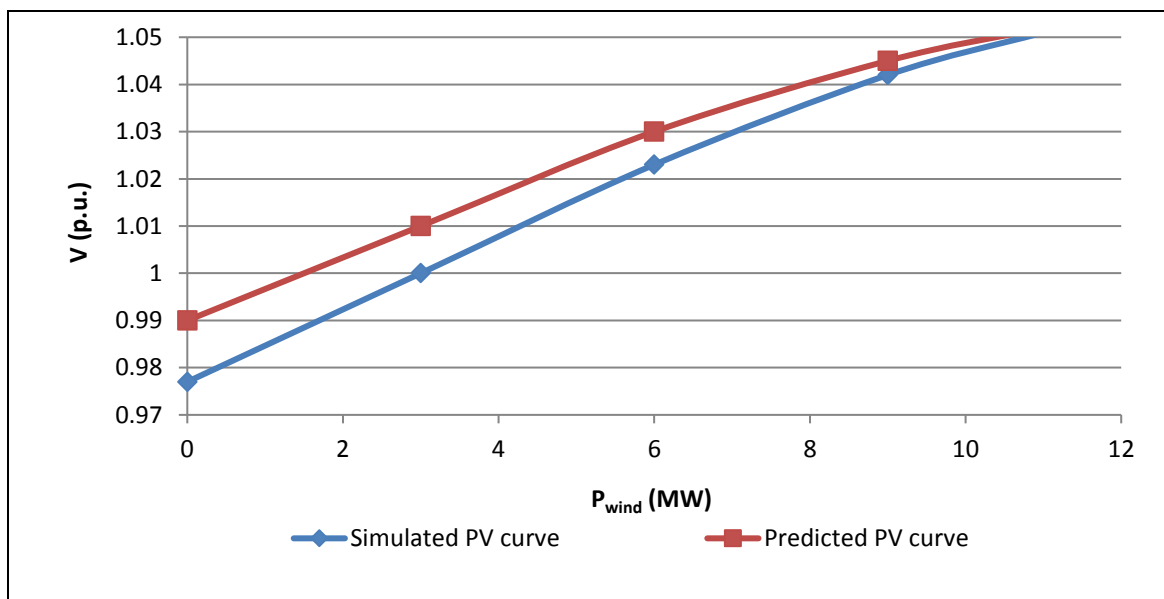


Figure 5.9 PV characteristic for Scenario 8.

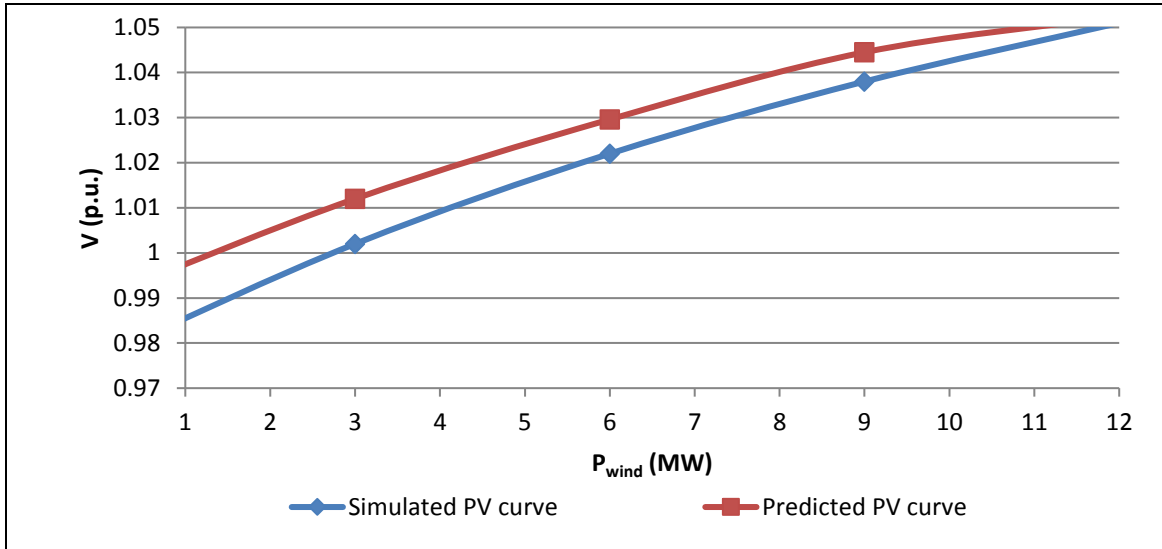


Figure 5.10 PV characteristic for Scenario 9.

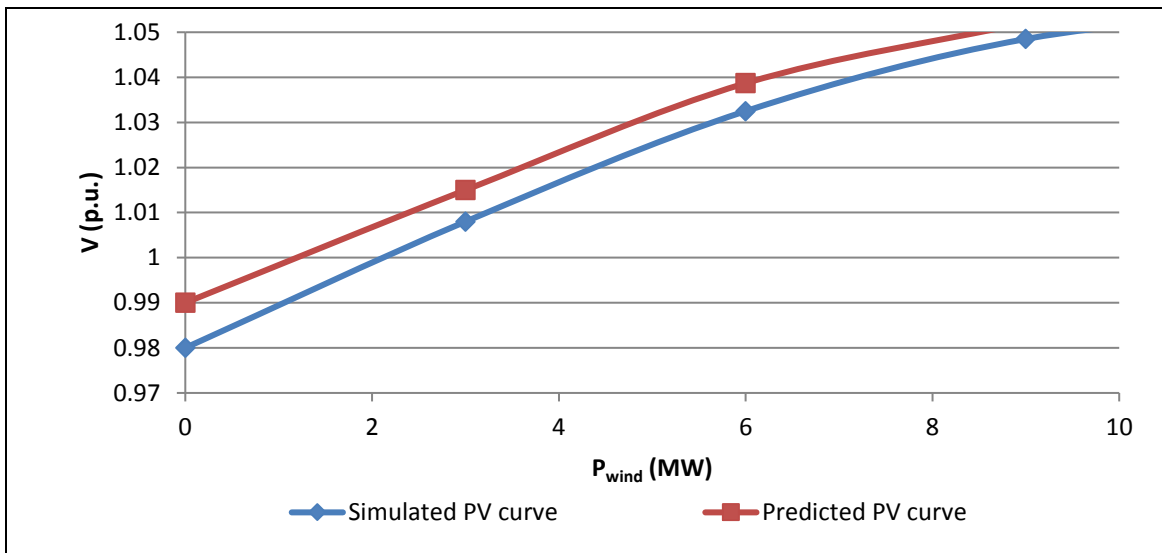


Figure 5.11 PV characteristic for Scenario 10.

Chapter 3 discussed the fact that, in DFIG–Based WPPs, small SCC and X/R_{PCC} ratios adversely impact voltage stability at a given PCC connection point when P_{wind} increases. As shown in Figure 5.10, the highest P_{wind} penetration is attainable in Scenario 9 where the SCC value is highest. X/R_{PCC} is highest in Scenario 10, but the small SCC in this scenario does not allow a high P_{wind} penetration. In this case, as shown in Figure 5.11, $P_{max-wind}$ is around 9 MW which is less than the $P_{max-wind}$ value in Scenario 9. Therefore, the results in Figures 5.8 to 5.11 confirm the findings presented in Chapter 3.

5.4.1 Voltage profile prediction in DFIG-Based WPPs

This section evaluates the accuracy of Eq. (4.41) in predicting V_{PCC} for DFIG-Based scenarios detailed in Table (5.1). The analysis of results shown in Table 5.4, for Scenarios 7 to 10, points the highest error to be around 1.4% and demonstrates that the error in most cases is less than 1%. Furthermore, in some cases such as those in Scenarios 7, 8, and 9, the percent error between predicted and simulated values is close to zero (Percent error < 0.3%). Therefore, the results validate that Eq. (4.41) can provide a significant accuracy in predicting V_{PCC} value in DFIG-Based WPP.

Table 5.4 Error between simulated and predicted V_{PCC} profile for Scenarios 7 to 10.

Scenarios	P_{wind} (MW)	$V_{simulated}$	$V_{predicted}$	Percent error (%)
Scenario 7	0	0.977	0.99	1.33
	3	1.005	1.015	1
	6	1.03	1.036	0.485
	9	1.047	1.05	0.28
Scenario 8	0	0.977	0.99	1.33
	3	1	1.01	1
	6	1.022	1.03	0.7828
	9	1.42	1.045	0.28
Scenario 9	0	0.977	0.99	1.33
	3	1.002	1.01	1
	6	1.022	1.0296	0.94
	9	1.038	1.045	0.7
	12	1.051	1.053	0.2
Scenario 10	0	0.98	0.99	1.02
	3	1.008	1.015	0.7
	6	1.0325	1.0387	0.6
	9	1.0485	1.0521	0.34

5.4.2 Step-voltage variation prediction in DFIG-Based WPPs

Similar to IG-Based WPPs, validation studies have been carried out for predicting ΔV_{PCC} using the relevant proposed equation (Eq. (4.41)) when $0.95 \text{ p.u.} < V_{PCC} < 1.05 \text{ p.u.}$ As an example, Figure 5.12 shows the predicted and simulated $P\Delta V$ characteristic at the PCC point plotted for Scenario 9, where the wind power penetration ensuring grid code requirements is the highest.

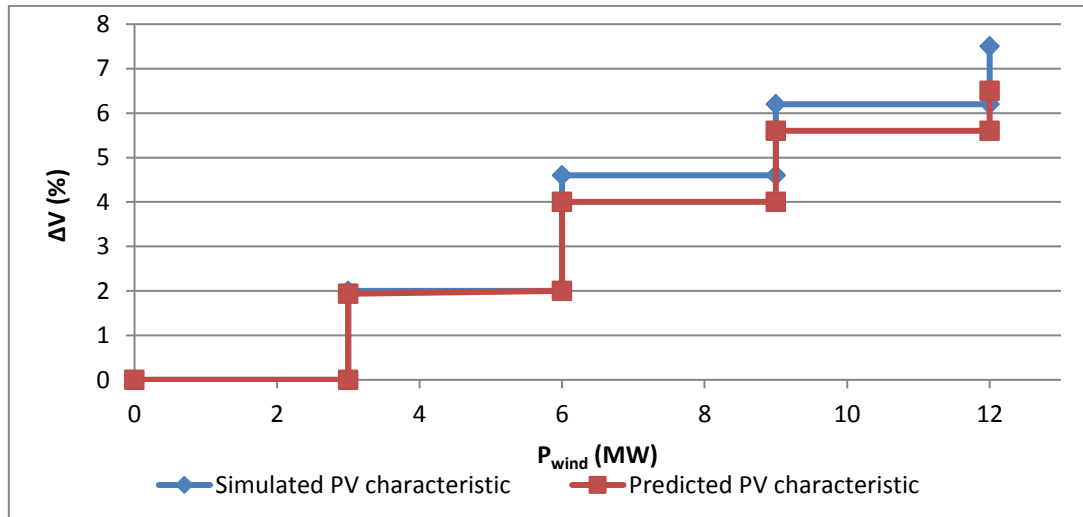


Figure 5.12 $P\Delta V$ characteristic for Scenario 9.

As shown in Figure 5.12, the predicted PV characteristic follows the PV characteristics gained by simulation results. The highest error is 1%. Despite the error between the predicted and simulated results, the results demonstrate that the proposed equation enables to predict the voltage variation violence. Both predicted and simulated result show that ΔV violates the grid code requirements ($\Delta V > 3\%$) when the increase in P_{wind} injection is 6 MW or over (for example when P_{wind} injection increases from 3 to 9 MW, i.e. two 3 MVA generators are simultaneously connected to the grid, or from 3 to 12 MW, i.e. when three 3 MVA generators are simultaneously connected to the grid).

As shown in Table 5.5, for each DFIG–Based scenario, the ΔV_{PCC} value was calculated from both simulation data and predicted by the analytical model for the 0.95 p.u. $< V_{PCC} < 1.05$ p.u range. This analysis enabled an observation on whether the voltage variations would satisfy or violate the grid code requirements. The V_{PCC} profile is within the allowable steady-state range for different P_{wind} injection levels shown in Table 5.5. However, both simulated and predicted results demonstrate that, in all four Scenarios, ΔV_{PCC} is greater than 3% when a large amount of P_{wind} (6 MW or over) is

injected to the grid. V_{PCC} variations therefore violate grid code requirements when two or more 3 MW generators are simultaneously connected to the grid.

From Table 5.5, it is clear that the results given from simulation confirm results estimated by the proposed Eq. (4.41). In all simulated cases, Eq. (4.41) has accurately predicted grid code violations in the permissible ΔV_{PCC} levels.

Table 5.5 Error between simulated and predicted ΔV_{PCC} for Scenarios 7 to 10.

Scenarios	P_{wind} (MW)		$\Delta V_{simulated}$ (%)		$\Delta V_{predicted}$ (%)	
	From	To	Value	Evaluating based on grid codes	Value	Evaluating based on grid codes
Scenario 7	0	3	2.86	Satisfies the grid code	2.5	Satisfies the grid code
	3	6	2.58	Satisfies the grid code	2.1	Satisfies the grid code
	6	9	1.65	Satisfies the grid code	1.32	Satisfies the grid code
	0	6	5.5	Violates the grid code	4.7	Violates the grid code
	0	9	7.2	Violates the grid code	6.1	Violates the grid code
	3	9	4.2	Violates the grid code	3.5	Violates the grid code
Scenario 8	0	3	2.35	Satisfies the grid code	2	Satisfies the grid code
	3	6	2.3	Satisfies the grid code	1.98	Satisfies the grid code
	6	9	1.86	Satisfies the grid code	1.5	Satisfies the grid code
	0	6	4.7	Violates the grid code	4	Violates the grid code
	0	9	6.65	Violates the grid code	5.6	Violates the grid code
	3	9	4.2	Violates the grid code	3.5	Violates the grid code
Scenario 9	0	3	2.5	Satisfies the grid code	2	Satisfies the grid code
	3	6	2	Satisfies the grid code	1.94	Satisfies the grid code
	6	9	1.56	Satisfies the grid code	1.5	Satisfies the grid code
	9	12	1.25	Satisfies the grid code	0.8	Satisfies the grid code
	0	6	4.6	Violates the grid code	4	Violates the grid code
	0	9	6.2	Violates the grid code	5.6	Violates the grid code
	0	12	7.5	Violates the grid code	6.5	Violates the grid code
	3	9	3.6	Violates the grid code	3.5	Violates the grid code
	3	12	4.9	Violates the grid code	4.3	Violates the grid code
6	12	2.8	Satisfies the grid code	2.3	Satisfies the grid code	
Scenario 10	0	3	2.86	Satisfies the grid code	2.53	Satisfies the grid code
	3	6	2.4	Satisfies the grid code	2.34	Satisfies the grid code
	6	9	1.55	Satisfies the grid code	1.3	Satisfies the grid code
	0	6	5.36	Violates the grid code	5	Violates the grid code
	0	9	6.98	Violates the grid code	6.3	Violates the grid code
	3	9	4	Violates the grid code	3.7	Violates the grid code

5.4.3 DFIG-Based WPP maximum allowable sizing prediction

In this section, $P_{max-wind}$ values from the actual PV characteristics are compared with the $P_{max-wind}$ values given by the proposed analytical model for Scenarios 7 to 10.

In Chapter 4, P_{wind} by the DFIG–Based WPPs was formulated as a function of V_{PCC} , SCC, and X/R_{PCC} , as in Eq. (4.45). This signifies that the $P_{max-wind}$ can be calculated by rearranging Eq. (4.45) and solving for P_{wind} when $V_{PCC} = 1.05$ p.u as given by Eq. (5.6).

Eq. (4.45) developed in Chapter 4:
$$P_{wind} = 0.347 \times \frac{\frac{X}{R} \times SCC}{Ln\left(\frac{0.101}{V - 0.99}\right)}$$

$$\xrightarrow{V = 1.05 (p.u.)} P_{max-wind} = 0.347 \times \frac{\frac{X}{R} \times SCC}{Ln\left(\frac{0.101}{1.05 - 0.99}\right)} \quad (5.5)$$

$$\rightarrow P_{max-wind} = 0.6663 \times \frac{X}{R} \times SCC \quad (5.6)$$

For each DFIG–Based scenario listed in Table 5.1, Eq. (5.6) was used for calculating the $P_{max-wind}$ value. Figure 5.13 presents the comparison of the simulated and predicted $P_{max-wind}$ values, for Scenarios 7 to 10.

As shown in Figure 5.13, the highest error between simulated and predicted $P_{max-wind}$ occurred in Scenario 10 where SCC value is smaller than that in the other Scenarios. This signifies that small SCC values impact the accuracy of the developed relation in predicting $P_{max-wind}$ in DFIG-Based WPP. However, as shown in Figure 5.13, the highest error is around 1 MW indicating the worst case accuracy is around 90%. In Scenario 7, where SCC value is larger than that in Scenario 10 but smaller than that in two other Scenarios, the difference between predicted and simulation results is around 0.5 MW, which is correspondence with 7% error. In Scenarios 9 and 8, the percent error is around 4% and 0%, respectively. Therefore, the results demonstrate that Eq. (5.6) has significant accuracy in predicting $P_{max-wind}$ in DFIG-Based WPPs.

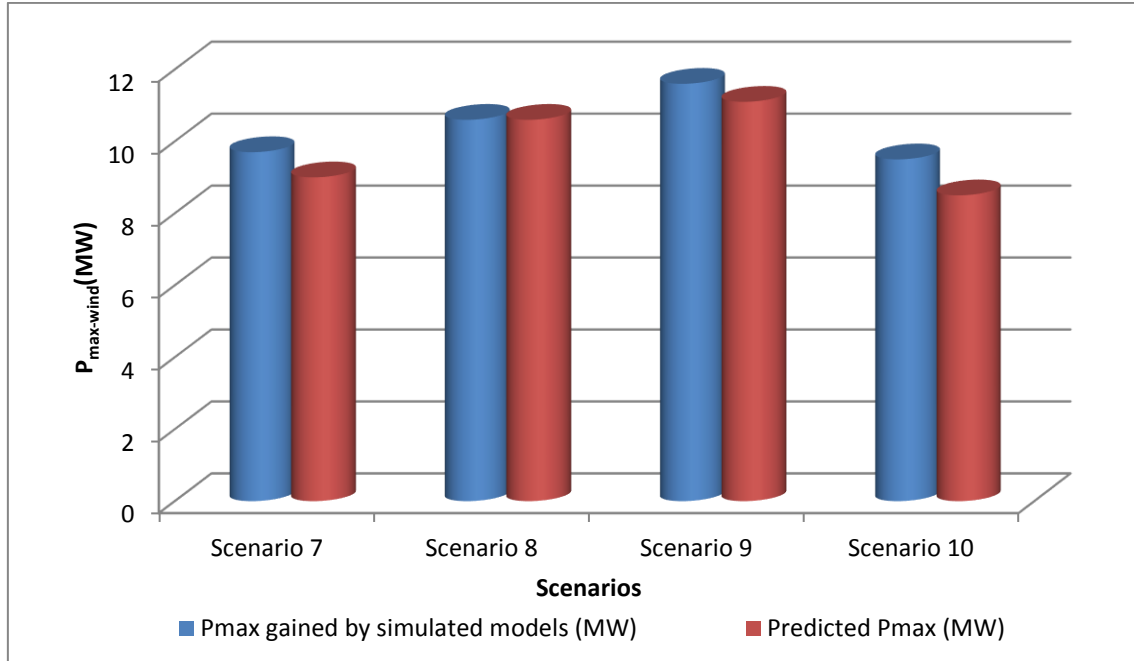


Figure 5.13 Predicted and simulated $P_{\max\text{-wind}}$ for Scenarios 7 to 10.

5.5 Conclusion

This chapter has presented the validation studies carried out for the voltage stability analytical model developed in Chapter 4 using different scenarios. The main idea was to investigate the capabilities of the proposed model in predicting three voltage stability criteria which are vital to the interconnection of WPPs to a distribution system. These criteria are: voltage profile at a PCC point, the step- V_{PCC} variation due to the change of wind power, and maximum permissible P_{wind} ensuring the grid code requirements.

Ten scenarios were considered based on the test systems used in Chapter 4 for acquiring simulation data and develop the analytical model. For each test system, the validation results demonstrated that the analytical model developed during the course of this research is capable of predicting the PV and $P\Delta V$ characteristics at a given connection point with specific X/R and SCC values. This enables to calculate the voltage stability criteria considered at a given PCC point.

In this Chapter, the validation studies were carried out assuming that voltage at the connection point of the test systems is regulated around 0.98 p.u. when the WPP is not connected to the distribution network ($V_{PCC_initial} = 0.98$ p.u.). However, different voltage values at the candidate PCC buses will impact the voltage behaviour in response to the injection of P_{wind} after the connection of WPP to those bus. This hinders to apply the analytical model developed in Chapter 4 for predicting the voltage stability criteria in test systems where $V_{PCC_initial}$ value is different from the default value ($V_{PCC_initial} \neq 0.98$ p.u.). In this regard, next Chapter investigates how the equations proposed in Chapter 4 can be further developed to take into account the possibility of different $V_{PCC_initial}$ values.

Chapter 6 - Development of the Proposed Analytical Model for Different Operating Conditions

6.1 Introduction

Preceding chapters have explained the details of the analytical predictive model developed in this research. This chapter is the final step of this research where the analytical model is developed and used for accurately predicting the voltage stability criteria at a PCC bus for any $V_{PCC_initial}$ value and PCC parameters. As mentioned in the preceding chapters, $V_{PCC_initial}$ signifies the value of PCC bus voltage when $P_{wind} = 0$ MW. The predictive assessment has been carried out based on three important voltage stability criteria, including: V_{PCC} profile, step-voltage variation at the PCC in response to the change of wind power (ΔV_{PCC}), and the maximum permissible wind power injection ensuring the grid code requirements ($P_{max-wind}$).

Voltage level is one of the most important defining factors for a distribution feeder. The loading condition noticeably affects voltages at distribution feeders. To lessen the loading problems and maintain the voltage value around the normal level at the distribution network buses, rural Australian networks make frequent use of voltage regulators. According to a case study report based on a comprehensive database of feeders, 68% of long rural feeders and 21% of short rural feeders feature at least one voltage regulator [162].

Referring to Chapter 4, in developing the analytical formulae, it was assumed that the operation of a voltage regulator results in $V_{PCC_initial}$ of around 0.98 p.u. The value of 0.98 p.u. was therefore taken as the default value for the $V_{PCC_initial}$ parameter. However, loading conditions and various voltage regulator set-point values may result in

$V_{PCC_initial}$ values which are different from this default value. $V_{PCC_initial}$ has a profound effect on the P_{wind} - V_{PCC} characteristic and on the steady-state voltage stability after the connection of WPP. In this regards, the proposed analytical model should ideally work for any $V_{PCC_initial}$ value.

The objective of this Chapter is to further develop the proposed analytical approach such that it satisfies a wide range of $V_{PCC_initial}$. This will make it possible to predict the voltage behaviour in response to the injection of P_{wind} for different loading conditions and $V_{PCC_initial}$ values. Developing the analytical model for any $V_{PCC_initial}$ value, the model will be validated using different scenarios involving a wide range of operating conditions.

6.2 Development of the analytical model for different $V_{PCC_initial}$

Referring to Chapter 4, the proposed analytical model that shows the mathematical relations between voltage, the PCC parameters (SCC and X/R_{PCC}), and P_{wind} , were developed assuming that $V_{PCC_initial} = 0.98$ p.u. As discussed in detail in Section 6.1, $V_{PCC_initial}$ significantly impacts the P_{wind} versus V_{PCC} characteristic, the ΔV_{PCC} , and the $P_{max-wind}$ value. The loading condition and set-point value of the voltage regulators impact the value of the $V_{PCC_initial}$. However, these factors would not change the X/R_{PCC} and SCC values. Hence, $V_{PCC_initial}$ value may be different from 0.98 p.u, which was assumed earlier when developing the analytical models. This section investigates how the equations proposed in Chapter 4 can further be developed to take into account the possibility of different $V_{PCC_initial}$ values.

Eight scenarios have been considered based on the four test distribution systems with the PCC parameters presented in Table 4.1 in Chapter 4. Four scenarios are concerned with the IG-Based WPPs and four scenarios relate to DFIG-Based WPPs. In

each scenario, it is assumed that PCC bus voltage is regulated such that $V_{PCC} \neq 0.98$ p.u. for the $P_{wind} = 0$ kW case ($V_{PCC_initial} \neq 0.98$ p.u.). Hereinafter, the new value of the $V_{PCC_initial}$ which differs from the default value is expressed by $V_{PCC_initial_new}$. Furthermore, the difference between $V_{PCC_initial_new}$ and the default value is expressed by $\Delta V_{PCC_initial}$. Similar to the previous sections, analysis has been carried out for different X/R_{PCC} values. For each scenario, the values of $V_{PCC_initial_new}$, $\Delta V_{PCC_initial}$, and the X/R_{PCC} value are shown in Table 6.1.

Table 6.1 PCC parameters for Scenarios with new $V_{PCC_initial}$ values.

Generator type	Scenario	Test system	X/R_{PCC}	$V_{PCC_initial_new}$ (p.u.)	$\Delta V_{PCC_initial}$ (p.u.)
IG-Based WPP	A	Test 1	0.3	0.99	0.01
	B	Test 2	3	0.97	- 0.01
	C	Test 3	0.3	1	0.02
	D	Test 4	4	0.99	0.01
DFIG-Based WPP	E	Test 1	0.5	1	0.02
	F	Test 2	0.4	0.97	- 0.01
	G	Test 3	0.3	1	0.02
	H	Test 4	0.6	0.99	0.01

For each scenario, two PV characteristics were plotted using data obtained from the simulation studies: one characteristic for $V_{PCC_initial}$ with the values shown in Table 6.1 ($V_{PCC_initial} = V_{PCC_initial_new}$), and another characteristic for the default $V_{PCC_initial} = 0.98$ p.u. The results are as presented in Figures 6.1 to 6.8.

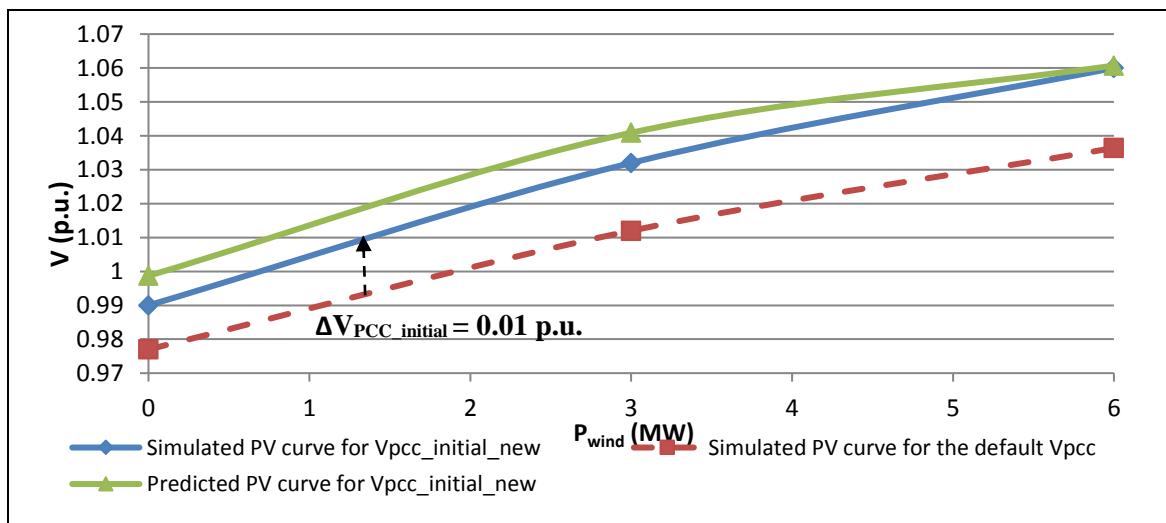


Figure 6.1 PV characteristic for Scenario A.

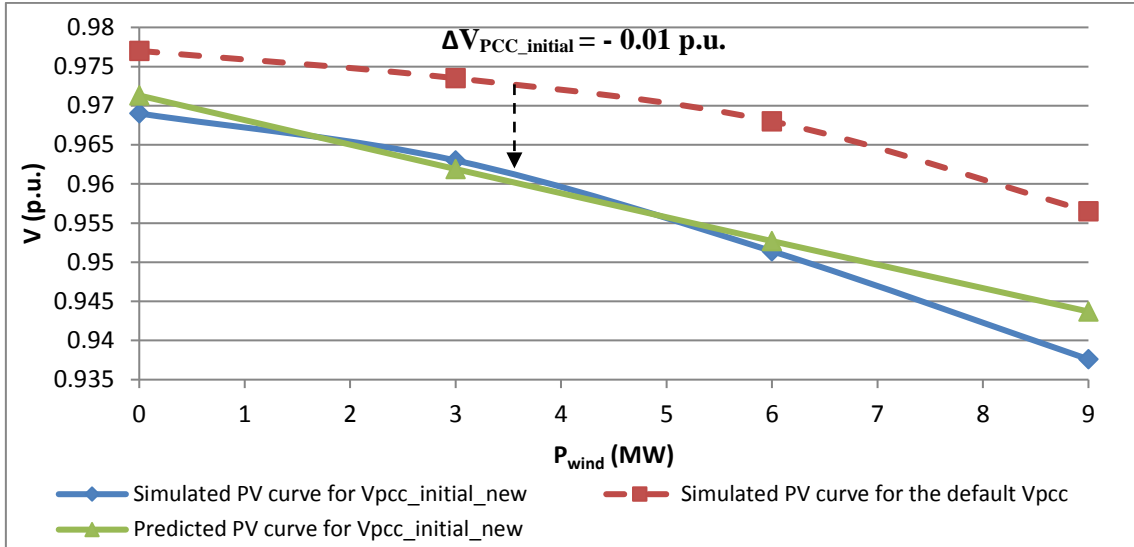


Figure 6.2 PV characteristic for Scenario B.

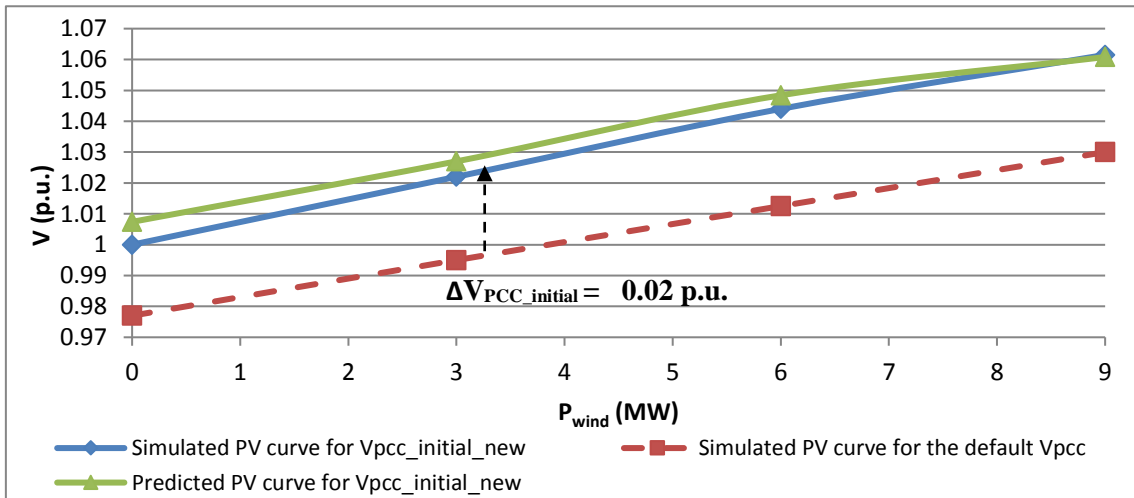


Figure 6.3 PV characteristic for Scenario C.

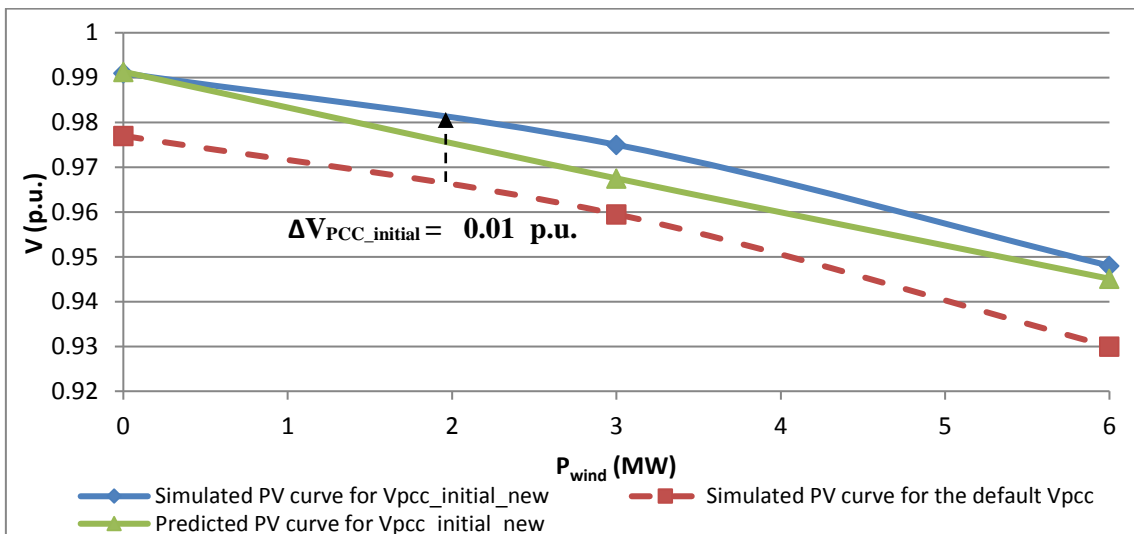


Figure 6.4 PV characteristic for Scenario D.

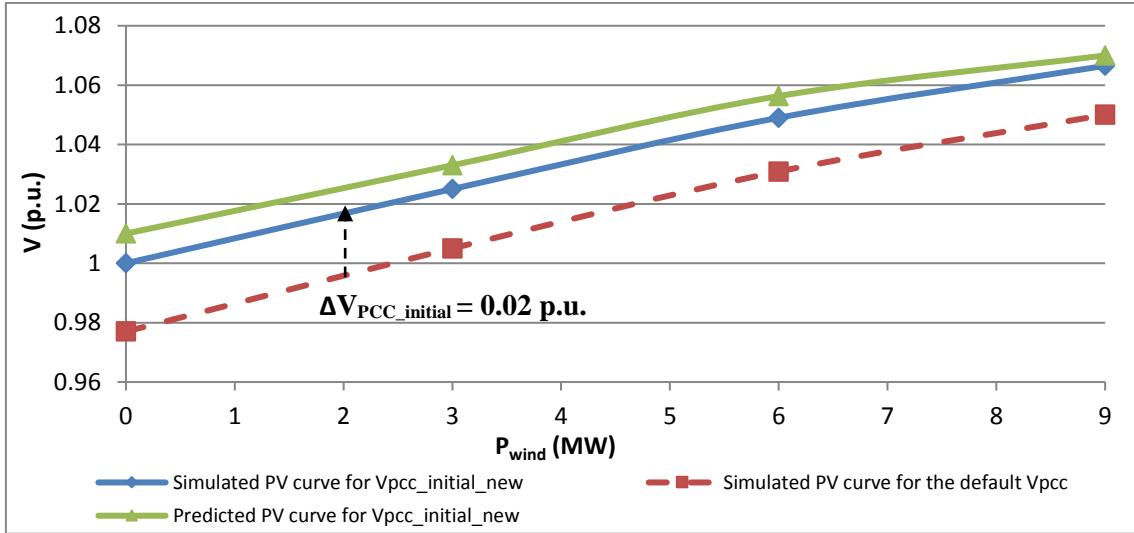


Figure 6.5 PV characteristic for Scenario E.

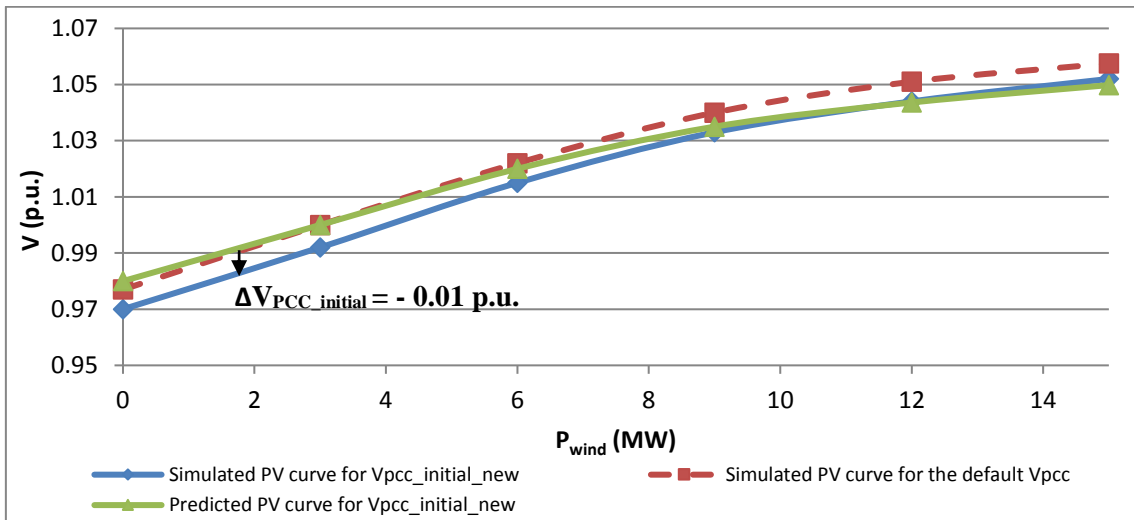


Figure 6.6 PV characteristic for Scenario F.

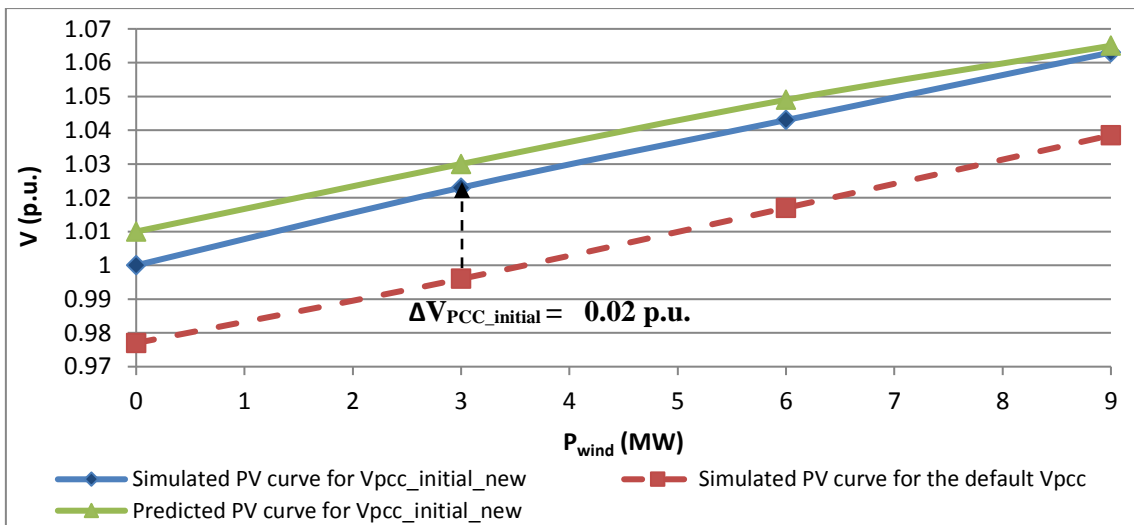


Figure 6.7 PV characteristic for Scenario G.

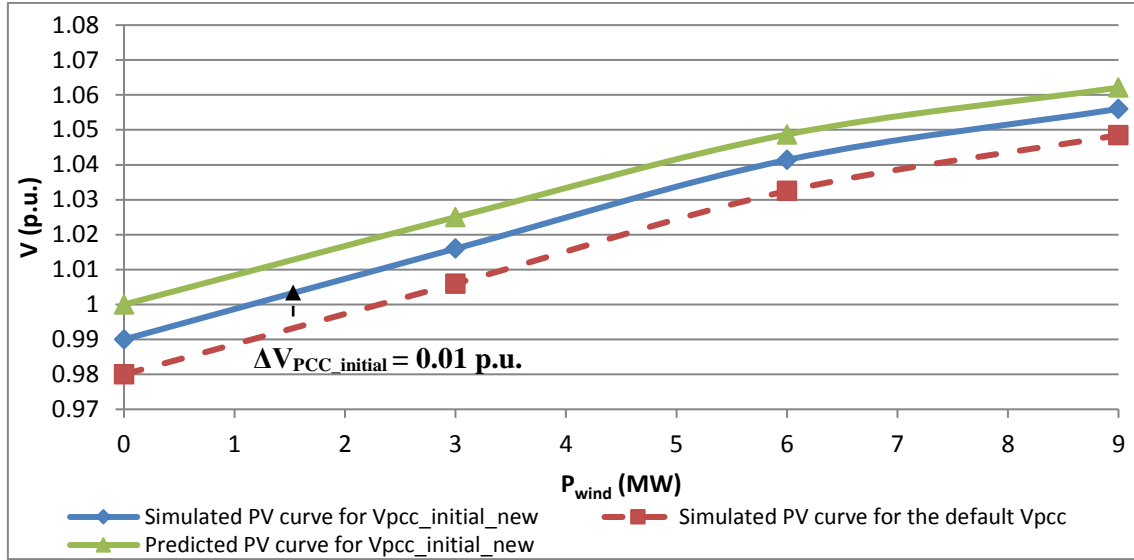


Figure 6.8 PV characteristic for Scenario H.

Comparing the simulated PV curves in Figures 6.1 to 6.8, it can be observed that the change of $V_{PCC_initial}$ does not change the shape of the PV characteristics. However, it shifts the characteristic upwards (for $V_{PCC_initial_new} > 0.98$ p.u.) or downwards (for $V_{PCC_initial_new} < 0.98$ p.u.) on the voltage axis. This indicates that, for a specific amount of P_{wind} , the voltage value in the PV characteristic plotted for $V_{PCC_initial_new}$ approximately equals with the sum of the voltage value in the PV characteristic plotted for the default $V_{PCC_initial}$ and the $\Delta V_{PCC_initial}$ value. This finding makes it possible to further develop the mathematical equations proposed in Chapter 4 for modelling the relations between voltage, P_{wind} , and the PCC parameters for different $V_{PCC_initial}$ values. In this respect, the $\Delta V_{PCC_initial}$ parameter has been added to the analytical model proposed in Chapter 4. Therefore, the equations can be rewritten in terms of the $V_{PCC_initial}$ parameter.

Eq. (6.1) to (6.7) show the mathematical formulation of the developed analytical model that can be used to predict PV characteristic for varying levels of IG wind power injection at PCC buses with an $X/R_{PCC} < 2$. Eq. (6.3) can now be used for predicting V_{PCC} and ΔV_{PCC} regarding different $V_{PCC_initial}$ values for different penetration of IG–

Based WPP. Eq. (6.7) enables to estimate how much P_{wind} must be provided by the IG to have a specific voltage value at a given connection point for different $V_{PCC_initial}$ values.

• **IG WPP with $X/R_{PCC} < 2$**

$$V = 0.9867 + 0.0912 e^{(-0.29 \times \frac{X}{R} \times \frac{SCC}{P_{wind}})} + \Delta V_{PCC_initial} \quad (6.1)$$

$$V = 0.9867 + 0.0912 e^{(-0.29 \times \frac{X}{R} \times \frac{SCC}{P_{wind}})} + V_{PCC_initial} - 0.98 \quad (6.2)$$

$$V = 0.0912 e^{(-0.29 \times \frac{X}{R} \times \frac{SCC}{P_{wind}})} + V_{PCC_initial} + 0.0067 \quad (6.3)$$

$$\rightarrow \frac{V - V_{PCC_initial} - 0.0067}{0.0912} = e^{(-0.29 \times \frac{X}{R} \times \frac{SCC}{P_{wind}})} \quad (6.4)$$

$$\rightarrow \ln\left(\frac{V - V_{PCC_initial} - 0.0067}{0.0912}\right) = -0.29 \times \frac{X}{R} \times \frac{SCC}{P_{wind}} \quad (6.5)$$

$$\rightarrow P_{wind} = -0.29 \times \frac{\frac{X}{R} \times SCC}{\ln\left(\frac{V - V_{PCC_initial} - 0.0067}{0.0912}\right)} \quad (6.6)$$

$$\rightarrow P_{wind} = 0.29 \times \frac{\frac{X}{R} \times SCC}{\ln\left(\frac{0.0912}{V - V_{PCC_initial} - 0.0067}\right)} \quad (6.7)$$

Eq. (6.8) to (6.17) show the mathematical formulation of the developed voltage stability analytical model that can be used to predict PV characteristic for varying levels of IG wind power injection at PCC buses with an $X/R_{PCC} > 2$. Eq. (6.10) can now be used for predicting V_{PCC} and ΔV_{PCC} regarding different $V_{PCC_initial}$ values for different penetration of IG–Based WPP. Eq. (6.16) enables to estimate how much P_{wind} must be

provided by the IG to have a specific voltage value at a given connection point regarding different $V_{PCC_initial}$ values. Eq. (6.15) has two possible solutions, with Eq. (6.16) being the correct solution, where the constant value (10.675) is subtracted from the square root term. This is because, as discussed in Section 4.5 in Chapter 4, the sum of the constant value and the square root phrase makes P_{wind} greater than the grid SCC, which would not be correct.

• **IG WPP with $X/R_{PCC} > 2$**

$$V_{PCC} = 0.9813 - 0.0427 \times \left(\frac{X}{R} \times \frac{P_{wind}}{SCC} \right) + 0.002 \times \left(\frac{X}{R} \times \frac{P_{wind}}{SCC} \right)^2 + \Delta V_{PCC_initial} \quad (6.8)$$

$$V_{PCC} = 0.9813 - 0.0427 \times \left(\frac{X}{R} \times \frac{P_{wind}}{SCC} \right) + 0.002 \times \left(\frac{X}{R} \times \frac{P_{wind}}{SCC} \right)^2 + V_{PCC_initial} - 0.98 \quad (6.9)$$

$$V_{PCC} = V_{PCC_initial} + 0.0013 - 0.0427 \times \left(\frac{X}{R} \times \frac{P_{wind}}{SCC} \right) + 0.002 \times \left(\frac{X}{R} \times \frac{P_{wind}}{SCC} \right)^2 \quad (6.10)$$

$$\frac{\times \frac{1}{0.002}}{\rightarrow} 500V = \left(\frac{X}{R} \times \frac{P_{wind}}{SCC} \right)^2 - 21.35 \times \left(\frac{X}{R} \times \frac{P_{wind}}{SCC} \right) + 500 \times (V_{PCC_initial} + 0.0013) \quad (6.11)$$

$$\rightarrow 500 \times (V - V_{PCC_initial}) = \left(\frac{X}{R} \times \frac{P_{wind}}{SCC} \right)^2 - 21.35 \times \left(\frac{X}{R} \times \frac{P_{wind}}{SCC} \right) + 0.65 \quad (6.12)$$

$$\rightarrow 500 \times (V - V_{PCC_initial}) = \left(\frac{X}{R} \times \frac{P_{wind}}{SCC} \right)^2 - 21.35 \times \left(\frac{X}{R} \times \frac{P_{wind}}{SCC} \right) + 114 - 114 + 0.65 \quad (6.13)$$

$$\rightarrow 500 \times (V - V_{PCC_initial}) = \left(\frac{X}{R} \times \frac{P_{wind}}{SCC} - 10.675 \right)^2 - 113.35 \quad (6.14)$$

$$\rightarrow \frac{X}{R} \times \frac{P_{wind}}{SCC} - 10.675 = \pm \sqrt{500 \times (V - V_{PCC_initial}) + 113.35} \quad (6.15)$$

$$\left\{ \begin{array}{l} P_{wind} = SCC \times \frac{R}{X} \times \left(10.675 - \sqrt{500 \times (V - V_{PCC_initial}) + 113.35} \right) \quad (6.16) \quad \checkmark \\ P_{wind} = SCC \times \frac{R}{X} \times \left(10.675 + \sqrt{500 \times (V - V_{PCC_initial}) + 113.35} \right) \quad (6.17) \quad \times \end{array} \right.$$

Eq. (6.18) to (6.24) show the mathematical formulation of the developed voltage stability analytical model that can be used to predict PV characteristic for varying levels of DFIG wind power injection at PCC buses with an $X/R_{PCC} < 2$. Eq. (6.20) can now be used for predicting V_{PCC} and ΔV_{PCC} regarding different $V_{PCC_initial}$ values for different penetration levels of DFIG–Based WPP. Eq. (6.24) enables to estimate how much P_{wind} must be provided by DFIG to have a specific voltage value at a given connection point for different $V_{PCC_initial}$ values.

- **DFIG–Based WPP with $X/R_{PCC} < 2$**

$$V = 0.99 + 0.101 e^{(-0.347 \times \frac{X}{R} \times \frac{SCC}{P_{wind}})} + \Delta V_{PCC_initial} \quad (6.18)$$

$$V = 0.99 + 0.101 e^{(-0.347 \times \frac{X}{R} \times \frac{SCC}{P_{wind}})} + V_{PCC_initial} - 0.98 \quad (6.19)$$

$$\boxed{V = 0.101 e^{(-0.347 \times \frac{X}{R} \times \frac{SCC}{P_{wind}})} + V_{PCC_initial} + 0.01} \quad (6.20)$$

$$\rightarrow \frac{V - V_{PCC_initial} - 0.01}{0.101} = e^{(-0.347 \times \frac{X}{R} \times \frac{SCC}{P_{wind}})} \quad (6.21)$$

$$\rightarrow \ln \left(\frac{V - V_{PCC_initial} - 0.01}{0.101} \right) = -0.347 \times \frac{X}{R} \times \frac{SCC}{P_{wind}} \quad (6.22)$$

$$\rightarrow P_{wind} = -0.347 \times \frac{\frac{X}{R} \times SCC}{\ln \left(\frac{V - V_{PCC_initial} - 0.01}{0.101} \right)} \quad (6.23)$$

$$\rightarrow P_{wind} = 0.347 \times \frac{\frac{X}{R} \times SCC}{Ln\left(\frac{0.101}{V - V_{PCC_initial} - 0.01}\right)} \quad (6.24)$$

The PV characteristics predicted by Eqs. (6.3), (6.10), and (6.20) for the new $V_{PCC_initial}$ value ($V_{PCC_initial_new}$) were shown earlier in Figures (6.1) to (6.8), for Scenarios A to H.

The analytical models proposed in Chapter 4 for $P_{max-wind}$ estimation can also be further developed to take into account the actual $V_{PCC_initial}$ value. For this purpose, Eqs. (6.7), (6.16), and (6.24) have been developed to estimate $P_{max-wind}$ when $V_{PCC} = 1.05$ p.u. or $V_{PCC} = 0.95$ p.u. Hence, the $P_{max-wind}$ value can be calculated from Eqs. (6.25) to (6.27), for the IG and DFIG–Based WPPs.

- IG-Based WPPs with $X/R_{PCC} < 2$

$$P_{max-wind} = \frac{0.29 \times \frac{X}{R} \times SCC}{Ln\left(\frac{0.0912}{1.05 - V_{PCC_initial} - 0.0067}\right)} = 0.29 \times \frac{\frac{X}{R} \times SCC}{Ln\left(\frac{0.0912}{1.0433 - V_{PCC_initial}}\right)} \quad (6.25)$$

- IG-Based WPPs with $X/R_{PCC} > 2$

$$P_{max-wind} = SCC \times \frac{R}{X} \times \left(10.675 - \sqrt{500 \times (0.95 - V_{PCC_initial}) + 113.35}\right) \quad (6.26)$$

- DFIG-Based WPPs with $X/R_{PCC} < 2$

$$P_{max-wind} = 0.347 \times \frac{\frac{X}{R} \times SCC}{Ln\left(\frac{0.101}{1.05 - V_{PCC_initial} - 0.01}\right)} = 0.347 \times \frac{\frac{X}{R} \times SCC}{Ln\left(\frac{0.101}{1.04 - V_{PCC_initial}}\right)} \quad (6.27)$$

The final forms of the analytical steady-state voltage stability model proposed in this thesis is summarised in Table 6.2.

Table 6.2 Final proposed voltage stability analytical model

Proposed equation	Application
Eq. (6.3)	Projecting V_{PCC} and ΔV_{PCC} for IG–Based WPPs for $X/R_{PCC} < 2$
Eq. (6.10)	Projecting V_{PCC} and ΔV_{PCC} for IG–Based WPPs for $X/R_{PCC} > 2$
Eq. (6.20)	Projecting V_{PCC} and ΔV_{PCC} for DFIG–Based WPPs for $X/R_{PCC} < 2$
Eq. (6.25)	Projecting $P_{max-wind}$ for IG–Based WPPs for $X/R_{PCC} < 2$
Eq. (6.26)	Projecting $P_{max-wind}$ for IG–Based WPPs for $X/R_{PCC} > 2$
Eq. (6.27)	Projecting $P_{max-wind}$ for DFIG–Based WPPs for $X/R_{PCC} < 2$

6.3 Validating proposed equations for different $V_{PCC_initial}$ values

This section presents the analyses undertaken to validate the proposed equations, listed in Table 6.2, which can be used to project V_{PCC} , ΔV_{PCC} , and $P_{max-wind}$ for any potential connection bus in a distribution network, given the $V_{PCC_initial}$ value.

6.3.1 Voltage profile prediction

This section investigates the accuracy of the proposed Eqs. (6.3), (6.10), and (6.20) in predicting the voltage profile for Scenarios A to H. In this respect, for each scenario, the V_{PCC} value gained from the PV characteristics shown in Figures (6.1) to (6.8) are compared with the V_{PCC} values given by the proposed equations and results presented in Table 6.3. Analysing Table 6.3, it is clear that the highest error is around 1% and, in most cases, the error is less than 1%. This validation confirms the high accuracy of the proposed equations in predicting voltages at the PCC connection points for different $V_{PCC_initial}$ values.

Table 6.3 Error between simulated and predicted V_{PCC} profile for Scenarios A to H

Scenarios	P_{wind} (MW)	$V_{simulated}$	$V_{predicted}$	Percent error (%)
Scenario A	0	0.99	0.997	0.7
	3	1.032	1.04	0.77
	6	1.06	1.06	0
Scenario B	0	0.969	0.9703	0.1342
	3	0.963	0.9609	-0.2181
	6	0.9514	0.9517	0.0315
	9	0.9376	0.9427	0.544
Scenario C	0	1	1.0074	0.74
	3	1.02	1.027	0.6863

	6	1.044	1.0484	0.42
	9	1.0615	1.0608	-0.0659
Scenario D	0	0.991	0.9913	0.0303
	3	0.975	0.9675	-0.7692
	6	0.948	0.9451	-0.3059
Scenario E	0	1	1.01	1
	3	1.025	1.033	0.78
	6	1.049	1.0563	0.6959
	9	1.0665	1.07	0.3282
Scenario F	0	0.97	0.98	1.03
	3	0.992	1	0.8
	6	1.015	1.02	0.5
	9	1.033	1.035	0.19
	12	1.044	1.0436	-0.0383
	15	1.052	1.05	-0.2
Scenario G	0	1	1.01	1
	3	1.023	1.03	0.7
	6	1.043	1.049	0.6
	9	1.063	1.065	0.2
Scenario H	0	0.99	1	1.01
	3	1.016	1.025	0.886
	6	1.0414	1.0487	0.7
	9	1.056	1.0621	0.5777

6.3.2 Step-voltage variation prediction

In this section, the accuracy of the proposed analytical models (Eqs. (6.3), (6.10), and (6.20)) in predicting the step- V_{PCC} variation due to the change of P_{wind} (ΔV_{PCC}) is evaluated for Scenarios A to H. As an example, Figure 6.9 shows the $P\Delta V$ characteristics gained from predicted and simulation results for one of the IG-Based scenarios (Scenario B) and one of the DFIG-Based scenarios (Scenario E). From Figure 6.9, it is observed that both simulated and predicted PV characteristics show that ΔV at the PCC point of the test system with smaller SCC and X/R, i.e. test system in Scenario E, is more serious than ΔV at the PCC point of the test system with larger SCC and X/R, i.e. test system in Scenario B. In Scenario E, it is clear that ΔV_{PCC} violates the grid code requirements ($\Delta V_{PCC} > 3$) when P_{wind} increase from 0 to 6 MVA (two 3 MVA

generators are simultaneously connected to the grid). However, for the same increase in P_{wind} in Scenario B, ΔV_{PCC} does not exceed 3%, and therefore complies with the Australian grid codes.

Table 6.4 shows the numerical result related to ΔV_{PCC} for all Scenarios, when $0.95 \text{ p.u.} < V_{PCC} < 1.05 \text{ p.u.}$ Both simulated and predicted results show that the highest ΔV_{PCC} occurred in Scenario A where the SCC and X/R_{PCC} are both small. According to Table 6.4, the ΔV_{PCC} value is greater than 3% when only one 3 MVA generator is connected to the grid. However, the smallest ΔV_{PCC} is concerned with Scenario B where SCC and X/R_{PCC} are both large. In Scenario F, where the P_{wind} penetration ensuring $0.95 \text{ p.u.} < V_{PCC} < 1.05 \text{ p.u.}$ is higher than the other Scenarios, ΔV_{PCC} satisfies the standard range if the increase in P_{wind} is 3 MW, for example when P_{wind} increases from 0 to 3 MVA or from 6 to 9 MVA. However, ΔV_{PCC} violates the grid code requirements when two or more 3 MVA generators are simultaneously connected to the grid.

An analysis of Table 6.4 enables grid codes compliance check, i.e. to verify if $\Delta V_{PCC} \leq 3 \%$ (compliance with the grid codes) or $\Delta V_{PCC} \geq 3 \%$ (grid codes violation). Comparing the simulated and predicted results in Table 6.9, it is clear that, in all scenarios, the proposed equations were accurate in estimating ΔV_{PCC} , projecting the correct grid codes compliance or violation outcome.

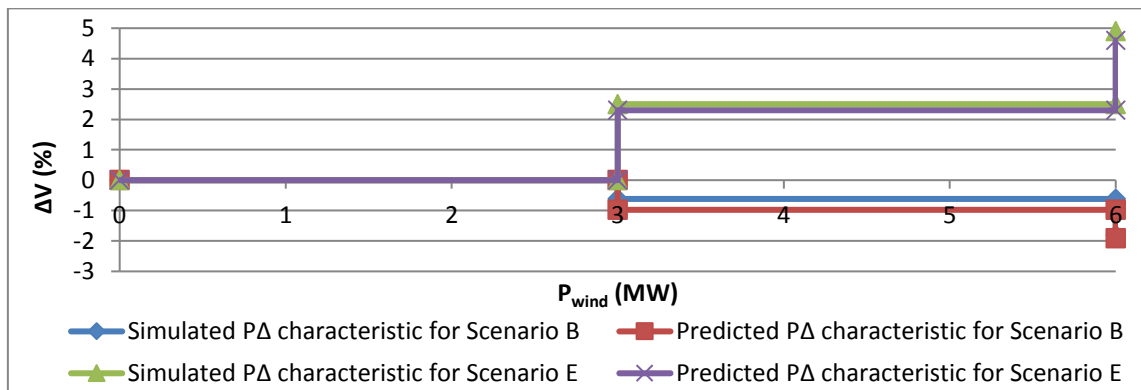


Figure 6.9 PΔV characteristic for Scenarios B and E.

Table 6.4 Error between simulated and predicted ΔV_{PCC} for Scenarios A to H.

Scenario	P_{wind} (MW)		$\Delta V_{simulated}$ (%)		$\Delta V_{predicted}$ (%)	
	From	To	Value	Evaluating based on grid codes	Value	Evaluating based on grid codes
Scenario A	0	3	4.24	Violates the grid code	4.3	Violates the grid code
	3	6	2.5	Satisfies the grid code	1.92	Satisfies the grid code
	0	6	7	Violates the grid code	6.3	Violates the grid code
Scenario B	0	3	-0.62	Satisfies the grid code	-0.97	Satisfies the grid code
	3	6	-1.2	Satisfies the grid code	-0.96	Satisfies the grid code
	0	6	-1.81	Satisfies the grid code	-1.91	Satisfies the grid code
Scenario C	0	3	2	Satisfies the grid code	1.94	Satisfies the grid code
	3	6	2.35	Satisfies the grid code	2.1	Satisfies the grid code
	0	6	4.4	Violates the grid code	4.1	Violates the grid code
Scenario D	0	3	-1.61	Satisfies the grid code	-2.4	Satisfies the grid code
	3	6	-2.77	Satisfies the grid code	-2.31	Satisfies the grid code
	0	6	-4.34	Violates the grid code	-4.66	Violates the grid code
Scenario E	0	3	2.5	Satisfies the grid code	2.3	Satisfies the grid code
	3	6	2.34	Satisfies the grid code	2.25	Satisfies the grid code
	0	6	4.9	Violates the grid code	4.6	Violates the grid code
Scenario F	0	3	2.27	Satisfies the grid code	2.04	Satisfies the grid code
	3	6	2.32	Satisfies the grid code	2	Satisfies the grid code
	6	9	1.77	Satisfies the grid code	1.5	Satisfies the grid code
	9	12	1.065	Satisfies the grid code	0.83	Satisfies the grid code
	12	15	0.77	Satisfies the grid code	0.6	Satisfies the grid code
	0	6	4.64	Violates the grid code	4.1	Violates the grid code
	0	9	6.5	Violates the grid code	5.62	Violates the grid code
	0	12	7.63	Violates the grid code	6.5	Violates the grid code
	0	15	8.45	Violates the grid code	7.1	Violates the grid code
	3	9	4.13	Violates the grid code	3.5	Violates the grid code
	3	12	5.24	Violates the grid code	4.36	Violates the grid code
	3	15	6.04	Violates the grid code	5	Violates the grid code
	6	12	2.86	Satisfies the grid code	2.3	Satisfies the grid code
	6	15	3.64	Violates the grid code	3	Violates the grid code
9	15	1.84	Satisfies the grid code	1.43	Satisfies the grid code	
Scenario G	0	3	2.3	Satisfies the grid code	1.98	Satisfies the grid code
	3	6	1.95	Satisfies the grid code	1.84	Satisfies the grid code
	0	6	4.3	Violates the grid code	3.86	Violates the grid code
Scenario H	0	3	2.62	Satisfies the grid code	2.5	Satisfies the grid code
	3	6	2.5	Satisfies the grid code	2.31	Satisfies the grid code
	0	6	5.2	Violates the grid code	4.87	Violates the grid code

6.3.3 WPP maximum allowable sizing prediction

Figure 6.10 shows the comparison of the maximum permissible size of WPP ($P_{max-wind}$) ensuring that $0.95 \text{ p.u.} < V_{PCC} < 1.05 \text{ p.u.}$ In this regards, $P_{max-wind}$ values obtained from the simulated PV characteristics are compared with the values given by

Eqs. (6.25) to (6.27). As shown in Figure 6.10, the predicted values track the simulated results with a relatively small margin of error.

For IG-Based Scenarios, i.e. Scenarios A to D, the highest error is related to the case with small X/R_{PCC} and SCC (Scenario A). As shown in Figure 6.10, the difference between simulation and predicted results in Scenario A was around 1 MW, which is correspondence with 13% error. Furthermore, the highest error in DFIG-Based Scenarios (Scenarios E to H) is concerned with the case with the smallest SCC value (Scenario H). From Figure 6.10, it can be observed that the error in Scenario H is around 1 MW (Percent error = 13%). Therefore, the worst case accuracy in both IG and DFIG-Based Scenarios is around 87%. In other Scenarios, the error was around 0.5 MW. This confirms that the developed analytical model can accurately estimate $P_{max-wind}$ at a given connection point for a specific $V_{PCC_initial}$.

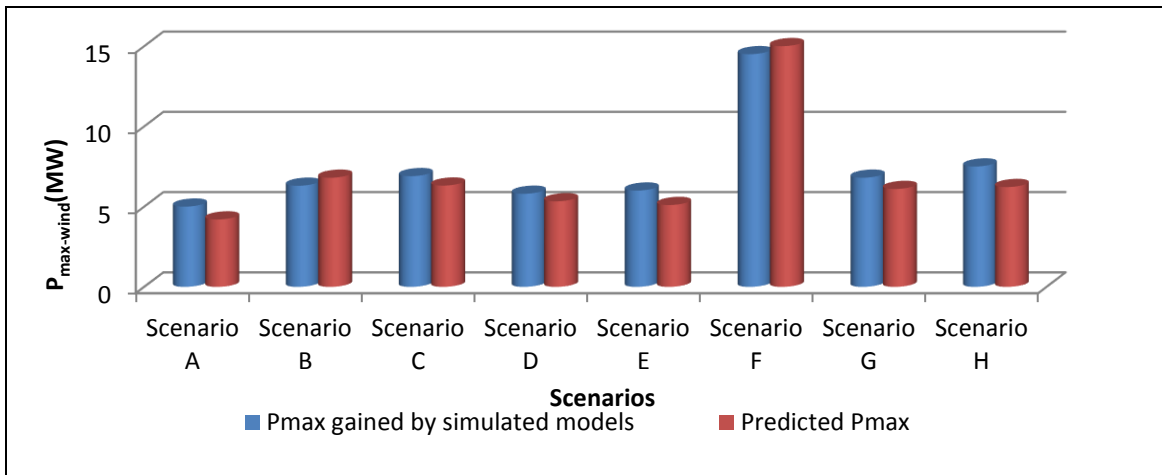


Figure 6.10 Predicted and simulated $P_{max-wind}$ for Scenarios A to H.

6.4 Further verification studies

In this section, the accuracy of the final proposed equations is validated using further test systems (with different PCC parameters and $V_{PCC_initial}$ values) in order to increase the validity of the developed steady-state voltage stability model by considering different topologies and PCC parameters. The test systems are based on the

IEEE 9-bus and 37-bus distribution models shown in Figures 3.2 and 3.3. For each test system, network bus voltages have been computed by performing a MATLAB based load-flow analysis, which provided the researcher with the $V_{PCC_initial}$ values for a range of buses.

Analysis was carried out using IG and DFIG-Based WPP models. For each test system, the system topology, the WPP type, PCC bus, the grid's SCC and X/R values, and finally the $V_{PCC_initial}$ value have been listed in Table 6.5. It is noted that a realistic range of initial V_{PCC} has been in these scenarios. Validation studies were then carried out to verify the accuracy of the proposed analytical model against the three voltage stability criteria considered in this thesis for each one of the scenarios. Similar to the previous sections, the validation analysis studies were carried out using the predicted and simulated PV characteristics plotted for each test system.

Table 6.5 New test systems topologies, PCC parameters, and $V_{PCC_initial}$ values

Test system	WPP Type	Topology	PCC Bus	SCC (MVA)	X/R _{PCC}	$V_{PCC_initial}$ (p.u.)
Test 5	IG-Based WPP	IEEE 37 - bus system	37	33	0.55	1
Test 6	IG-Based WPP	IEEE 9 - bus system	1	46	3.5	0.985
Test 7	IG-Based WPP	IEEE 9 - bus system	5	64	3	0.97
Test 8	DFIG – based WPP	IEEE 37 - bus system	24	30	0.4	0.99
Test 9	DFIG-Based WPP	IEEE 37 - bus system	12	17	1	1
Test 10	DFIG-Based WPP	IEEE 9 - bus system	8	68	0.4	0.98
Test 11	IG-Based WPP	IEEE 9 - bus system	9	54	0.3	1.01
Test 12	DFIG-Based WPP	IEEE 37 - bus system	25	21	0.3	0.965

6.4.1 PV characteristics for the new test systems

In this section, the PV characteristics obtained from simulation models and those predicted by the final equations listed in Table 6.2, are compared for test scenarios listed in Table 6.5. Similar to Section (6.2), the PV characteristics were predicted using Eq (6.3) for the IG-Based WPPs with $X/R_{PCC} > 2$, Eq (6.10) for the IG-Based WPP with

$X/R_{PCC} > 2$, and Eq (6.20) for the DFIG–Based WPPs. Simulated and predicted PV characteristics are as shown in Figures 6.11 to 6.14 for $0.95 \text{ p.u.} < V_{PCC} < 1.05 \text{ p.u.}$

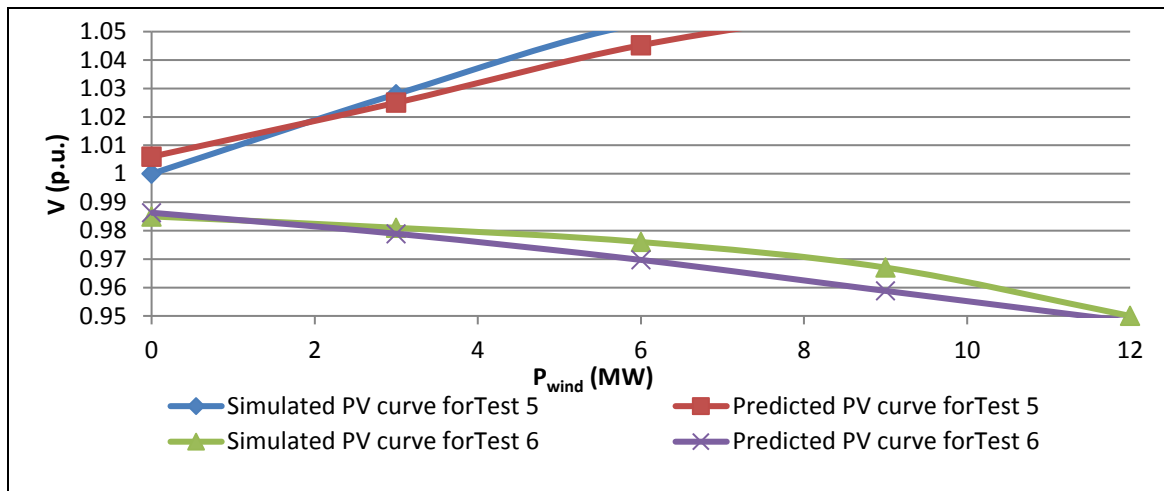


Figure 6.11 PV characteristic for Tests 5 and 6.

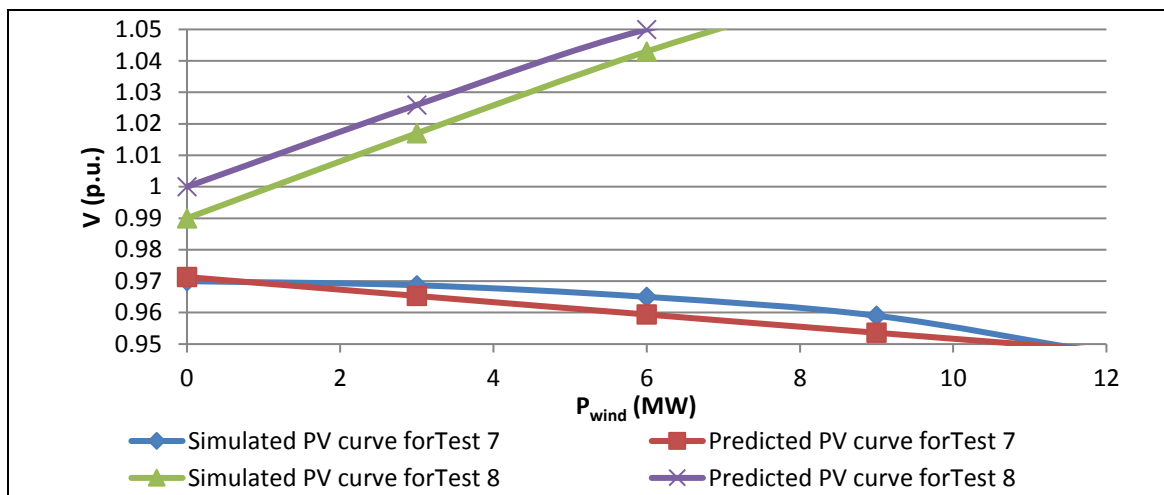


Figure 6.12 PV characteristic for Tests 7 and 8.

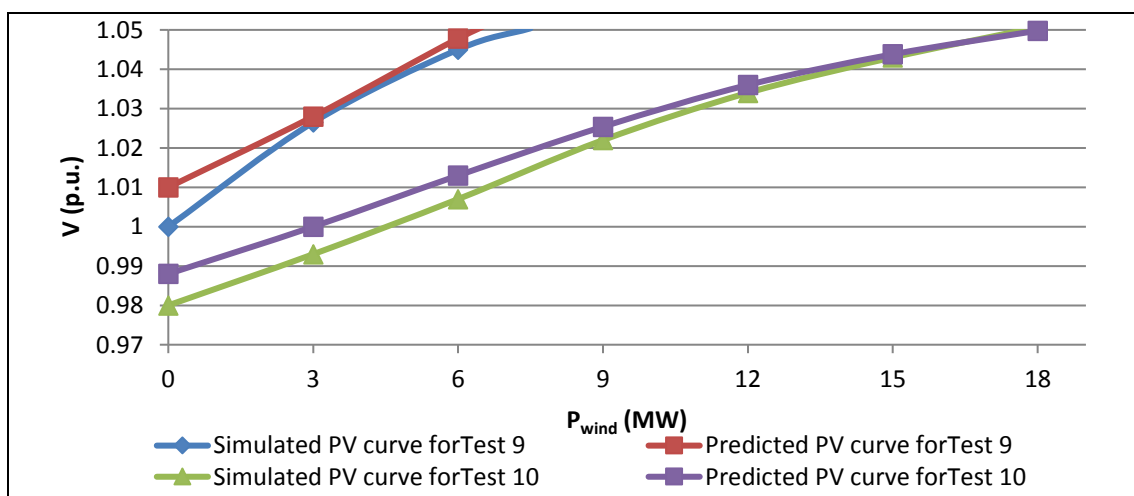


Figure 6.13 PV characteristic for Tests 9 and 10.

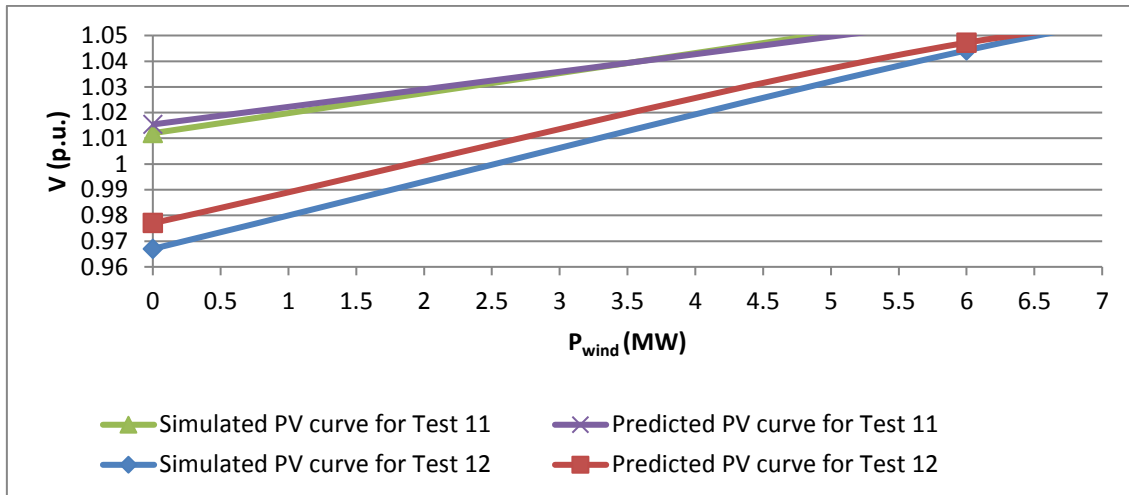


Figure 6.14 PV characteristic for Tests 11 and 12

The results in Figures 6.11 to 6.13 confirm the hypothesis put forward in Chapter 3 that the highest wind power penetration is attainable at PCC points with a high SCC value. Figure 6.13 confirms the hypothesis by showing that P_{wind} injection will be the highest in Test 10, where the SCC values are at their highest levels at potential PCC points within IEEE 9-bus system.

Although SCC in Test 9 is lower than that in the other test systems, wind power penetration in Test 9 is approximately the same with that in Tests 5, 8, and 12. This is because, as shown in Table 5.10, the X/R_{PCC} ratio in Test 9 is closer to 2 in comparison with the lower X/R_{PCC} ratio observed in Tests 5, 8, and 12.

Referring to Table 6.5, $V_{PCC_initial}$ value in Test 12 is smaller than that in Tests 8 and 5, while in all three test systems $X/R_{PCC} < 2$. Although the SCC value in Test 12 is smaller than the SCC value in Tests 5 and 8, comparing the results in Figures 6.11, 6.12, and 6.14 demonstrates that the maximum permissible wind power penetration in both test systems is approximately the same. Moreover, the SCC value in Test 11 is greater than all three Tests 5, 8, and 12, while in all four test systems $X/R_{PCC} < 2$. However, a larger $V_{PCC_initial}$ in Test 11 makes the maximum permissible wind power penetration smaller than that in Tests 5, 8, and 12. This indicates that a large $V_{PCC_initial}$ adversely

impacts on the $P_{\max\text{-wind}}$ value at connection points with a small X/R ratio. This is because as demonstrated in Chapter 3, V_{PCC} would increase as P_{wind} generation increases for small X/R_{PCC} ratios.

The $V_{\text{PCC_initial}}$ value in Test 7 is smaller than that in Test 6, while in both test systems $X/R_{\text{PCC}} > 2$ (refer to Table 6.5). Although the SCC value in Test 7 is greater than that in Test 6, comparing the results in Figures 6.11 and 6.12 demonstrates that $P_{\max\text{-wind}}$ value in both test systems is approximately the same. This indicates that a small $V_{\text{PCC_initial}}$ adversely impacts on the $P_{\max\text{-wind}}$ value at connection points with a large X/R ratio. This is because as demonstrated in Chapter 3, V_{PCC} would decrease as P_{wind} generation increases for large X/R_{PCC} ratios.

6.4.2 Voltage profile prediction for the new test systems

This section investigates the accuracy of the proposed Eqs. (6.3), (6.10), and (6.20) in predicting the V_{PCC} value for Test systems 5 to 10 using the PV characteristics presented in Figures 6.11 to 6.14. Table 6.6 shows the simulated and predicted V_{PCC} values and the percentage error between the simulated and predicted results for each test system

Table 6.6 Error between simulated and predicted V_{PCC} profile for Tests 5 to 10.

Test system	P_{wind} (MW)	$V_{\text{simulated}}$	$V_{\text{predicted}}$	Percent error (%)
Test 5	0	1	1.006	0.6
	3	1.026	1.025	- 0.1
	6	1.053	1.046	- 0.67
Test 6	0	0.985	0.9863	0.13
	3	0.981	0.9789	- 0.21
	6	0.976	0.9697	- 0.64
	9	0.967	0.9588	- 0.85
	12	0.95	0.948	- 0.21
Test 7	0	0.97	0.9713	0.13
	3	0.9687	0.9653	- 0.35
	6	0.965	0.9594	-0.58
	9	0.959	0.9536	- 0.56
	12	0.947	0.9479	- 0.1

Test 8	0	0.99	1	1
	3	1.017	1.026	0.88
	6	1.043	1.05	0.7
Test 9	0	1	1.01	1
	3	1.025	1.028	0.15
	6	1.045	1.048	0.27
Test 10	0	0.98	0.99	0.95
	3	0.993	1	0.47
	6	1.007	1.01	0.37
	9	1.022	1.025	0.23
	12	1.034	1.036	0.09
	15	1.043	1.0438	0.07
	18	1.0507	1.0498	- 0.08
Test 11	0	1.01	1.016	0.6
	3	1.035	1.035	0
	6	1.055	1.056	0.1
Test 12	0	0.965	0.975	1
	3	1.005	1.012	0.69
	6	1.044	1.047	0.28

From the results presented in Table 6.6, it is clear that the highest error between simulated and predicted V_{PCC} values is only 1% which occurred in only three cases: in Tests 8, 9, and 12. However, in many cases, the error is less than 0.5 %. For test system with $V_{PCC_initial}$ far from the default value, the validation results demonstrate that the error between predicted and reference V_{PCC} profile is small. For example, in some cases, such as in Test 11, the error between predicted and reference values is zero. Hence, similar to the validation results shown in the previous sections, the proposed Eqs. (6.3), (6.10), and (6.20) provide significant accuracy in predicting the voltage profile at a given connection point.

6.4.3 Step-voltage variation prediction for the new test systems

As an example, Figure 6.15 represents the $P\Delta V$ characteristics at the PCC point for one of the IG-Based test systems (Test 6) and one of the DFIG-Based test systems (Test 10), when $0.95 \text{ p.u.} < V_{PCC} < 1.05 \text{ p.u.}$ Furthermore, the numerical results showing the ΔV_{PCC} value for different wind power penetration have been presented in Table 6.7. An analysis of Table 6.7, for each test system, enabled an investigation on confirming

whether the analytical model can accurately predict ΔV_{PCC} and project compliance or violation of the grid codes. For example, in Test 5, the ΔV_{PCC} value for switching an extra 3MW capacity on top of the existing 3 MW was measured as 2.6 % from the Simulink model whereas the prediction of the analytical model is 2 %. Even though the analytical prediction has around 76% accuracy, it can correctly project that such switching of an extra 3MW capacity would comply with the grid codes in terms of the allowable limits of step voltage fluctuations.

In Test 12, where both SCC and X/R are small, the simulated and predicted results demonstrate that the voltage variation violates the grid code requirements in all WPP penetration levels. Referring to Table 6.6, the V_{PCC} profile satisfies the grid code requirements ($0.95 \text{ p.u.} < V_{PCC} < 1.05 \text{ p.u.}$) when the WPP penetration is around 6 MW. However, both simulated and predicted results in Table 6.6 show that the small X/R and SCC at PCC of Test 12 adversely impact the V_{PCC} variation. In Test 10, a large SCC seen at the PCC allows a large number of generators to be connected to the grid. In Table 6.7, the results demonstrate that the proposed model enables to predict whether ΔV_{PCC} satisfies or violates the standard range for all possible generators switching modes in Test 10. Hence, the results demonstrate that proposed Eqs. (6.3), (6.10), and (6.20) are accurate in predicting ΔV_{PCC} for different wind power penetration levels.

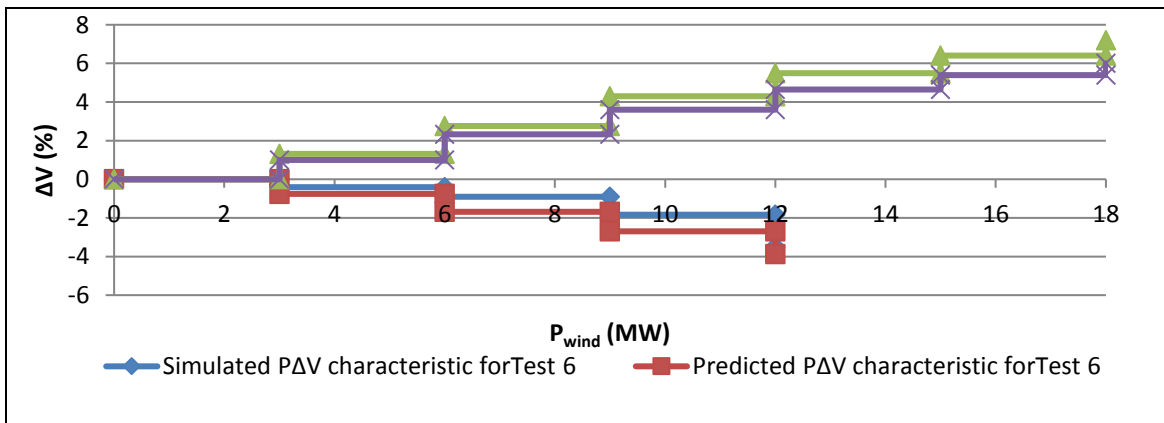


Figure 6.15 PΔV characteristic for Tests 6 and 10.

Table 6.7 Error between simulated and predicted ΔV_{PCC} for Tests 5 to 10.

Test system	P_{wind} (MW)		$\Delta V_{simulated}$ (%)		$\Delta V_{predicted}$ (%)	
	From	To	Value	Evaluating based on grid codes	Value	Evaluating based on grid codes
Test 5	0	3	2.6	Satisfies the grid code	2	Satisfies the grid code
	3	6	2.6	Satisfies the grid code	2	Satisfies the grid code
	0	6	5.3	Violates the grid code	4	Violates the grid code
Test 6	0	3	-0.41	Satisfies the grid code	-0.75	Satisfies the grid code
	3	6	-0.51	Satisfies the grid code	-0.94	Satisfies the grid code
	6	9	-0.92	Satisfies the grid code	-1.12	Satisfies the grid code
	9	12	-1.76	Satisfies the grid code	-1.13	Satisfies the grid code
	0	6	-0.91	Satisfies the grid code	-1.68	Satisfies the grid code
	0	9	-1.83	Satisfies the grid code	-2.5	Satisfies the grid code
	0	12	-3.5	Violates the grid code	-3.88	Violates the grid code
	3	9	-1.43	Satisfies the grid code	-2	Satisfies the grid code
	3	12	-3.16	Violates the grid code	-3.16	Violates the grid code
	6	12	-2.66	Satisfies the grid code	-2.25	Satisfies the grid code
	Test 7	0	3	-0.13	Satisfies the grid code	-0.62
3		6	-0.38	Satisfies the grid code	-0.6	Satisfies the grid code
6		9		Satisfies the grid code	-0.6	Satisfies the grid code
9		12	-1.25	Satisfies the grid code	-0.6	Satisfies the grid code
0		6	-0.52	Satisfies the grid code	-1.23	Satisfies the grid code
0		9	-1.13	Satisfies the grid code	-1.82	Satisfies the grid code
0		12	-2.37	Satisfies the grid code	-2.41	Satisfies the grid code
3		9	-1	Satisfies the grid code	-1.2	Satisfies the grid code
3		12	-2.24	Satisfies the grid code	-1.8	Satisfies the grid code
Test 8	0	3	2.7	Satisfies the grid code	2.6	Satisfies the grid code
	3	6	2.5	Satisfies the grid code	2.4	Satisfies the grid code
	0	6	5.3	Violates the grid code	5	Violates the grid code
Test 9	0	3	2.65	Satisfies the grid code	1.8	Satisfies the grid code
	3	6	1.8	Satisfies the grid code	1.9	Satisfies the grid code
	0	6	4.5	Violates the grid code	3.75	Violates the grid code
Test 10	0	3	1.32	Satisfies the grid code	1	Satisfies the grid code
	3	6	1.41	Satisfies the grid code	1.3	Satisfies the grid code
	6	9	1.49	Satisfies the grid code	1.25	Satisfies the grid code
	9	12	1.17	Satisfies the grid code	1.03	Satisfies the grid code
	12	15	0.87	Satisfies the grid code	0.75	Satisfies the grid code
	15	18	0.74	Satisfies the grid code	0.6	Satisfies the grid code
	0	6	2.75	Satisfies the grid code	2.32	Satisfies the grid code
	0	9	4.3	Violates the grid code	3.6	Violates the grid code
	0	12	5.5	Violates the grid code	4.65	Violates the grid code
	0	15	6.4	Violates the grid code	5.4	Violates the grid code
	0	18	7.2	Violates the grid code	6	Violates the grid code
	3	9	2.7	Satisfies the grid code	2.5	Satisfies the grid code
	3	12	4.1	Violates the grid code	3.6	Violates the grid code
	3	15	5	Violates the grid code	4.4	Violates the grid code
	3	18	5.8	Violates the grid code	5	Violates the grid code
6	12	2.68	Satisfies the grid code	2.5	Satisfies the grid code	
6	15	3.57	Violates the grid code	3.1	Violates the grid code	

	6	18	4.34	Violates the grid code	3.65	Violates the grid code
	9	15	2	Satisfies the grid code	1.8	Satisfies the grid code
	9	18	2.8	Satisfies the grid code	2.4	Satisfies the grid code
	12	18	1.6	Satisfies the grid code	1.33	Satisfies the grid code
Test 11	0	3	2.4	Satisfies the grid code	1.87	Satisfies the grid code
	3	6	1.95	Satisfies the grid code	2	Satisfies the grid code
	0	6	4.45	Violates the grid code	3.95	Violates the grid code
Test 12	0	3	4.2	Violates the grid code	3.8	Violates the grid code
	3	6	3.8	Violates the grid code	3.5	Violates the grid code
	0	6	8	Violates the grid code	7.5	Violates the grid code

6.4.4 WPP maximum allowable sizing prediction for the new test systems

In this section, the accuracy of the proposed analytical model in estimating $P_{\max\text{-wind}}$ is verified for the test systems listed in Table 6.5. The objective is to test if the developed analytical model can predict $P_{\max\text{-wind}}$ for compliance with the grid codes, i.e. maximum P_{wind} injection levels allowable for maintaining the steady-state voltage within the $0.95 < V_{\text{PCC}} < 1.05$ range without requiring any further static or dynamic reactive compensation solutions.

For this purpose, Eqs. (6.25) to (6.27) have been used to calculate the $P_{\max\text{-wind}}$ for Tests 5 to 12, and compare with the simulation results. Figure 6.16 shows the simulated and predicted $P_{\max\text{-wind}}$ values for each test.

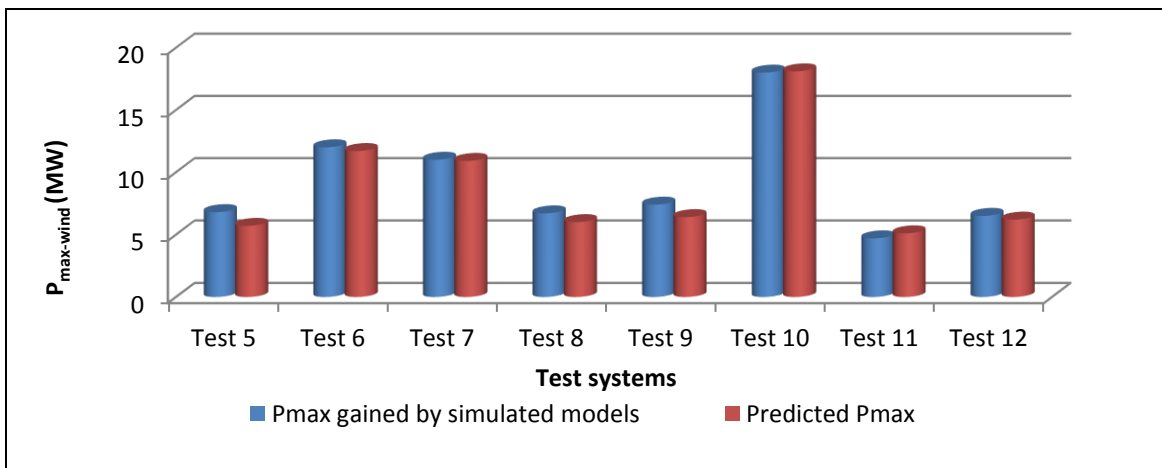


Figure 6.16 Predicted and simulated $P_{\max\text{-wind}}$ for Tests 5 to 10.

As shown, the highest error in IG-Based test systems (Test 5 to 7) is related to Test 5 where both X/R_{PCC} and SCC values are small. This is because, as mentioned in

Chapter 5 and Section 6.3.3, small SCC values impact the accuracy of the proposed analytical model in estimating $P_{\max\text{-wind}}$ in IG-Based WPP with a small X/R_{PCC} ratio ($X/R_{\text{PCC}} < 2$). From Figure 6.16, it is observed that the error in Test 5 is around 1 MW (Percent error = 16%). However, the error in other IG-Based test systems (Tests 6, 7, and 11) is less than 0.5 MW.

In DFIG-Based test systems (Tests 8 to 10), the highest error is around 1 MW (Percent error = 13%) in Test 9 where the SCC value is smaller than the two other test systems. This is because, as discussed in Chapter 5, small SCC values slightly impact the accuracy of the equation proposed for predicting $P_{\max\text{-wind}}$ in DFIG-Based WPP. In the other DFIG-Based test systems (Tests 8, 10, and 12) the error is around 0.5 MW.

Therefore, results in Figure 6.16 demonstrate that the worst case accuracy in IG and DFIG-Based test systems is 84% and 87%, respectively. Therefore, the results confirm the accuracy of the proposed analytical model in predicting $P_{\max\text{-wind}}$.

6.5 Conclusion

In this chapter, the analytical model proposed in the previous Chapters was developed for carrying out an initial predictive assessment on voltage stability at a given connection point with any $V_{\text{PCC_initial}}$ value. For this purpose, the effect of $V_{\text{PCC_initial}}$ on P_{wind} versus V_{PCC} characteristic was investigated using eight scenarios.

It was demonstrated that different $V_{\text{PCC_initial}}$ values shift the characteristics upward or downward on the voltage axis. Using this finding, the initial proposed analytical model was developed to calculate PCC voltage profile, ΔV_{PCC} , and $P_{\max\text{-wind}}$ for different $V_{\text{PCC_initial}}$ values. Development of the initial proposed analytical model for considering the effect of the $V_{\text{PCC_initial}}$ parameter enabled to predict the voltage stability

criteria for different loading conditions and different set–point values of the voltage regulators.

The developed analytical model was, then, verified for further case studies and test systems with different PCC parameters and $V_{PCC_initial}$ value. Generally, the validation results presented in this Chapter demonstrated that the analytical model developed during the course of this research is capable of predicting the PV and P Δ V characteristics at potential distribution network interconnection points for IG and DFIG-Based WPPs with specific X/R and SCC values. This enables to calculate V_{PCC} profile, ΔV_{PCC} , and $P_{max-wind}$ at the candidate PCC points.

Hence, the author could come up with a novel SCC and X/R based voltage stability model for an initial predictive assessment on the important voltage stability criteria at penetrated WPP connection sites within a distribution system. The proposed model has high accuracy and enables stability analysis computations without the need to carry out complex and time consuming computational tasks.

Chapter 7 - Conclusions and Future Work

7.1 Introduction

This research presents an analytical voltage stability model as a new approach for the initial site and size analysis of potential distribution network interconnection points for WPPs. The approach relied on the analysis of potential interconnection points in terms of their SCC and X/R ratios, which enabled author to develop a voltage stability hypothesis based on the SCC and X/R ratio seen at a potential connection point. Two key types of WTGs widely used in the WPPs were observed, IG and DFIG. For each generator type, author formulated mathematical approximations supported by the GA optimization method for voltage-stability analysis in that generator type. Taking advantage of the proposed method, an engineer can promptly conduct an initial predictive assessment on voltage stability and maximum injection levels at candidate PCC buses regarding the value of SCC and X/R seen from those buses.

Many approaches have been proposed in the literature to find optimal size allocation of DG systems in distribution networks. The majority of these approaches are based on Artificial Intelligence (IA) or Optimal Power flow analytical approaches. IA and analytical approaches proposed in the literature require complex and time consuming computational tasks or modelling of test systems. These challenges could be removed using an analytical voltage stability model based on mathematical relations between PCC bus voltage and the PCC parameters, i.e. X/R_{PCC} and SCC. However, relatively no effort has been made towards optimal WPP size allocating using such an analytical model.

Nevertheless, there are some publications focusing on the relation between voltage and the PCC parameters of a distribution network penetrated by WPPs. Majority of these investigated the effect of X/R_{PCC} variation on V_{PCC} and step- V_{PCC} variations under constant SCC value using graphical representations. However, none developed an analytical model based on mathematical relations between V_{PCC} , the grid's SCC, and X/R_{PCC} ratio. Therefore, development of mathematical relations between V_{PCC} and the key parameters such as the SCC and X/R ratio is a noticeable gap.

The research work presented in this thesis has proposed a new analytical model introduces six equations listed in Table 7.1. The equations enable to predict three voltage stability criteria which have a pivotal role in the interconnection of IG and DFIG-Based WPPs to a distribution system. These criteria are: PCC bus voltage profile (V_{PCC}), the step-voltage variation due to the increase in wind power injection at a given PCC point (ΔV_{PCC}), and maximum permissible wind active power ensuring the grid code requirements ($P_{\max-wind}$).

Table 7.1 Proposed voltage stability analytical model

Proposed equation	Application
$V = 0.0912e^{(-0.29 \times \frac{X}{R} \times \frac{SCC}{P_{wind}})} + V_{initial} + 0.0067$	Projecting V_{PCC} and ΔV_{PCC} for IG-Based WPPs for $X/R_{PCC} < 2$
$V = V_{initial} + 0.0013 - 0.0427 \times (\frac{X}{R} \times \frac{P_{wind}}{SCC}) + 0.002 \times (\frac{X}{R} \times \frac{P_{wind}}{SCC})^2$	Projecting V_{PCC} and ΔV_{PCC} for IG-Based WPPs for $X/R_{PCC} > 2$
$V = 0.101e^{(-0.347 \times \frac{X}{R} \times \frac{SCC}{P_{wind}})} + V_{PCC_initial} + 0.01$	Projecting V_{PCC} and ΔV_{PCC} for DFIG-Based WPPs for $X/R_{PCC} < 2$
$P_{\max-wind} = 0.29 \times \frac{\frac{X}{R} \times SCC}{Ln(\frac{0.0912}{1.0433 - V_{initial}})}$	Projecting $P_{\max-wind}$ for IG-Based WPPs for $X/R_{PCC} < 2$

$P_{\max-wind} = SCC \times \frac{R}{X} \times \left(10.675 - \sqrt{500 \times (0.95 - V_{initial}) + 113.35} \right)$	Projecting $P_{\max-wind}$ for IG-Based WPPs for $X/R_{PCC} > 2$
$P_{\max-wind} = 0.347 \times \frac{\frac{X}{R} \times SCC}{Ln \left(\frac{0.101}{1.04 - V_{PCC_initial}} \right)}$	Projecting $P_{\max-wind}$ for DFIG-Based WPPs for $X/R_{PCC} < 2$

The novel SCC and X/R based voltage-stability model has high accuracy and enables stability analysis computations without the need to carry out complex and time consuming computational tasks, which is a significant advantage over existing site and size analysis approaches. Furthermore, the proposed analytical model removes the need to investigate the effect of distribution network configuration and its component specifications on PCC bus voltage stability. This is due to the fact that the effect of these factors has been considered and modelled in the proposed analytical approach using SCC and X/R parameters. Validation studies carried out in Section 6.4 in Chapter 6 demonstrated that the proposed model can accurately predict the voltage stability criteria for different X/R and SCC values seen from different PCC points. Therefore, although the coefficient values of the developed equations were determined using data obtained from a limited number of PCC points (refer to Chapter 4), the proposed model and the determined coefficients can be applied for the initial voltage stability assessment of any distribution network WPP interconnection point.

7.2 Key contributions of the research

The voltage stability analytical model developed in this research focused on the mathematical relation between voltage and the key PCC parameters of distribution networks to enable a predictive assessment on the important voltage stability criteria at candidate distribution network buses for WPP interconnection. Therefore, key contributions of the research spans over different areas which are itemized below.

- **Voltage stability analysis using IEEE models**

Most of the research works present in the literature talk about the impact of the interconnection of WPPs to distribution networks on the PCC bus voltage in general terms and using simple scenarios. However, this research addresses issues concerned with the interconnection of WPPs to distribution networks through detailed voltage stability analysis studies carried out using IEEE standard distribution test systems simulated by MATLAB. The analysis studies considered two common types of WTGs: IG and DFIG.

For the IG-Based WPP, PV analysis demonstrated that at PCC points with an $X/R_{PCC} < 2$, V_{PCC} increases for increasing levels of P_{wind} and it declines at PCC points with an $X/R_{PCC} > 2$. $X/R_{PCC} = 2$ was observed as the optimal ratio where V_{PCC} would have the lowest variations in response to the change of P_{wind} . It was observed that ΔV at PCC points with a small SCC was greater than that at PCC points with a large SCC. The QV analysis demonstrated that the rate of change in voltage in response to changes in the reactive power at PCC points with a large X/R ratio is higher than that at PCC points with a large X/R ratio. The V-SCR characteristics showed that for weak connection points, where $SCR < 10$, PQ requirements will be problematic in an IG-Based WPP for both small ($X/R_{PCC} < 2$) and large ($X/R_{PCC} > 2$) ranges of X/R_{PCC} .

For the DFIG-Based WPP, PV analysis showed that DFIG is not suitable for low X/R ratio PCCs as DFIG is not able to regulate V_{PCC} within the standard range at PCC points with a small X/R ratio when wind power penetration is high. QV analysis revealed that, similar to IG-Based WPPs, the rate of voltage variation due to the increase in reactive power variation at PCC points with a large X/R is higher than that at PCC points with a small X/R ratio. For DFIG-Based WPPs with $SCR < 10$, V-SCR

analysis evinced the voltage stability requirements would be problematic at connection points with small X/R_{PCC} ratio.

- **Development of an analytical model for projecting V_{PCC} and ΔV_{PCC}**

As one of the major contributions of this research, it was revealed that the voltage profile and voltage variation can be estimated at a given connection point regarding the SCC and X/R values seen at that point and the WPP generator type. For this purpose, a sensitivity analysis has been performed to plot V_{PCC} - X/R_{PCC} characteristics for different IEEE test systems with different SCR values. The V_{PCC} - X/R_{PCC} characteristics were, then, used to develop the general forms of mathematical relations between the parameters considered. For the IG-Based WPP, the relations were developed for two key X/R regions of interest, the $X/R_{PCC} < 2$, and $X/R_{PCC} > 2$ regions. Furthermore, for the DFIG-Based WPP, the equations were developed for the $X/R < 2$ region. A GA-Based approach was later used to determine the coefficient values of these relations.

An exponential function was proposed for the IG-Based WPPs with $X/R_{PCC} < 2$ case, a second-order polynomial function was proposed for $X/R_{PCC} > 2$ case, and an exponential function was proposed for the DFIG-Based WPPs with $X/R_{PCC} < 2$ case. Validation studies confirmed the accuracy of the proposed method in predicting V_{PCC} profile and the step-voltage variation grid codes compliance check, i.e. to verify $\Delta V_{PCC} \leq 3\%$ (compliance with the grid codes) or $\Delta V_{PCC} \geq 3\%$ (grid codes violation).

- **Development of an analytical model for WPP maximum allowable size predicting**

Upon developing the relations between voltage and the PCC parameters, the proposed relations were rewritten in terms of P_{wind} as a function of V_{PCC} , X/R_{PCC} , and SCC. The proposed relations enabled to estimate $P_{max-wind}$ which could be injected by an

IG or DFIG_Based WPP to distribution system. The verification results showed that the accuracy of the proposed relations was slightly impacted in IG-Based WPPs with small SCC and X/R_{PCC} and DFIG-Based WPPs with small SCC value. However, the worst case accuracy amongst the all scenarios investigated was around 85%.

The proposed equations simplify the WPP sizing and siting in a distribution system by removing the need to carry out time consuming computational tasks.

7.3 Future Work

The research presented in this thesis is an important contribution to the knowledge in WPP siting and sizing field. However, it can still be extended in several ways by removing some of the scope limitations assumed in this research or by using it as a stepping-stone to investigate other aspects of WPP optimal placement and sizing. Regardless of their nature, these extensions will make the proposed model more comprehensive and reliable.

Referring to Chapter 3, voltage stability limit is another important parameter in voltage stability analysis studies. As mentioned therein, in a QV curve, the voltage stability limit is the extremum point where further absorption of Q by IG results in $dV/dQ < 0$ and voltage collapse. Therefore, the voltage stability limit can be determined using the relation between voltage and reactive power injected/absorbed by the WPP.

However, the analytical method proposed in this thesis models the relation between voltage and active power. Therefore, the calculation of the voltage stability limit using the proposed analytical model is subject to the development of a model for the reactive power parameter. In this regard, one possible research idea is related to develop the proposed voltage stability analytical model to show the mathematical relations between voltage and the WPP reactive power at a given connection point.

Apart from the voltage stability limit, developing the proposed analytical model for showing the relation between voltage and reactive power enables to calculate V_{PCC} and ΔV_{PCC} at a given connection point for a specific Q_{wind} values.

The equations proposed in this research show mathematical relations between the PCC parameters and the steady-state voltage at a given PCC point. However, the proposed equations can be developed and extended to model the relation between PCC parameters and voltage under transient stability. Such a voltage stability model will enable to predict the voltage behaviour under fault conditions and dynamic performance of the WPP. The reader may refer to [163, 164], where insightful analytical approaches have been proposed for the transient voltage stability analysis in distribution generators based on IG and DFIG.

In this research, the V_{PCC} and $P_{max-wind}$ formulation proposed for the IG-Based WPPs was developed as a polynomial function with the order of 2 and an exponential function for two X/R regions, ($X/R < 2$ and $X/R > 2$). As another extension to this research, this formulation can be developed as a single function, such as a polynomial function with a high rank, which satisfies the whole X/R region and removes the need for dividing the X/R region into two parts. This may increase the applicability of the analytical model for predicting voltage stability at PCC points with X/R around 2. However, the accuracy of such an equation must be compared with the mathematical relations proposed in this research to ensure that the error is not high. Furthermore, apart from GA-Based approach used in this research, the value of the developed equations can be determined using other artificial intelligence approaches, such as Particle Swarm Optimisation (PSO), or Artificial Neural Network (ANN), or least squares curve fitting methods, such as Levenberg–Marquardt algorithm and gradient

descent. Consequently, the error of the new equations has to be compared with the error of the voltage stability analytical model proposed in this research.

Finally, the proposed voltage stability model was developed and validated using IEEE test feeder models. Although, the use of IEEE standard models has wide range of applications in electrical engineering studies, the validation of the presented model using real life test cases is important and will be addressed in future studies to further complement this research. The application of the proposed analytical approach to the real world distribution networks may offer additional insights into further validating the accuracy of the proposed model. Therefore, as part of future work, the author is considering to simulate real-life distribution network models to further test the application of the developed analytical model. This includes modelling and simulating a distribution network model from Victoria, where a wind power plant is being proposed for further integration. However, simulation and modelling the real world distribution systems may require the use of professional engineering software, such as PSS/e.

From a practical perspective, the application of the proposed analytical model to the real world distribution systems may impose additional complexity and challenges. For instance, the effect of On-Load Tap Changer (OLTC) connected to the secondary, or low-voltage side of the power transformer was not considered in the simulated test distribution models. This leads to pessimistic results as the analysis studies considered the worst condition where additional voltage regulation is not provided by the tap changer. However, the ignorance of the OLTC effect is one the practical issues which may impact the accuracy of the analytical model in WPP optimal placement and sizing. Furthermore, having access to data obtained from real world networks, such as the X/R

value seen at distribution network buses or summer and winter load data, may be a complicated process.

References

- [1] S. Tampakis, G. Tsantopoulos, G. Arabatzis, and I. Rerras, "Citizens' views on various forms of energy and their contribution to the environment," *Renewable and Sustainable Energy Reviews*, vol. 20, pp. 473-482, 2013.
- [2] T. S. Ustun, C. Ozansoy, and A. Zayegh, "Recent developments in microgrids and example cases around the world—A review," *Renewable and Sustainable Energy Reviews*, vol. 15, pp. 4030-4041, 2011.
- [3] C. Jin, X. Sheng, and P. Ghosh, "Optimized Electric Vehicle Charging With Intermittent Renewable Energy Sources," *Selected Topics in Signal Processing, IEEE Journal of*, pp. 1-10, 2014.
- [4] T. S. Ustun, C. Ozansoy, and A. Zayegh, "Distributed Energy Resources (DER) object modeling with IEC 61850-7-420," in *Power Engineering Conference (AUPEC), 2011 21st Australasian Universities*, 2011, pp. 1-6.
- [5] S. M. Alizadeh, C. Ozansoy, and T. Alpcan, "The impact of X/R ratio on voltage stability in a distribution network penetrated by wind farms," in *Power Engineering Conference (AUPEC), 2016 Australasian Universities*, 2016, pp. 1-6.
- [6] Y. A. Kaplan, "Overview of wind energy in the world and assessment of current wind energy policies in Turkey," *Renewable and Sustainable Energy Reviews*, vol. 43, pp. 562-568, 2015.
- [7] G. M. Shafiullah, A. M.T. Oo, A. B. M. Shawkat Ali, and P. Wolfs, "Potential challenges of integrating large-scale wind energy into the power grid—A review," *Renewable and Sustainable Energy Reviews*, vol. 20, pp. 306-321, 2013.
- [8] S. Grunau and F. W. Fuchs, "Effect of wind-energy power injection into weak grids," *Institute for Power Electronics and Electrical Drives, Christian-Alberchts-University, Kiel, Germany*, 2012.
- [9] G. Liu, X. Cao, W. Wang, T. Ma, W. Yang, and Y. Chen, "Adaptive control strategy to enhance penetration of PV power generations in weak grid," in *2014 International Power Electronics and Application Conference and Exposition*, 2014, pp. 1217-1221
- [10] J. Morren, S. d. Haan, and J. A. Ferreira, "Contribution of DG units to voltage control: Active and reactive power limitations," in *Power Tech, 2005 IEEE Russia*, 2005, pp. 1-7.
- [11] A. Larsson, "Practical Experience with Power Quality and Wind Power," *Wind Power in Power Systems*, p. 349, 2005.

- [12] M. Shukla and A. Sekar, "Study of the effect of X/R ratio of lines on voltage stability," in *System Theory, 2003. Proceedings of the 35th Southeastern Symposium on*, 2003, pp. 93-97.
- [13] M. Tonso, J. Moren, S. W. H. de Haan, and J. A. Ferreira, "Variable inductor for voltage control in distribution networks," in *Power Electronics and Applications, 2005 European Conference on*, 2005, pp. 10 pp.-P.10.
- [14] T. Neumann, C. Feltes, and I. Erlich, "Response of DFG-based wind farms operating on weak grids to voltage sags," in *Power and Energy Society General Meeting, 2011 IEEE*, 2011, pp. 1-6.
- [15] Y. Zhou, D. D. Nguyen, P. C. Kjaer, and S. Saylor, "Connecting wind power plant with weak grid - Challenges and solutions," in *2013 IEEE Power & Energy Society General Meeting*, 2013, pp. 1-7.
- [16] Australian Energy Market Operator (AEMO), "Wind integration: International experience WP2: Review of grid codes," *2nd October*, 2011.
- [17] S. G. Naik, D. Khatod, and M. Sharma, "Sizing and siting of distributed generation in distribution networks for real power loss minimization using analytical approach," in *Power, Energy and Control (ICPEC), 2013 International Conference on*, 2013, pp. 740-745.
- [18] D. Q. Hung, N. Mithulananthan, and R. Bansal, "Analytical expressions for DG allocation in primary distribution networks," *IEEE Transactions on energy conversion*, vol. 25, pp. 814-820, 2010.
- [19] I. Pisica, C. Bulac, and M. Eremia, "Optimal Distributed Generation Location and Sizing Using Genetic Algorithms," in *Intelligent System Applications to Power Systems, 2009. ISAP '09. 15th International Conference on*, 2009, pp. 1-6.
- [20] F. S. Abu-Mouti and M. El-Hawary, "Optimal distributed generation allocation and sizing in distribution systems via artificial bee colony algorithm," *IEEE transactions on power delivery*, vol. 26, pp. 2090-2101, 2011.
- [21] I. J. Hasan, M. R. A. Ghani, and C. K. Gan, "Optimum distributed generation allocation using PSO in order to reduce losses and voltage improvement," in *Clean Energy and Technology (CEAT) 2014, 3rd IET International Conference on*, 2014, pp. 1-6.
- [22] D. K. Khatod, V. Pant, and J. Sharma, "Evolutionary programming based optimal placement of renewable distributed generators," *IEEE Transactions on Power Systems*, vol. 28, pp. 683-695, 2013.
- [23] J.H. Teng, "A direct approach for distribution system load flow solutions," *IEEE Transactions on Power Delivery*, vol. 18, pp. 882 - 887, 2013.

- [24] C. Ozansoy, A. Zayegh and A. Kalam, "Time Synchronisation in Distributed Substation Systems," *In. Proceedings of the AUPEC'08 Conference*, Sydney, Australia, December 2008
- [25] Power quality manager, "Supply standards: Electricity supply standard," ed: Essential energy, 2011.
- [26] U. F. Melkior, M. er, an, M. Z. Iler, et al., "The reliability of the system with wind power generation," in *2016 17th International Scientific Conference on Electric Power Engineering (EPE)*, 2016, pp. 1-6.
- [27] T. Custem and C. Vournas, "Voltage stability of the electric power systems," *Kluwer Academic*, Norwell, 1998.
- [28] Berizzi A, "The Italian 2003 blackout," in *IEEE power engineering society general meeting*, Denver, 2004, pp. 1673–1679.
- [29] N. Ghasemi, M. Abedi, H. Rastegar, and G. Gharepetian, "Hybrid distributed generation units PEM fuel cell and microturbine," in *Industrial Technology, 2008. ICIT 2008. IEEE International Conference on*, 2008, pp. 1-6.
- [30] S. M. Alizadeh, M. Sedighzadeh, and D. Arzaghi-Haris, "Optimization of micro-turbine generation control system using genetic algorithm," in *Power and Energy (PECon), 2010 IEEE International Conference on*, 2010, pp. 589-593.
- [31] X. Han, J. Guo, and P. Wang, "Adequacy study of a wind farm considering terrain and wake effect," *Generation, Transmission & Distribution, IET*, vol. 6, pp. 1001-1008, 2012.
- [32] C. Mishra, S. P. Singh, and J. Rokadia, "Optimal power flow in the presence of wind power using modified cuckoo search," *Generation, Transmission & Distribution, IET*, vol. 9, pp. 615-626, 2015.
- [33] F. Ugranli, C. Ersavaş, and E. Karatepe, "Neural network based distributed generation allocation for minimizing voltage fluctuation due to uncertainty of the output power," in *Innovations in Intelligent Systems and Applications (INISTA), 2011 International Symposium on*, 2011, pp. 415-419.
- [34] A. Kunwar, R. Bansal, and O. Krause, "Steady-state and transient voltage stability analysis of a weak distribution system with a remote doubly fed induction generator-based wind farm," *Energy Science & Engineering*, vol. 2, pp. 188-195, 2014.
- [35] M. Gunsan and C. Ozansoy, "Analysis of Wind Power Potential in Western Regions of Melbourne," *In. Proceedings of the Solar'09 Conference*, Townsville, Australia, October 2009.
- [36] W. Li, Y. Chun-Jui, H. Min-Han, W. Cheng-Tai, and L. Chieh-Lung, "Analysis of voltage variations and short-circuit ratios of a large-scale offshore wind farm connected to a practical power system," in *2013 IEEE Power & Energy Society General Meeting*, 2013, pp. 1-5.

- [37] A. Bagheri, A. Habibzadeh, and S. Alizadeh, "Comparison of the effect of combination of different DG types on loss reduction using APSO algorithm," *Canadian Journal on Electrical and Electronics Engineering*, vol. 2, pp. 468-474, 2011.
- [38] C. A. Patel, K. Mistry, and R. Roy, "Loss allocation in radial distribution system with multiple DG placement using TLBO," in *Electrical, Computer and Communication Technologies (ICECCT), 2015 IEEE International Conference on*, 2015, pp. 1-5.
- [39] K. Nadhir, D. Chabane, and B. Tarek, "Firefly algorithm for optimal allocation and sizing of Distributed Generation in radial distribution system for loss minimization," in *Control, Decision and Information Technologies (CoDIT), 2013 International Conference on*, 2013, pp. 231-235.
- [40] P. Chiradeja and R. Ramakumar, "An approach to quantify the technical benefits of distributed generation," *IEEE Transactions on Energy Conversion*, vol. 19, pp. 764-773, 2004.
- [41] H. Hedayati, S. A. Nabaviniaki, and A. Akbarimajd, "A Method for Placement of DG Units in Distribution Networks," *IEEE Transactions on Power Delivery*, vol. 23, pp. 1620-1628, 2008.
- [42] H. L. Willis, "Analytical methods and rules of thumb for modeling DG-distribution interaction," in *Power Engineering Society Summer Meeting, 2000. IEEE*, 2000, pp. 1643-1644.
- [43] T. Gözel and M. H. Hocaoglu, "An analytical method for the sizing and siting of distributed generators in radial systems," *Electric Power Systems Research*, vol. 79, pp. 912-918, 2009.
- [44] C. Wang and M. H. Nehrir, "Analytical approaches for optimal placement of distributed generation sources in power systems," *IEEE Transactions on Power Systems*, vol. 19, pp. 2068-2076, 2004.
- [45] L. F. Ochoa and G. P. Harrison, "Minimizing energy losses: Optimal accommodation and smart operation of renewable distributed generation," *IEEE Transactions on Power Systems*, vol. 26, pp. 198-205, 2011.
- [46] A. Golieva, "Low Short Circuit Ratio Connection of Wind Power Plants," TU Delft, Delft University of Technology, 2015.
- [47] S. M. Alizadeh and C. Ozansoy, "The role of communications and standardization in wind power applications – A review," *Renewable and Sustainable Energy Reviews*, vol. 54, pp. 944-958, 2016.
- [48] Australian Electricity Market Operator, "Wind integration: International experience," *WP2: Review of Grid Codes*, 2011.

- [49] European network of transmission system operators for electricity (entose), "Network Code for Requirements for Grid Connection Applicable to all Generators (NC RfG)," March 2013.
- [50] R. Langella, A. Testa, and et al. "IEEE Guide—Adoption of IEC/TR 61000-3-7: 2008, Electromagnetic compatibility (EMC)—Limits—Assessment of emission limits for the connection of fluctuating installations to MV, HV and EHV power systems," 2012.
- [51] R. Secretariat, "Grid Connection Code for Renewable Power Plants (RPPs) Connected to the Electricity Transmission System (TS) or the Distribution System (DS) in South Africa," ed: NERSA. Sahin, YG & Aras, F, 2007.
- [52] G. O. Suvire and P. E. Mercado, "Wind farm: Dynamic model and impact on a weak power system," in *Transmission and Distribution Conference and Exposition: Latin America, 2008 IEEE/PES*, 2008, pp. 1-8.
- [53] K. M. Muttaqi, A. D. T. Le, M. Negnevitsky, and G. Ledwich, "A coordinated voltage control approach for coordination of OLTC, voltage regulator and DG to regulate voltage in a distribution feeder," in *Industry Applications Society Annual Meeting*, 2013, pp. 1-8.
- [54] Y. Zhou, D. D. Nguyen, P. C. Kjaer, and S. Saylor, "Connecting wind power plant with weak grid - Challenges and solutions," in *2013 IEEE Power & Energy Society General Meeting*, 2013, pp. 1-7.
- [55] T. Sarkar, A. K. Dan, and S. Ghosh, "Effect of X/R ratio on low voltage distribution system connected with constant speed wind turbine," in *2016 2nd International Conference on Control, Instrumentation, Energy & Communication (CIEC)*, 2016, pp. 417-421.
- [56] R. Reginato, M. G. Zanchettin, and M. Tragueta, "Analysis of safe integration criteria for wind power with induction generators based wind turbines," in *2009 IEEE Power & Energy Society General Meeting*, 2009, pp. 1-8.
- [57] Kothari and et al., *Renewable Energy Sources and Emerging Technologies*: Prentice-Hall of India Pvt. Limited.
- [58] S. Hartge and F. Fischer, "FACTS capabilities of wind energy converters," in *European Wind Energy Conference*, Athens, 2006.
- [59] S. Bose, R. W. Delmerico, N. M. Elkachouty, J. P. Lyons, N. W. Miller, R. A. Walling, et al., "Continuous reactive power support for wind turbine generators," ed: Google Patents, 2005.
- [60] Operator Australian Energy Market, "Wind turbine plant capabilities report" 2013.
- [61] D. M. Patel, A. Nagera, and D. Y. Joshi, "Power quality improvement with Static Compensator on grid integration of wind energy system," in *Engineering (NUI CONE), 2011 Nirma University International Conference on*, 2011, pp. 1-6.

- [62] A. Moharana and R. K. Varma, "Subsynchronous resonance in single-cage self-excited-induction-generator-based wind farm connected to series-compensated lines," *IET Generation, Transmission & Distribution*, vol. 5, pp. 1221-1232, 2011.
- [63] T. Sunil and N. Loganathan, "Power quality improvement of a grid-connected wind energy conversion system with harmonics reduction using FACTS device," in *Advances in Engineering, Science and Management (ICAESM), 2012 International Conference on*, 2012, pp. 415-420.
- [64] M. Ngo Duc, "Application of bidirectional power converters to overcome some disadvantages of a SVC substation in Thainguyen, Vietnam," in *Electric Utility Deregulation and Restructuring and Power Technologies (DRPT), 2011 4th International Conference on*, 2011, pp. 509-513.
- [65] S. W. Mohod and M. V. Aware, "A STATCOM-control scheme for grid connected wind energy system for power quality improvement," *Systems Journal, IEEE*, vol. 4, pp. 346-352, 2010.
- [66] L. Duck-Su, K. Soo-Nam, C. Young-Chan, B. Byung-San, and H. Jong-Sung, "Development of wind power stabilization system using BESS and STATCOM," in *Innovative Smart Grid Technologies (ISGT Europe), 2012 3rd IEEE PES International Conference and Exhibition on*, 2012, pp. 1-5.
- [67] M. J. Ghorbanian, F. Goodarzvand, A. Poudaryaei, and W. N. L. Mahadi, "Power quality improvement of grid connected doubly fed induction generator using STATCOM and BESS," in *Engineering Technology and Technopreneuship (ICE2T), 2014 4th International Conference on*, 2014, pp. 110-115.
- [68] H. Emanuel, M. Schellschmidt, S. Wachtel, and S. Adloff, "Power quality measurements of wind energy converters with full-scale converter according to IEC 61400-21," in *Electrical Power Quality and Utilisation, 2009. EPQU 2009. 10th International Conference on*, 2009, pp. 1-7.
- [69] M. Fischer and A. Mendonca, "Representation of variable speed full conversion Wind Energy Converters for steady state short-circuit calculations," in *Power and Energy Society General Meeting, 2011 IEEE*, 2011, pp. 1-7.
- [70] K. Divya and P. N. Rao, "Models for wind turbine generating systems and their application in load flow studies," *Electric Power Systems Research*, vol. 76, pp. 844-856, 2006.
- [71] High speed induction generators. Available in ABB group website: <http://new.abb.com/motors-generators/generators/generators-for-wind-turbines/high-speed-induction-generators>
- [72] L. Pham, "A review of full scale converter for wind turbines," *Electrical and Renewable Energy Engineering Department, Oregon Institute of Technology*, Wilsonville, pp. 1-8.

- [73] Schneider electric, "Industrial electrical network design guide-Part7: Reactive energy compensation," 2009.
- [74] S. Gopiya-Naik, D. Khatod, and M. Sharma, "Optimal allocation of distributed generation in distribution system for loss reduction," in *Proc. IACSIT Coimbatore Conferences*, 2012, pp. 42-46.
- [75] H. Khan and M. A. Choudhry, "Implementation of Distributed Generation (IDG) algorithm for performance enhancement of distribution feeder under extreme load growth," *International Journal of Electrical Power & Energy Systems*, vol. 32, pp. 985-997, 2010.
- [76] N. Acharya, P. Mahat, and N. Mithulananthan, "An analytical approach for DG allocation in primary distribution network," *International Journal of Electrical Power & Energy Systems*, vol. 28, pp. 669-678, 2006.
- [77] D. Q. Hung and N. Mithulananthan, "Multiple distributed generator placement in primary distribution networks for loss reduction," *IEEE Transactions on industrial electronics*, vol. 60, pp. 1700-1708, 2013.
- [78] S. Mishra, D. Das, and S. Paul, "A simple algorithm to implement active power loss allocation schemes in radial distribution systems," *Journal of The Institution of Engineers (India): Series B*, vol. 93, pp. 123-132, 2012.
- [79] A. Farooq and K. Hamid, "An Efficient and Simple Algorithm for Matrix Inversion," *International Journal of Technology Diffusion (IJTD)*, vol. 1, pp. 20-27, 2010.
- [80] F. Soleymani, "A rapid numerical algorithm to compute matrix inversion," *International Journal of Mathematics and Mathematical Sciences*, vol. 2012, 2012.
- [81] E. Carpaneto, G. Chicco, and J. S. Akilimali, "Branch current decomposition method for loss allocation in radial distribution systems with distributed generation," *IEEE Transactions on Power Systems*, vol. 21, pp. 1170-1179, 2006.
- [82] L. Ochoa, C. Borges, G. Ault, A. Alarcon, R. Currie, F. Pilo, *et al.*, "State of the art techniques and challenges ahead for DG planning and optimization," 2013.
- [83] S. N. Singh, "Distributed generation in power systems: An overview and key issues," in *24th Indian Engineering Congress*, 2009.
- [84] E. Wenger, *Artificial intelligence and tutoring systems: computational and cognitive approaches to the communication of knowledge*: Morgan Kaufmann, 2014.
- [85] I. Pisica, C. Bulac, and M. Eremia, "Optimal distributed generation location and sizing using genetic algorithms," in *Intelligent System Applications to Power Systems, 2009. ISAP'09. 15th International Conference on*, 2009, pp. 1-6.

- [86] M. Gandomkar, M. Vakilian, and M. Ehsan, "A genetic-based tabu search algorithm for optimal DG allocation in distribution networks," *Electric Power Components and Systems*, vol. 33, pp. 1351-1362, 2005.
- [87] *Modelling requirements*. Available in Australian Energy Market Commission (AEMO) webpage: <https://www.aemo.com.au/Electricity/National-Electricity-Market-NEM/Network-connections/Modelling-requirements>.
- [88] A. Grilo, P. Meira, J. Vieira, W. Freitas, and R. Bansal, "Analytical tools to assess the voltage stability of induction-based distributed generators," *International Journal of Electrical Power & Energy Systems*, vol. 36, pp. 31-39, 2012.
- [89] N. P. W. Strachan and D. Jovicic, "Stability of a Variable-Speed Permanent Magnet Wind Generator With Weak AC Grids," *IEEE Transactions on Power Delivery*, vol. 25, pp. 2779-2788, 2010.
- [90] N.E. Clausen, "Planning and development of wind farms: Environmental impact and grid connection," DTU Wind Energy 2013.
- [91] J. Bech, "Wind turbine control for a weak grid by reducing active power output," ed: Google Patents, 2014.
- [92] C. Ozansoy and K. Frearson, "IEC 61850 based islanding detection and load shedding in substation automation systems," *Turkish Journal of Electrical Engineering & Computer Sciences*, vol. 24, no. 6, pp. 4858-4873, December 2016.
- [93] J. W. Feltes and B. S. Fernandes, "Wind turbine generator dynamic performance with weak transmission grids," in *2012 IEEE Power and Energy Society General Meeting*, 2012, pp. 1-7.
- [94] J. Schmall, S. H. Huang, L. Ying, J. Billo, J. Conto, and Z. Yang, "Voltage stability of large-scale wind plants integrated in weak networks: An ERCOT case study," in *2015 IEEE Power & Energy Society General Meeting*, 2015, pp. 1-5.
- [95] E. Muljadi, C. P. Butterfield, B. Parsons, and A. Ellis, "Effect of Variable Speed Wind Turbine Generator on Stability of a Weak Grid," *IEEE Transactions on Energy Conversion*, vol. 22, pp. 29-36, 2007.
- [96] R. Piwko, N. Miller, J. Sanchez-Gasca, Y. Xiaoming, D. Renchang, and J. Lyons, "Integrating Large Wind Farms into Weak Power Grids with Long Transmission Lines," in *2005 IEEE/PES Transmission & Distribution Conference & Exposition: Asia and Pacific*, 2005, pp. 1-7.
- [97] F. I. Bakhsh, M. Irshad, and S. Islam, "New Model Variable Frequency Transformer (NMVFT)—A Technology for V/f Control of Induction Motors," in *International Conference on Advances in Electrical and Electronic*, 2010, pp. 21-22.

- [98] R. J. Piwko and E. V. Larsen, "Variable Frequency Transformer - FACTS Technology for Asynchronous Power Transfer," in *2005/2006 IEEE/PES Transmission and Distribution Conference and Exhibition*, 2006, pp. 1426-1428.
- [99] S.H. Huang, J. Schmall, J. Conto, J. Adams, Y. Zhang, and C. Carter, "Voltage control challenges on weak grids with high penetration of wind generation: ERCOT experience," in *Power and Energy Society General Meeting, 2012 IEEE*, 2012, pp. 1-7.
- [100] J. O. Tande and K. Uhlen, "Wind turbines in weak grids-constraints and solutions," in *Electricity Distribution, 2001. Part 1: Contributions. CIRED. 16th International Conference and Exhibition on (IEE Conf. Publ No. 482)*, 2001, p. 5 pp. vol. 4.
- [101] J. Conto, "Grid challenges on high penetration levels of wind power," in *2012 IEEE Power and Energy Society General Meeting*, 2012, pp. 1-3.
- [102] J. C. Molburg, J. Kavicky, and K. Picel, *The Design Construction, and Operation of Long-distance High-voltage Electricity Transmission Technologies*: Argonne National Laboratory, Environmental Science Division, 2007.
- [103] M. Farzaneh, S. Farokhi, and W. Chisholm, *Electrical design of overhead power transmission lines*: McGraw Hill Professional, 2012.
- [104] B. C. Wadell, *Transmission line design handbook*: Artech House Publishers, 1991.
- [105] A. Seneviratne, "Standard: Distribution Design Manual Vol 5 –Overhead Bare Conductor Distribution " 2014.
- [106] M. Reta-Hernández, "Transmission Line Parameters," Taylor & Francis Group, LLC2006.
- [107] A. J. Sinclair and J. A. Ferreira, "Analysis and design of transmission-line structures by means of the geometric mean distance," in *AFRICON, 1996., IEEE AFRICON 4th*, 1996, pp. 1062-1065 vol.2.
- [108] A. Parizad, S. Dehghan, H. Saboori, and A. Kazemi, "Transmission network augmentation planning considering the impact of corona power loss," in *PowerTech, 2011 IEEE Trondheim*, 2011, pp. 1-6.
- [109] F. W. Grover, *Inductance calculations: working formulas and tables*: Courier Corporation, 2004.
- [110] J. Morren, S. W. de Haan, and J. Ferreira, "Distributed generation units contributing to voltage control in distribution networks," in *Universities Power Engineering Conference, 2004. UPEC 2004. 39th International*, 2004, pp. 789-793.

- [111] N. H. Woodley, A. Sundaram, T. Holden, and T. C. Einarson, "Field experience with the new platform-mounted DVR/sup TM/," in *Power System Technology, 2000. Proceedings. PowerCon 2000. International Conference on*, 2000, pp. 1323-1328 vol.3.
- [112] P. Parihar and G. G. Karady, "Characterization of a thyristor controlled reactor," *Electric Power Systems Research*, vol. 41, pp. 141-149, 1997/05/01 1997.
- [113] B. N. Rao, N. Senroy, and A. R. Abhyankar, "Analysis of OLTC behaviour in a wind power integrated distribution system," in *Power and Energy Engineering Conference (APPEEC), 2014 IEEE PES Asia-Pacific*, 2014, pp. 1-5.
- [114] F. Sulla, J. Svensson, and O. Samuelsson, "Wind turbines voltage support in weak grids," in *2013 IEEE Power & Energy Society General Meeting*, 2013, pp. 1-5.
- [115] R. Navarro-Perez and R. Prada, "Voltage collapse or steady-state stability limit," in *Proceedings of the International Seminar on Bulk Power System Voltage Phenomena II*, 1993, pp. 75-84.
- [116] P. N. K. Sreelatha, J. Praveen, and V. Kamaraju, "Effect of unsymmetrical faults on distribution lines with different line X/R ratios and voltage restoration using DVR with Space vector control," in *Computing, Electronics and Electrical Technologies (ICCEET), 2012 International Conference on*, 2012, pp. 92-97.
- [117] A. M. Massoud, S. Ahmed, P. N. Enjeti, and B. W. Williams, "Evaluation of a Multilevel Cascaded-Type Dynamic Voltage Restorer Employing Discontinuous Space Vector Modulation," *IEEE Transactions on Industrial Electronics*, vol. 57, pp. 2398-2410, 2010.
- [118] J. D. Barros and J. F. Silva, "Multilevel Optimal Predictive Dynamic Voltage Restorer," *IEEE Transactions on Industrial Electronics*, vol. 57, pp. 2747-2760, 2010.
- [119] C. N. M. Ho and H. S. H. Chung, "Implementation and Performance Evaluation of a Fast Dynamic Control Scheme for Capacitor-Supported Interline DVR," *IEEE Transactions on Power Electronics*, vol. 25, pp. 1975-1988, 2010.
- [120] A. Prasai and D. M. Divan, "Zero-Energy Sag Correctors-Optimizing Dynamic Voltage Restorers for Industrial Applications," *IEEE Transactions on Industry Applications*, vol. 44, pp. 1777-1784, 2008.
- [121] N. H. Woodley, "Field experience with Dynamic Voltage Restorer (DVR/sup TM/MV) systems," in *Power Engineering Society Winter Meeting, 2000. IEEE*, 2000, pp. 2864-2871 vol.4.
- [122] C. Vournas, P. Sauer, and M. Pai, "Relationships between voltage and angle stability of power systems," *International Journal of Electrical Power & Energy Systems*, vol. 18, pp. 493-500, 1996.

- [123] Thierry Van Cutsem and C. Vournas, *Voltage stability of electric power systems* vol. 441: Springer Science & Business Media, 1998.
- [124] Australian Energy Market Operator (AEMO), "Update report – black system event in South Australia (SA) on 28 September 2016," 2016.
- [125] J. Hossain and H. R. Pota, "Power System Voltage Stability and Models of Devices," in *Robust Control for Grid Voltage Stability: High Penetration of Renewable Energy*, ed: Springer, 2014, pp. 19-59.
- [126] Y. Chi, Y. Liu, W. Wang, and H. Dai, "Voltage stability analysis of wind farm integration into transmission network," in *2006 International Conference on Power System Technology*, 2006, pp. 1-7.
- [127] Y. Tamura, K. Sakamoto, and Y. Tayama, "Voltage instability proximity index (VIPI) based on multiple load flow solutions in ill-conditioned power systems," in *Decision and Control, 1988., Proceedings of the 27th IEEE Conference on*, 1988, pp. 2114-2119.
- [128] J. Carpentier, R. Girard, and E. Scano, "Voltage collapse proximity indicators computed from an optimal power flow," in *Proc. 8th Power System Computation Conf.(PSCC)*, 1984, pp. 671-678.
- [129] F. Galiana, "Load flow feasibility and the voltage collapse problem," in *Decision and Control, 1984. The 23rd IEEE Conference on*, 1984, pp. 485-487.
- [130] P. Kessel and H. Glavitsch, "Estimating the voltage stability of a power system," *IEEE Transactions on Power Delivery*, vol. 1, pp. 346-354, 1986.
- [131] A. Tiranuchit and R. Thomas, "A posturing strategy against voltage instabilities in electric power systems," *IEEE Transactions on Power Systems*, vol. 3, pp. 87-93, 1988.
- [132] C. L. DeMarco and T. J. Overbye, "An energy based security measure for assessing vulnerability to voltage collapse," *IEEE Transactions on Power Systems*, vol. 5, pp. 419-427, 1990.
- [133] L. Zhang, Y. Honggeng, D. Zhilin, and L. Yadong, "Online estimation of short circuit ratio for HVDC transmission systems," *Electric Power Science and Engineering*, vol. 3, p. 005, 2012.
- [134] W.C. Yang, T. Chen, J. Wu, and S. Chen, "Modeling and Operation Analysis of Meshed Distribution Systems with Distributed Generation," in *WSEAS International Conference. Proceedings. Mathematics and Computers in Science and Engineering*, 2009.
- [135] G. K. Babu and R. K. Samala, "Load flow analysis of 9 bus radial system using BFSLF algorithm," *International Journal of Electronics and Communication Engineering (IJECE)*, vol. 4, pp. 17-22, 2015.

- [136] R. Anilkumar, G. Devriese, and A. K. Srivastava, "Intelligent volt/VAR control algorithm for active power distribution system to maximize the energy savings," in *Industry Applications Society Annual Meeting*, 2015 IEEE, 2015, pp. 1-8.
- [137] T. R. Kempner, M. Oleskovicz, and A. Q. Santos, "Optimal allocation of monitors by analyzing the vulnerability area against voltage sags," in *2014 16th International Conference on Harmonics and Quality of Power (ICHQP)*, 2014, pp. 536-540.
- [138] I. Ziari, G. Ledwich, A. Ghosh, D. Cornforth, and M. Wishart, "Optimal allocation and sizing of DGs in distribution networks," in *IEEE PES General Meeting*, 2010, pp. 1-8.
- [139] A. Sharma and B. K. Panigrahi, "Optimal relay coordination suitable for grid-connected and islanded operational modes of microgrid," in *2015 Annual IEEE India Conference (INDICON)*, 2015, pp. 1-6.
- [140] R. Sirjani, A. Mohamed, and H. Shareef, "An improved harmony search algorithm for optimal capacitor placement in radial distribution systems," in *Power Engineering and Optimization Conference (PEOCO), 2011 5th International*, 2011, pp. 323-328.
- [141] S. G. B. Dasan, K. Sharon Ravichandran, and R. P. K. Devi, "Steady-state analysis of Grid connected WECS using FACTS controller," in *Emerging Trends in Electrical and Computer Technology (ICETECT), 2011 International Conference on*, 2011, pp. 127-132.
- [142] Overhead Line Conductors report, Available in Oman Cables Industry (SAOG) website: <http://omancables.com/wp-content/uploads/2017/01/Overhead-Line-Conductor.pdf>
- [143] C. Lin, J. N. Jiang, C. Y. Tang, and T. Runolfsson, "A study on the impact of control on PV curve associated with doubly fed induction generators," in *Power Systems Conference and Exposition (PSC), 2011 IEEE/PES*, 2011, pp. 1-7.
- [144] K. Et, *Renewable Energy Sources And Emerging Technologies*: Prentice-Hall Of India Pvt. Limited.
- [145] Y. F. JingJing Zhao, DongDong Li, KaiKai Wang, "Reactive Power Compensation Strategy of DGIF Wind Park," Springer Science Business Media, New York 2014.
- [146] Y. Wang, "Voltage Stability Assessment Using PQ Region Incorporating Wind Power," The University of Wisconsin-Milwaukee United States, 2013.
- [147] J. F. Frenzel, "Genetic algorithms," *IEEE Potentials*, vol. 12, pp. 21-24, 1993.
- [148] P. Koehn, "Combining genetic algorithms and neural networks: The encoding problem," 1994.
- [149] D. Samajpati, "Distributed Generation Allocation For Power Loss Minimization And Voltage Improvement Of Radial Distribution Systems Using Genetic Algorithm," 2014.

- [150] S. T. Ng, M. Skitmore, and K. F. Wong, "Using genetic algorithms and linear regression analysis for private housing demand forecast," *Building and Environment*, vol. 43, pp. 1171-1184, 2008.
- [151] D. X. Zheng, S. T. Ng, and M. M. Kumaraswamy, "Applying a genetic algorithm-based multiobjective approach for time-cost optimization," *Journal of Construction Engineering and management*, vol. 130, pp. 168-176, 2004.
- [152] S. Chiraphadhanakul, P. Dangprasert, and V. Avatchanakorn, "Genetic algorithms in forecasting commercial banks deposit," in *Intelligent Processing Systems, 1997. ICIPS'97. 1997 IEEE International Conference on*, 1997, pp. 116-121.
- [153] Y. Ju, C. Kim, and J. Shim, "Genetic-based fuzzy models: interest rate forecasting problem," *Computers & industrial engineering*, vol. 33, pp. 561-564, 1997.
- [154] D. Kim and C. Kim, "Forecasting time series with genetic fuzzy predictor ensemble," *IEEE Transactions on Fuzzy systems*, vol. 5, pp. 523-535, 1997.
- [155] B. Jeong, H.-S. Jung, and N.-K. Park, "A computerized causal forecasting system using genetic algorithms in supply chain management," *Journal of Systems and Software*, vol. 60, pp. 223-237, 2002.
- [156] P. Guo, X. Wang, and Y. Han, "The enhanced genetic algorithms for the optimization design," in *2010 3rd International Conference on Biomedical Engineering and Informatics*, 2010, pp. 2990-2994.
- [157] M. Srinivas and L. M. Patnaik, "Genetic algorithms: a survey," *Computer*, vol. 27, pp. 17-26, 1994.
- [158] M. Srinivas and L. M. Patnaik, "Adaptive probabilities of crossover and mutation in genetic algorithms," *IEEE Transactions on Systems, Man, and Cybernetics*, vol. 24, pp. 656-667, 1994.
- [159] K. Strike, K. E. Emam, and N. Madhavji, "Software Cost Estimation with Incomplete Data," *IEEE Trans. Softw. Eng.*, vol. 27, pp. 890-908, 2001.
- [160] S. D. Conte, H. E. Dunsmore, and V. Y. Shen, *Software engineering metrics and models*, Menlo Park, Calif: Benjamin Cummings, 1986.
- [161] T. M. Khoshgoftaar, J. C. Munson, B. B. Bhattacharya, and G. D. Richardson, "Predictive modeling techniques of software quality from software measures," *IEEE Transactions on Software Engineering*, vol. 18, pp. 979-987, 1992.
- [162] A. Berry, T. Moore, J. Ward, S. Lindsay, and K. Proctor, "National Feeder Taxonomy—Describing a Representative Feeder Set for Australian Electricity Distribution Networks," *Report for CSIRO*, 2013.

[163] A. Grilo, M. Salles, F. Trindade, and W. Freitas, "An analytical insight into large-disturbance stability of doubly fed induction generators," *Electric Power Systems Research*, vol. 122, pp. 29-32, 2015.

[164] A. P. Grilo, A. de Assis Mota, L. T. M. Mota, and W. Freitas, "An analytical method for analysis of large-disturbance stability of induction generators," *IEEE Transactions on power systems*, vol. 22, pp. 1861-1869, 2007.

Appendix A – MATLAB/Simulink Models of Test Systems

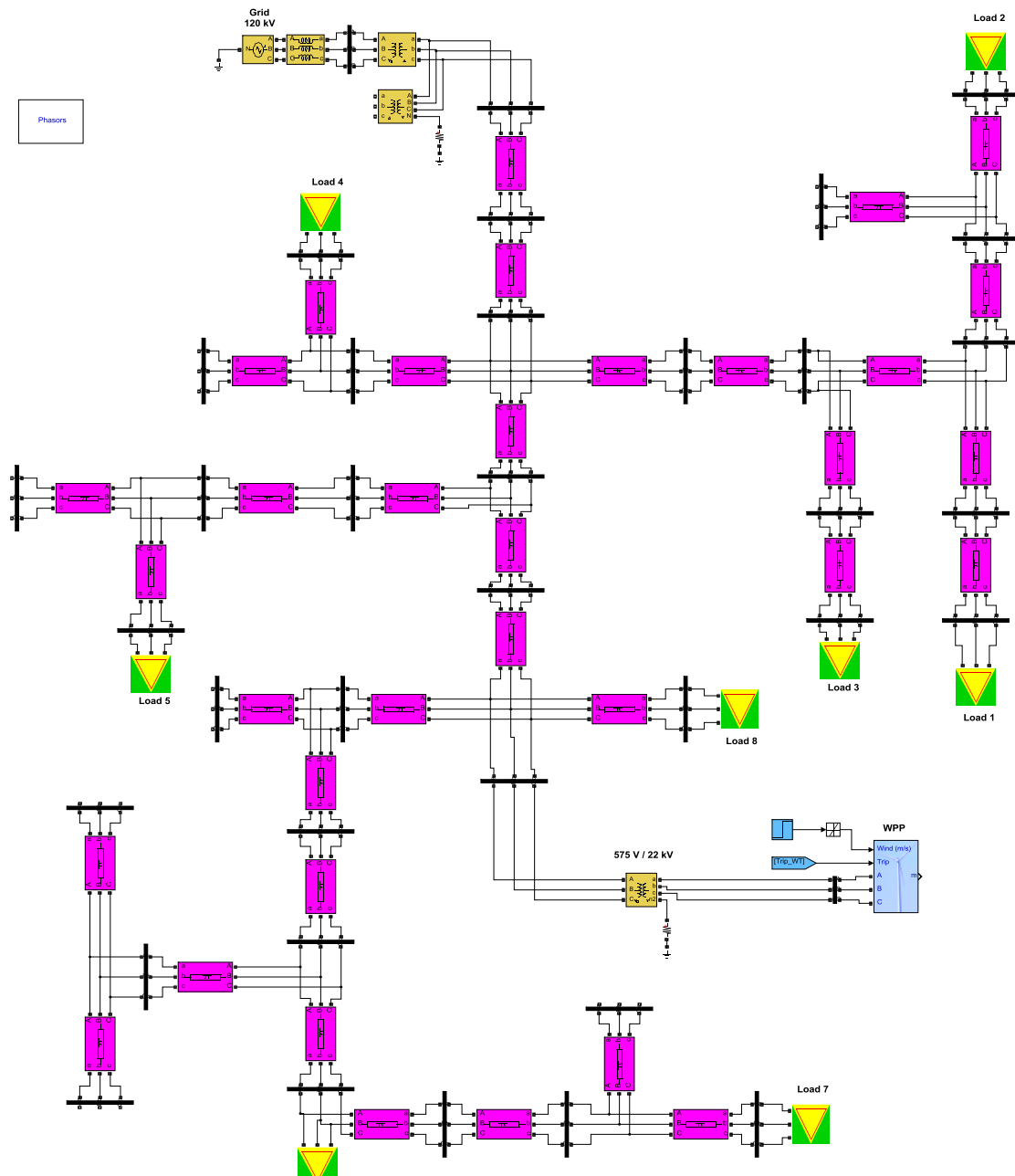


Figure A.1 MATLAB / Simulink model of the 37-bus test distribution system

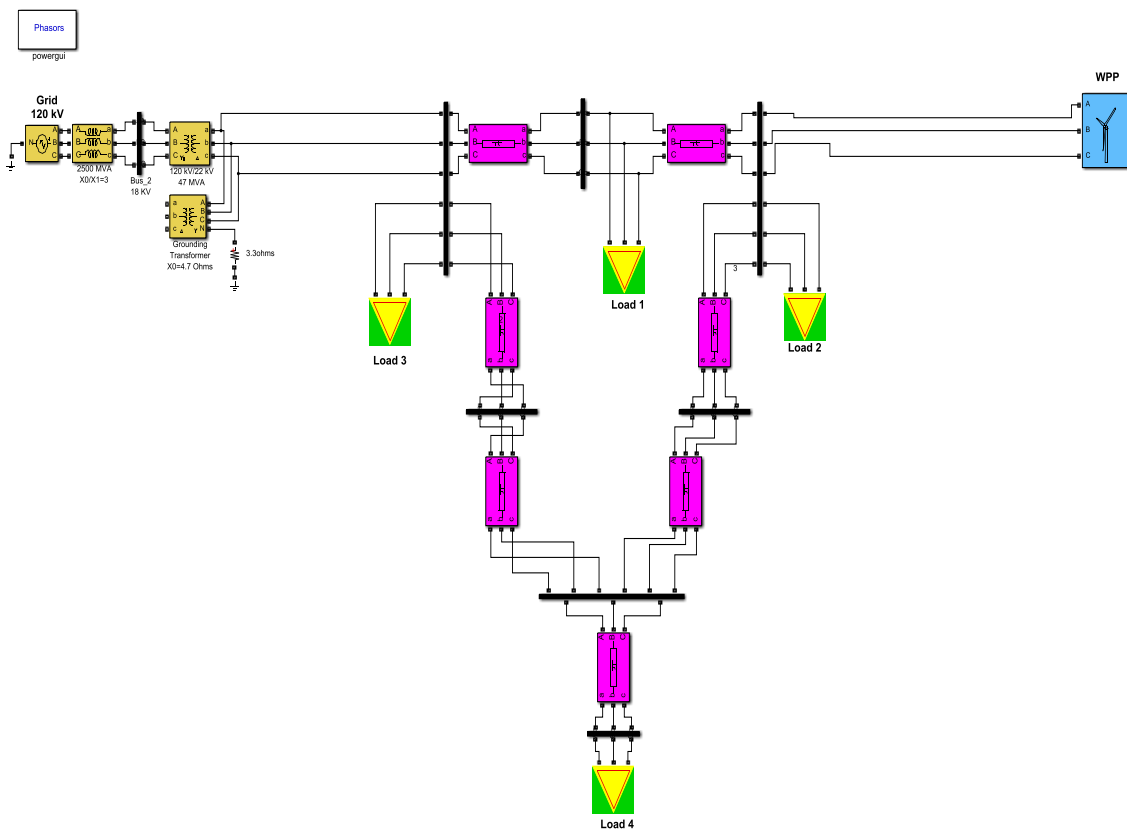


Figure A.2 MATLAB / Simulink model of the 9-bus test distribution system

Appendix B - Test Systems Specifications

Table B.1 Distribution transformer parameters.

Parameter	Unit	Value
Nominal power	P_n (MVA)	47.5
Frequency	f_n (Hz)	50
Primary winding phase to phase voltage	V_1 (kV)	120
Primary winding resistance	R_1 (p.u.)	0.0027
Primary winding inductance	L_1 (p.u.)	0.08
Secondary winding phase to phase voltage	V_2 (kV)	22
Secondary winding resistance	R_2 (p.u.)	0.0027
Secondary winding inductance	L_2 (p.u.)	0.08
Magnetization resistance	R_m (p.u.)	500
Magnetization inductance	L_m (p.u.)	500

Table B.2 Wind turbine generator parameters.

	Parameter	Unit	Value	
			IG	DFIG
Generator data	Nominal power	P_n (MVA)	3	3
	Frequency	f_n (Hz)	50	50
	Line to line voltage	V (kV)	575	575
	Stator resistance	R_s (p.u.)	0.004843	0.007
	Stator leakage inductance	L_s (p.u.)	0.1248	0.17
	Rotor reactance (referred to stator)	R_r' (p.u.)	0.004377	0.005
	Rotor leakage inductance (referred to stator)	L_r' (p.u.)	0.1791	0.156
	Magnetizing inductance	L_m (p.u.)	6.77	2.9
Turbine data	Pitch angle controller gains	K_p	5	500
		K_i	25	-
	Maximum pitch angle	Pitch_angle _{max} (°)	45	45

Table B.3 Wind farm transformer parameters.

Parameter	Unit	Value
Nominal power	P_n (MVA)	4
Frequency	f_n (Hz)	50
Primary winding phase to phase voltage	V_1 (kV)	22
Primary winding resistance	R_1 (p.u.)	0.00084
Primary winding inductance	L_1 (p.u.)	0.025
Secondary winding phase to phase voltage	V_2 (kV)	575
Secondary winding resistance	R_2 (p.u.)	0.00084
Secondary winding inductance	L_2 (p.u.)	0.025
Magnetization resistance	R_m (p.u.)	500
Magnetization inductance	L_m (p.u.)	Infinite

Table B.4 Load data.

Load No.	Load value (MVA)	Total load (MVA)
1	6.3	21
2	1.5	
3	1.5	
4	1.5	
5	2.1	
6	3.2	
7	4.2	
8	1	

Table B.5 Conductor data [138].

Parameter	Unit	Value
Conductor type	-	AAAC
Code number	No.	250
Nominal area	mm ²	288.0
No. / Nominal diameter of wires	No. / mm	19 / 4.39
Approximate overall diameter	mm	21.95
Approximate weight	kg/km	790.8
Nominal breaking load	KN	84.88
Nominal DC resistance at 20° C	ohm/km	0.1151

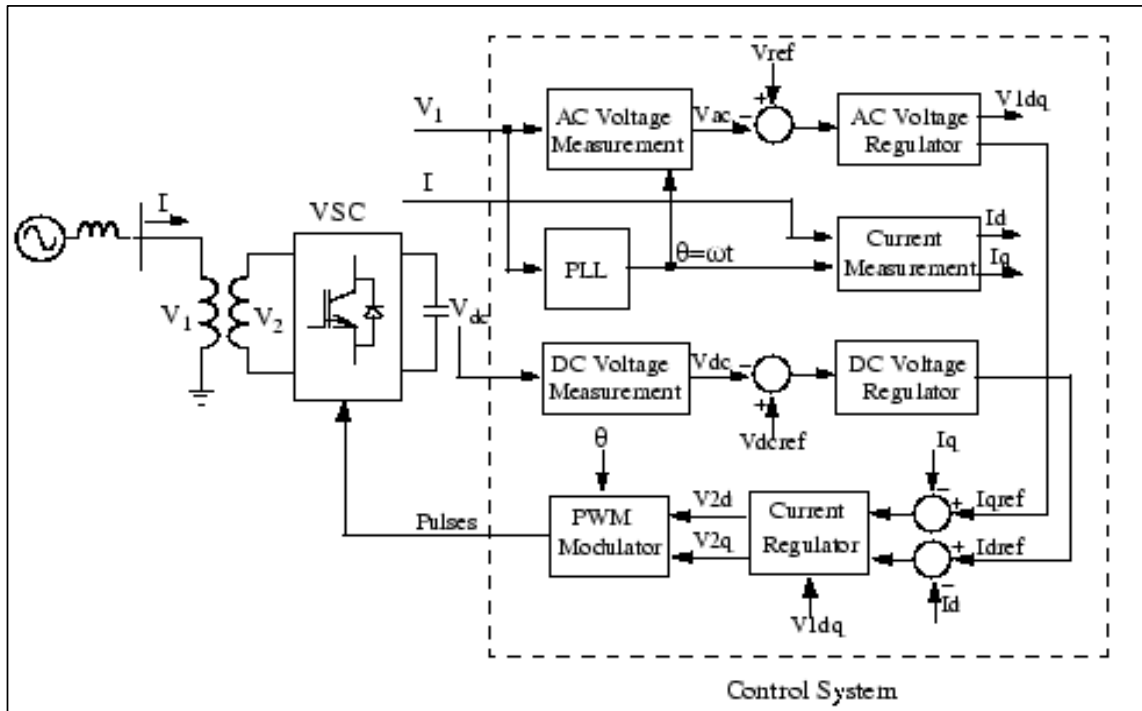


Figure B.1 Single-line diagram of STATCOM and its control system

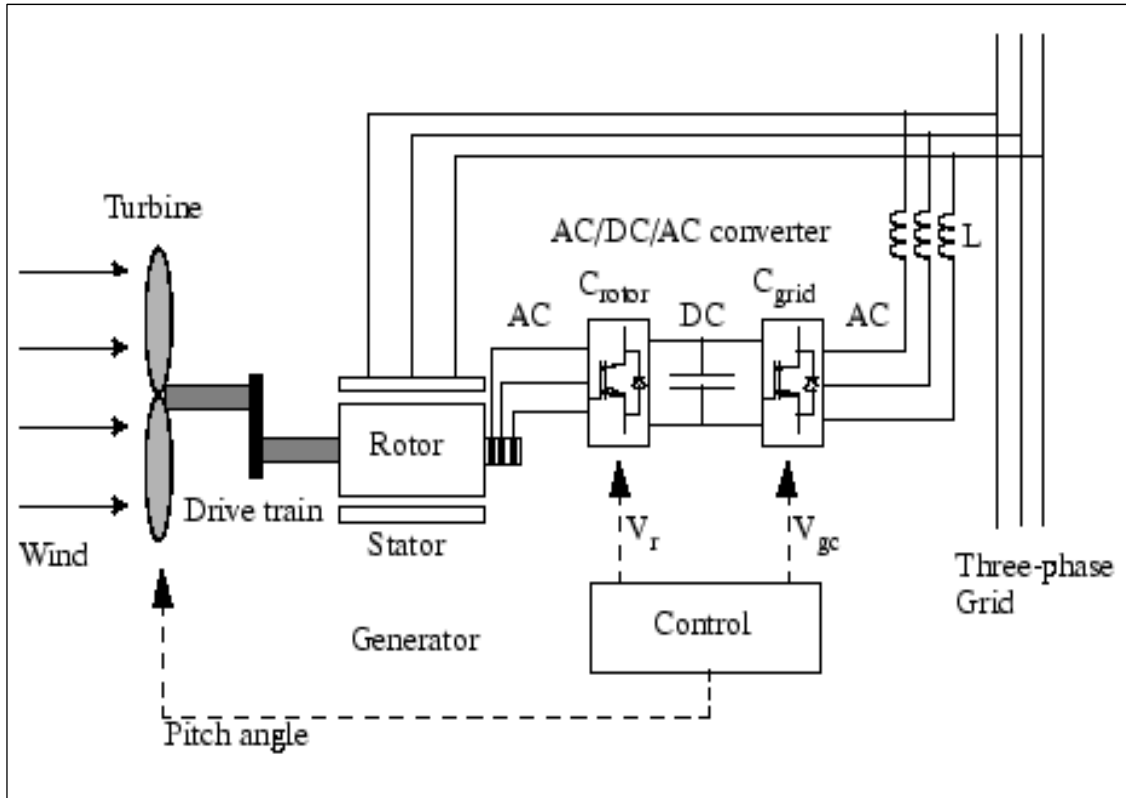


Figure B.2 Block diagram of Doubly-Fed Induction Generator (DFIG) system

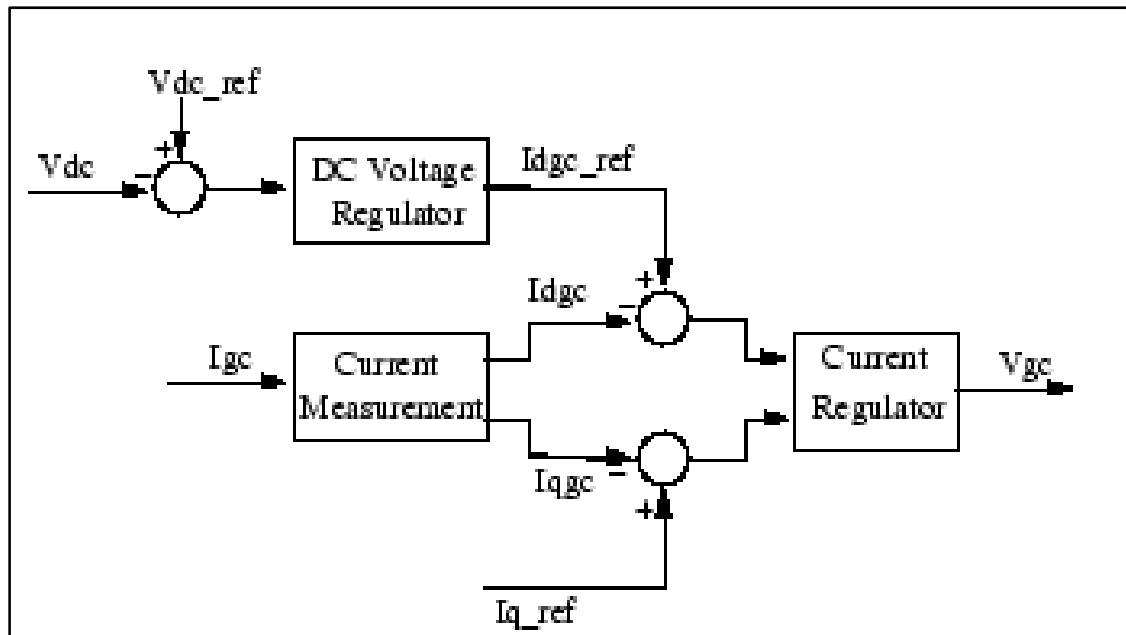


Figure B.3 Block diagram of the grid-side converter control system used in DFIG

Appendix C – MATLAB Codes for Fitness Function 1

```
function SSD = FF1(K)
Asr0 = K(1);
Asr1 = K(2);
Asr2 = K(3);
% Declare Fitness Function 1 named FF1 which accepts vector K as input variable and returns
output variable Sum of Standard Deviation (SSD). K is a row vector with length = 3. The
elements in vector k represent the value of coefficients, in Eq. (4.7), i.e. Asr0, Asr1, and Asr2.
Output parameter (SSD) is the sum of the standard deviation of reference vs. predicted V-X/R
characteristics for Tests 1 to 4 characterised in Table 4.1 in Chapter 4.

xr_1 = [0.3 0.35 0.4 0.45 0.5 0.6 0.7 0.8 0.9 1.3 1.45 1.6 1.85 2.2 2.35
2.45 2.6];
v_ref_1 = [1.07 1.0522 1.035 1.027 1.022 1.0155 1.01 1.005 1 0.9865 0.983
0.98 0.9755 0.9715 0.966 0.9585 0.95];
SCR_1 = 3;
% Assign the reference X/R and voltage data points obtained for Test 1 into variable xr_1 and
variable v_ref_1, respectively. Furthermore, define the SCR value for Test 1.

v_pre_1=Asr0*exp(Asr1*(xr_1*SCR_1))+Asr2;
% For Test 1, calculate voltage value named v_pre_1 using Eq. (4.7).

Error = 0;
s = size(v_pre_1);
for i = 1: s(1)
    Error = Error + (v_ref_1(i)- v_pre_1(i))^2;
end
SD(1) = sqrt(Error) / s(1)
% Calculate standard deviation between v_ref_1 and v_pre_1 and assign it into variable SD(1).

xr_2 = [0.27 0.3 0.38 0.44 0.5 0.57 0.65 0.87 1.23 1.52 1.88
2.07 2.17 2.3 2.4 2.5 2.66 2.8 2.95 3.15 3.3];
v_ref_2 = [1.05 1.042 1.028 1.024 1.019 1.014 1.001 0.999 0.9878
0.982 0.976 0.975 0.973 0.972 0.971 0.97 0.967 0.963 0.96 0.955 0.95];
% Assign the reference X/R and voltage data points obtained for Test 2 into variable xr_2 and
variable v_ref_2, respectively. Furthermore, define the SCR value for Test 2.

v_pre_2 = Asr0*exp(Asr1*(xr_2*SCR_2))+Asr2;
% For Test 2, calculate voltage value named v_pre_2 using Eq. (4.7).

Error = 0;
s = size(v_pre_2);
for i = 1: s(1)
    Error = Error + (v_ref_2(i)- v_pre_2(i))^2;
end
SD(2) = sqrt(Error) / s(1)
```

% Calculate standard deviation between v_ref_2 and v_pre_2 and assign it into variable SD(2).

```
xr_3 = [0.34 0.41 0.5      0.63    0.7    0.8    1.1    1.3    1.7    1.88 2.1
2.2    2.34 2.64      2.86    2.95    3.06    3.25    3.42    3.62    3.82
4.15 4.3    4.5];
```

```
v_ref_3 = [1.026 1.02    1.015    1.0065 1.003 0.998 0.9895 0.985 0.978 0.976
0.974 0.973    0.972    0.97    0.967 0.966 0.964 0.962 0.96    0.9574
0.955 0.953 0.9515 0.95];
```

```
SCR_3 = 6;
```

% Assign the reference X/R and voltage data points obtained for Test 3 into variable xr_3 and variable v_ref_3, respectively. Furthermore, define the SCR value for Test 3.

```
v_pre_3 = Asr0*exp(Asr1*(xr_3*SCR_3))+Asr2;
```

% For Test 3, calculate voltage value named v_pre_3 using Eq. (4.7).

```
Error=0;
```

```
s = size(v_pre_3);
```

```
for i = 1 : s(1)
```

```
    Error = Error + (v_ref_3(i)- v_pre_3(i))^2;
```

```
end
```

```
SD(3) = sqrt(Error) / s(1)
```

% Calculate standard deviation between v_ref_3 and v_pre_3 and assign it into variable SD(3).

```
xr_4 = [0.35    0.4048    0.5    0.57    0.67    0.8    0.98    1.2    1.4 1.62
1.85    2.1    2.3    2.5    2.75    3    3.565    3.8    4.1    4.4 4.8
5 5.75];
```

```
v_ref_4 = [1.016 1.012    1.009 1.008    1.0045 1 0.995 0.99 0.985 0.982 0.979
0.9765 0.974 0.973 0.9714 0.97 0.968 0.963 0.961 0.96 0.9576 0.9558 0.954
0.95];
```

```
SCR_4 = 7;
```

% Assign the reference X/R and voltage data points obtained for Test 4 into variable xr_4 and variable v_ref_4, respectively. Furthermore, define the SCR value for Test 4.

```
v_pre_4 = Asr0*exp(Asr1*(xr_4*SCR_4))+Asr2;
```

% For Test 3, calculate voltage value named v_pre_3 using Eq. (4.7).

```
Error=0;
```

```
s=size(v_pre_4);
```

```
for i = 1:s(1)
```

```
    Error = Error + (v_ref_4(i)- v_pre_4(i))^2;
```

```
end
```

```
SD(4) = sqrt(Error) / s(1);
```

% Calculate standard deviation between v_ref_4 and v_pre_4 and assign it into variable SD(4).

```
SSD = sum(SD);
```

% Calculate the sum of error between predicted and reference voltage values for Tests 1 to 4.